ANALYSIS OF DEFORMATIONS, STRESSES,

AND FORCES IN WEBS ENCOUNTERING

SPREADING ROLLERS

By

RONALD DAVID DELAHOUSSAYE

Bachelor of Science
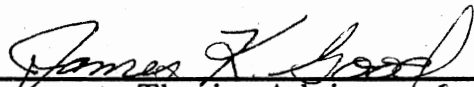Louisiana Tech University
Ruston, Louisiana
1979

Master of Science in Mechanical Engineering
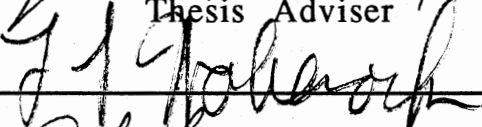Georgia Institute of Technology
Atlanta, Georgia
1982

Submitted to the Faculty of the
Graduate College of the
Oklahoma State University
in partial fulfillment of
the requirements for
the Degree of
DOCTOR OF PHILOSOPHY
December, 1989

ANALYSIS OF DEFORMATIONS, STRESSES,
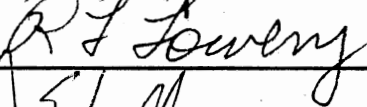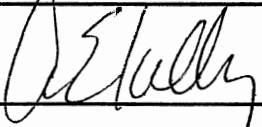
AND FORCES IN WEBS ENCOUNTERING

SPREADING ROLLERS

Thesis   Approved:

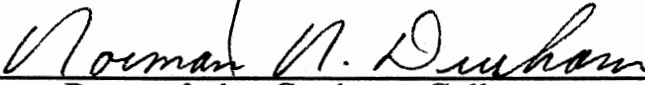_____
Thesis   Adviser

_____

_____

_____

_____
Dean of the Graduate College

ACKNOWLEDGMENTS

TABLE OF CONTENTS

LIST OF TABLES

LIST OF FIGURES

CHAPTER I

THE RESEARCH PROBLEM

Introduction

A web is defined as any material in continuous flexible strip form [1]. The flexibility of the web is derived from the fact that the material thickness is small compared to the length and width of the material. Many of the goods produced by modern industry involve the use of material in web form. These industries include automotive, aircraft, paper, textiles, printing, metal processing, electronics, building materials, etc. Common web materials include paper, textiles, plastics, metals, and many others. The manufacture of products using web materials and the manufacture of the web material itself involves a wide variety of processes. These processes include rolling, casting, extrusion, printing, coating, laminating, cleaning, slitting, folding, etc.

Web materials are usually delivered in the form of rolls, because of their compactness and ease of handling. Most web handling systems include equipment to unwind the roll of web material, transport it through the various manufacturing processes, and rewind it onto a roll. The material is usually supported, guided, and propelled by rollers. Some of these rollers are driven by external means to propel the web down the line. Others are driven

solely by the friction of the contacting web and are used for control and support of the web.

The commercial pressures for increased productivity require higher and higher line speeds. As the speed of the line increases, the static and dynamic forces acting on the web become more extreme, increasing the likelihood of defects in the material. Wrinkling is one of the most common web defects.

Wrinkles can form for a variety of reasons, including nonuniform material properties, and nonuniform loading. Wrinkles in a free web span between two supporting rollers are common and do not necessarily damage the web. These wrinkles are aligned with the direction of travel down the machine and indicate a lack of tension in the cross machine direction. Permanent damage can occur when the wrinkle crosses a roller, or when the wrinkle is wound into a roll. Both of these situations can result in a crease or crack in the material, or other problems.

Several devices have been developed to remove wrinkles from webs or prevent them from forming. The most common spreading devices are the D-Bar spreader, the curved axis (Mt. Hope) roller, and the concave roller. The curved axis roller and concave roller are the objects of this study. Each of these devices operate by inducing tensile stresses in the web in the cross machine direction. In addition, a nonuniform stress profile is also induced in the machine direction. The proper design of a system using either of these rollers involves choosing system parameters to provide stress levels sufficient to prevent wrinkle formation, but not so excessive as to damage the web. The purpose of this study is to develop and verify

a method of determining the deformations and stresses induced by the use of these two types of spreading rollers.
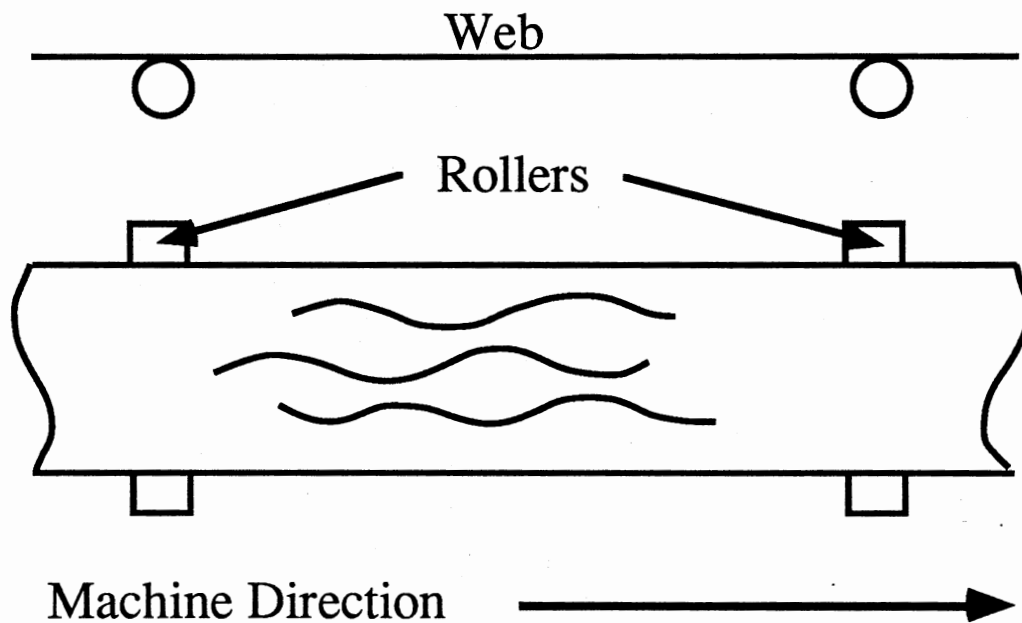
Figure 1-1. Wrinkles in a Web Span Between Rollers

The Curved Axis Roller

The curved axis roller is formed using a nonrotating bowed shaft. The bow in the shaft may be permanently fixed or variable by mechanical means. A set of bearings are placed over the shaft at even, closely spaced intervals. A tight flexible covering is placed over the set of bearings. The covering and the bearings rotate together as a unit. Figure 1-2 is a schematic drawing of a curved axis

roller. As the covering rotates, points on the upper portion of the covering are moved out towards the end of the roller. This is caused by the bow in the shaft. Portions of the web in contact with the covering are also moved outward, provided there is sufficient frictional force between the covering and the web.
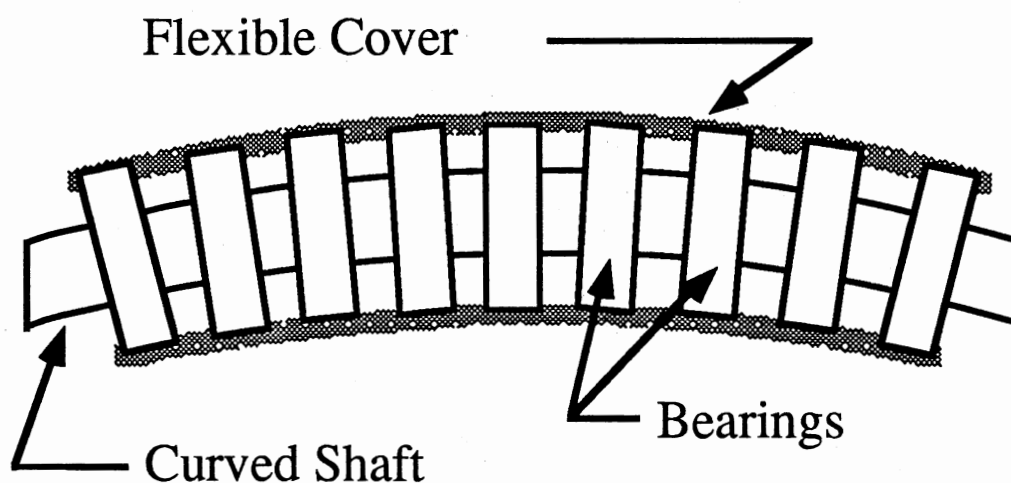
Figure 1-2. A Curved Axis Roller

Although the curve axis roller is a relatively complex device when compared to most other rollers, its method of operation is intuitively simple. The roller is able to spread the web because points on the surface of the roller itself are moving outward. This is one of the advantages of the curved axis roller. Even when there is slippage between the web and the roller, as long as the material remains in contact with the roller, this simple spreading mechanism

remains effective. The curved axis roller does have several disadvantages. The first is the relative complexity and expense of this type of roller. The other disadvantages occur because of the need for a flexible covering on this device. The covering is not as durable as aluminum or steel rollers, particularly in harsh environments. The cover can be damaged by extreme temperatures and chemicals used in the manufacturing process. Also the behavior of the covering can change with time. The surface traction of the covering can change, reducing the effective spreading forces. The surface can deform into the spaces between the bearings, so that it no longer has the shape of a curved cylinder. Because of the alternating tensile and compressive stresses induced in the covering with each revolution of the roller, it can have a relatively short fatigue life. This results in cracking of the covering. In spite of these disadvantages, the curved axis roller is being used successfully in many web handling applications.

The Concave Roller

The concave roller is a much simpler device than the curved axis roller. The construction of the concave roller is very much like the cylindrical rollers used in most web handling equipment. The major difference is that the roller is not cylindrical, but instead has a smaller diameter at the center, and a larger diameter at the ends. The curve describing the roller profile can be circular, parabolic, linear, or a combination of these and other curves. Figures 1-3 and 1-4 show concave rollers with circular and linearly tapered profiles. The concave roller is closely related to the crowned roller which has

been used for many years as a means of keeping power transmission belts centered on their pulleys. Figure 1-5 shows a crowned roller.

The spreading mechanism of the concave roller is not as easily understood as that of the curved axis roller. The spreading action of the concave roller is caused by the elastic deformation of the web in the cross machine direction when a nonuniform displacement is applied to the web in the machine direction. The nonuniform surface profile of the concave roller causes these nonuniform displacements. A more complete description of this spreading mechanism will be given in subsequent chapters.

The concave roller is much more dependent on surface traction between the web and the roller than is the curved axis roller. Without sufficient friction, the concave roller can actually increase the likelihood of wrinkles. This is the primary disadvantage of the concave roller. The primary advantage of the concave roller over the curved axis roller is its similarity to the cylindrical roller. The concave roller can be made of the same materials, and have the same bearing configuration as the other rollers on the machine. This means that the concave roller can be designed to survive in the same environment as other rollers on the machine.

Circular Surface
Profile
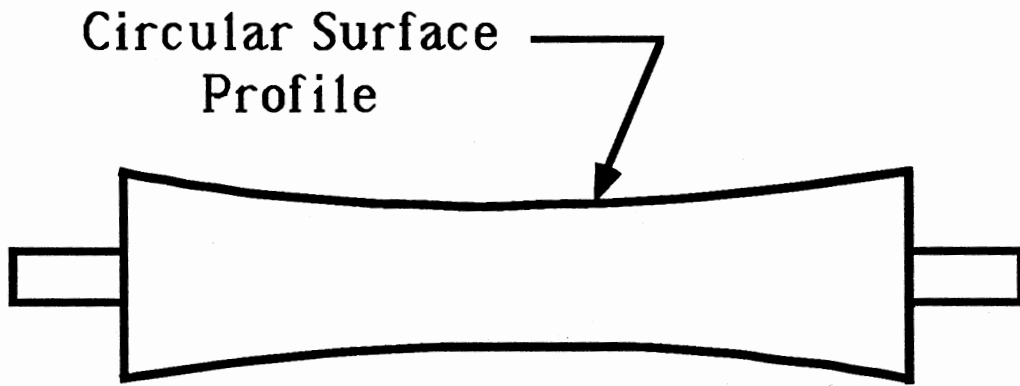
Figure 1-3. A Circular Profile Concave Roller

Linear Tapered
Profile
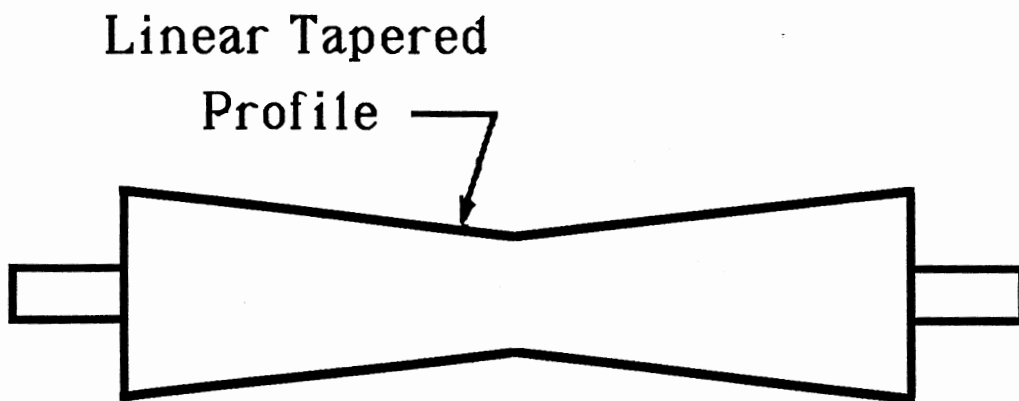
Figure 1-4. A Linearly Tapered Concave Roller

Crowned Profile
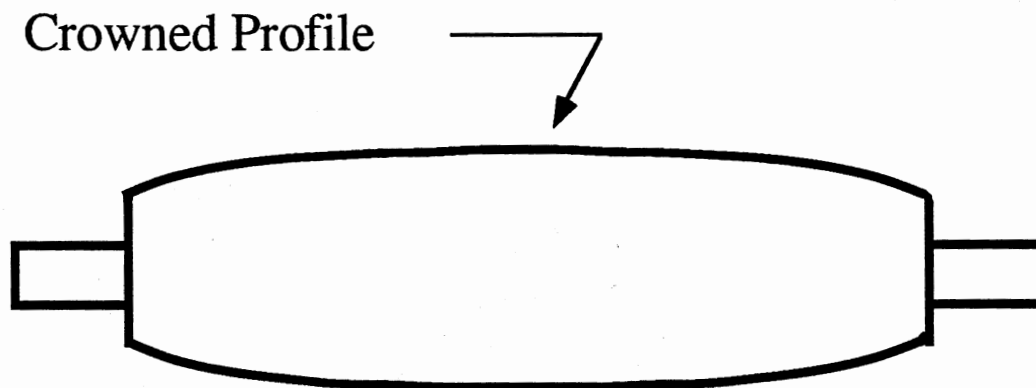
Figure 1-5. A Crowned Roller

Summary of Research Objectives

Objective

The primary objective of this research is to develop a method for predicting the elastic deformations and stresses of webs encountering concave and curved axis rollers. The Finite Element method is used to relate the web displacements, forces, and stresses. Because of the nonlinear nature of the traction between the web and the roller, an iterative Finite Element solution technique must be used.

Subobjectives

In addition to the primary objective, there are also several sub-objectives.

(1) The accuracy of the Finite Element model must be verified experimentally. This involves measuring the changes in the width of the web at strategic places before and after it encounters the concave or curved axis roller. These measurements are compared to the values predicted by the model.

(2) The model is used to examine the effects of variations in roller geometry and web material properties on the effectiveness of these spreading rollers. This allows the significant parameters to be identified.

(3) For the results of this research to be truly useful, the computer model must be accessible, relatively fast, and must present the results of the computations in an easily understandable form. Program accessibility is enhanced by using several techniques to reduce the memory requirements of the program to the point where it can be run on a personal computer. In addition, techniques have been used to minimize computation time required.

CHAPTER II

LITERATURE REVIEW

Introduction

This chapter contains a review of the literature pertaining to the design and analysis of spreading rollers. The literature can be grouped into five general categories.

(1) Analysis of crowned rollers used as centering devices

(2) Analysis of the lateral motion of webs applied to web guidance

(3) General discussions and recommendations on the use of spreading devices based on industrial experience

(4) Experimental investigations

(5) Analytical investigations

Crowned Rollers

The crowned roller is a device very similar in construction to the concave roller. Although the crowned roller is a compressing device, and the concave roller is a spreading device, the theory behind the operation of these two devices is identical. Crowned rollers have been recognized for years as a simple and effective device for centering belts in belt driven power transmission systems.

Swift [2] recognized that because the crown is detrimental to the longevity of the belt and reduces the frictional qualities of the drive, the smallest crown necessary should be used. To facilitate this, he developed a design model based on treating the belt as a beam bending due to an applied couple. He also developed the idea of an idle arc on the roller in which the tension in the belt is constant. This results in a strain profile in the belt which conforms to the geometry of the pulley. This strain profile is the primary factor in the centering effect of the crowned roller, and the spreading effect of the concave roller.

Sassaki, Hira, Abe, Yangagishima, Shimoyama, and Tahara [3] performed both analytical and experimental investigations on the effect of crowned rollers used in the annealing furnace of a steel mill. They were particularly interested in the tendency of the steel strip to buckle and wrinkle in the furnace. A one fifth scale web transport system was built to study a variety of roller crown profiles, and their tendency to cause buckling in aluminum foil. The profiles they studied included various magnitudes of crown radius and linear taper combined with cylindrical sections. They recognized that the nonuniform strain profile imposed by the roller on the material contributed to the tendency of the steel to buckle. In order to quantify this effect, they used a finite element model of a flat strip subjected to nonuniform longitudinal displacements. They determined that the strain profile caused compressive stresses in the material and this was the primary cause of buckling.

Theory of Web Guidance

Shelton [4] used the idea of the idle arc as described by Swift to develop the principle of web transport and three corollaries. The principle of web transport is stated as follows:

> If the friction between a moving web and a roller is sufficient to prevent slippage at the line of entering contact, the conditions at a given point in the entering span immediately upstream from the line of entering contact are transported toward, then around the roller in a plane which is perpendicular to the axis of rotation of the roller and which passes through the initial location of the point.

This principle is applied in much of the work in web guidance and control, and is used in developing the boundary conditions for the curved axis and concave roller models.

Shelton and Reid [5],[6] developed models for the lateral dynamics of webs and applied these models to web guide control systems. These web guide control systems generally rely on lateral shifting and pivoting of intermediate rollers to steer the web. The most important principle governing these devices is that the web will seek to align itself perpendicular to a roller in the entry span to that roller. Shelton used the equation for beam bending to model the lateral motion of the web due to the moments induced by the steering rollers. Shelton [7] also used the principles of web transport to investigate the dynamics of web tension control. In this report, he developed the web span continuity equation given in equation (2.1). The steady state form of this equation is used in developing the

models for the curved axis and concave rollers. Figure 2-1 shows the roller system described by the continuity equation.

$$(1-\varepsilon_A) V_1 dt - (1-\varepsilon_B) V_2 dt = d[L_B(1-\varepsilon_B)] \qquad (2.1)$$
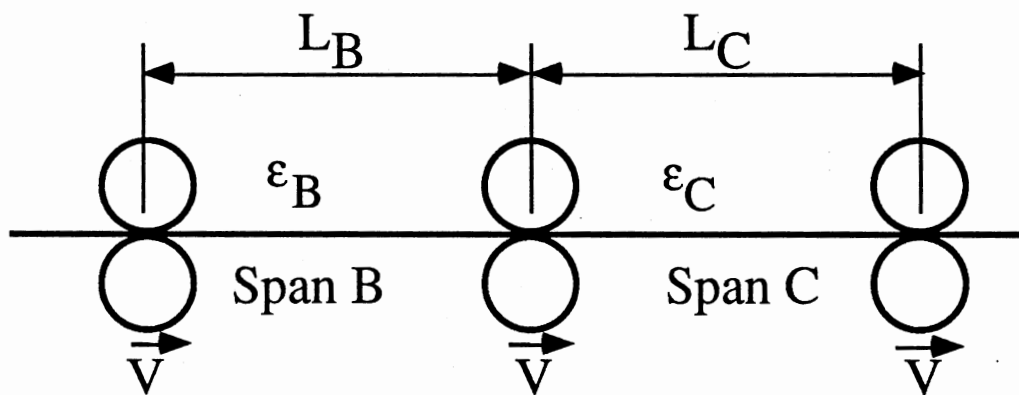
Figure 2-1. Reference Geometry for the Continuity Equation

Pfeiffer [8] used the web transport principle and simple concepts from both narrow and wide web systems to offer rules of thumb for web guidance. He describes the spreading mechanism of the curved axis roller and the D-bar spreader. He also discusses factors governing the traction between the web and the roller.

Industrial Experience

The curved axis roller and the concave roller have been used in industry for many years. The insight gained from observing real

applications of these devices is useful in understanding the spreading mechanism exhibited by these devices.

Butler [9] describes a novel application of the concave roller. Concave rollers are being used to remove a condition called "bow" from fabric. Bow occurs in fabric when the fibers of the material are shifted in the machine direction, and no longer align properly in the cross machine direction as shown in figure 2-2.
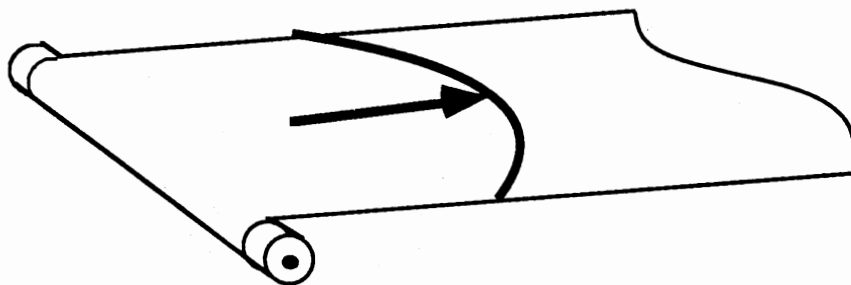
Figure 2-2. Bow in a Fabric Web

Butler states that the velocity gradient across the width of the concave roller is able to remove symmetrical bows by moving the outer fibers faster than the inner fibers. With proper design of the concave roller, the outer fibers can be shifted back into alignment with the inner fibers. This application is a graphic demonstration of the basic spreading mechanism of the concave roller. The nonuniform strains are applied across the web because of a nonuniform velocity across the face of the roller.

Gallahue [10] describes the use of the curved axis roller to separate the web strips after passing through a slitter. He recommends that two curved axis rollers be placed in series in a configuration so that all of the slits travel the same distance. This configuration minimizes the strains applied to the web material, and improves the quality to the wound roll by reducing the likelihood of interleaving or dishing.

Daly [11] investigated the factors controlling traction between webs and their carrying rolls. Proper traction is a critical factor in the performance of both the concave roller and the curved axis roller. Daly reports that the significant variables governing traction are:

(1)   Web tension

(2)   Web speed

(3)   Wrap angle

(4)   Roll diameter

(5)   Web porosity

(6)   Web moisture

(7)   Paper grade

In his analysis, he concludes that air entrainment is the common and overriding factor in web traction. He then recommends the following methods of increasing web traction:

(1)   Use of vented rolls by grooves of holes

(2)   Use of porous body rolls

(3)   Use of porous rolls evacuated

(4)   Use of a nip roll (with nip control)

(5)   Use of a vacuum doctor at incoming wedge

(6)   Use of stationary air floated tables to carry the web, creating a fixed traction condition

Lucas [12] and [13] performed a study of the effectiveness of two of the common spreading devices; the curved axis roller and the D-bar spreader. He described the mechanism by which each of these devices works. He focused primarily on the use of these devices in separating web strips after slitting, and prior to winding on a roll. He lists the following problems associated with these spreading devices:

(1)   Good slit separation at the machine center, with poor spread at the edges

(2)   Good spread at low speeds and poor spread at high speeds

(3)   Good spread at high web tensions and poor spread at low web tensions

(4)   Poor wound roll edge quality

(5)   Web snapoffs at slitter or spreader

(6)   Crowding of slits at wound roll

(7)   Thrusting of wound rolls against core boxes

(8)   Roll dishing

In his investigation, he discovers that excessive curvature of the curved axis roller can actually decrease the amount of spreading.

He states that the elasticity of the material allows the web to spread only to a limited degree, and that the roller curvature should be compatible with this limited spreading. He also states that the effects of even the best spreading device are wasted if the web is not guided reliably.

Experimental Investigations

Magill [14] developed a transducer capable of measuring bi-axial tension in webs. The transducer uses a circular vacuum ring placed in contact with the web to apply a uniform pressure to the web. When the vacuum is applied, the ring acts as an edge support as the web deforms down into the ring. A moire' grating is placed over the web to produce a fringe pattern. The size and shape of the fringe pattern can be related to the bi-axial tension state in the web. Figure 2-3 is a schematic drawing of this device.

The vacuum ring was manufactured in three different diameters; 1, 1.5, and 2 inches. A curved axis roller was used to apply a bi-axial tension field into a web. The device was successful at detecting the tension in the machine direction, and in the cross machine direction. Because of the size of the vacuum ring, this device's spacial resolution is somewhat coarse. Also, because of the size of the ring and the frame, it was not possible to take measurements near the roller. This limits the usefulness of this device in studying the stress distribution induced by the roller.
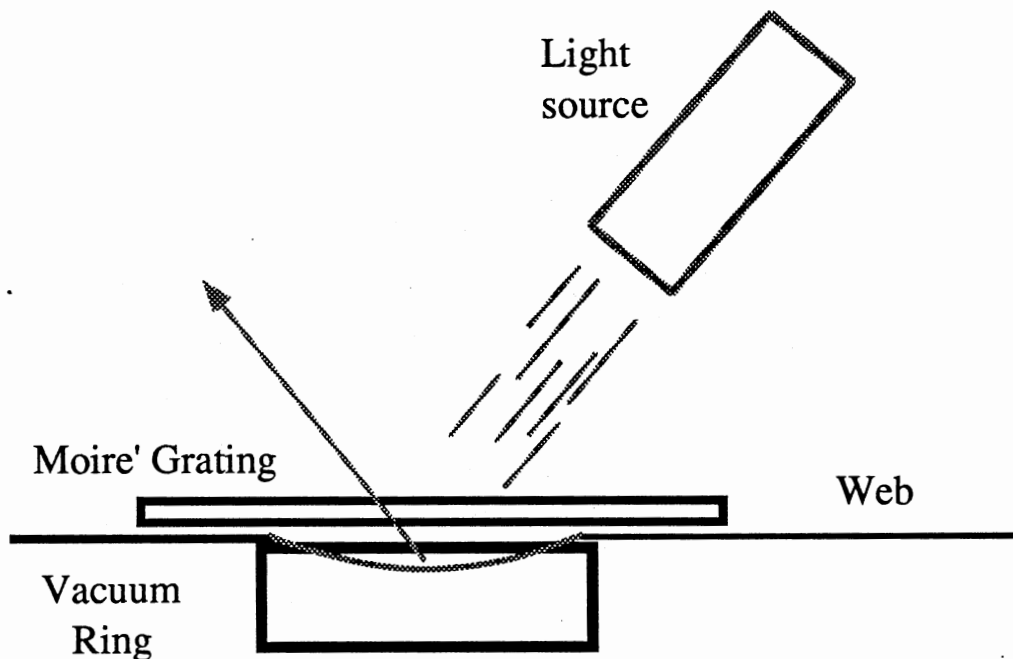
Figure 2-3. Device to Measure Bi-axial Tensions in Webs

Analytical Investigations

Feiertag [15] developed a mathematical model for the spreading of an idealized web by a curved axis roller. He then used this model to develop design criteria for using the curved axis roller in wrinkle prevention, as guide rollers, and for slit separation. Figure 2-4 shows the spreading behavior of both real and idealized webs.
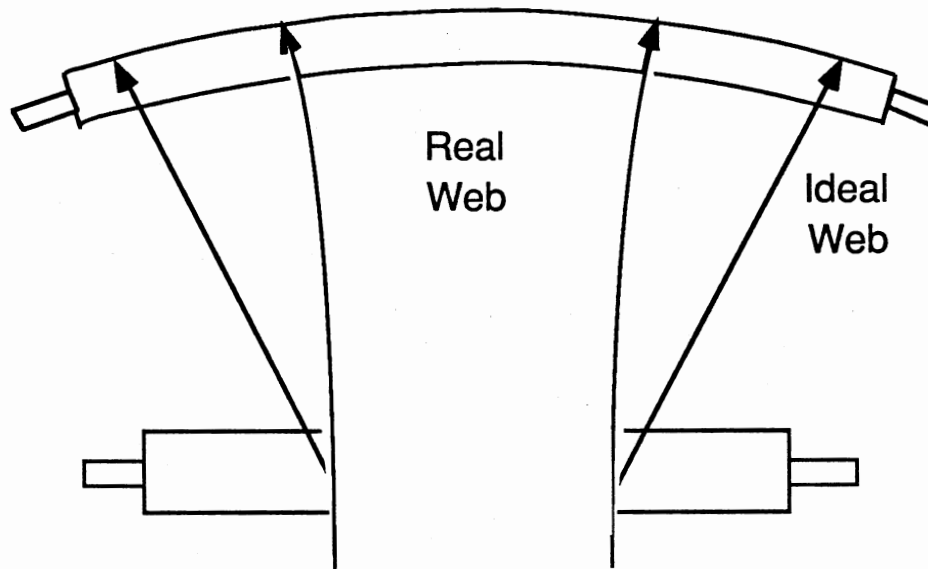
Figure 2-4. Spreading of Real and Idealized Webs

An idealized web is a web that has tensile stiffness in the
machine direction, but no stiffness in the cross machine direction.
This is a suitable model for a wrinkled web. From his analysis,
Feiertag concluded that less roller curvature should be used, and
much longer entry spans should be used.

Reynolds [16] developed a two-dimensional finite element
model of the curved axis roller. He used triangular linear simplex
elements in his model. Because of the simple elements used, the
number of elements had to be quite large. The program was also
highly iterative, often requiring more than 100 iterations to converge
on a solution. The combination of these two facts limit the program

to running on a mainframe computer to give reasonable turn-around times.

Reynolds ran five different problems to examine the behavior of his model. He was primarily investigating the sensitivity of his model to various iteration methods. He did not perform any type of parametric study.

Leport [17] developed a three-dimensional model of the concave roller. He also used the triangular linear simplex element. He used the technique of assembling 2-D flat plate elements in 3-D space as described by Segerlind. This assembly in 3-D allows the normal forces generated by the roller to be calculated by the finite element code. This is not possible with a 2-D model.

Leport modeled concave rollers having both circular profiles and linear taper profiles. His model also required large amounts of computer memory and many iterations to converge.

Kliewer [18] continued working with Leport's model, searching for a reasonable set of geometric boundary conditions. Boundary conditions were needed that provided continuity of strains, and also satisfied the web transport conditions as stated by Shelton. After trying many different boundary conditions, Kliewer succeeded in finding a reasonable solution. To satisfy the boundary conditions with strain continuity, he developed the following algorithm:

(1)   Use the continuity equation to calculate the location on the roller having the same strain as the average line strain.

(2)　Use these strains and a simple tension model to calculate a set of forces resulting from these strains.

(3)　Make a preliminary finite element run using these forces as boundary conditions. This run gives a set of machine direction displacements corresponding to the applied forces.

(4)　Apply the deformations from the preliminary run to the nodes at the entry to the roller.

(5)　Use the estimated strains from step 1 to lock in the machine direction positions of the remaining nodes on the roller (no slip in the machine direction).

(6)　Lock together rows of nodes to simulate the no slip condition in the cross machine directions.

Using this model, Kliewer investigated the effects of seven system parameters on the spreading ability of the concave roller. Those system parameters are:

(1)　Circular arc profile of the concave roller

(2)　Modulus of elasticity

(3)　Material thickness

(4)　Poisson's ratio

(5)　Coefficient of friction

(6)　Wrap angle

(7)　Line tension

His investigation generated a large amount of data for web stresses, strains, and deflection in concave roller systems.

Because Kliewer's model is based on the work of Leport, it is also a very large computer model, requiring eight megabytes of CPU memory, and an average of 40 minutes of IBM 3081 CPU time to run one analysis. He recommends that techniques be applied to reduce the size and increase the efficiency of the computer model. In addition, he recommends that a method be found to experimentally verify the program results.

Summary

This chapter presents a survey of the literature on the current knowledge and research needs related to the curved axis and the concave roller. This survey indicates that these devices have been used for many years with very little quantitative understanding of the parameters affecting their performance. Preliminary work has been done to create useful computer models that can increase our understanding of these devices. These models have not been validated by experimental means. In addition, these models require an excessive amount of mainframe computing resources to run and therefore are not sufficiently accessible or useful.

CHAPTER III

TECHNIQUES FOR EFFICIENT MODELING OF
SPREADING ROLLERS

Introduction

The purpose of this project is to develop and verify a model capable of predicting the elastic behavior of webs encountering curved axis and concave rollers. The web / roller system can be modeled as a membrane conforming elastically to a three dimensional surface, with surface tractions between the membrane and the surface. The equilibrium state between the surface tractions and membrane deformations is governed by the rotational motion of the surface (the roller). This summary of the model describes a complex set of boundary conditions that must be applied to the equations of elasticity.

Finite Element Modeling (FEM) has proven to be an effective means of modeling problems described by sets of partial differential equations with complex boundary conditions. This chapter summarizes the equations for modeling 2-D plane stress using FEM. It also summarizes the modeling techniques commonly used in a general purpose FEM system. These general techniques have a computational overhead that greatly increases the memory requirements and computation time required to model these

23

spreading roller systems. The remainder of this chapter describes the techniques used in developing efficient Finite Element models of the curved axis roller and the concave roller.

Basic Finite Element Analysis Techniques

The Finite Element Equations for 2-D Plane Stress

The finite element method is a means of approximating the behavior of continuous systems. The domain of the continuous system is divided into a finite number of regions or elements. Within each element, the system behavior is described by an approximating function. The problem of solving a small set of partial differential equations and boundary conditions is replaced by the problem of solving a large but finite set of algebraic equations.

The equations used in applying the Finite Element method to 2-D plane stress elasticity problems will be briefly described. It is assumed that the reader has some familiarity with both the theory of elasticity and the Finite Element method.

Figure 3-1 shows a representative 2-D linear triangular finite element with deflections given at node points i, j, and k. The deflections u and v at any other point in the element can be determined using equation 3.1 [19],[20].

$$\left\{ \begin{array}{c} u(x,y) \\ v(x,y) \end{array} \right\} = [N] \ \{U^{(e)}\} \qquad\qquad (3\text{-}1)$$
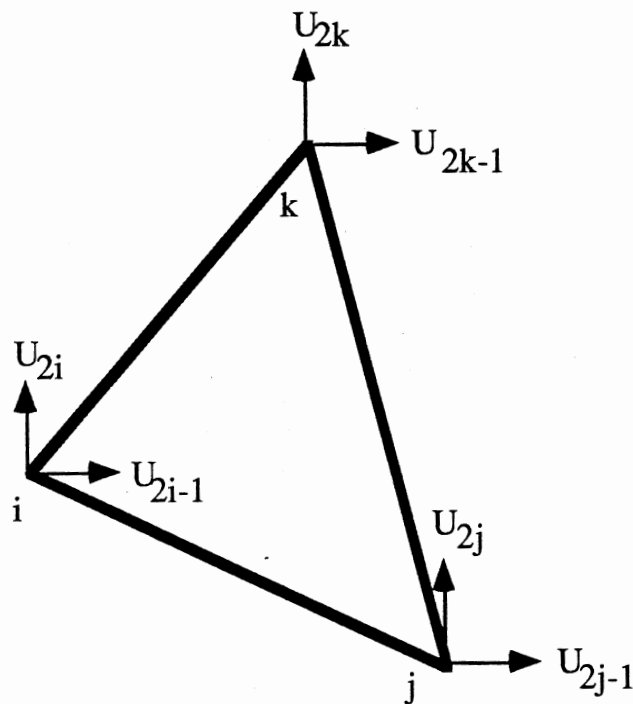
Figure 3-1.   Nodal Deformations of a Linear Triangular Element

[N]   is a matrix of elemental shape functions and $U^{(e)}$ is a column vector of the element nodal displacements.   Both the accuracy and complexity of the element model are governed by the types of function used as elemental shape functions, and the number

of nodes used in defining the element. The linear triangle element shown in figure 3-1 is the simplest and probably the most commonly used type of element. More accurate elements can be obtained by increasing the complexity of the shape functions, and correspondingly increasing the number of nodes defining the element.

If the nodal deformations are known, the element strains can be computed by equation (3.2).

$$\{\varepsilon\} = \begin{bmatrix} \varepsilon_x \\ \varepsilon_y \\ \gamma_{xy} \end{bmatrix} = \begin{bmatrix} \dfrac{\partial u}{\partial x} \\ \dfrac{\partial v}{\partial y} \\ \dfrac{\partial u}{\partial y} + \dfrac{\partial y}{\partial x} \end{bmatrix} = [B]\{U\} \qquad (3.2)$$

[B] is a matrix containing partial derivatives of the shape functions [N]. For linear shape functions, [B] is a matrix of constants. This means that the strain within the element is approximated as a constant. Non-linear shape functions can be used to allow variation of strain within the element. For non-linear shape functions, [B] is a matrix of functions that must be evaluated at the point within the element where the strains are to be calculated.

Hooke's law is used to represent the relationship between elemental strains and stresses. It states that the state of stress at any point is linearly related to the state of strain at that point as shown in equation (3.3).

$$\{\sigma\} = \begin{bmatrix} \sigma_x \\ \sigma_y \\ \tau_{xy} \end{bmatrix} = [D]\{\epsilon\} \tag{3.3}$$

For isotropic materials in a state of plane stress the coefficients of [D] are expressed in terms of the two commonly used material properties, Young's Modulus and Poisson's Ratio.

$$[D] = \frac{E}{(1-\nu^2)} \begin{bmatrix} 1 & \nu & 0 \\ \nu & 1 & 0 \\ 0 & 0 & \frac{(1-\nu)}{2} \end{bmatrix} \tag{3.4}$$

For orthotropic materials in a state of plane stress, four independent material coefficients are required. Equation (3.5) shows the coefficients of [D] for orthotropic materials expressed in terms of five material properties.

$$[D] = \frac{1}{(1-\nu_x\nu_y)} \begin{bmatrix} E_x & \nu_y E_x & 0 \\ \nu_x E_y & E_y & 0 \\ 0 & 0 & G \end{bmatrix} \tag{3.5}$$

But, four of the properties are related as shown in equation (3.6).

$$E_x \nu_y = E_y \nu_x \tag{3.6}$$

For materials where the shear modulus G is not known, equation (3.7) is a useful approximation.

$$G = \frac{1}{\frac{(1+\nu_x)}{E_x} + \frac{(1+\nu_y)}{E_y}} \tag{3.7}$$

For isotropic materials, equation (3.7) yields the familiar relationship between Young's Modulus, Shear Modulus, and Poisson's Ratio.

$$G = \frac{E}{2(1+\nu)} \tag{3.8}$$

The principle of minimum potential energy is used to develop the equilibrium equation for plane stress. The total potential energy of the system is the sum of the strain energy in the material, and the work done by the external loads. Using the relations between nodal displacements, and element strains and stressed defined above, the element equilibrium equation can be written as:

$$[F]^{(e)} = [K]^{(e)} [U]^{(e)} \tag{3.9}$$

$$[K]^{(e)} = \int_V [B]^T [D] [B] dV \tag{3.10}$$

[F] is a vector of forces applied at the nodes and [K] is the element stiffness matrix.

The application of these equations involves assembling the stiffness matrices for each element into a global stiffness matrix. The global stiffness matrix and the force vector are modified to account for any known nodal forces and displacements. The set of equations are solved for the unknown nodal displacements. Those displacements can then be used to solve for the elemental stresses and strains.

The Eight Node Isoparametric Element

The linear triangle element is adequate for many types of problems. To model complex geometry, a large number of very small elements can be used to provide good accuracy even in areas of high stress gradients. Given sufficient computing resources, this is an acceptable approach. An alternative means of improving accuracy is to use higher order elements. The linear triangle uses linear shape functions, and therefore calculates a linear variation for element deformations, and constant element strains and stresses. Quadratic shape functions give quadratic deformation variations, and linear stress and strain variations across the element. This higher order variation in stress and strain means that fewer elements are needed to achieve the same accuracy as the linear element. Fewer elements mean that less computer memory is required for storing the global stiffness matrix, and less time is required to solve the structural equilibrium equations.

The eight node quadratic isoparametric element was selected as the element to be used in modeling the concave roller and the curved axis roller. This element is shown in figure 3-2.
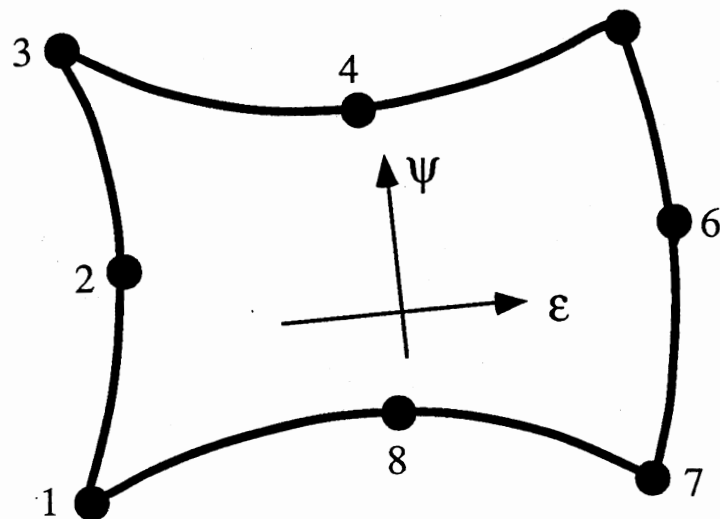
Figure 3-2. Eight Node Quadratic Isoparametric Element

This element uses quadratic shape functions of the parameters ε and ψ to map the curved sides of the element to a unit square. Because of this non-linear mapping of the shape functions, the element stiffness matrix cannot be integrated directly. Instead, Gauss Quadrature numerical integration is used. The procedure for performing the mapping and integration is described in Segerlind's text [20].

<u>Modeling Shells as an Assembly of Planar</u>

<u>Elements</u>

Zienkiewicz's text [19] on Finite Element methods illustrates using a collection of planar elements to model three dimensional shells.
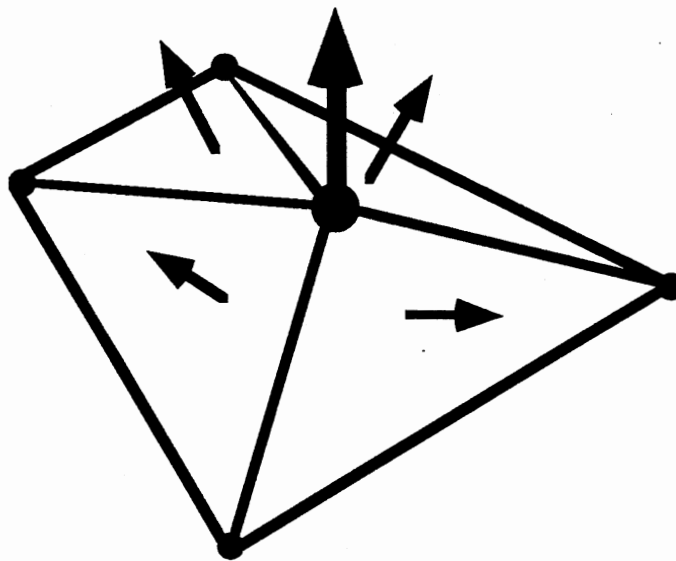
Figure 3-3.   A 3-D Shell Modeled with Flat Plate Elements

Figure 3-3 shows a simple pyramid shape being modeled by triangular flat plate elements. The directions of the surface normals are shown for each element. The direction of the deformations for the node shared by the four elements is also shown. The process for

building the 3-D stiffness matrix of a shape composed of flat elements involves the following steps.

(1) Build the elemental stiffness matrix for the element in a 2-D local coordinate system.

(2) Copy the values from the 2-D stiffness matrix into a 3-D temporary matrix.

(3) Rotate the 3-D flat matrix into the proper 3-D orientation using a rotation matrix based on the direction of the surface normal for the element.

(4) Assemble the 3-D temporary matrix into the global stiffness matrix.

(5) If desired, the global stiffness matrix can be modified so that nodal forces and deflections are aligned with an independent coordinate system for each node.

Steps (3) and (5) involve the proper application of coordinate transformations to the element and global stiffness matrices.

Transforming the Element Stiffness Matrix
from Local to Global Coordinates

It is often simpler to calculate the element stiffness matrix in a coordinate system that is not aligned with the global coordinate system. In particular, when modeling a 3-D shell with planar elements, the element stiffness terms must first be calculated in a 2-D planar system, and are the rotated to the correct orientation in the

global coordinate system.   Figure 3-4 shows an element in both the local (x,y,z) and global (X,Y,Z) system.

Local Element Coordinates

Element
rotated to
the Global
system
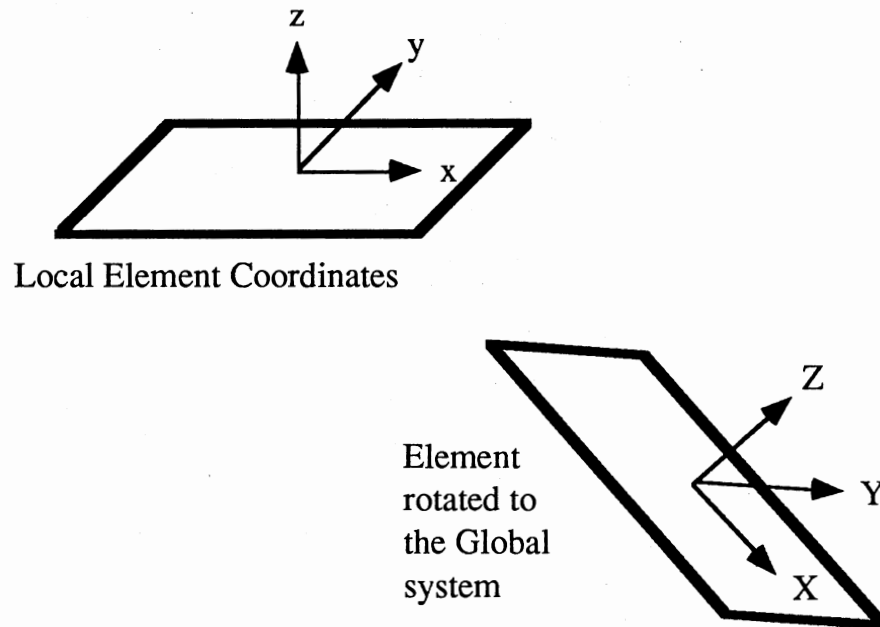
Figure 3-4.   Element Rotated From Local to Global Coordinates

The geometry of the specific system being analyzed will define a 3 by 3 transformation matrix $[t_{lg}]$ that will transform forces and deformations from the local system to the global system as shown in equation (3.11).

$$\begin{bmatrix} X \\ Y \\ Z \end{bmatrix} = \begin{bmatrix} t_{lg} \end{bmatrix} \begin{bmatrix} x \\ y \\ z \end{bmatrix} \qquad (3.11)$$

A larger transformation matrix is required to transform all of the nodal displacements or forces for an element. This matrix $[T_{lg}]$ is formed by placing copies of $[t_{lg}]$ on the diagonal of a 3N by 3N matrix where N is the number of nodes in the element.

$$[T_{lg}] = \begin{bmatrix} [t_{lg}] & & 0 \\ & \ddots & \\ 0 & & [t_{lg}] \end{bmatrix} \tag{3.12}$$

$$F_g = [T_{lg}] F_l \tag{3.13}$$

$$U_g = [T_{lg}] U_l \tag{3.14}$$

These equations can be substituted into the local element stiffness equations to define the transformation from the local element stiffness matrix to the global element stiffness matrix.

$$[F_g] = [T_{lg}] [K_l] [T_{lg}]^T [U_g] \tag{3.15}$$

$$[F_g] = [K_g] [U_g] \tag{3.16}$$

$$[K_g] = [T_{lg}] [K_l] [T_{lg}]^T \tag{3.17}$$

Defining Individual Nodal Coordinate Directions

Once the global stiffness matrix is assembled, it is sometimes convenient to assign local coordinate systems to individual nodes. This local or skewed coordinate system defines the directions of boundary conditions imposed on the node, as well as the directions of the calculated forces and displacements. This process involves modifying entire rows and columns of the global stiffness matrix with coordinate transformation matrices. The concept is essentially the same as the method described in the previous section except that the transformation is applied uniquely to each node in the model. The process of skewing a single node in the model is illustrated in figure 3-5 using the transformation matrix from equation (3.11).

First, the rows of the global stiffness matrix containing the equations for the node being skewed are pre-multiplied by the transpose of the transformation matrix. Then the columns containing the coefficients of the displacements for the node being skewed are post-multiplied by the transformation matrix.

Applied Force Boundary Conditions

Externally applied forces are the simplest boundary conditions to implement in a finite element program. They are included by simply entering the force values into the appropriate term of the force vector. If the nodal coordinate directions have been skewed, the forces must correspond to the new nodal directions. If the forces

do not correspond to those directions, they can be modified using the coordinate transformation matrix.
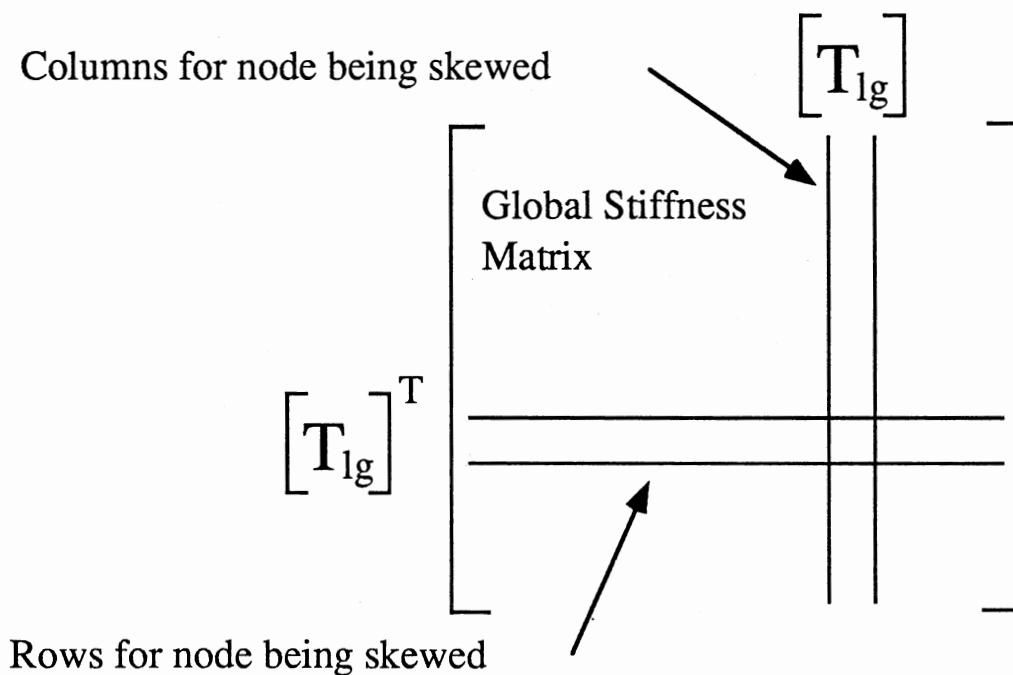
Figure 3-5.   Skewing Coordinates for a Single Node

Fixed Displacement Boundary Conditions.

In most Finite Element models, some of the nodal displacements are known in advance and are part of the set of boundary conditions that drive the model to a specific solution. These fixed displacements must be incorporated into the set of equations without disturbing the symmetry and the banding of the

global stiffness matrix. A simple procedure to accomplish this is illustrated in figure 3-6.

Column vector $\mathbf{K}^i$
for DOF being specified

Global Stiffness Matrix

Clear the Row
vector for DOF being
specified
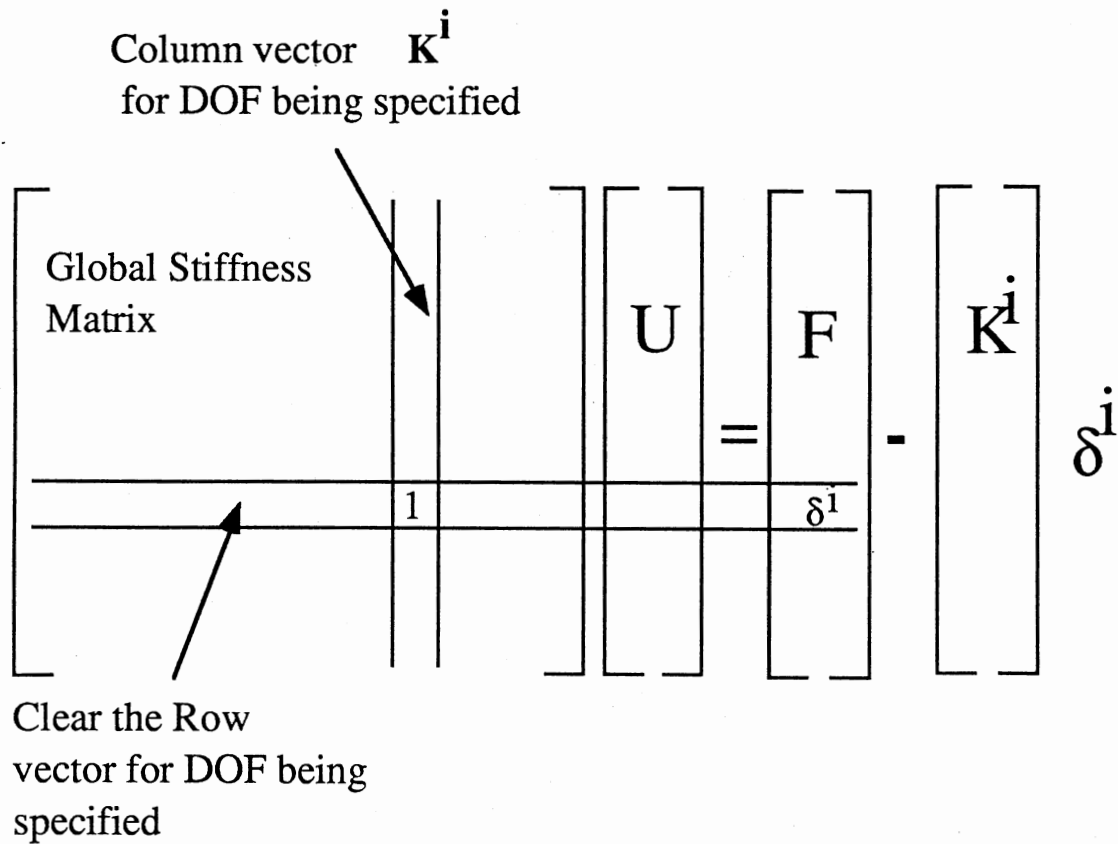
Figure 3-6. Modification of Equation for Known Displacements

(1) Subtract the product of column i and the known displacement from the force vector.

(2) Zero all values in column i of the stiffness matrix.

(3) Zero all values in row i of the stiffness matrix.

(4) Enter 1 on the diagonal

(5) Enter the value of the known displacement in row i of the force vector.

This procedure effectively removes equation i from the stiffness matrix and transfers its effect to the force vector. It does this without effecting the matrix bandwidth or symmetry. The row and column of zeroes in the stiffness matrix could be removed to decrease storage requirements and increase solution speed.

Multi-point Constraints

Another type of boundary condition occurs where a linear relationship is required between the displacements of several nodes. The simplest type of multi-point constraint requires that two degrees of freedom must have the same displacement. In essence, these degrees of freedom are locked together. Another simple multi-point constraint requires that two degrees of freedom remain a constant distance apart. Both of these constraints are required in modeling the spreading rollers.

Conceptually, these types of constraints state that part of the solution to the problem is known in advance, and a degree of freedom is removed from the problem. In practice, another degree of freedom is often added to the problem along with the equation for the constraint. This extra degree of freedom is the constraint force required to enforce the displacement relationship. The additional degree of freedom can be added to the system of equations in a way that preserves the symmetry of the system. Unfortunately, the

bandwidth of the system can be increased drastically. This procedure is shown in figure 3-7.
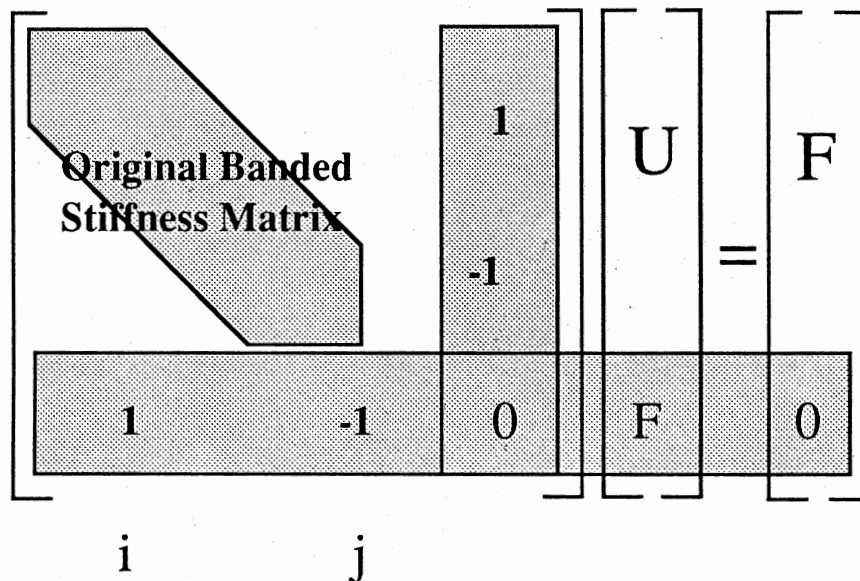
Figure 3-7. Terms Added to Lock Together DOF i and j

Techniques Used to Increase Computational Efficiency

It was noted in the previous section that the methods given for incorporating boundary information into the system of equations were intended for general purpose models. These methods were not optimized for efficient storage requirements, or computation speed. For specific problems, more efficient methods are possible.

Several techniques were developed to improve the efficiency of the programs developed to analyze spreading rollers. Without these techniques, analysis of these rollers would not be reasonable on current versions of personal computers. Although virtual memory techniques would allow eventual solution of these models, the time required for solution would be on the order of days. This long solution time would make these models virtually useless to engineers needing a solution to a problem. These techniques are described in the following sections.

Use of Shared Element Shapes to Reduce Element Integration Time

The undeformed meshes for both the concave roller and the curved axis roller models have identical topology. This mesh is shown in a flat view in figure 3-8.
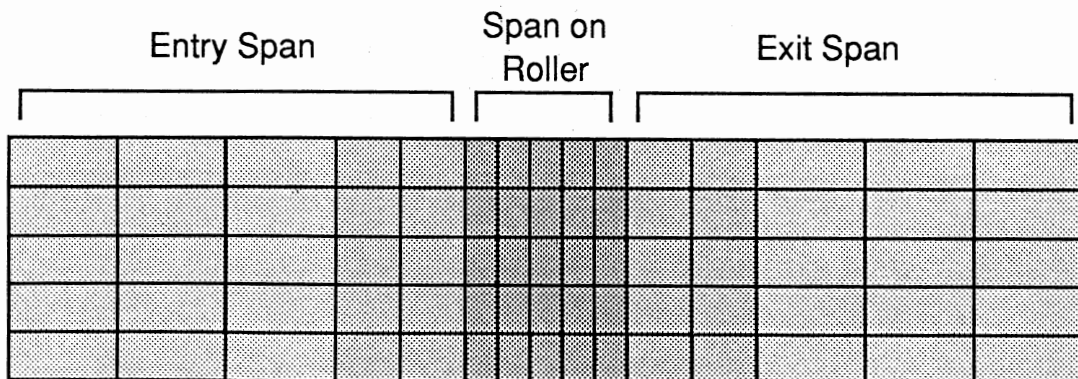
Figure 3-8. Flat View of the FEM Mesh

Figure 3-8 shows that only three unique element shapes are used in a model containing 75 elements. Although two elements of the same shape might have quite different stiffness properties when transformed to the 3-D global coordinate system, their local coordinate stiffness properties are identical. This means that the numerical integration of the element matrices need only be done for three elements instead of 75. This does not reduce memory requirements for the model, but it does save time.

Implementation of Skewed Nodal Coordinates at the Element Level

The procedure described earlier for skewing nodal coordinates required modification of the 3-D global stiffness matrix after all elements were assembled. This requires storage space for the X, Y, and Z DOF equations for each node in the model.

The geometric model of both the curved axis and concave roller is constructed so that all local Z deformations are known. This will be shown in a later section. Because of this, it should not be necessary to store any of the equations for the Z direction. Elimination of these equations reduces storage requirements for the model tremendously. Not only is the number of equations reduced by one third, but the bandwidth of the system of equations is also reduced by one third. Both of these together reduce memory requirements to less than one-half the original requirements. In addition, the time required to solve this smaller set of equations is reduced by an even larger amount.

These savings in memory requirements and computation time are available only if the nodal coordinates can be skewed without actually storing the equations for the Z DOF's. In addition, the effects of the Z-direction stiffness terms must not be lost. Two procedures were developed to do precisely that.

The coordinates for each node in the model can be skewed in the element stiffness matrices instead of the global stiffness matrix. The procedure is similar to that of rotating the entire element stiffness matrix from its local system to its global location. Instead of building a 3N by 3N transformation matrix with the same 3 by 3 matrix on the diagonal, a 3N by 3N matrix with different 3 by 3 matrices on the diagonal is built. Each 3 by 3 matrix contains the values required to transform a specific node in the element. This total skewing matrix will be different for each element, but each time a node appears in an element, it is transformed by the same 3 by 3 matrix. The process of transforming the element to its 3-D location, and skewing the nodal coordinates is performed by one combined matrix. This process is shown in figure 3-9.

Retaining the effects of the Z-direction stiffness terms without assembling them is relatively simple once the previous problem has been solved. All of the Z-direction terms can be treated just like any other known displacement boundary conditions. The effects of the stiffness terms and the known displacements can be put into the appropriate force vector terms. Because no Z equations are stored in the global stiffness matrix, the stiffness matrix does not have to be modified.

$$[T^e] = \begin{bmatrix} t^e & & & & \\ & \bullet & & & \\ & & \bullet & & \\ & & & \bullet & \\ & & & & t^e \end{bmatrix}$$

Transformation of the element from local to global coordinates.

Transformation of each node in the element to the skewed coordinates.

$$[T_s] = \begin{bmatrix} t^T_{first} & & & \\ & \bullet & & \\ & & t^T_i & \\ & & & \bullet \\ & & & & t^T_{last} \end{bmatrix}$$

$$[T_{es}] = [T_s][T^e]$$

Combine the two transformations into one matrix.

Transform the element from local to skewed global.

$$[K^{global}_{skewed}] = [T_{es}][K_{local}][T_{es}]^T$$

Figure 3-9.   Skewed Transformation at the Element Level

Encode all Single and Multi-point Constraints
for Inclusion at the Element Assembly Level

It was pointed out in a previous section that the simple method for incorporating multi-point constraints destroyed the narrow bandwidth of the unmodified set of equations. For the mesh used to model the spreading rollers, this increase in bandwidth would increase memory requirements by a factor of eight. This would prevent the model from running on a PC in a reasonable amount of time.

A technique was found to incorporate the multi-point constraints into the system of equations by removing degrees of freedom instead of adding extra degrees of freedom. In addition, the single point constraints can be treated as a simple form of the multi-point constraint and can be incorporated into the system of equations in exactly the same way. When this technique is combined with a judicious node numbering scheme, the theoretical minimum memory requirement is approached.

A general multi-point constraint relationship between two points is given in equation (3.18). It requires that two of the degrees of freedom of the system lie on a straight line. The constraints needed to model the spreading rollers are simpler than that shown in equation (3.18). For modeling these rollers, only a simple offset between the degrees of freedom is required. This is shown in equation (3.19) and (3.20).

$$C_i X_i + C_j X_j = D_{ij} \qquad\qquad (3.18)$$

$$X_j - X_i = D_{ij} \qquad\qquad (3.19)$$

$$X_j = X_i + D_{ij} \qquad\qquad (3.20)$$

For a single point constraint, the degree of freedom X_i is the zero degree of freedom, the fixed coordinate system. In that sense, the single point constraint is a simple form of the multi-point constraint. Figure 3-10 illustrates one procedure for incorporating the multi-point constraint given in equation (3.19).

The steps illustrated in Figure 3-10 are as follows:

(1) Transfer the coefficients of X_j to the coefficients of X_i by adding the values of column j to column i. This satisfies the portion of the constraint that says $X_j = X_i$.

(2) To maintain the symmetry of the system of equations, add the coefficients of row j to row i. This does not change the solution to the set of equations.

(3) Subtract the coefficients in column j multiplied by the offset D from the force vector.
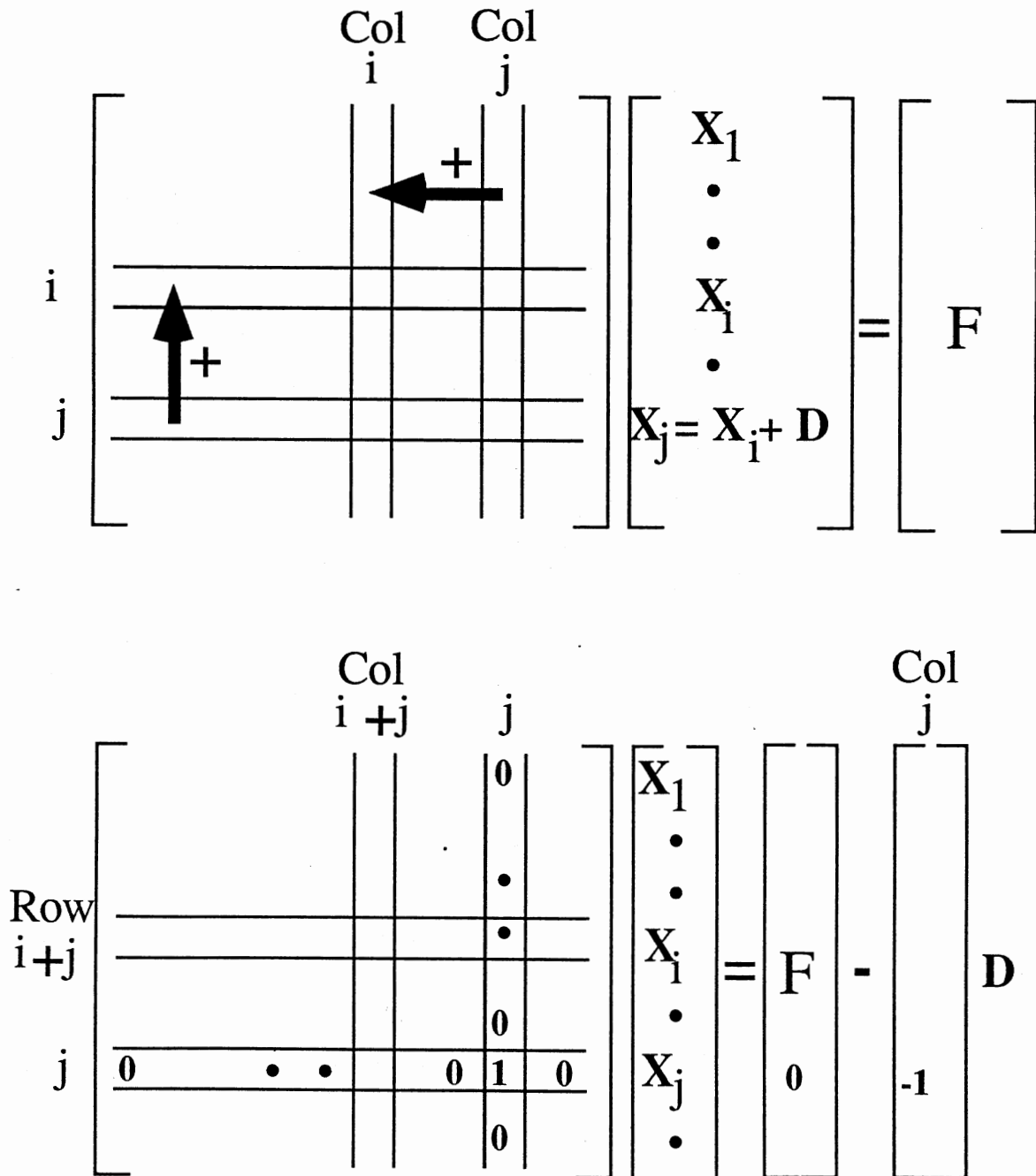
Figure 3-10. Procedure to Incorporate Multi-point Constraint

(4) At this point, degree of freedom j has been removed from the system of equations and its effect has been transferred to degree of freedom i and the force vector. Therefore, all coefficients of degree of freedom j must be removed from the set of equations. This can be done by setting all of them to zero. To prevent creation of a singular matrix, a 1 can be placed on the diagonal of degree of freedom j.

(5) To make this procedure apply to single point constraints, the value of D is placed in row j of the force vector. This will cause the system to calculate the value of D for degree of freedom j.

(6) If the constraint is a multi-point constraint, the value calculated for degree of freedom j is incorrect. After solving the equations, the value of degree of freedom j should calculated by inserting the value of degree of freedom i into the original constraint equation.

The procedure described above has the advantage of enforcing single and multi-point constraints without requiring additional equations or drastically increasing the system bandwidth. It has the disadvantage of leaving an equation in the system that has an incorrect but harmless value. Another possibly unavoidable disadvantage is that the equation bandwidth may be increased, but by a lesser amount than that of the simpler method. If a multi-point constraint relates two degrees of freedom separated by a distance greater than the original bandwidth, the system bandwidth must be

increased. In a general FEM program, this is unavoidable, and must be planned for. Most commercial FEM programs use a node numbering optimization scheme to minimize the system bandwidth.

With the mesh chosen for the roller models, judicious selection of a node numbering scheme combined with a modification of the procedure described above can prevent this problem from occurring. The modification of the constraint procedure is described first.

A close inspection of the procedure described above reveals the following:

(1) All of the stiffness coefficients associated with DOF j are transfered to DOF i by adding row and column j to row and column i, and to the force vector.

(2) The coefficients of row and column j are then discarded (set to zero).

(3) Equation j is modified to give a harmless but possibly incorrect answer for DOF j.

(4) The correct answer for DOF j must be calculated from the constraint equation.

Items (1) and (2) above suggest the following modifications to the constraint algorithm:

(1) Before building any of the element matrices, assemble a Lock vector that describes the DOF's that are to be locked to other DOF's or fixed in the global coordinate system.

This vector has an entry for each degree of freedom in the system.

(2)   Also, assemble a vector of displacement offsets. This vector combined with the Lock vector contains all of the information required to specify both the single and multi-point constraints.

(3)   Use the Lock vector to determine the system bandwidth. If a DOF is locked to another DOF or fixed in space, do not reserve space in the global stiffness matrix for that DOF's equation.

(4)   When assembling each element, use the Lock vector to redirect the locked coefficients to the proper location. This is equivalent to adding rows and columns of coefficients in the previous method. Also, use the offset vector to distribute the coefficients into the force vector.

These modifications produce a stiffness matrix identical to the unmodified procedure with the exception that many of the unnecessary equations are never stored. A sample Lock and Offset vector is shown and described in Figure 3-11.

DOF	Lock Vector	Offset Vector	Constraint Equation
1	1	0	No Constraint
2	2	0	No Constraint
.	.	.	.
.	.	.	.
5	1	1.5	$X_5 = X_1 + 1.5$
6	2	3.5	$X_6 = X_2 + 3.5$
.	.	.	.
9	0	3.0	$X_9 = 3.0$
10	10	0	No Constraint

Figure 3-11.   Sample Lock and Offset Vectors and Their Constraints

Judicious Choice of a Node Numbering Scheme

Inclusion of constraint information at the element level can significantly reduce the memory requirements of a model, particularly when combined with an optimum node numbering scheme.   It will be shown in the next section that the nodes contacting the roller on both spreading devices are totally constrained.   Therefore, with proper node numbering, the coefficients of the nodes on the roller need never be stored.   Figures 3-12

through 3-15 show two possible node numbering schemes and their corresponding storage requirements.

The first is the simplest scheme in which nodes are numbered sequentially from the beginning of the entry span to the end of the exit span. Figure 3-13 shows that the bandwidth of the system of equations is relatively small when constraints are ignored. But, when the multi-point constraints are applied to the nodes on the roller the bandwidth increases dramatically. This is because the constraint equations cause the nodes at the end of the entry span to be directly related to the nodes at the beginning of the exit span.
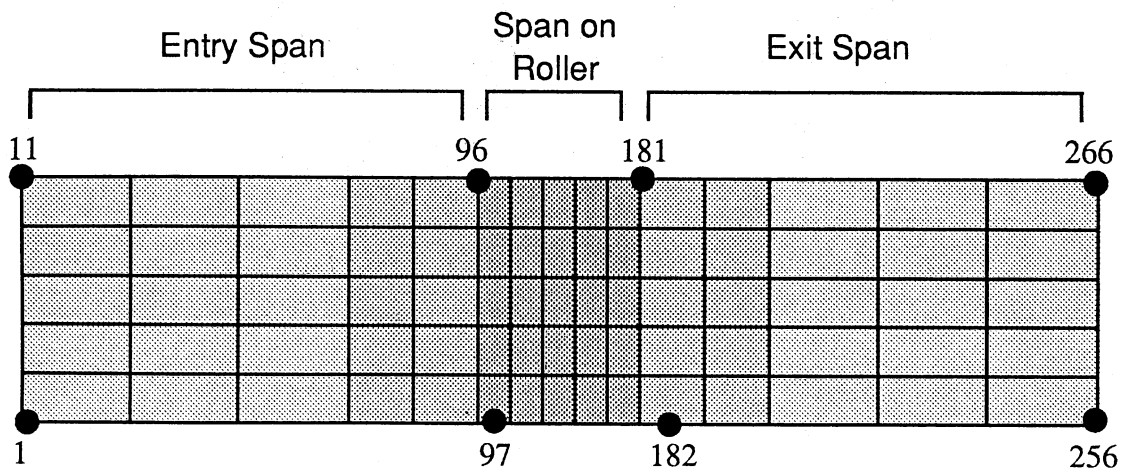
Figure 3-12. Sequential Node Numbering Scheme
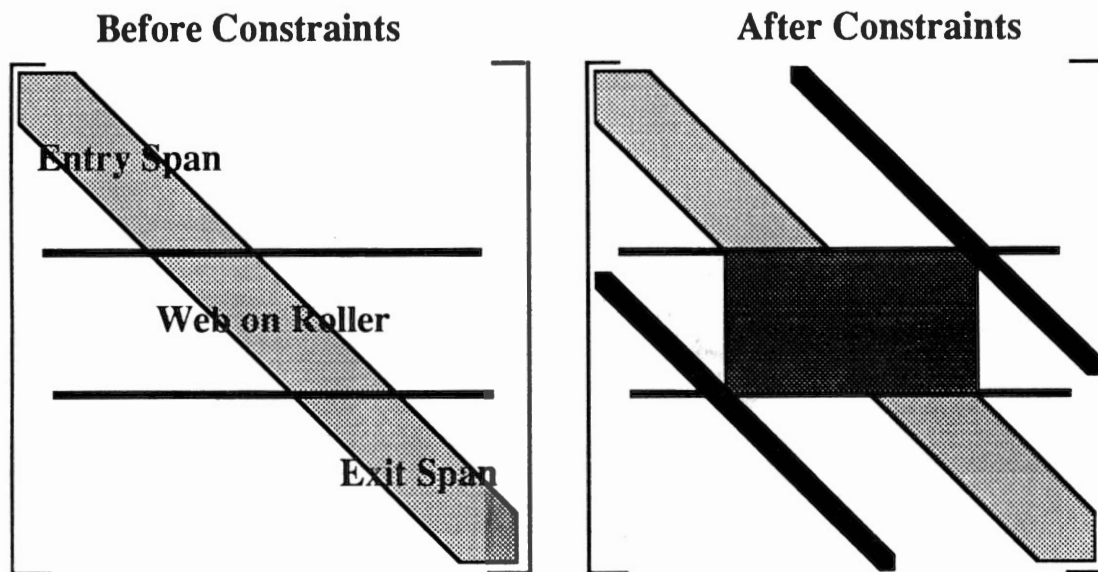
Figure 3-13. Sequential Numbering Bandwidth

The numbering scheme implemented in the spreading roller modeling program is shown in Figure 3-14. In this scheme, the entry span is numbered sequentially from 1 to 96. Then the exit span is numbered sequentially from 97 to 181. Finally the nodes on the roller are numbered from 182 to 266. When the elements are assembled without regard for constraints, a system of equations with a very large bandwidth results. This is shown in Figure 3-15. When the constraint equations for the nodes on the roller are applied, all of the coefficients for those nodes disappear. The resulting matrix has only the stiffness coefficients for the nodes on the entry and exit spans. And, because of the numbering scheme, the resulting bandwidth is very small.
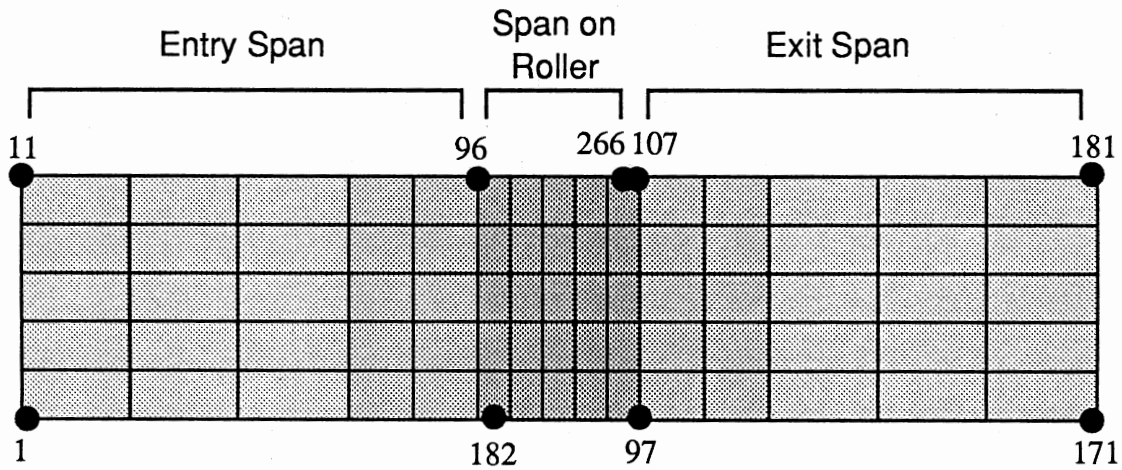
Figure 3-14. Non-Sequential Numbering Scheme
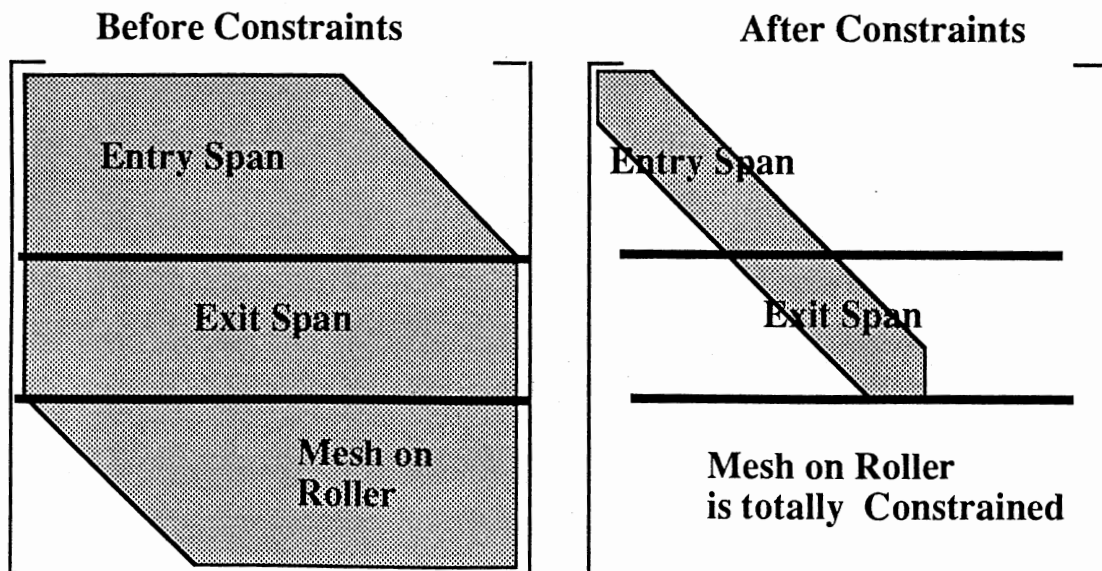
Figure 3-15. Non-Sequential Bandwidth

When the techniques described in the previous sections are combined with the non-sequential numbering scheme, a very compact set of equations is the result. Memory is allocated to store only the coefficients of nodes on the entry and exit spans. Because the nodal coordinates are skewed when the element matrix is built, only the 2-D coefficients are stored. Because the stiffness effects of the constrained degrees of freedom are distributed at element assembly time, the coefficients of the nodes on the roller are never stored.

This economy in memory requirements provides two major benefits. Because memory requirements are relatively small, the entire stiffness matrix can be stored in high speed memory. Virtual memory techniques which cause a tremendous slow down in program execution speed are not required. In addition, the reduced size of the system of equations allows those equations to be solved in single precision with very good accuracy. It is the combination of both of these factors that makes it feasible to run the spreading roller analysis code on PC class machines.

CHAPTER IV

SPREADING ROLLER MODELS

Introduction

The techniques described in the previous chapter were used in developing finite element models of the concave roller and the curved axis roller. As indicated, the Finite Element method requires a complete description of the geometric and elastic properties of the system being modeled, and the boundary conditions to be applied. In addition, modeling of the spreading rollers requires an iterative search to enforce the condition of normal entry to the roller. Each of these features of the spreading roller model is described in this chapter for both the concave roller and the curved axis roller.

Spreading Roller Model Surface Geometry

The total surface geometry model of the spreading rollers requires the following information:

(1)   The nominal dimensions of all the parts of the model. This includes the length and width of the web, the shape and orientation of the roller, and the angle of wrap between the web and the roller.

(2)   The unstrained coordinates of the discretized shape. These are the locations of the nodes used to define the elements.

(3)   The directions of a coordinate system normal to the nominal deformed surface at each node location.

(4)   The known nodal deformations described in the node normal coordinate system. This includes all deformations normal to the surface, as well as any known deformations in the plane of the web surface.

This geometry information is calculated independently for the three major sections of the roller models: the entry span, the web contacting the roller, and the exit span. The following sections describe this geometry for both the concave roller and the curved axis roller.

The Concave Roller Geometry

Figure 4-1 is a schematic showing the nominal geometry of a web over a concave roller. The dimensions indicated in the figure are the basis for calculating the nodal locations, directions, and deformations required by the concave roller model. Figure 4-2 shows that the geometry of the concave roller system has an axis of symmetry parallel to the direction of motion of the web (the machine direction). The roller model takes advantage of this symmetry by storing information for only one half of the total geometry. In addition, the figure indicates the directions of the global coordinate

system for the model. The origin of the coordinate system is located at the center of the roller.

In addition to the machine direction line of symmetry, the concave roller system has a line of symmetry in the cross machine direction. It is located on the roller at one half of the indicated wrap angle. Although this is a geometric line of symmetry, the boundary conditions to be described later are not symmetric about this line. For this reason, this symmetry is not used in the model.
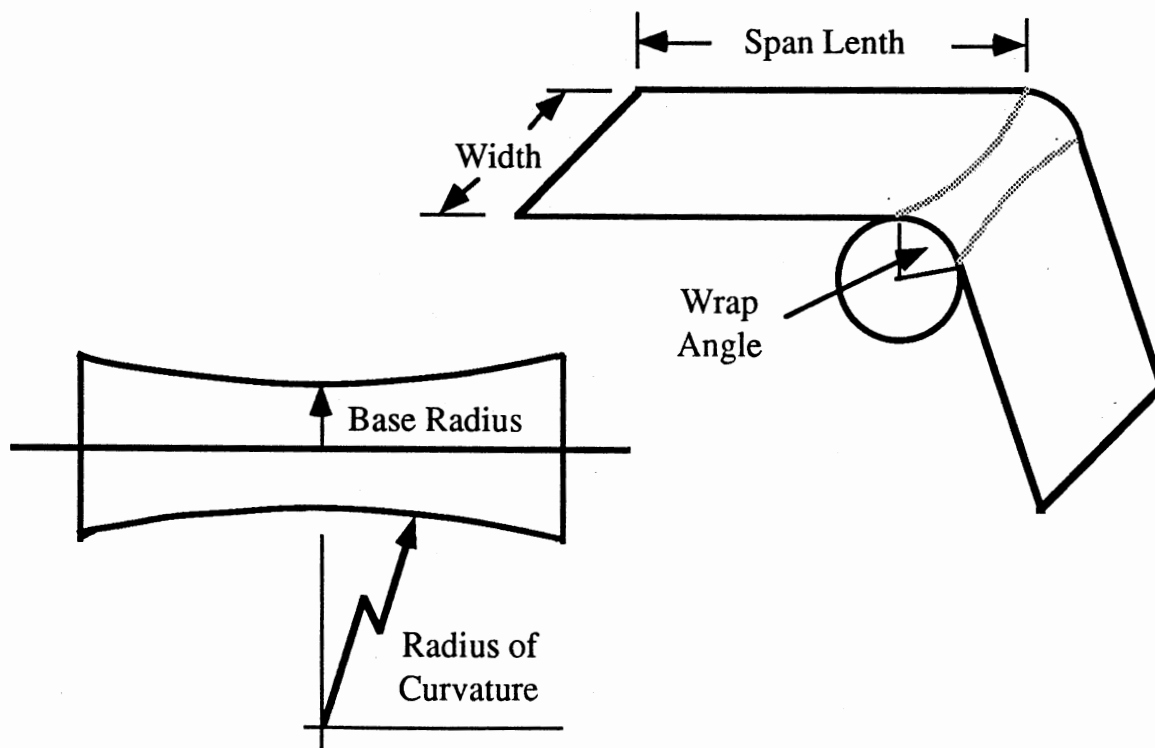
Figure 4-1.   Concave Roller Nominal Dimensions
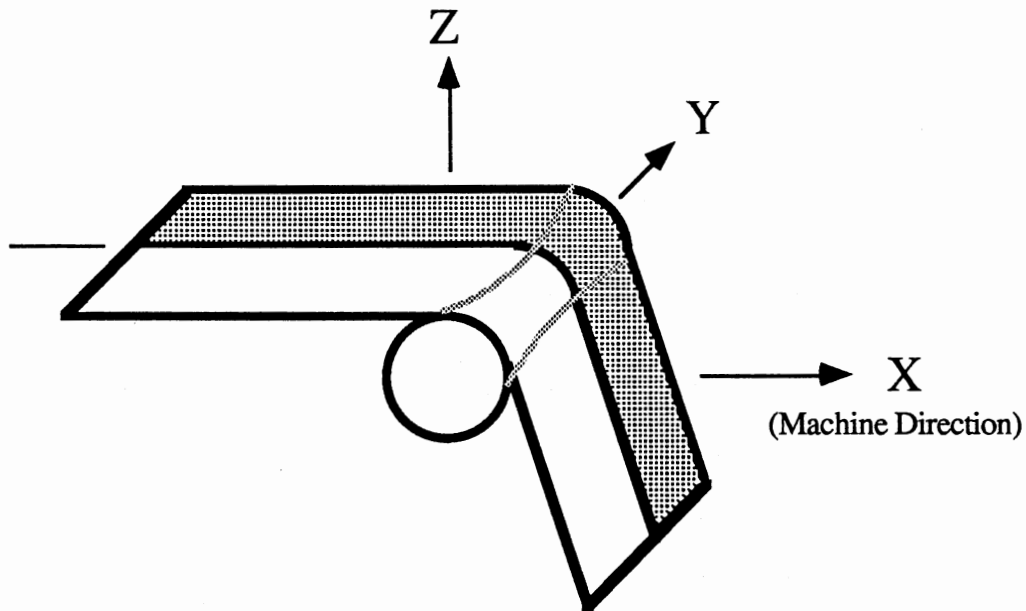
Figure 4-2.   Line of Symmetry for the Concave Roller

Because the roller geometry is not a simple cylinder, the web material cannot conform itself to the surface of the roller without being strained.   In order to properly calculate the strains and stresses imposed on the web when conforming to the roller shape, the web FEM mesh is first assembled as if it were wrapped around a cylindrical roller.   This roller has a diameter equal to the average diameter of the concave roller.   This is shown in figure 4-3.
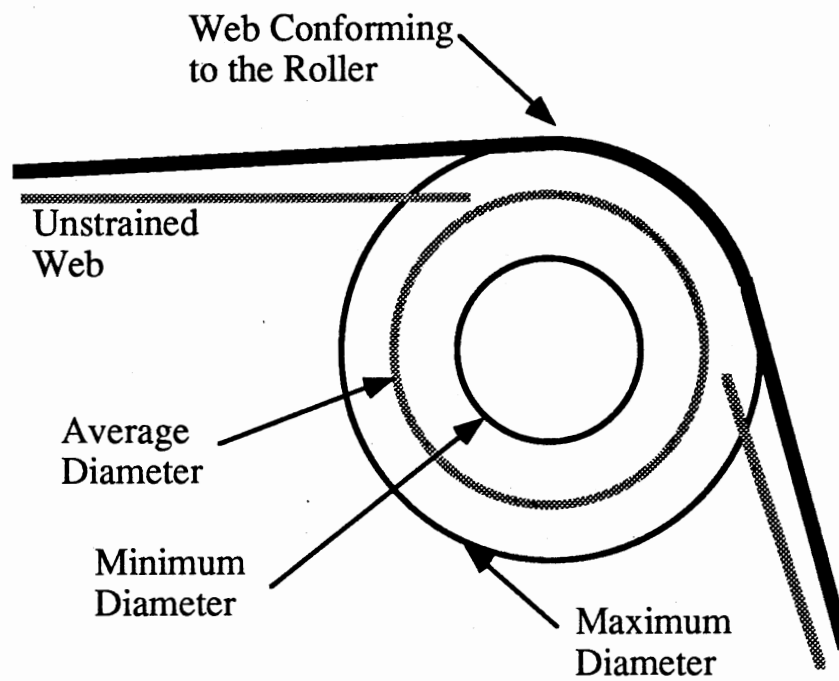
Figure 4-3. Web Deformed from Average Roller Diameter

From this unstrained position, the web is then deformed to conform to the roller as shown in the figure. Because the diameter of the roller varies in the cross machine direction, the magnitude of the deformation also varies. The figure shows the deformation at the outer edge of the web. For the simple geometry of the concave roller, all of the deformation required to conform the web to the roller are in the direction normal to the surface of the roller. This is modeled in the program as the local Z coordinate. Because all of the Z coordinate deformations are known in advance, those degrees of

freedom are not stored explicitly in the FEM stiffness. Instead, the effect of those deformations is assembled into the system force vector as described in Chapter III.

For each node location in the model, the directions of a coordinate system normal to the surface must be calculated. For the concave roller, these directions can be calculated as the concatenation of two simple rotations. The first is a rotation about the global X axis to align the coordinate system with the curvature of the roller at a point on top of the roller. The second is a rotation of this new coordinate system about the global Y axis to align the system with the wrap angle at the node location. These rotations are shown in figures 4-4 and 4-5.
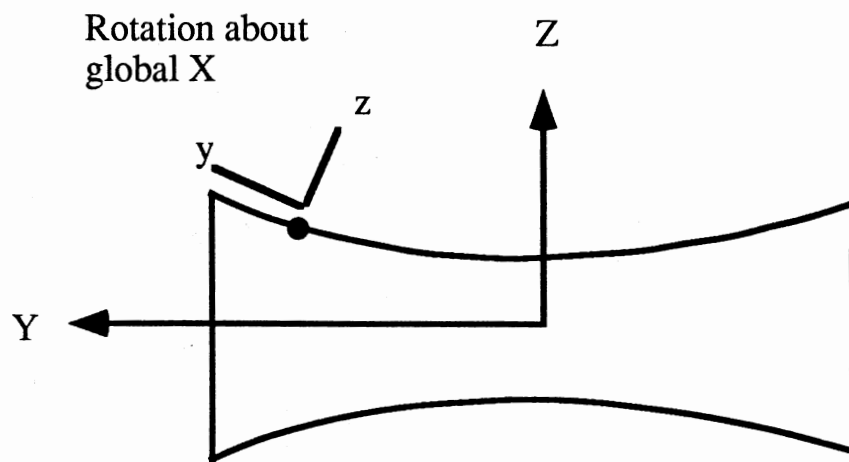
Figure 4-4.   First Rotation About the Global X Axis
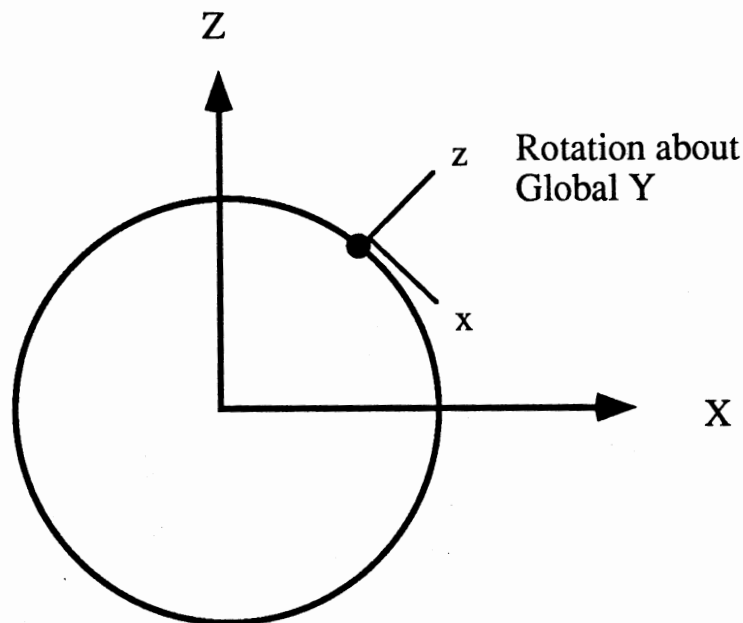
Figure 4-5.   Second Rotation About the Global Y Axis

The Curved Axis Roller Geometry

Figure 4-6 is a sketch showing the significant dimensions of the curved axis roller system. The dimensions are similar to those of the concave roller. An additional dimension is needed because the curved axis roller is not symmetric about its own rotational axis. Because of this, an angle indicating the orientation of the bow plane must be specified. The curved axis roller system also has a line of symmetry parallel to the machine direction located at the midspan of the web as shown in figure 4-7. This symmetry is also used by the program to reduce memory needs.
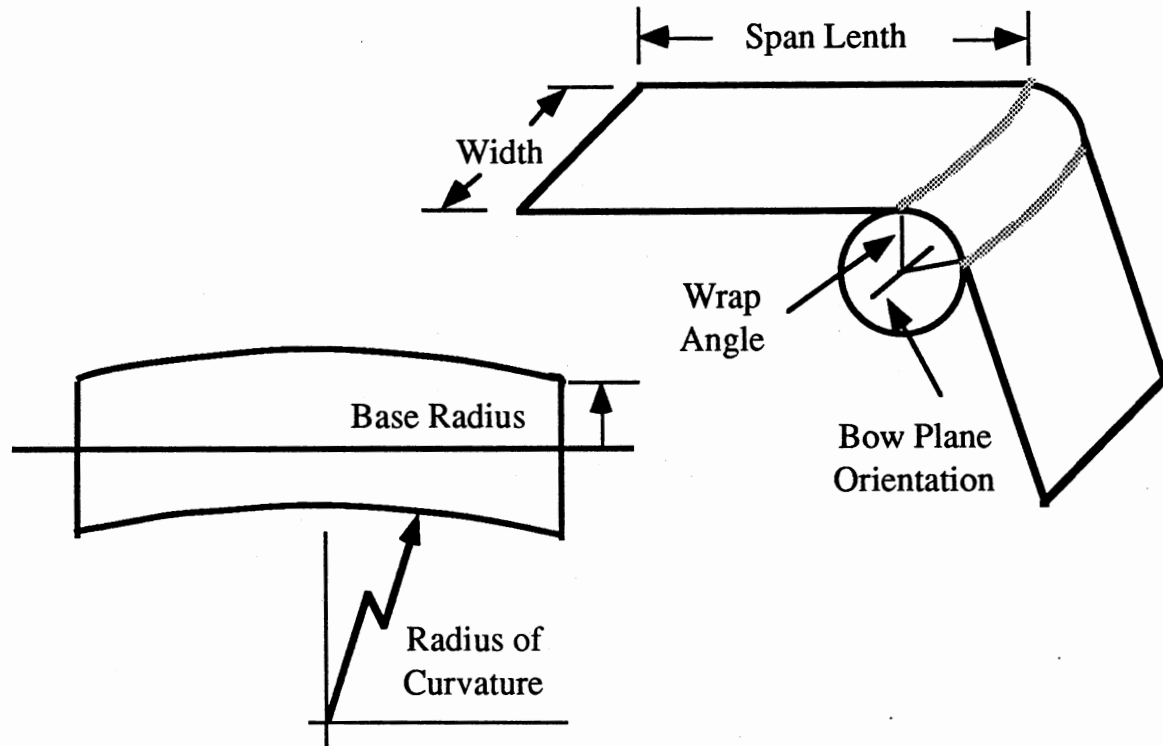
Figure 4-6.   Curved Axis Roller Dimensions
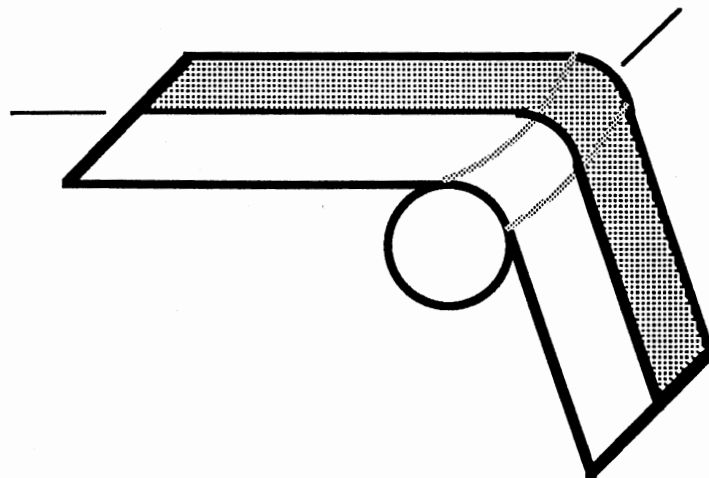
Figure 4-7.   Curved Axis Roller Model Symmetry

The curved axis roller also has a shape that cannot be matched by a web in an unstrained condition. As in the concave roller, the unstrained FEM mesh must be assembled using an average cylindrical roller. In the case of the curved axis roller, the roller diameter is constant, but the location of the center of the roller varies across the width of the web. Therefore, the unstrained model is assembled around a roller having the same diameter as the curved axis roller, and located at the average position of the curved axis roller. This is shown in figure 4-8.

Figure 4-8 shows that a point on the unstrained web is displaced in both the machine direction, and the direction normal to the surface. For the portions of the web actually in contact with the roller, the eventual boundary conditions will include known displacements for all degrees of freedom in both the machine direction and the normal direction. For those nodes not in contact with the roller, only the displacements normal to the surface are known in advance. In both cases, the geometry of figure 4-8 is used to calculate the normal direction displacements.

As in the concave roller model, a local coordinate system for each node in the model must be found. Again the coordinate system is aligned so that the local Z direction is normal to the surface of the web. This is again represented by the concatenation of two simple rotations. The first is a rotation about the global Z direction to align the coordinates with the roller bow. The second is a rotation of this new coordinate system about the roller's axis of rotations to align it with the roller wrap angle at that point. These rotations are shown in figures 4-9 and 4-10.

Web Conforming at the
Ends of the Roller

Ends of the
Roller

Unstrained Web

Center of the
Roller

Average Roller
Position
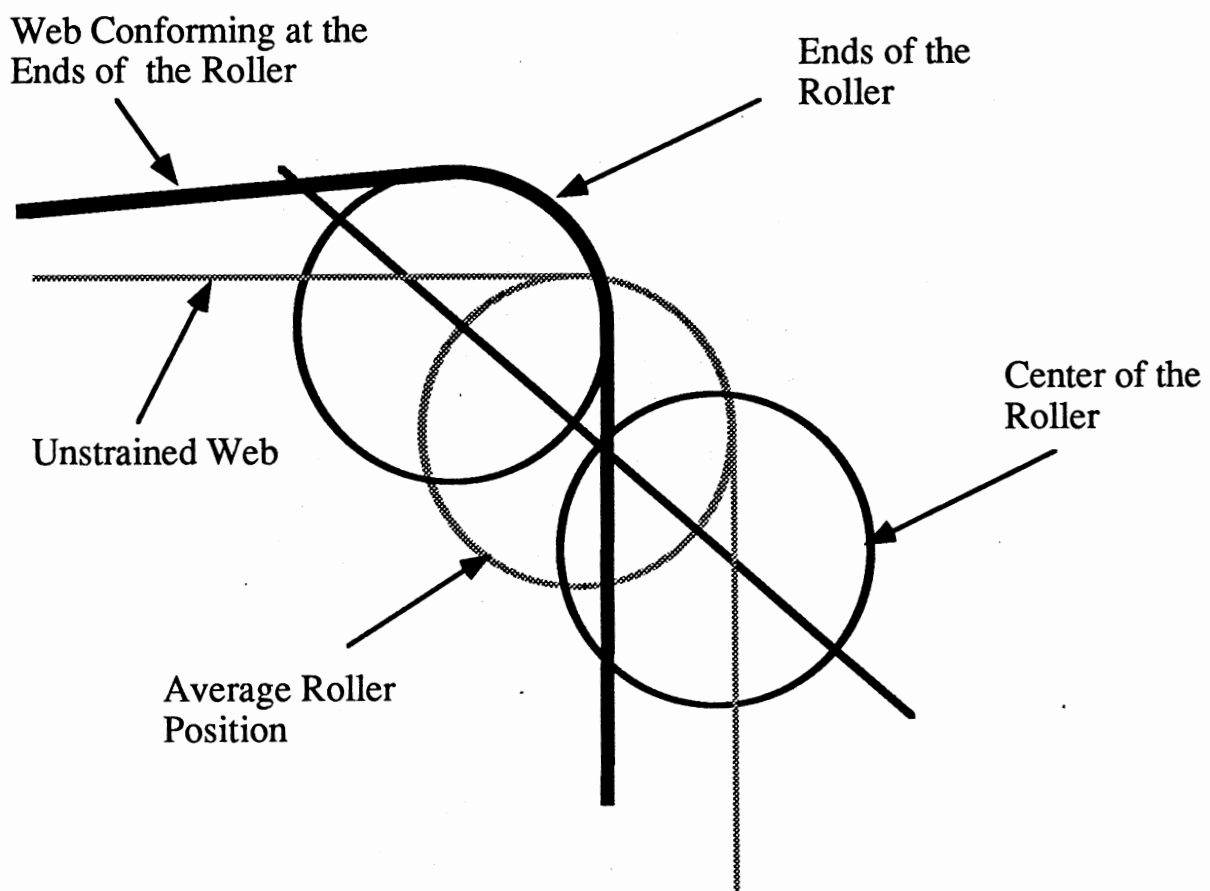
Figure 4-8.   Web Deformed from Average Roller Position
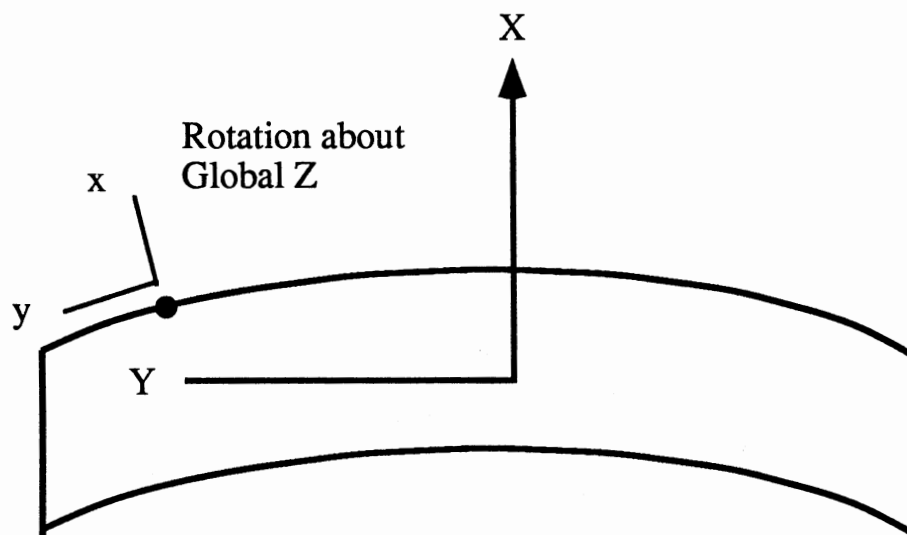
Figure 4-9. First Rotation About the Global Z Axis
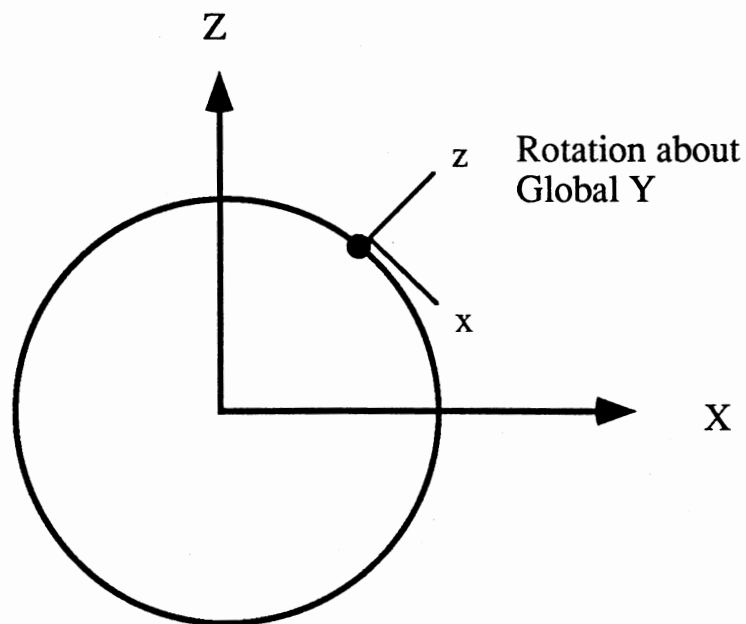
Figure 4-10. Second Rotation About the Global Y Axis

The Boundary Conditions for the Models

The most critical factor in correctly predicting deformations and stresses in the spreading rollers is the application of the proper boundary conditions. The boundary conditions used in the models are:

(1) Zero Y-direction (cross machine direction) displacements at all nodes on the centerline of the web. Because of the axis of symmetry in both of the rollers at the centerline of the web, only one half of the web is modeled. The web centerline is therefore one of the boundaries of the remaining portion of the web that is modeled.

(2) Fixed X-direction (machine direction) displacements at the beginning of the entry span and the end of the exit span. These displacements are calculated from the simple 1-D tension model using the dimensions of the web and the line tension.

(3) Fixed X-direction displacements at all nodes in contact with the roller. The first row on nodes on the roller is the zero displacement reference point for displacements due to line tension. In both the concave and the curved axis roller models, additional X-directions displacements are added to the displacements due to line tension.

(4) Multi-point constraints in the Y-direction for all nodes in contact with the roller.

Constraint sets (1) and (2) are identical in both of the spreading roller models. The constraints in (3) and (4) are different for each of the models. These constraints arise from three physical properties of the web / roller system.

First, the state of strain in the free span immediately upstream from the roller contact point is identical to the state of strain on the roller immediately after the contact point. The second is: given sufficient friction, the web material will remain in contact with the surface of the roller. This is the No Slip boundary condition. Finally, given sufficient friction, the web material will be oriented normal to the roller at the initial point of contact with the roller. This is the Normal Entry boundary condition. Each of these will be described for both types of rollers.

Concave Roller Model Boundary Conditions

The governing effect in the behavior of the concave roller is the velocity of points on the surface of the roller in contact with the web. The velocity magnitude varies across the width of the roller. The velocity direction is uniform and is aligned parallel to the machine direction. This is caused by a uniform roller angular velocity combined with a non-uniform roller diameter and is shown in figure 4-11.
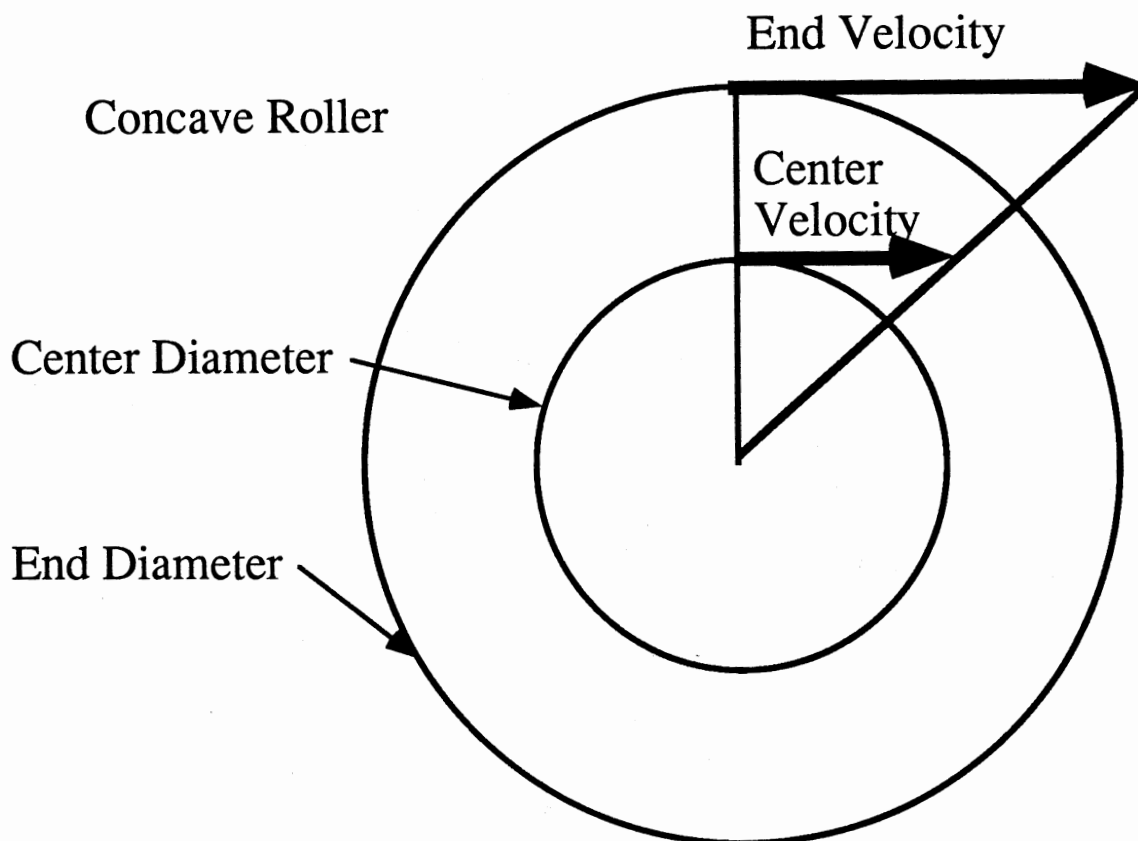
Figure 4-11. Velocity Variation on the Concave Roller

Because the roller velocity at the edge of the web if faster than the velocity at the center, the concave roller tries to shear the material at the edge of the web ahead of the material at the center. This is a local effect which causes a higher machine direction stress at the edge of the web that at the centerline of the web immediately before the web contacts the roller. These shearing displacements are shown in figure 4-12.
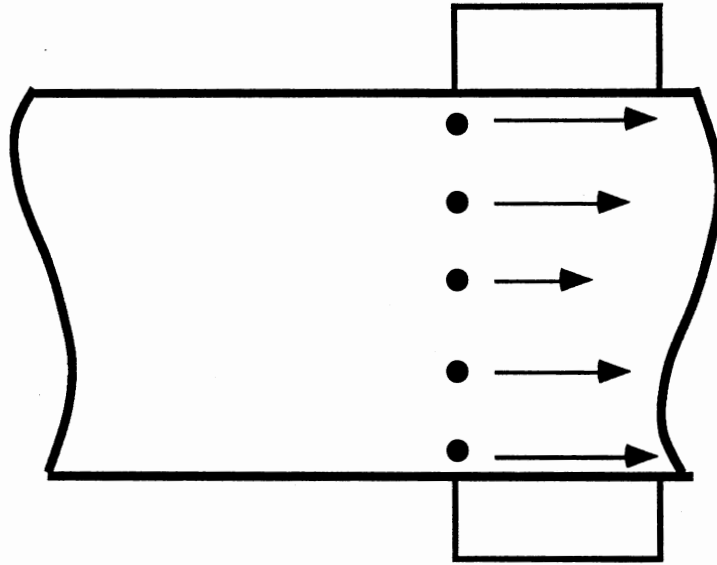
Figure 4-12. Machine Direction Shearing of the Web

These shearing displacements are calculated from a simple FEM model of the entry span using the following procedure.

(1) The strain profile of the material on the web due to the roller diameter profile is calculated. This is a differential strain profile. The strain at the location on the roller which has the same diameter as the average roller diameter is defined to be zero. '

(2) Using this differential strain profile and a simple 1-D tension model, the differential force at each node required to maintain this strain profile is calculated.

(3) A 2-D FEM model of the entry span is assembled.

(4) The nodes at the beginning of the entry span are frozen to zero machine direction displacements.

(5) The differential force profile is applied to the other end of the entry span.

(6) This FEM analysis yields a set of differential displacements. These displacements are the shearing displacements that are applied as boundary conditions to the full model of the roller.

Each of the nodes on the roller are first given a machine direction displacement compatible with the nominal line tension. These displacements do not vary across the width of the roller, but do vary in the machine direction. Then the appropriate differential displacement is added to the displacement of each node on the roller. These displacements do not vary in the machine direction, but do vary across the width of the roller. The total machine direction displacement for each node on the roller is the sum of these two displacements.

There is another effect which induces a machine direction strain profile on the nodes of the roller. For constant mass flow in the machine direction, the material in contact with the roller at the edge of the web must have a higher MD strain than the material at the center of the roller. This compensates for the higher velocity at the edge of the web. Because of the way the unstrained web is assembled, this effect is induced without additional machine direction displacements. This is illustrated in figure 4-13.

Nodes Displaced
in the Outward Normal Direction
to Conform to the Roller

Elements Receive
Additional MD
Strains

Unstrained
Elements

Average Roller
Diameter
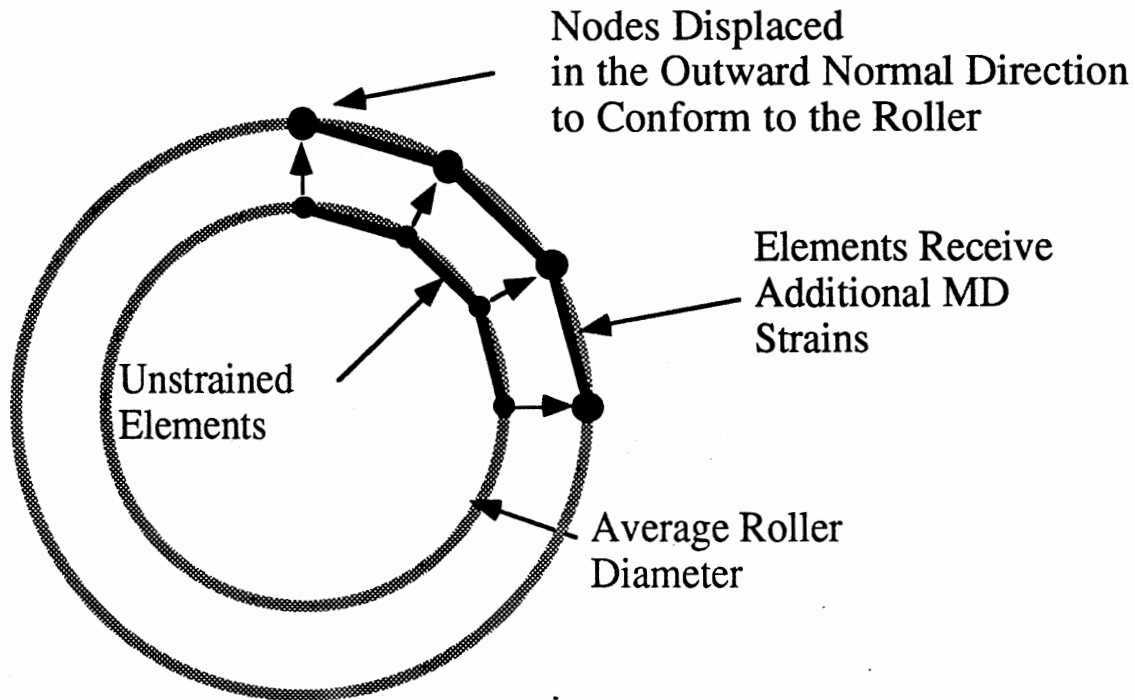
Figure 4-13. Machine Direction Strains Induced by Local Z-direction Displacements

The final boundary conditions required for the concave roller enforce the no slip condition over the roller. Given sufficient friction, a point on the web should travel at precisely the same velocity (magnitude and direction) as the point it is contacting on the roller. The previous boundary conditions assured that the velocity magnitude is matched. Additional constraints are required to match the velocity direction. Because the concave roller is axisymmetric about a line through its center of rotation, all points on the surface of

the roller move in a circle. These circles are all in planes that are perpendicular to the axis of rotation. This means that the Y location of any point on the roller remains constant. If the point on the web contacts the roller without slipping, then that point should also remain in a plane having a constant Y location. This can be formulated as a multi-point constraint. It is required that all nodes on the roller have the same Y-displacement as the node having the same nominal Y coordinate that first contacts the roller. This is illustrated in figure 4-14.

When all of the constraints are combined, all of the degrees of freedom of the nodes on the roller are either fixed or are related to another node by a multi-point constraint. This fact combined with the techniques of Chapter III allows the model to be stored in a relatively small amount of computer memory and to execute with relatively high speed.

Curved Axis Roller Model Boundary Conditions

The governing effect in the behavior of the curved axis roller is also the velocity of the points of the roller in contact with the web. As its name implies, the curved axis roller is a simple cylindrical roller whose axis of rotation is not a straight line, but an arc of a circle. Because all cross-sections of the roller have the same diameter, all points on the surface of the roller have the same velocity magnitude. It is the curvature of the roller axis that causes a variation in the direction of the velocity vector.
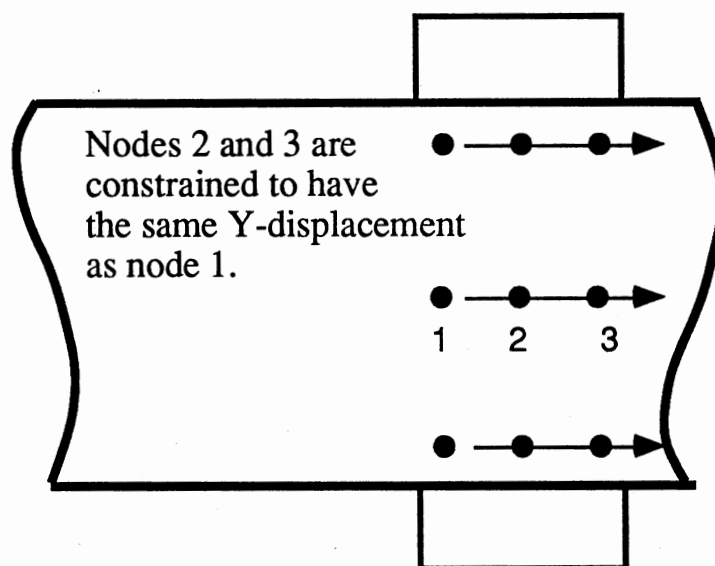
Figure 4-14. Y-lock Multi-point Constraints Over the Roller

Although the curved axis roller is more complicated mechanically than the concave roller, its governing boundary conditions are more simple. Because all velocity magnitudes on the roller are equal, there is no tendency for the roller to shear any strip of web ahead of any other strip. This means that the FEM calculations on the entry span that were required for the concave roller are not necessary for the curved axis roller. In addition to the boundary conditions shared with the concave roller, two other boundary conditions must be applied.

The process of making the unstrained web deform to the shape of the roller requires deformations both in the local Z direction and the local X direction. This is shown in figure 4-15.

The magnitude of the local X and Z displacements varies across the width of the roller. The figure shows that the nodes on the roller

remain the same distance apart both before and after the required displacements. This means that there are no induced machine direction strains on the roller as were found in the concave roller.

These displacements applied to the nodes on the roller (which are applied as boundary conditions to force the initially unstrained web to become strained and conform to the curved axis roller geometry) do cause one problem. The first row of nodes in contact with the roller are also the last row of nodes in the entry span. The applied boundary displacements cause this first row of nodes to receive a machine direction displacement profile relative to the entry span that would induce local machine direction strains in the entry span. This is shown in figure 4-16. Because there is no physical reason for these displacements to exist (no velocity magnitude differential across the roller to induce this displacement / strain profile), they should not be left in the model. To remove these extraneous displacements the following procedure is used:

(1) Start with the zero local displacements of the unstrained web.

(2) Apply the fixed displacements in the X and Z direction required to make the web conform to the roller.

(3) Subtract the local X displacement of the first node on the roller from that node and from all nodes that follow it on the roller.

(4) Add in the local machine direction displacements at each node on the roller to apply the nominal line tension at those nodes.
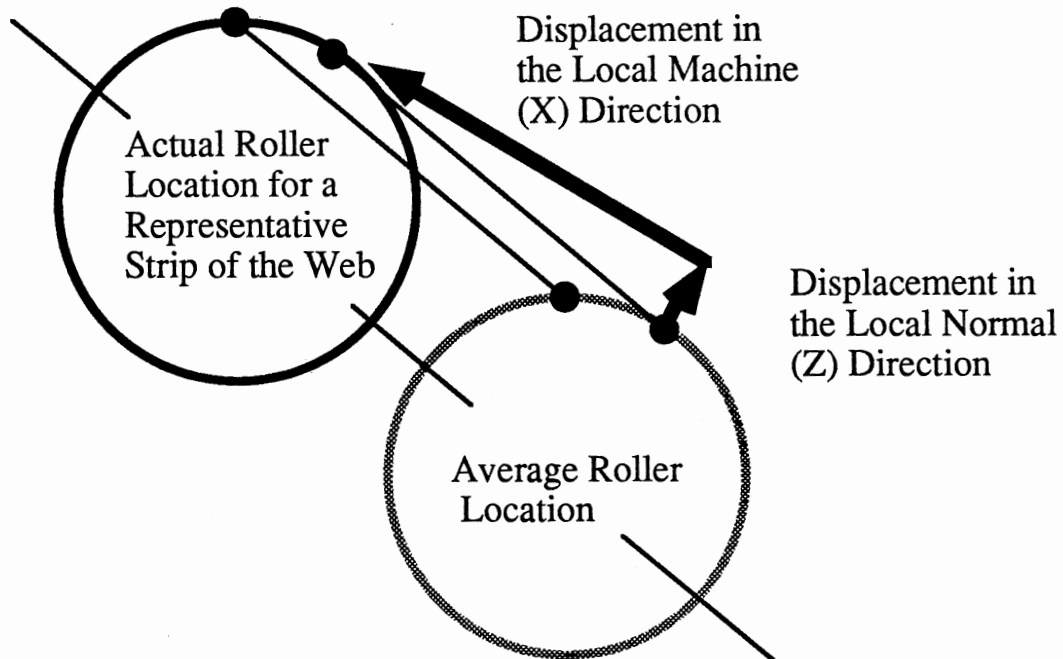
Figure 4-15. X and Z Displacements Required to Conform the Web to the Roller
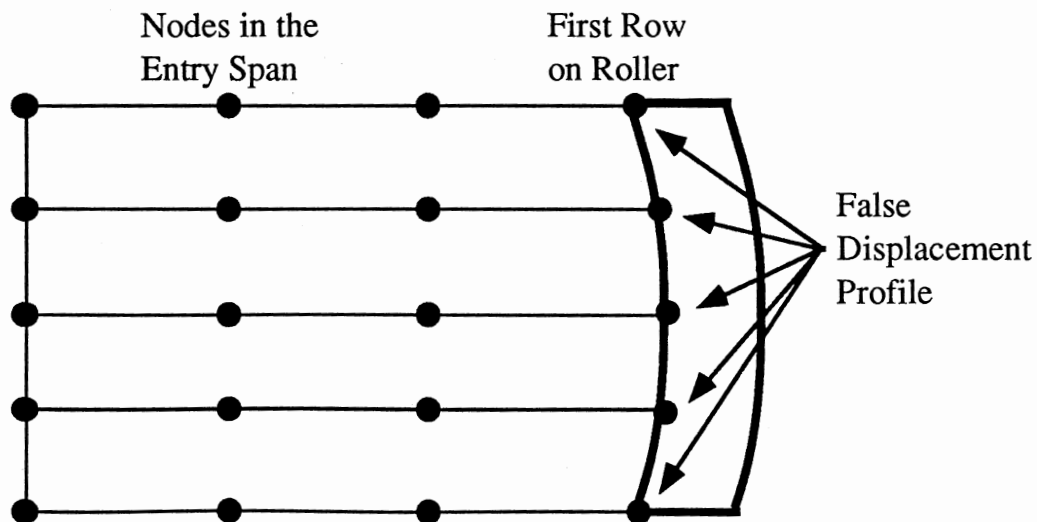
Figure 4-16. False MD Displacement Profile in the Entry Span Resulting from Applied Roller Displacements

As in the concave roller model, a final boundary condition is required to enforce the no slip condition. As before, all points on the roller move in a circle located in a plane perpendicular to the roller axis of rotation. Because the axis of rotation is not a straight line, these planes are not parallel. Instead, these planes extend radially from a line passing through the center of curvature of the axis. Because the planes are not parallel, the velocity vectors are not parallel. This is the principal reason for the spreading effect of the curved axis roller.

A multi-point constraint may still be used to relate all of the nodes on the roller to the initial point of contact. The constraint requires that all of the points on the roller having the same nominal Y location should continue to remain in a plane. They are forced to remain in the same plane as the velocity vectors. This plane is the local X-Z plane at each node on the roller. This type of constraint requires that a pair of nodes be separated by a constant offset in the local Y direction. This constraint is shown in figure 4-17. Node 2 is locked to node 1 with a constant offset. Node 3 is also locked to node 1 with a different constant offset. The offsets of the two constraints are selected so that nodes 1, 2, and 3 remain in the proper plane.
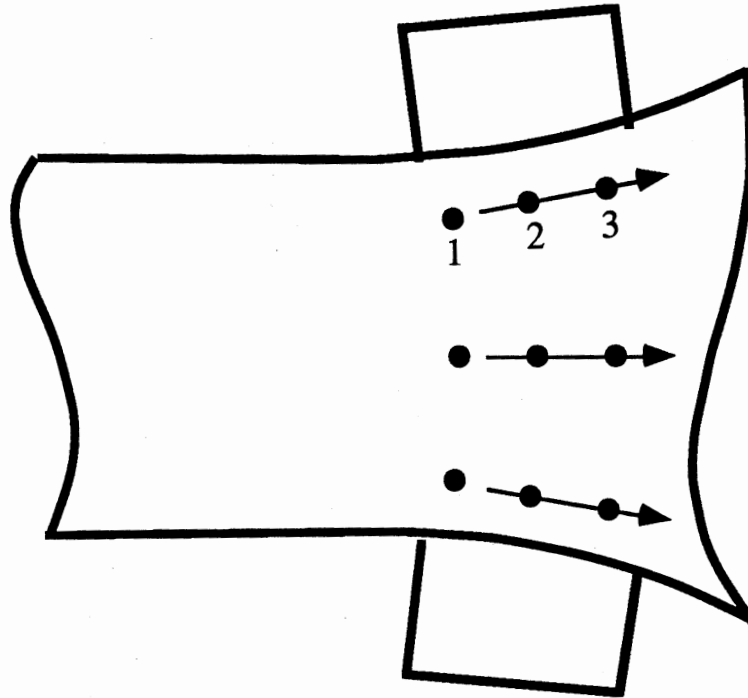
Figure 4-17. Multi-point Constraints for the Curved Axis Roller

The Spreading Process

The next stage in modeling the spreading rollers is the actual spreading process. This process requires an iterative search for a set of cross machine direction displacements that are compatible with the condition of normal entry to the roller. There are two reasonable approaches to finding the proper set of displacements. One approach is to apply known displacements to the nodes at the end of the entry span in a systematic way until the proper displacements are found.

The other approach is to apply forces to those same nodes in a systematic way until the proper displacements are found.

The first approach seems initially to be the most direct and efficient method. This is quickly shown not to be the case. Application of known displacements requires a modification of both the stiffness matrix and the force vector. This requires that the stiffness matrix be inverted at each new stage in the search, increasing the total computation time by a tremendous amount.

While the second approach seems less direct, it is actually much more efficient. Application of known forces requires modification of only the force vector. Because of this, the stiffness matrix only needs to be inverted one time. Each new stage in the search requires only a multiplication of the new force vector by the inverted stiffness matrix.

The search process can be posed as a nonlinear least squares curve fitting problem which in effect is a multidimensional nonlinear optimization problem. It can be stated as follows:

> Find the set of applied forces which minimize the sum of the squares of the deviations from normal entry to the roller. The minimum value of this sum in known in advance to be zero.

The set of applied forces can be selected in two ways. A force can be chosen independently for each node at the end of the entry span. This gives as many independent variables for the optimization

process as there are nodes across the width of the web. For the mesh chosen, this would give an eleven dimensional optimization problem.

A better approach is to use a function to define the force distribution across these nodes. The problem then becomes one for finding the proper values for the coefficients of this function to minimize the least square error. This can greatly reduce the order of the optimization problem. The simplest choice for the forcing functions are simple polynomials.

The lowest order polynomial is a simple constant but this does not allow any variation of force across the roller width. It seems unlikely that this would allow all of the nodes to approach normal entry to the roller.

The next order polynomial is a straight line. The line is defined by two coefficients, and does allow a force variation. If the linear force profile allows sufficient variation in force to approach zero error, then the problem is reduced from an eleven variable optimization problem to a two variable problem. This turns the problem from one that would probably never converge to a reasonable solution into one that should converge in a relatively short time.

The linear force function was implemented in the spreading roller analysis program. This simple function allows the search to converge in a matter of minutes to very acceptable accuracy. The Nelder-Mead Simplex method was used to perform the optimization process. The objective function for the search is given in equation (4.1).

$$\sum_{i=1}^{N_w} \left(\left(\text{Slope before roller} \right) - \left(\text{Slope after roller} \right) \right)^2 \qquad (4.1)$$

The spreading process for both the concave roller and the curved axis roller is illustrated in figures 4-18 and 4-19. In each case, the nodes on the roller have been locked together with the slope given by the multi-point constraint. For the concave roller the slope is zero, and for the curved axis roller, the slope is non-zero. For each device, before the proper spreading is achieved, the slopes immediately before the roller do not match the slopes on the roller. The value of the objective function is not zero. After the spreading analysis is complete, all of the slopes before the roller match the slopes on the roller within a small error tolerance. This causes the objective function to be very nearly zero. This geometric state satisfies the normal entry condition for the web and roller.
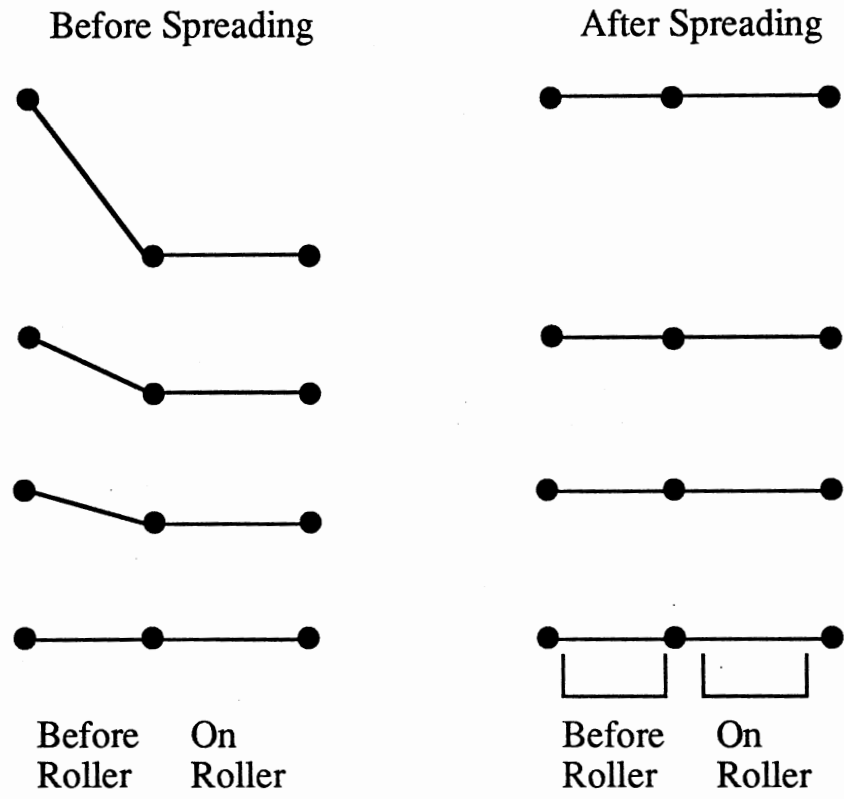
Figure 4-18. Illustration of Spreading the Concave Roller

Before Spreading   After Spreading

Before   On   Before   On
Roller   Roller   Roller   Roller
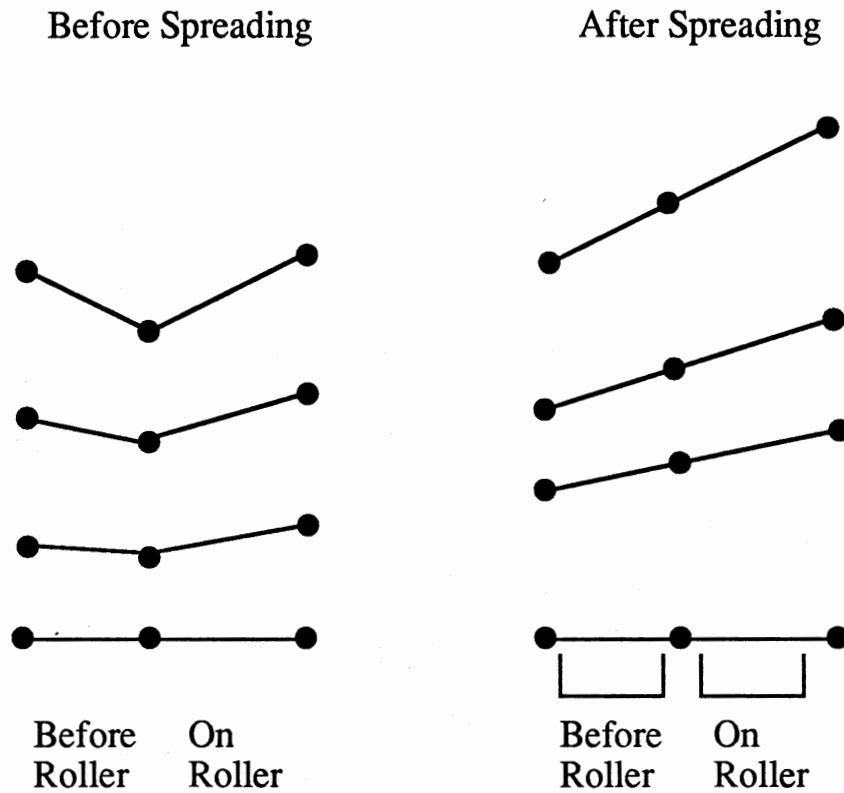
Figure 4-19. Illustration of Spreading the Curved Axis Roller

Calculation of Forces and Stresses

With all displacements now known, the spreading roller program is able to calculate element stresses and element forces. This is done in exactly the same way for both of the roller models.

Element Friction Calculation

The underlying principle of every stage of the modeling process has been that geometry drives the boundary conditions applied to the model. In describing each boundary condition, it was

stated that the force or deformation would occur, assuming that there is sufficient friction available. The results of the entire model assume that sufficient friction is available at each stage. Therefore, a necessary result from the model is the friction forces required to produce the displacements and stresses predicted by the program.

To calculate the coefficients of friction for the model, the magnitude of the forces at each node on the roller in all three local coordinate directions must be known. Because of the modifications made to the global stiffness matrix to incorporate the boundary conditions, the nodal forces cannot be calculated immediately. First, the portion of the stiffness matrix in contact with the roller must be reassembled in full 3-D. In this stiffness matrix, the boundary conditions have not been included. The known nodal displacements can be multiplied by this matrix to obtain the nodal forces for all three directions. The coefficient of friction at each node can be calculated by dividing the vector sum of the local X and Y forces by the magnitude of the local Z force. Each of these forces and the coefficient of friction is reported by the program.

Element Stress Calculations

With all displacements known for the model, equations (3.2) and (3.3) may be used to calculate the element stresses. Because each of the nodal displacements are given in a 3-D local coordinate system, they must be transformed into the average 2-D coordinate system of the planar element. This is done by reversing the process described in figure 3-9. The stresses in the average X-Y coordinate system are calculated for each node in the element and for the center

of the element. In addition, the principal stresses are calculated at those same locations.

Summary

The entire process for calculating deformations, forces, and stresses for webs on spreading rollers has been described in this chapter. The necessary geometry has been defined, as well as the values to be calculated from that geometry. The necessary boundary conditions have also been described. The process of solving for the correct geometric spreading to achieve normal entry has been posed as a multi-dimensional, nonlinear optimization problem with a minimum functional value of zero. From the spreading analysis, all deformations for each node in the model are determined. From these values, the element stresses and forces may be calculated.

CHAPTER V

MEASUREMENT OF WEB SPREADING

Introduction

In order to verify the accuracy of the Finite Element models, data from actual web systems had to be obtained for both the curved axis roller and the concave roller. Because the models predict both web stresses and displacements, either property could have been used for verification. The web edge displacements were chosen as the property to be measured for two reasons.

The first reason is that the Finite Element method models displacements more accurately than it models stresses. The 8-node isoparametric element allows quadratic variation of displacement over the element, while allowing only linear variation of stress and strain. Therefore, the displacements predicted by the model should be more accurate than the stresses.

The second reason is that it is easier to collect accurate displacement data at very precise locations along the edge of the web. The web bi-axial tension measuring device developed by Magill [14] measures the average web tension over a one inch circular region. This does not provide sufficient resolution for validating the model because the predicted stresses in the web near the roller vary significantly over a one inch region. Comparison of

85

measured and predicted edge displacements should provide the best data for judging the accuracy of the models.

Two different devices were tried in measuring the change in the edge displacement of the web as it approached the spreading rollers. The first was a laser based position sensor, and the second was an optical based device.

The Laser Position Detector

Figure 5-1 shows a schematic drawing of a laser based position detector. This is a commercially available device that can measure the location of the centroid of a laser beam to a rated accuracy of 0.0005 inches. Sensors are available to measure position in one direction only, or in two dimensions.

A laser beam can be spread into a line of light using a cylindrical glass rod as a lens. This is shown in figure 5-2. The centroid of the portion of the line falling on the detector can be determined by the detector. If the line crosses the entire active area of the detector, then the line centroid is located at the center of the detector. If the line falls on only a portion of the detector, then the centroid is shifted from the center. The location of the centroid gives an accurate indication of the length of the line. This could be used to advantage in measuring web edge displacements. By allowing the edge of the web to interrupt the beam of light, the change in position of the remaining portion of the beam hitting the detector gives the change in position of the edge of the web. A simple calibration method was devised to allow this setup to give the position of the

edge of the web directly. This calibration method is shown in figure 5-3.
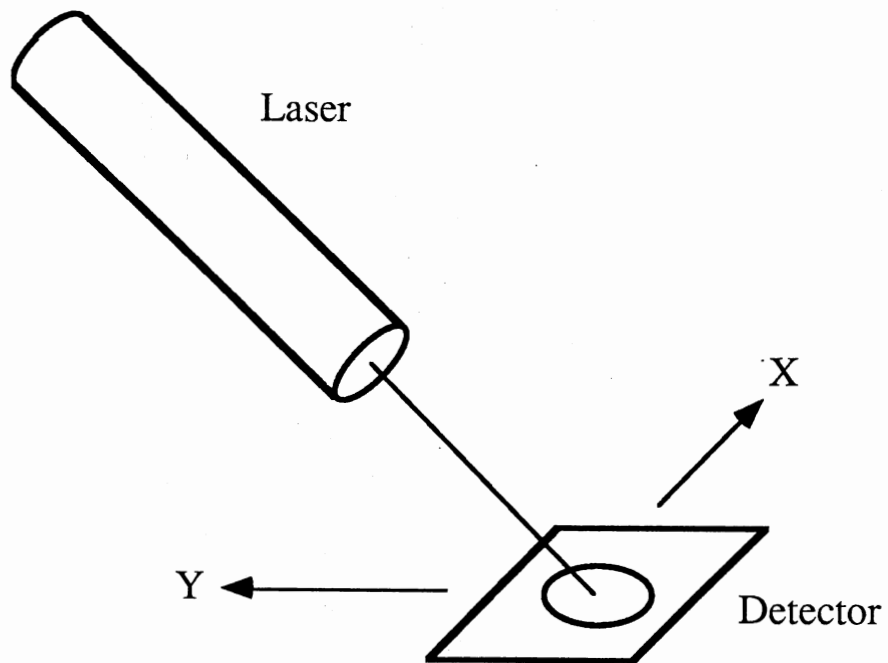
Figure 5-1. A Laser Position Detector
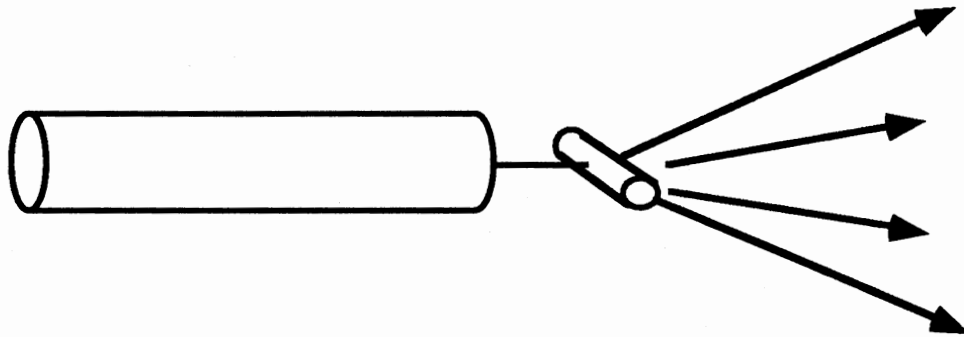
Figure 5-2. Spreading of a Laser Beam by a Glass Cylinder
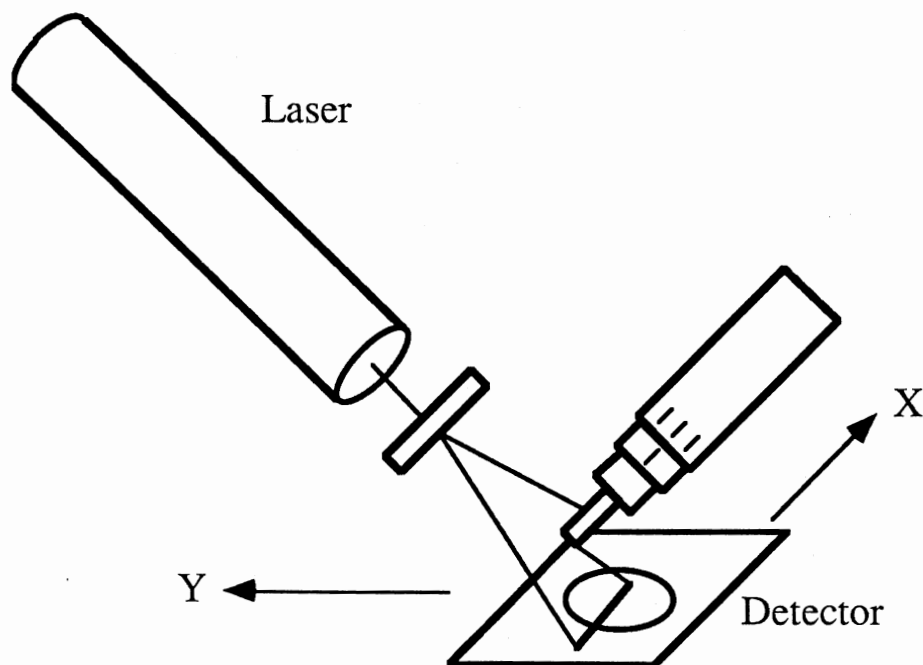
Figure 5-3. Calibration of the Position Detector

A set of four lasers and detectors were to be used to measure the position of the edge of the web at four locations. Two sets were to be used to determine the relative width of the web upstream from the spreading roller, and two were to be used at the position predicted to give the maximum web spreading. The change in the web width could be compared to the spread predicted by the Finite Element models. Figure 5-4 shows a side view of the fixture holding the lasers, detectors and the rollers.
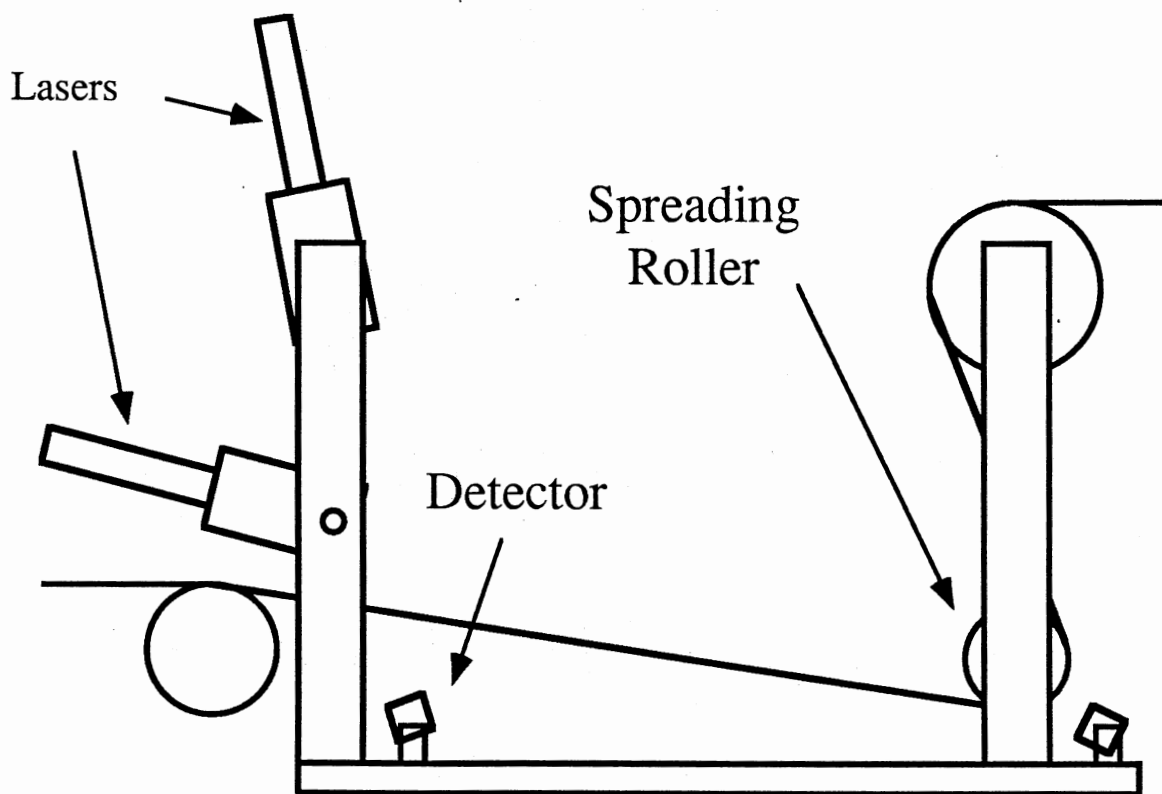
Figure 5-4. Fixture for Position Detectors, Lasers and Rollers

Results from the Laser Based Displacement
Measurements

Unfortunately, the laser based measurements did not have the accuracy expected, and both the roller model program and the actual devices yielded smaller displacements than anticipated.

The laser position detector was able to measure very small changes in displacement as long as the timespan between the two measurements was not more than a few seconds. Unfortunately the sensors tended to drift so that the absolute position of the beam on an individual sensor could not be determined closer than about 0.002 inches. With web spreads on the order of 0.004 to 0.008 inches being predicted, this was clearly unacceptable.

The results of this device are reported here to point out its potential value as a web spread measurement tool. It should be possible to develop a high speed online calibration device to work in conjunction with the laser position detector. A computer controlled micrometer head could be installed at each sensor location for online calibration in a fraction of a second. This is recommended as a future project.

Optical Edge Displacement Measurement

An optical device, Bausch and Lomb Super Gauge no. 38.21.32, with markings indicating 0.001 inch intervals was ultimately used to measure the web edge displacements. This device was used as a backup system in case of problems with the laser based system. Because of the calibration problems encountered with the laser

device, the optical system was the more accurate system. Since this device was intended as a backup system, the laser mounting apparatus was designed also to be used for measurements with the optical device. This setup is shown in figure 5-5.
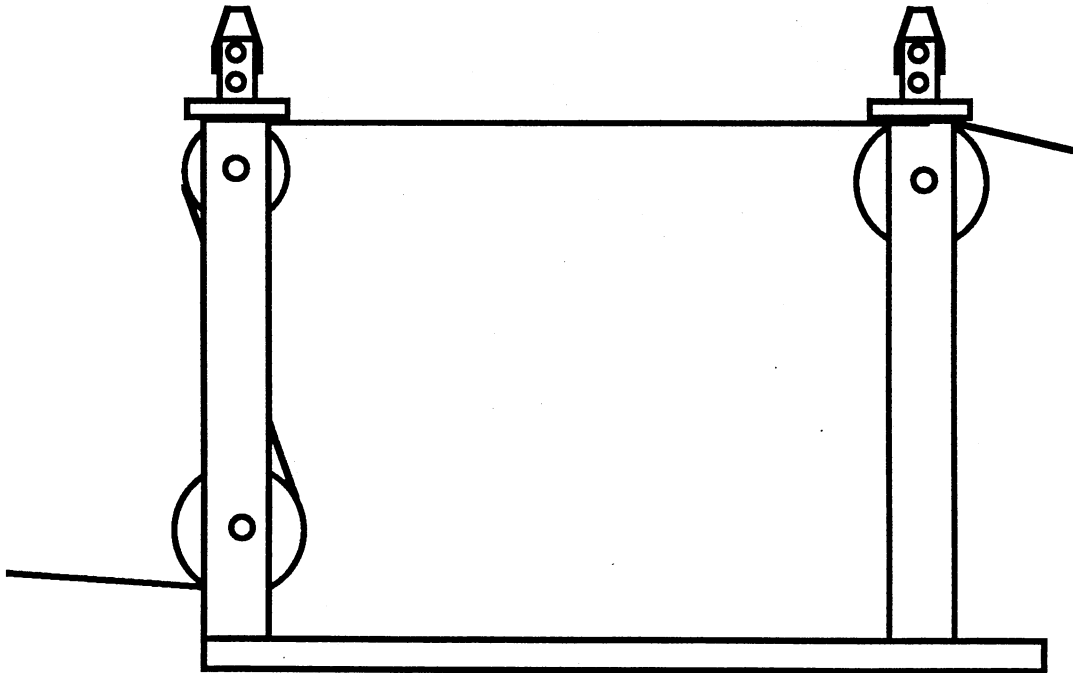
Figure 5-5. The Optical Web Spreading Measurement System

Although the device was marked to indicate 0.001 inches, with practice, it was possible to consistently estimate web edge locations to the nearest 0.00025 inches. Because of the extremely small spreads being measured, this estimation was crucial to obtaining useful results. In an attempt to compensate for the poor accuracy of

the device, five readings were taken for the web edge positions in each spread measurement. Any web width measurement that lay well outside the range of the other four measurements was discarded. The average of all remaining readings was used in calculating the web spread.

Spreading Measurements for the Concave Roller

Initial results using the optical device to measure the spreading produced by the concave roller were very discouraging. The measurements consistently showed a decrease (negative spread) in the web width downstream of the concave roller. Variations in the measurement technique gave no improvement. It was finally decided that the friction required to spread the web was larger than the amount supplied by the nominal line tension.

A large increase in the line tension was not feasible because of the relatively low yield strength of the material. To increase the available friction, a very light coating of 3-M aerosol glue was applied to the roller and allowed to dry. This glue gave the roller a slight tackiness. Although the coefficient of friction was not measured, a definite increase in the coefficient of friction was observed. Subsequent web measurements began to show positive spread values on the order of 1 to 2 thousandths of an inch.

Spreading Measurements for the Curved Axis Roller

The curved axis roller exhibited a positive web spreading on the first test. This was encouraging, and indicated that the curved axis roller is able to spread the web with lower friction forces than the concave roller.

CHAPTER VI

STUDY OF MODEL BEHAVIOR

Introduction

The models described in Chapters III and IV were implemented in a group of FORTRAN programs running on an IBM-PC/AT class computer. The source code listings and users manual for these programs are included in a separate document titled "Users Manual and Program Listing for SPREAD Version 1.1". The purpose of this chapter is to examine the deformations, forces, and stresses predicted by the roller models for a wide range of input parameter values.

For each roller model, a base set of input parameters was chosen. The deformation and stress distribution over the surface of the web are examined for these base parameter values. The parameters are then systematically varied about the base values. For each run of the program, only one parameter is changed from the base case. This study does not consider variations of combinations of parameter values because of the extreme computation time that would be required. The numerical values generated by these computer runs are given in Appendix A.

This study was done for three principal reasons:

(1) To give additional credibility to the computer models by illustrating that the models predict trends in the behavior of the system that agree with behavior expected from reasoning and prior experience.

(2) To identify other trends in the behavior of the system caused by variations in the input parameters.

(3) To generate analytical data for comparison to the measured spreading data for program verification.

Deformations and Stresses in the Base Parameter Runs

Explanation of the Plots

The distributions of deformations, stresses, and friction forces over the surface of the web are calculated by the spreading model programs. Because of the large amount of numerical data generated by the programs to describe these distributions, graphical post processors were written. The post processors use X-Y plots to display the spreading deformations, and 3-D contour lines to display the stress distributions. These plots condense the program output into a form that greatly enhances understanding of the models.

The plots generated by the post processors attempt to present the data in a form that conveys as much information as possible in

the limited space provided by a typical computer display. Because of this, an explanation of these plots is required.
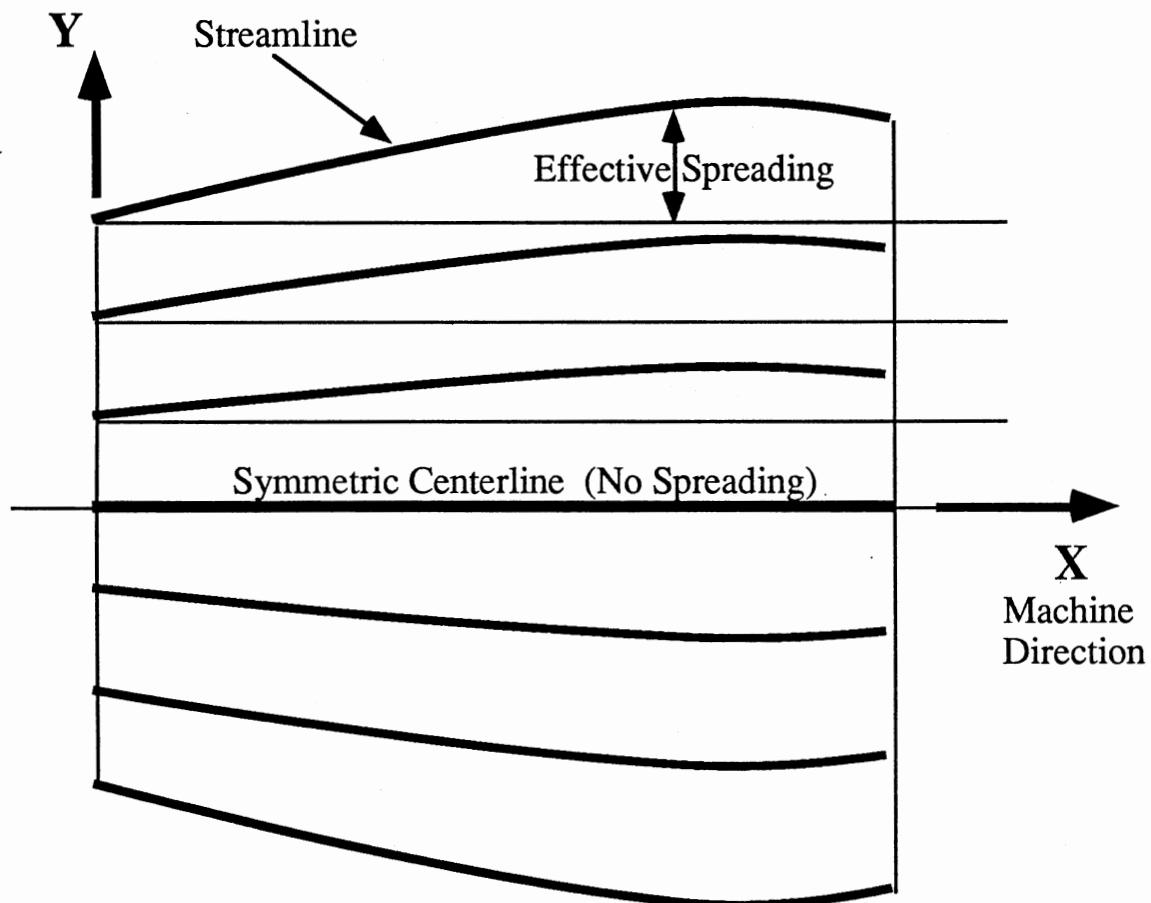
Figure 6-1. Effective Spreading of Web Streamlines

Figure 6-1 shows a segment of a web with exaggerated cross machine direction displacements indicated by the heavy lines. These lines represent the streamlines of points on the web sharing common undeformed cross machine direction (Y) locations. The lighter lines

represent the Y-location of the streamline at the beginning of the model. The deviation between the light and heavy lines represents the effective spreading of the material at that Y-location.

This effective spreading is plotted on an X-Y graph. The spreading is indicated on the Y-axis, and the machine direction location is indicated on the X-axis as shown in figure 6-3. For the values used as the base parameters in both the curved axis and concave runs, the span before the roller is 12 inches long and occupies the left side of the displacement plot from X=0 to X=12. The material on the roller begins at X=12 and continues for a distance equal to the length of web material in contact with the roller (defined by the roller diameter and the wrap angle). This location is not shown explicitly on the plot, but for both types of spreading rollers, it is indicated by a pronounced change to a negative slope in the spread data.

Figure 6-2 shows an example of one of the stress plots with additional markings added to assist in its interpretation. The entire web is shown in this figure. The symmetric centerline of the model and both the machine and cross-machine directions are shown. In this figure, the stress contour lines are drawn on only one half of the model. If the other half were to be drawn, the contour lines would be a mirror image of the lines that are shown. On the stress plots generated by the post processor, only this half of the model is shown to take maximum advantage of the display area. In addition, portions of the web far upstream and downstream from the roller have been omitted. It will be shown that there is little information of interest on these parts of the web.

Maximum Shear Stress
Concave Roller Base Run   .... th = 0.0012

STRESS LEVELS

Cross-Machine Direction

Max Stress =   933.08
Min Stress =   445.17

Symmetric Centerline

1		905.97 psi
2		851.76 psi
3		797.55 psi
4		743.34 psi
5		689.12 psi
6		634.91 psi
7		580.70 psi
8		526.48 psi
9		472.27 psi

* **These parts of the model are not shown in the Stress Plots**

Machine Direction
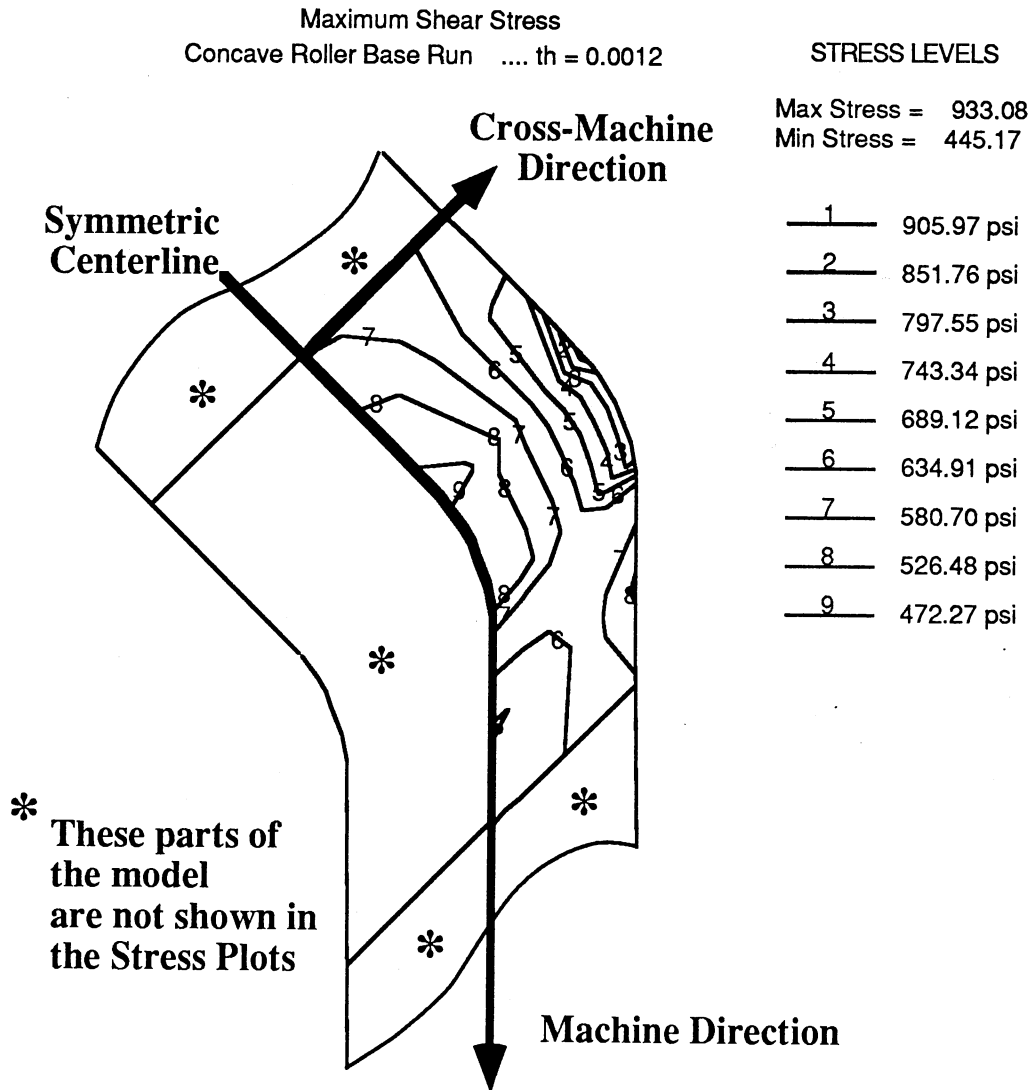
Figure 6-2.   Sample Annotated Stress Plot

Base Run for the Concave Roller

The base set of parameters for both rollers were chosen to match the web materials and equipment used in the initial experimental efforts. In both cases, the web material was coated polypropylene. The base parameters for the concave roller runs are given in Table I.

TABLE I.

CONCAVE ROLLER BASE PARAMETER VALUES

Thickness	0.0012 inches
Machine Direction Modulus	157000 psi
Cross Direction Modulus	117000 psi
Machine Direction Poisson's Ratio	0.16
Web Width	6 inches
Web Span Before the Roller	12 inches
Line Tension	1.5 pli
Roller Radius	1.125 inches
Roller Profile Radius	1250 inches
Wrap Angle	90 degrees

Effective Spreading of Equidistant Points from Centerline
Concave Roller Base Run   .... th = 0.0012
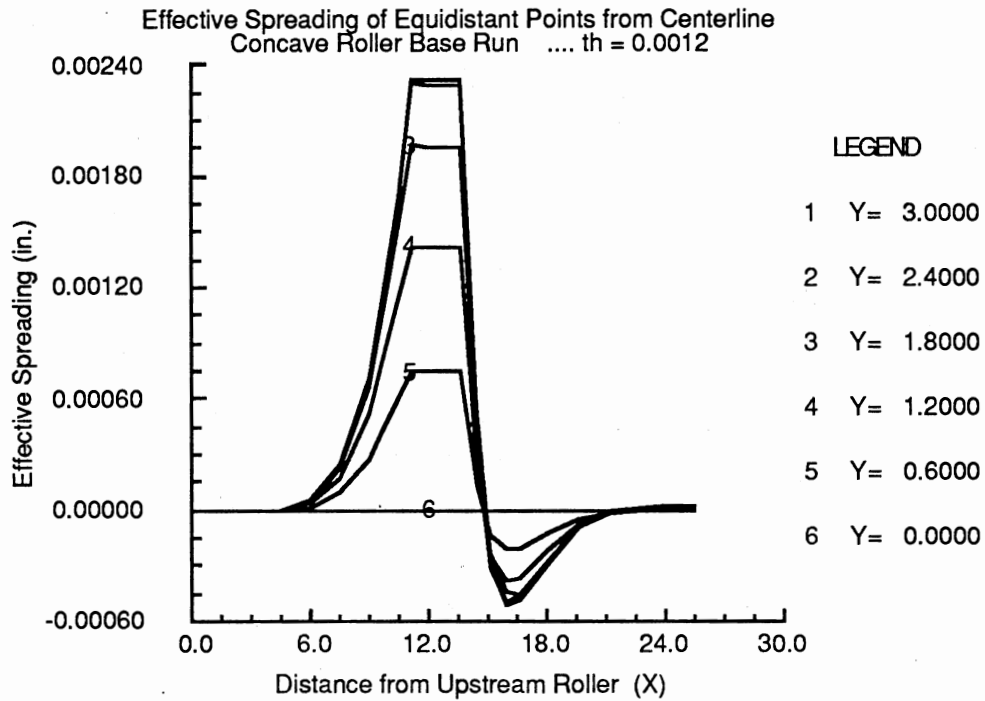
Figure 6-3.   Concave Roller Base Run Effective Spreading

Figure 6-3 shows the effective spreading for the base parameters of the concave roller.   This plot shows several important properties of the concave roller model.

The first thing to notice is that the spread lines have zero slope beginning slightly before the point of contact with the roller (X=12), and ending at the last point of contact with the roller.   This represents two of the essential properties of the concave roller model.   First, the no slip boundary condition causes the displacements at the entrance of the roller to be transported over the

roller. In addition, normal entry condition says that given sufficient friction, the web will spread so that streamlines approach the roller normal to the line of initial contact. For both of these, the normal direction is parallel to the machine direction, therefore the lines have zero slope.

The next thing to notice is that the spread lines converge to zero at the left and right sides of the plot. This does not mean that each of these streamlines have zero displacement at the ends or even the same displacement. Remember that each of these curves represents the deviation in displacement relative to the point at the beginning of the entry span. Each of the points at the beginning of the entry span have undergone a displacement because of the Poisson contraction. In this plot, the deviation of the curve from zero effective spreading represents the additional displacement beyond the Poisson contraction. At the left and right end, the only displacement in the web is the Poisson contraction. This means that the spreading effect is restricted to the area near the roller. For the parameter values chosen for the base case, the roller affects the web material about one web width (6 in.) upstream and downstream of the roller.

The final thing to note from these curves is the relative spreading. The curve at Y=0 has zero effective spreading everywhere. Because Y=0 is the symmetric centerline of the model, this is to be expected. It is also significant that the space between curves near the centerline is greater than the space between curves near the edge of the web. The total spreading force at any point along the width of the web is related to the distance of that point

from the edge of the web. The total spreading force approaches zero as the point approaches the edge of the web.
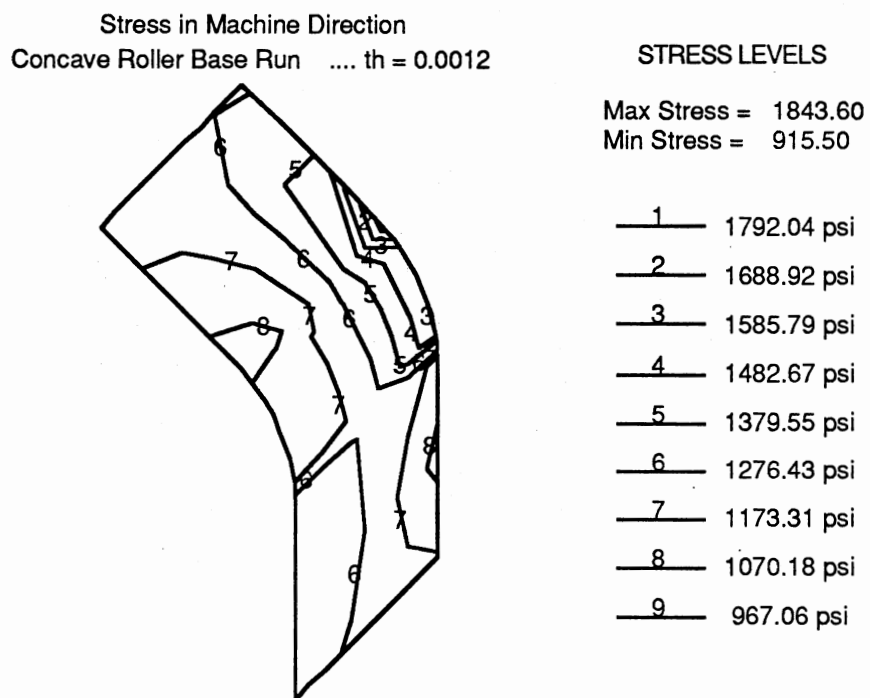
Figure 6-4.   Concave Roller Base Run MD Stresses

Figure 6-4 shows the distribution of machine direction stresses. It shows that there is extreme variation in the MD stress, with a maximum (max) stress of 1843 psi, and a minimum (min) stress of 915.5 psi. The variation is greatest near the roller, while the stresses approach a uniform value farther away from the roller. This uniform value is the nominal MD stress induced by the line tension.

The stresses are greatest near the edge of the roller, and smallest near the center of the roller. This was expected from simple geometric reasoning. The outer edges of the roller have a larger radius. The material must undergo larger strains and stresses to conform to this larger radius. In addition, the velocity at the outer edges is greater than the velocity at the center of the roller. This tends to shear the edges of the web ahead of the center, causing greater stresses near the edge. An interesting feature common to all of the stress plots for the concave roller is also shown in figure 6-4. The stress contours in the area where the web is in contact with the roller are all parallel to the machine direction. This is again a consequence of the no slip boundary condition which says that the state of strain immediately before the roller is transported over the surface of the roller.

Figure 6-5 shows the cross machine direction stress distribution for the concave roller model. The range of stresses in the cross machine direction is not as large as the range of machine direction stresses. The primary feature shown in the figure is the character of the CD stress distribution. The stresses are greatest near the center of the roller, decreasing to near zero at the edge of the roller. This stress distribution is consistent with the spreading displacement plot. The material at the edge of the roller has no spreading force applied to it. The material at the center of the roller is being pulled outward by the friction forces acting on the entire web, therefore incurring higher stresses.
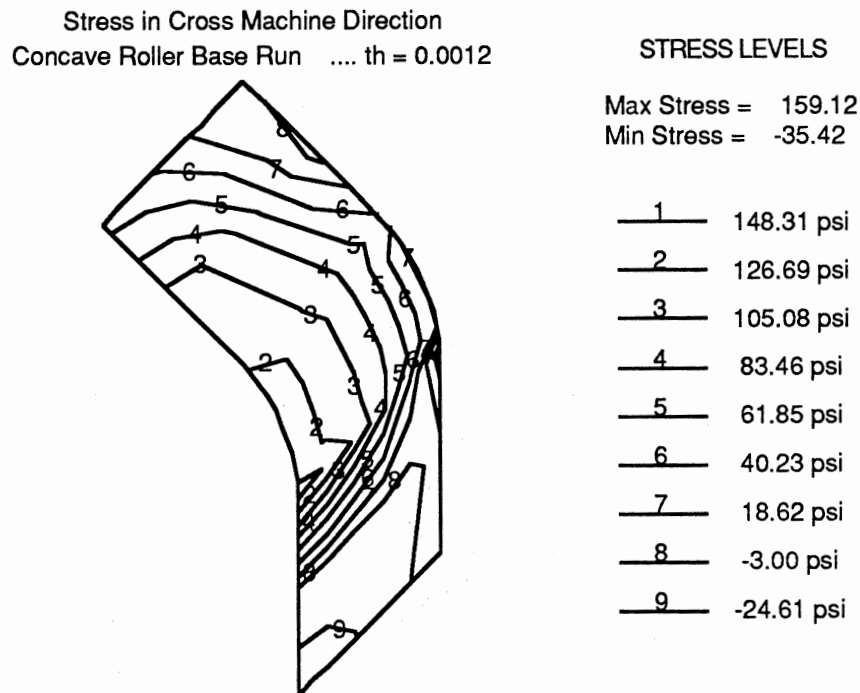
Figure 6-5.   Concave Roller Base Run CD Stresses

It was surprising to see a large region of compressive CD stresses in the exit span.   The magnitudes of those compressive stresses are small compared to the maximum CD tensile stress but are still significant.   The existence of these compressive stresses can be explained as follows.   The larger radius at the edge of the concave roller tends to shear the material at the edges of the web ahead of the material at the center.   This shearing induces a MD stress profile with significantly larger tensile stresses near the edge of the web than at the center of the web.   This stress profile acts as a force couple bending the edges of the web in toward the center at the exit span, causing compressive CD stresses in the exit span.

Figure 6-6 shows the shear stress distribution for the concave roller model. The shear stress distribution is consistent with the behavior expected from the roller geometry. The material at the edges of the roller is sheared ahead of the material at the center, therefore the shear stresses are higher at the edge. Because the web centerline is a line of symmetry, the shear stresses decrease to zero at the web centerline. The stress variation is greatest near the roller, decreasing to zero in the entry and exit span.

Figures 6-7, 6-8 and 6-9 show the principal stresses in the maximum and minimum directions, and the maximum shear stresses. Because of the relatively large MD stresses as compared to the CD stresses, it is not surprising to see that the maximum principal stress distribution is very similar to the MD stress distribution. Also, the minimum principal stress distribution is very similar to the CD stress distribution. The shape of the maximum shear stress distribution resembles the MD stress distribution, although the magnitudes are significantly different.

Shear Stress
Concave Roller Base Run   .... th = 0.0012

STRESS LEVELS

Max Stress =   277.90
Min Stress =   -16.54

1	261.54 psi
2	228.83 psi
3	196.11 psi
4	163.40 psi
5	130.68 psi
6	97.96 psi
7	65.25 psi
8	32.53 psi
9	-0.18 psi
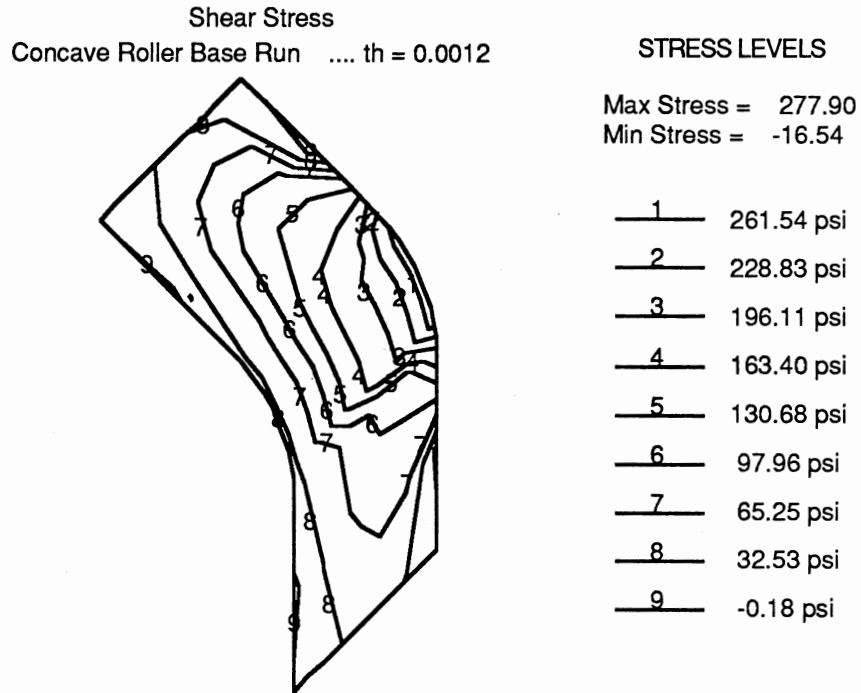
Figure 6-6.   Concave Roller Base Run Shear Stresses

Principal Stress in Max. Direction
Concave Roller Base Run   .... th = 0.0012

STRESS LEVELS

Max Stress =   1878.85
Min Stress =   916.45

1	1825.38 psi
2	1718.45 psi
3	1611.52 psi
4	1504.58 psi
5	1397.65 psi
6	1290.72 psi
7	1183.78 psi
8	1076.85 psi
9	969.92 psi
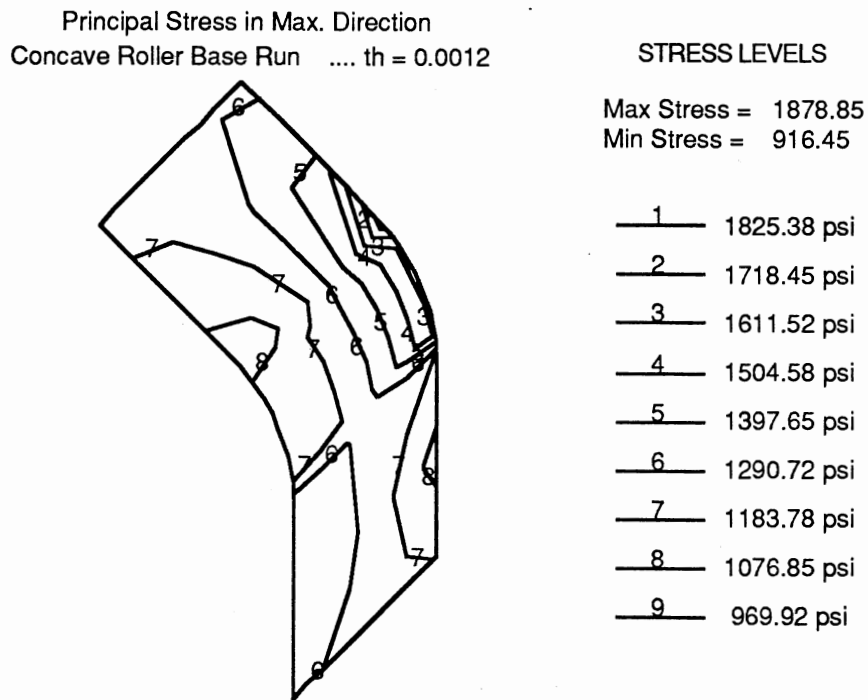
Figure 6-7.   Concave Roller Base Run Max Principal Stresses

Principal Stress in Min. Direction
Concave Roller Base Run   .... th = 0.0012
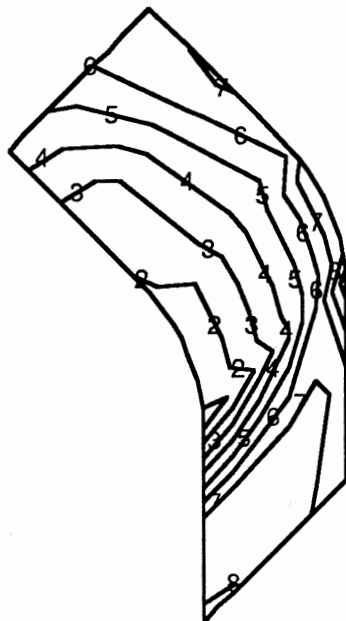
STRESS LEVELS

Max Stress =   158.47
Min Stress =   -69.27

1		145.82 psi
2		120.51 psi
3		95.21 psi
4		69.90 psi
5		44.60 psi
6		19.29 psi
7		-6.01 psi
8		-31.32 psi
9		-56.62 psi

Figure 6-8.   Concave Roller Base Run Min Principal Stresses

Maximum Shear Stress
Concave Roller Base Run   .... th = 0.0012
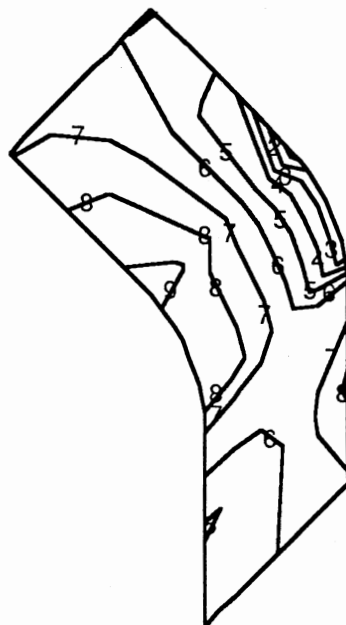
STRESS LEVELS

Max Stress =   933.08
Min Stress =   445.17

1		905.97 psi
2		851.76 psi
3		797.55 psi
4		743.34 psi
5		689.12 psi
6		634.91 psi
7		580.70 psi
8		526.48 psi
9		472.27 psi

Figure 6-9.   Concave Roller Base Run Max Shear Stresses

Base Run for the Curved Axis Roller

The base set of parameters used with the curved axis roller model are shown in table II. The parameters are essentially the same as those used with the concave roller model. The only differences are the roller radius, and the bow plane angle. Because the concave roller is an axisymmetric device, the bow plane angle has no meaning. The bow plane angle of 45 degrees was used with the experimental apparatus. In practice, this is the most commonly used orientation for the curved axis roller. The parameter study of the next section will show several reasons why this is the case.

Figure 6-10 shows the effective spreading for the base parameters for the curved axis roller. This plot shows several important features of the curved axis roller model.

The first thing to notice is that the slope of the curves is not zero in the area where the web contacts the roller. The amount of spreading does not remain constant over the surface of the roller. Instead, additional spreading occurs. This was expected from the geometry of the roller. The spreading effect of the curved axis roller occurs as a result of two separate mechanisms. The first and most obvious mechanism is the spreading action of the roller cover rotating on the curved shaft. The second is the steering of web streamlines so that they approach the roller normal to the line of contact. The slope of the streamlines at the end of the entry span is the same as the slope over the roller. The plot exhibits both of these effects, an increase in spreading over the roller with a smooth transition in the entry span.

TABLE II.

CURVED AXIS ROLLER BASE PARAMETER VALUES

Thickness	0.0012	inches
Machine Direction Modulus	157000	psi
Cross Direction Modulus	117000	psi
Machine Direction Poisson's Ratio	0.16	
Web Width	6	inches
Web Span Before the Roller	12	inches
Line Tension	1.5	pli
Roller Radius	0.75	inches
Roller Profile Radius	1680	inches
Wrap Angle	90	degrees
Bow Plane Angle	45	degrees

Effective Spreading of Equidistant Points from Centerline
Curved axis roller base run
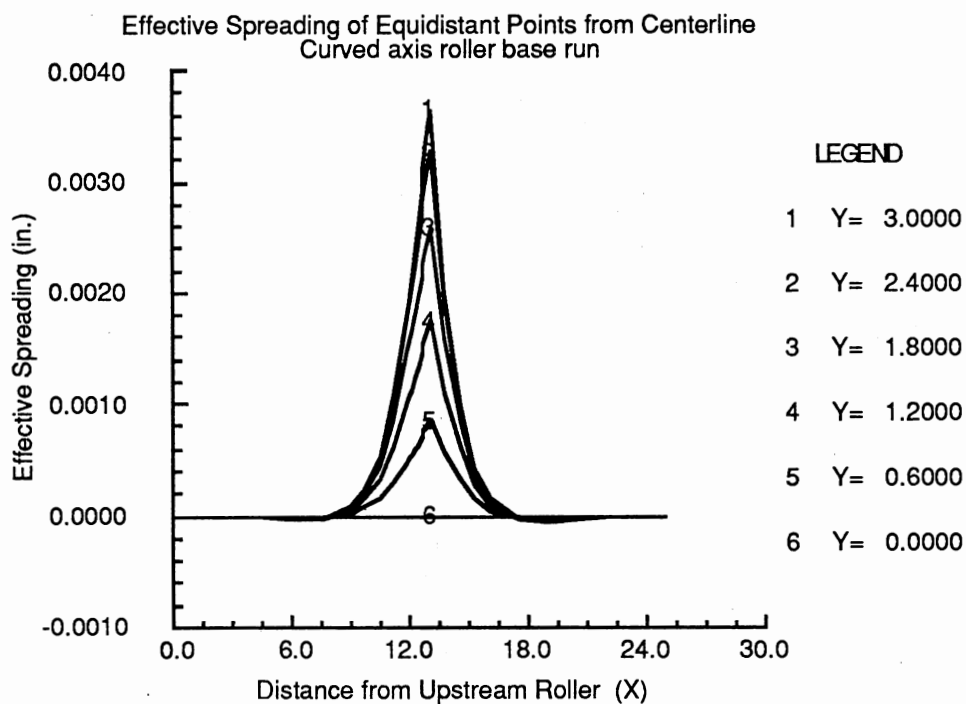
Figure 6-10. Curved Axis Roller Base Run Effective
Spreading

As in the concave roller, the slope of the curves become negative nearly instantly as the web leaves the roller. There are no friction forces in this region to sustain the spreading that was developed over the roller. The displacement streamlines also converge to zero as in the concave roller. The span length affected by the roller is again approximately one web width before and after the roller.

Stress in Machine Direction
Curved axis roller base run

STRESS LEVELS

Max Stress = 1353.35
Min Stress = 1180.45

——1——	1343.74 psi
——2——	1324.53 psi
——3——	1305.32 psi
——4——	1286.11 psi
——5——	1266.90 psi
——6——	1247.69 psi
——7——	1228.48 psi
——8——	1209.27 psi
——9——	1190.06 psi
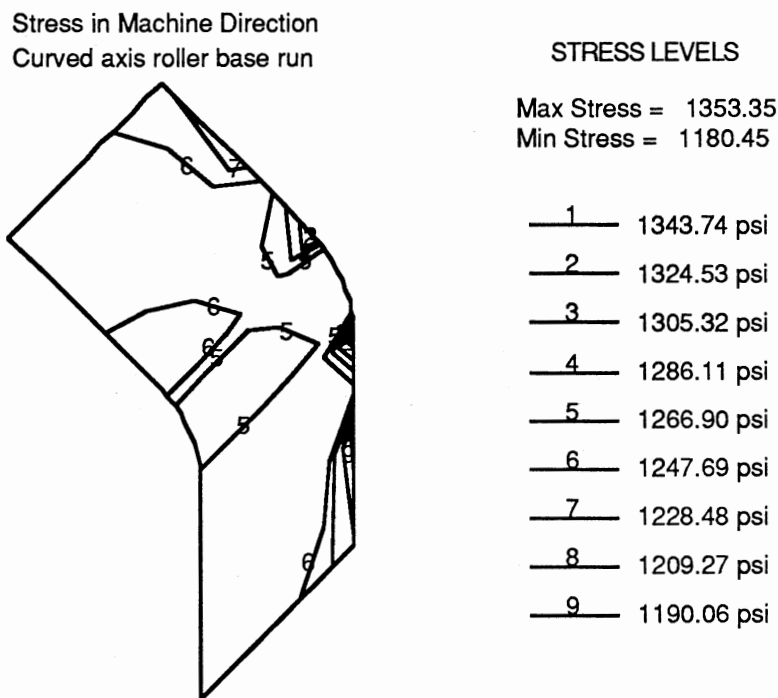
Figure 6-11.   Curved Axis Roller Base Run MD Stresses

Figure 6-11 shows the distribution of machine direction stresses in the curved axis roller model. The first thing noticed is that the range of MD stresses in the curved axis roller is not nearly as large as that of the concave roller. In addition, the high and low stresses occur in very localized regions. Over most of the web, the MD stresses are essentially uniform and equal to the nominal stress in the line. The near uniformity of the MD stresses should not be surprising. All cross-sections of the curved axis roller have the same diameter. Therefore, the MD strains over the roller should be nearly

uniform. Also, there is no shearing action as was seen in the concave roller model.

Figure 6-12 shows the cross machine direction stress distribution for the curved axis roller model. At first glance, it looks very similar to the CD stress distribution for the concave roller. The largest stresses are on the roller at the center of the web, with the stresses dropping to near zero at the edge of the web. There are two essential differences. The first is the absence of parallel contour lines over the surface of the roller. Because additional spreading occurs over the roller, the CD stresses continue to increase over the roller. The second difference is the absence of the large region of compressive stresses in the exit span. The shearing mechanism that caused these compressive stresses in the concave roller is not present in the curved axis roller.

There is a region of compressive stress indicated at the edge of the web in the entry span. In contrast to the concave roller, both the magnitude of the stress, and the size of the region are relatively small.

Figure 6-13 shows the shear stress distribution for the curved axis roller model. Both the range and the magnitudes of the shear stress distribution are smaller than those of the conave roller. This is consistent with the previous plots; the curved axis roller does not exhibit the same shearing mechanism as the concave roller.

Stress in Cross Machine Direction
Curved axis roller base run
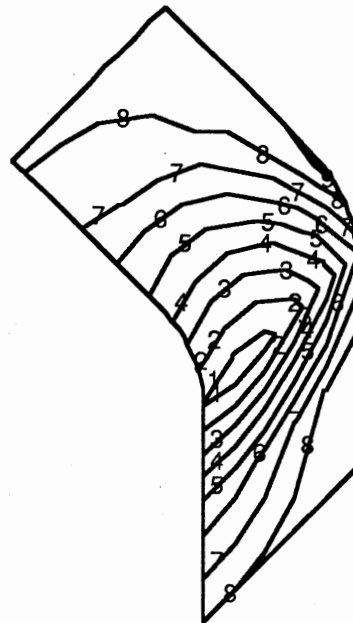
STRESS LEVELS

Max Stress =   176.83
Min Stress =   -20.71

1	165.86 psi
2	143.91 psi
3	121.96 psi
4	100.01 psi
5	78.06 psi
6	56.11 psi
7	34.16 psi
8	12.21 psi
9	-9.74 psi

Figure 6-12. Curved Axis Roller Base Run CD Stresses

Shear Stress
Curved axis roller base run
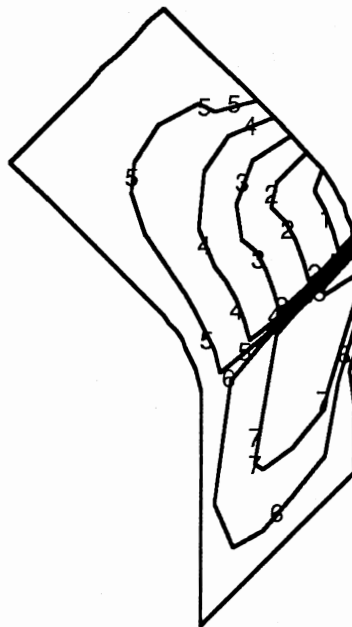
STRESS LEVELS

Max Stress =   76.29
Min Stress =   -57.56

1	68.85 psi
2	53.98 psi
3	39.11 psi
4	24.24 psi
5	9.37 psi
6	-5.51 psi
7	-20.38 psi
8	-35.25 psi
9	-50.12 psi

Figure 6-13. Curved Axis Roller Base Run Shear Stresses

The plot shows that the shear stress has a value of zero at all points on the web symmetric centerline. On the roller surface, the shear stress increases to a maximum value at the edge of the web. In the entry span, the shear stresses quickly dissipates to a nearly uniform value of zero. In the exit span, the shear stresses are slightly negative near the roller, and dissipating to a nearly uniform value of zero.

Figures 6-14, 6-15 and 6-16 show the principal stresses in the maximum and minimum directions, and the max. shear stresses. As in the concave roller model, the max. and min. principal stress distributions are essentially the same as the MD and CD stress distributions respectively.

The shape of the max shear stress distribution has features similar to the shape of the MD stress distribution, small regions of higher stresses near the edge of the web at the entry and exit spans. The range of max shear stress variations is relatively small.

Principal Stress in Max. Direction
Curved axis roller base run
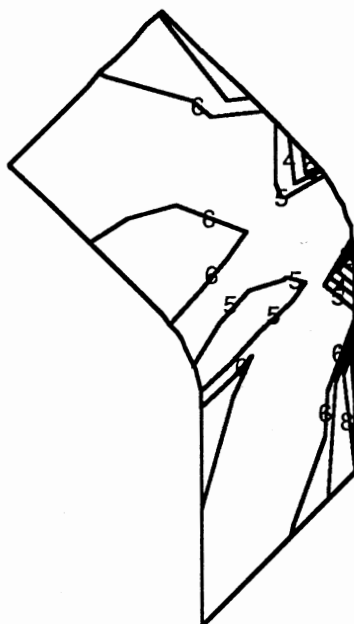
STRESS LEVELS

Max Stress = 1363.60
Min Stress = 1180.65

1	1353.44 psi
2	1333.11 psi
3	1312.78 psi
4	1292.45 psi
5	1272.13 psi
6	1251.80 psi
7	1231.47 psi
8	1211.14 psi
9	1190.81 psi

Figure 6-14.   Curved Axis Roller Base Run Max Principal Stresses

Principal Stress in Min. Direction
Curved axis roller base run

STRESS LEVELS

Max Stress = 176.06
Min Stress = -25.08

1	164.89 psi
2	142.54 psi
3	120.19 psi
4	97.84 psi
5	75.49 psi
6	53.14 psi
7	30.79 psi
8	8.44 psi
9	-13.91 psi

Figure 6-15.   Curved Axis Roller Base Run Min Principal Stresses

Maximum Shear Stress
Curved axis roller base run

STRESS LEVELS

Max Stress =   675.87
Min Stress =   537.60

——1——	668.19 psi
——2——	652.83 psi
——3——	637.46 psi
——4——	622.10 psi
——5——	606.73 psi
——6——	591.37 psi
——7——	576.01 psi
——8——	560.64 psi
——9——	545.28 psi
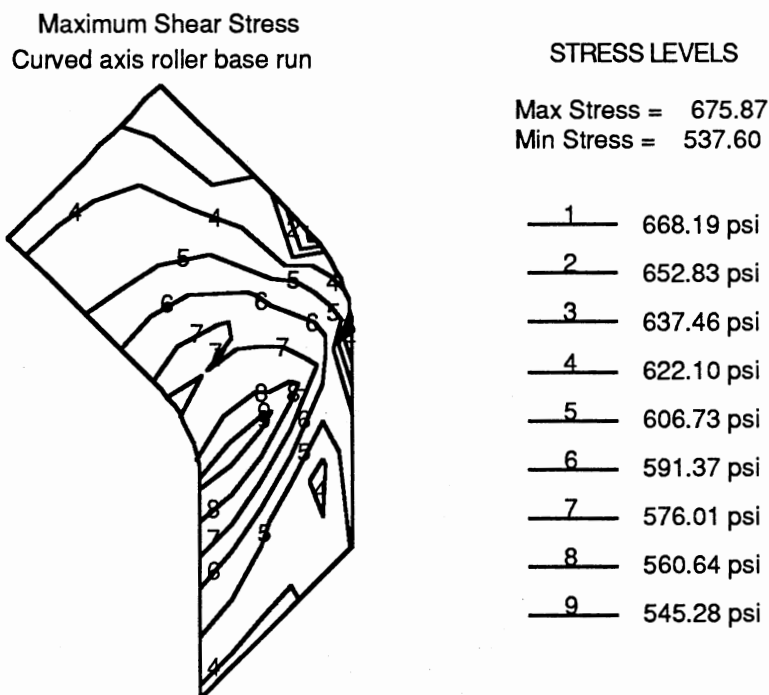
Figure 6-16.   Curved Axis Roller Base Run Max Shear
Stresses

Analysis of Parameter Variations

The previous section examined the deformation and stress
distribution over the entire web surface for a base set of parameter
values.   In this section, the parameters will be varied around those
base values.   This study required approximately 70 runs of the
computer model.   It is not feasible to discuss the resulting stress and
deformation plots for each of those runs.   Instead, representative
values will be tabulated from each of those runs, and combined in a
set of summary plots.   These summary plots will be examined for
trends in the response of the model to parameter variations.

These summary plots are organized in the following manner. For the range of values of a single parameter, and for each of the two roller types, the following four plots are generated:

(1) Maximum effective spreading displacement (spreading beyond the Poisson contraction at the point on the outer edge of the web where it exits the roller)

(2) Maximum coefficient of friction required to enforce the predicted displacements

(3) Maximum and minimum machine direction (MD) stresses on a combined plot

(4) Maximum and minimum cross machine direction (CD) stresses on a combined plot

In each of these plots, the values in the list above are plotted on the vertical axis, and the values of the parameter being varied are on the horizontal axis.

The values for the parameters used in this study are given in tables III and IV for the concave roller and curved axis roller respectively. The values shown in bold print are the base parameter values for the roller.

TABLE III.

CONCAVE ROLLER PARAMETER VALUES

Thickness (in)	0.0005	0.0009	**0.0012**	0.0018
Machine Direction Modulus (psi)	50000	117000	**157000**	200000
Cross Direction Modulus (psi)	50000	**117000**	157000	200000
Machine Direction Poisson's Ratio	0.1	**0.16**	0.2	0.3
Web Width (in)	3	**6**	9	12
Line Tension (pli)	1.0	**1.5**	2.0	3.0
Roller Radius (in)	0.75	**1.125**	2.0	3.0
Roller Profile Radius of Curvature (in)	**1250**	2000	3000	5000
Wrap Angle (deg)	30	60	**90**	120

TABLE IV.

CURVED AXIS ROLLER PARAMETER VALUES

Thickness (in)	0.0005	0.0009	**0.0012**	0.0018
Machine Direction Modulus (psi)	50000	117000	**157000**	200000
Cross Direction Modulus (psi)	50000	**117000**	157000	200000
Machine Direction Poisson's Ratio	0.1	**0.16**	0.2	0.3
Web Width (in)	3	**6**	9	12
Line Tension (pli)	1.0	**1.5**	2.0	3.0
Roller Radius (in)	0.5	**0.75**	1.0	1.25
Roller Profile Radius of Curvature (in)	756	**1680**	3000	5000
Wrap Angle (deg)	30	60	**90**	120
Bow Plane Angle (deg)	30	40	**45**	60

Web Thickness

Figures 6-17 through 6-20 show the effects of thickness variation on the concave roller, and figures 6-21 through 6-24 show the effects of thickness variation on the curved axis roller. The first plot in each of these groups is the maximum effective spreading vs. thickness plot. For both types of rollers, this curve is flat. Thickness has no effect on the amount that the web is spread. This behavior is consistent with a process that is driven by geometry and not by forces. In both of the web models, the primary boundary conditions are geometric. The web must conform to the shape of the roller. Points on the web are transported around the roller without slipping. Also, the web is spread until streamlines enter the roller normal to the wrap line. The only boundary conditions based on force are the MD displacements at the beginning of the entry span and the end of the exit span. These displacements are calculated from the nominal line tension.

The second plot in each group is maximum coefficient of friction vs. thickness. This is the maximum coefficient of friction over the entire surface of the roller that ensures the no slip boundary condition. The maximum friction curves for both models show a nearly linear dependence on the material thickness. The required friction increases as thickness increases. Again, this is consistent with a geometry driven process. A larger force is required to deform a thicker web a fixed amount than is required to deform a thinner web that same amount.

Concave Roller Data
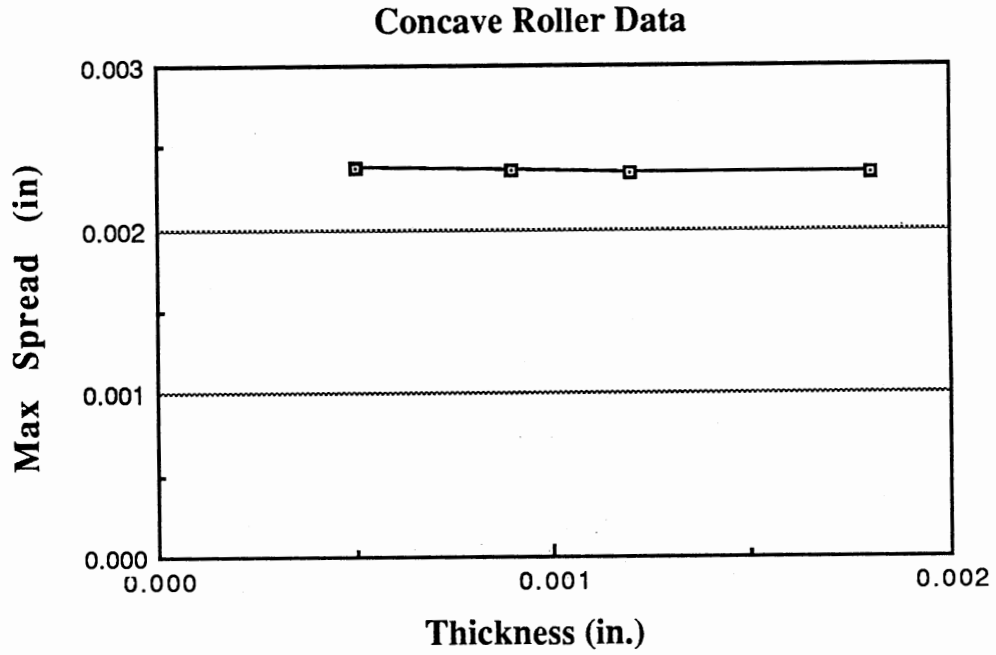
Figure 6-17.   Concave Roller - Spread vs. Thickness

Concave Roller Data
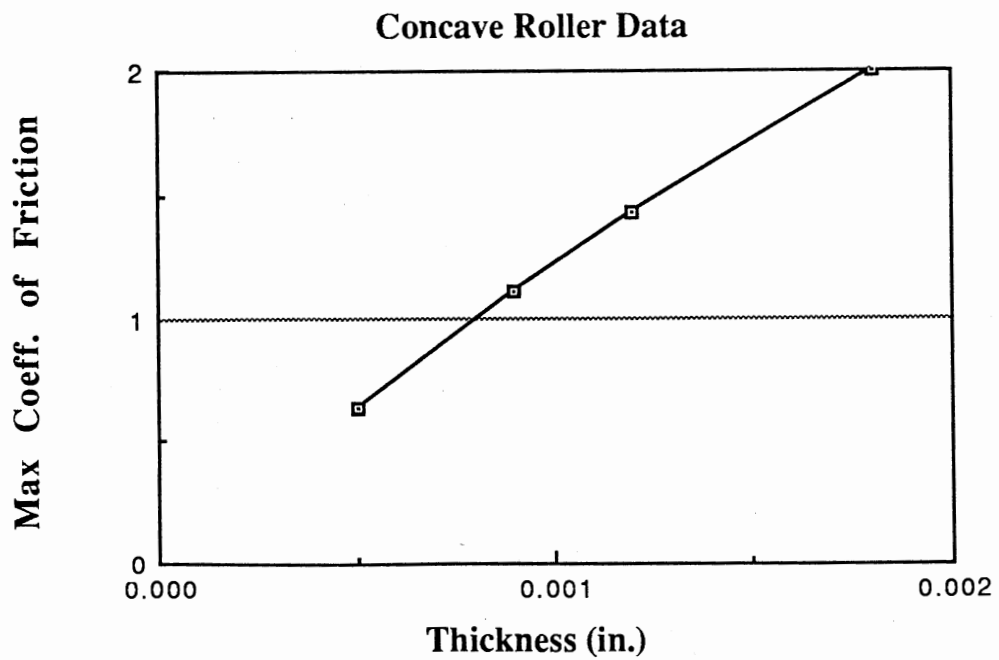
Figure 6-18.   Concave Roller - Friction vs. Thickness

Concave Roller Data
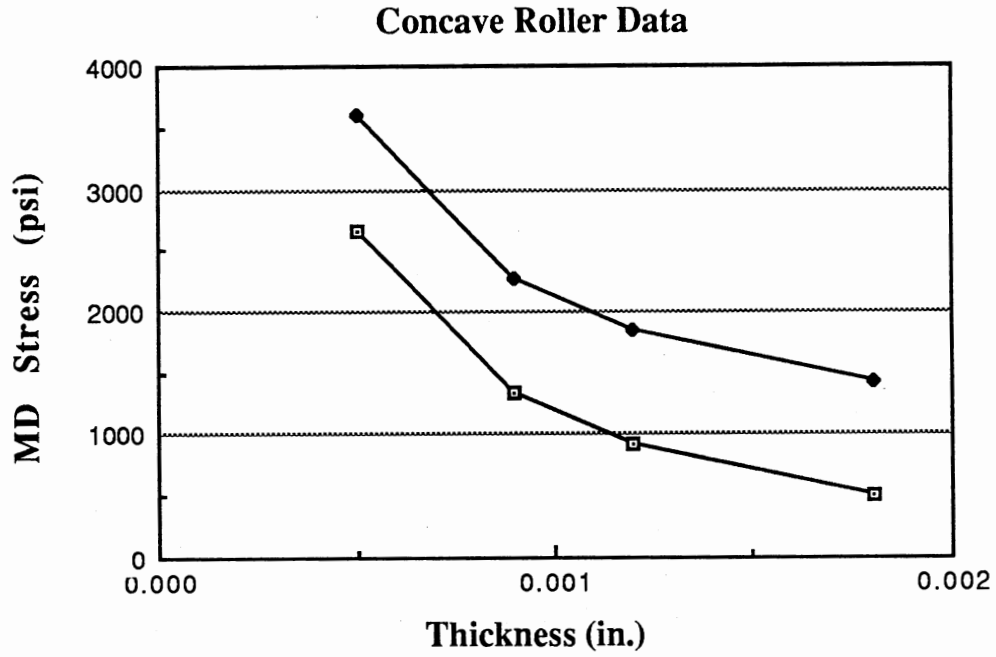
Figure 6-19. Concave Roller - MD Stress vs.
Thickness

Concave Roller Data
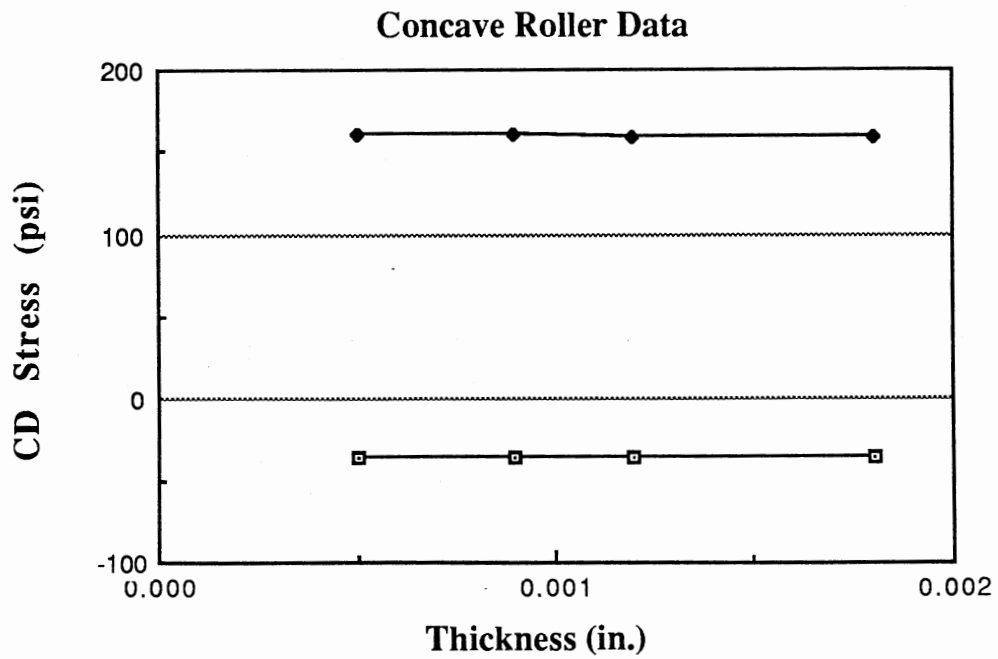
Figure 6-20. Concave Roller - CD Stress vs.
Thickness

Curved Axis Roller Data
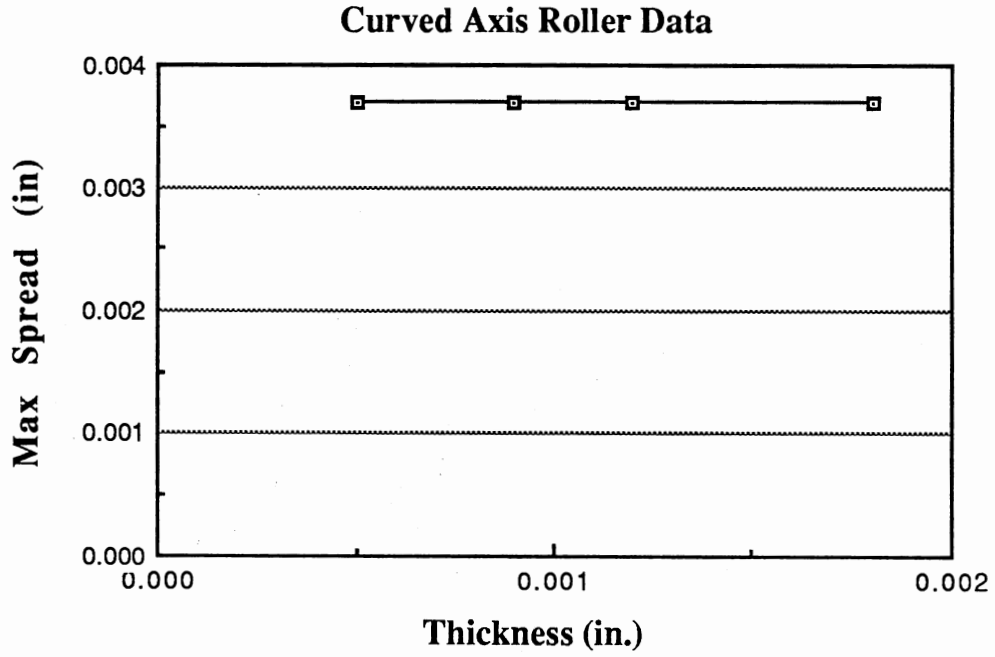
Figure 6-21.   Curved Axis Roller - Spread vs. Thickness

Curved Axis Roller Data
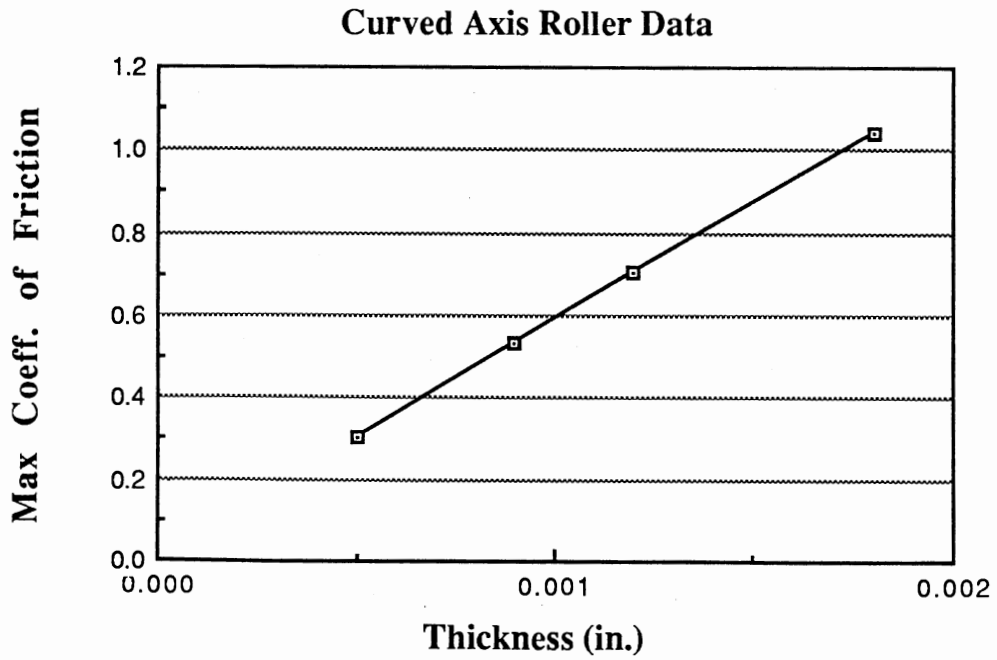
Figure 6-22.   Curved Axis Roller - Friction vs. Thickness

Curved Axis Roller Data
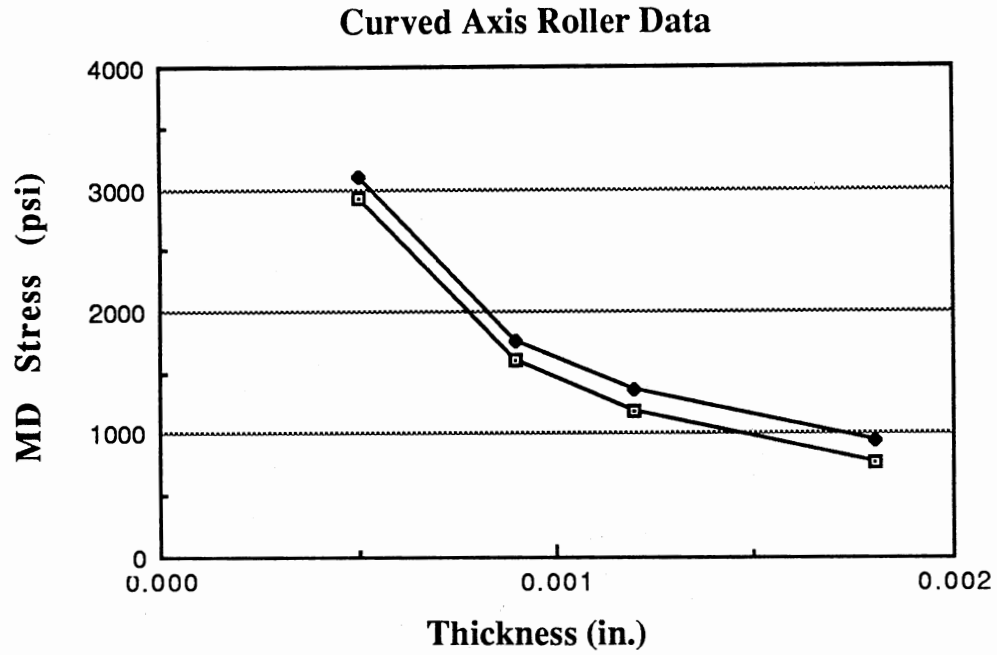
Figure 6-23.   Curved Axis Roller - MD Stress vs.
Thickness

Curved Axis Roller Data
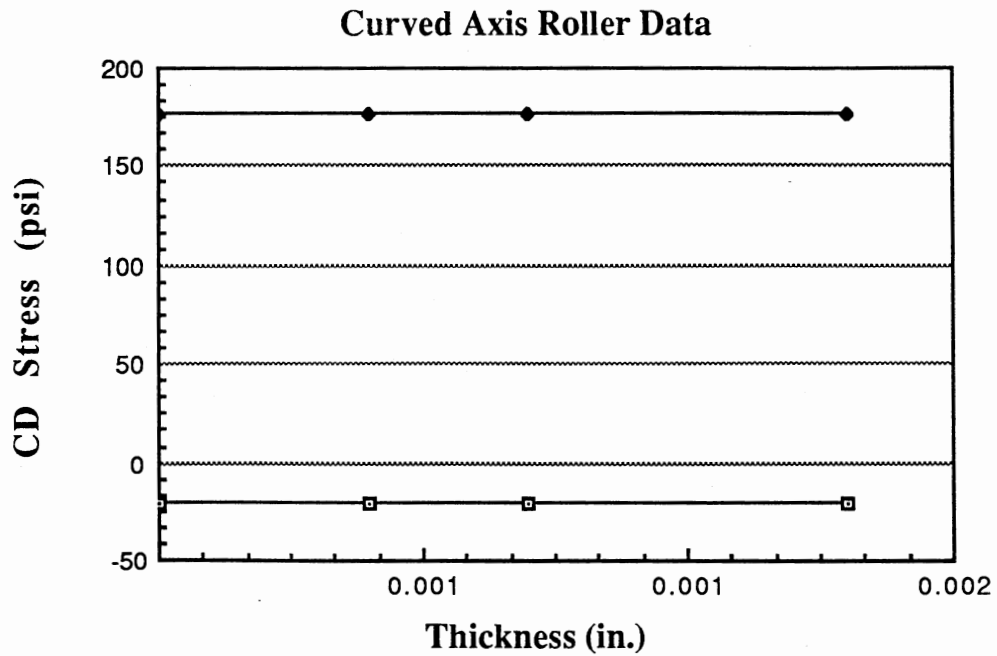
Figure 6-24.   Curved Axis Roller - CD Stress vs.
Thickness

The third plot in each group is the max and min machine direction stress vs. thickness. For a single run of the program, the single highest and lowest stress over the entire model are selected for this plot. For both the concave and the curved axis roller, both the max and min MD stresses decrease with increasing thickness. This occurs because of the displacements applied at the beginning and end of the model. These displacements are calculated from the nominal line tension. For a constant value of line tension, the average value of MD stress should decrease with increasing web thickness.

It is interesting to note that the max and min MD stress curves are nearly parallel for both types of rollers. This indicates that the average MD stress is governed by the web thickness but that the difference between the max and min stress is not. The stress difference is controlled by the geometry of the roller. In addition, the difference between the max and min MD stress is much larger in the concave roller than in the curved axis roller. This was also seen in the MD stress distribution plots of the previous section.

The curves for max and min cross machine direction stresses are flat indicating no variation with respect to web thickness. This again is consistent with the geometry driven spreading process.

Machine Direction Modulus

Figures 6-25 through 6-28 show the effects of machine direction modulus on the concave roller, and figures 6-29 through 6-32 show the effects of MD modulus on the curved axis roller. The shapes of all of the curves for the concave roller are nearly the same

as the corresponding curves for the curved axis roller. But in each case, variations in MD modulus have a significantly larger effect on the concave roller than on the curved axis roller.

For both types of rollers, the max spread increases with increasing MD modulus, although the increase is very small in the curved axis roller. The spreading mechanism in the concave roller is driven primarily by the stress-strain distribution in the machine direction, and is therefore more sensitive to variations in the MD modulus.

The maximum required friction also increases with MD modulus for both types of rollers. Again, the effect is much larger in the concave roller. This occurs for two different reasons. First, larger friction forces are required to accommodate the increased spreading. The second reason is that the MD strain variation on the concave roller is solely a function of the roller geometry. For the same geometry, the system induces the same strain variation over the roller. An increase in the MD modulus requires greater friction forces to maintain the same strain.

The curves for MD stress show the max and min stresses diverging for both rollers, with the max stress increasing and the min stress decreasing. Again, the variation of stresses is much larger for the concave roller. For both rollers, the slope of the max stress curve has a magnitude similar to the slope of the min stress curve, but of opposite sign. For constant line tension, the average value of MD stress is independent of the MD modulus, while the variation in MD stress is dependent on the MD modulus.

Concave Roller Data
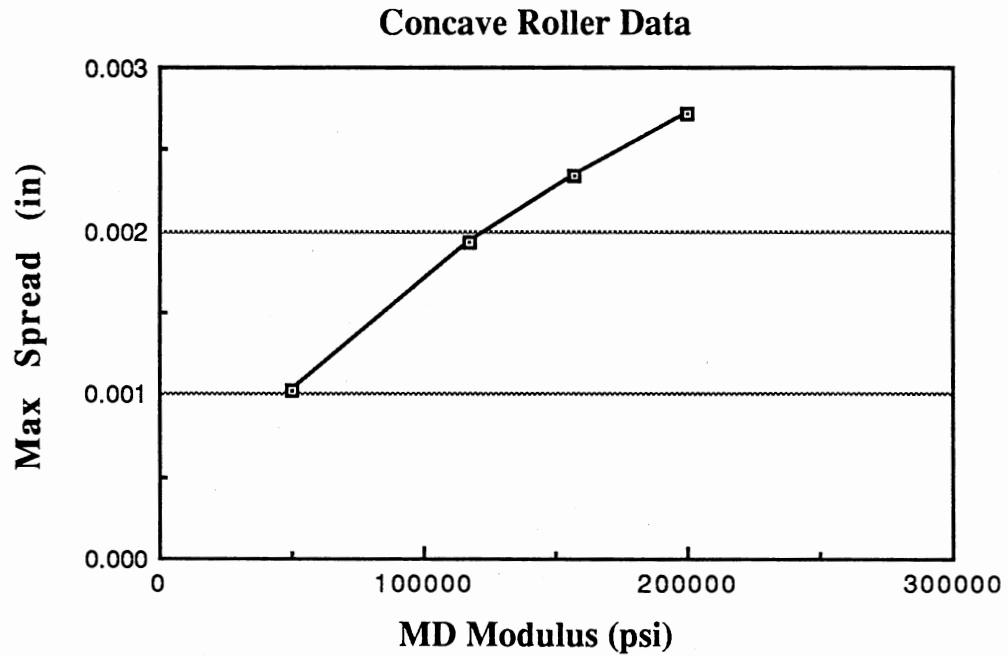
Figure 6-25.   Concave Roller - Spread vs. MD
Modulus

Concave Roller Data
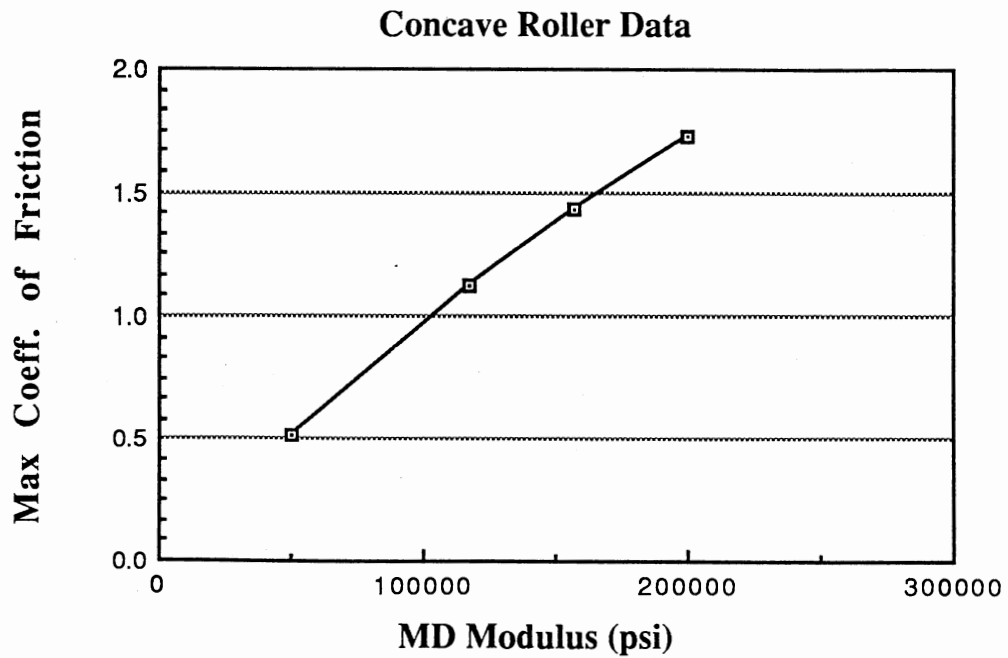
Figure 6-26.   Concave Roller - Friction vs. MD
Modulus

Concave Roller Data
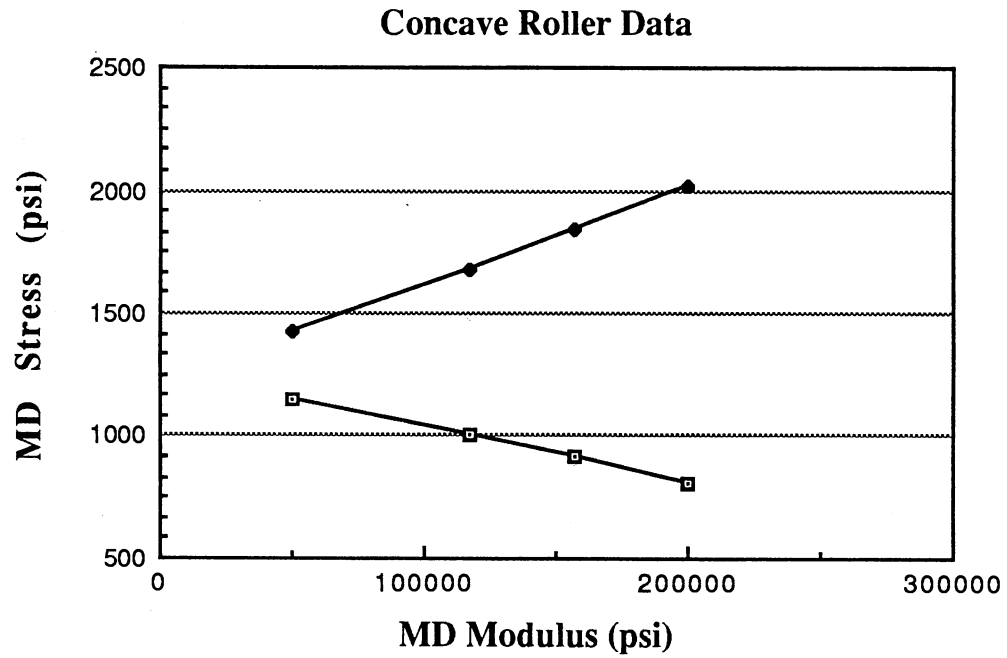
Figure 6-27. Concave Roller - MD Stress vs. MD
Modulus

Concave Roller Data
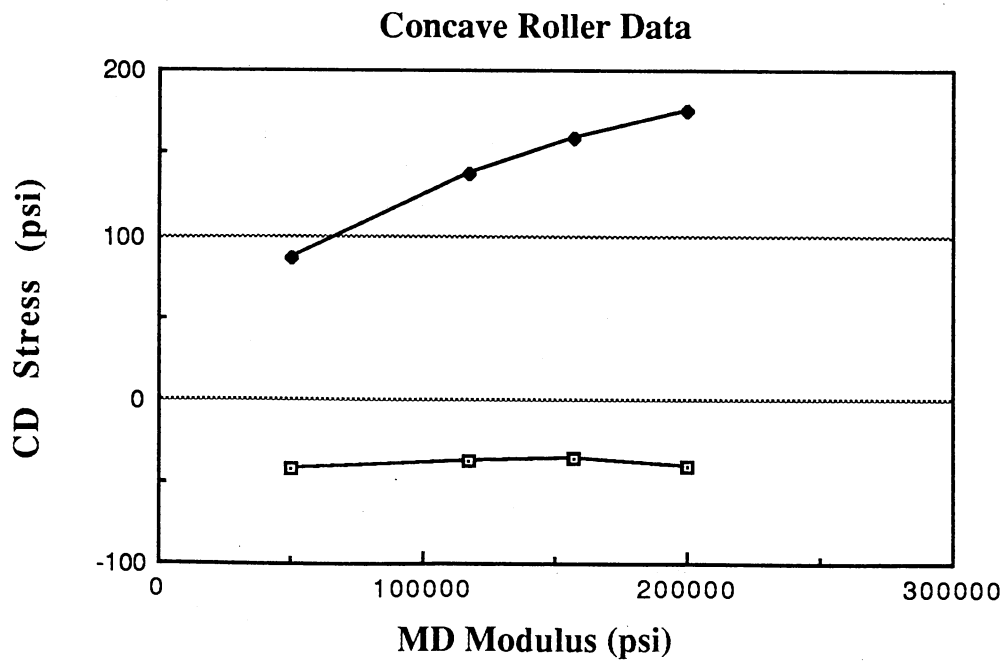
Figure 6-28. Concave Roller - CD Stress vs. MD
Modulus

Curved Axis Roller Data
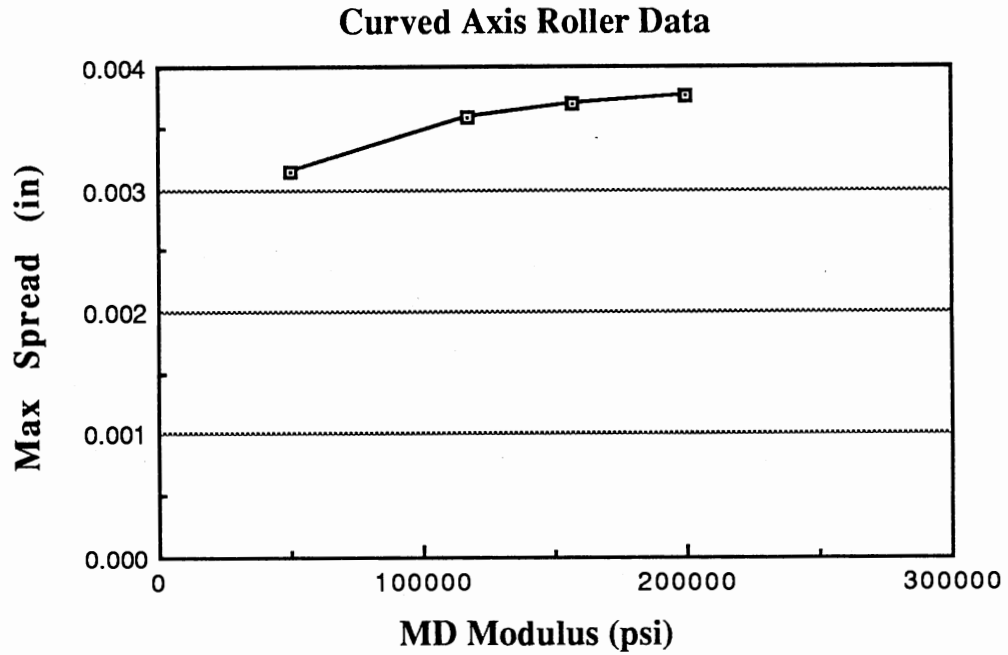
Figure 6-29. Curved Axis Roller - Spread vs. MD Modulus

Curved Axis Roller Data
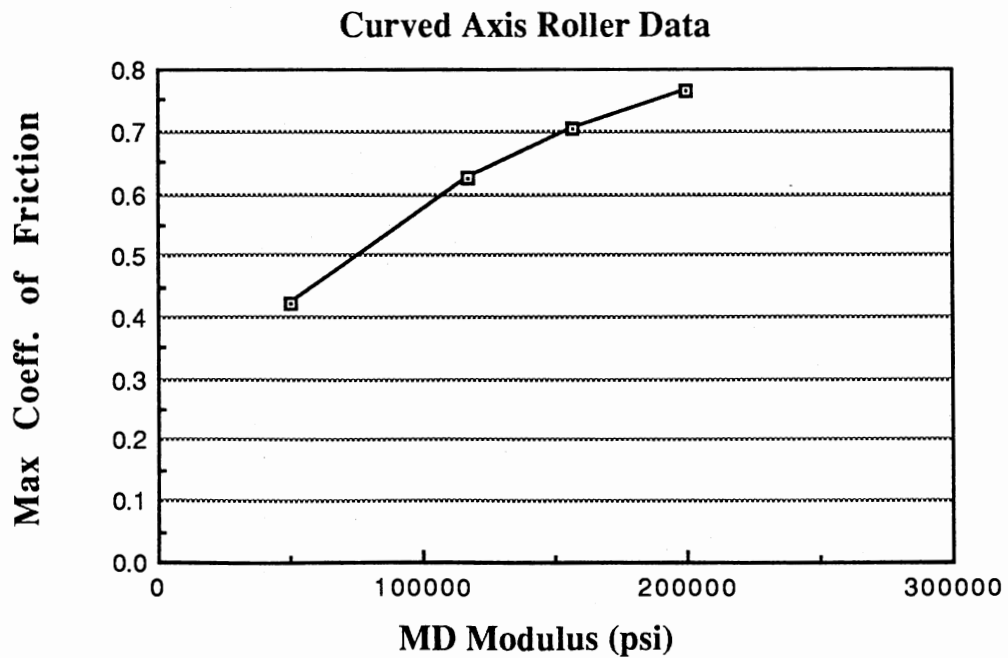
Figure 6-30. Curved Axis Roller - Friction vs. MD Modulus

Curved Axis Roller Data
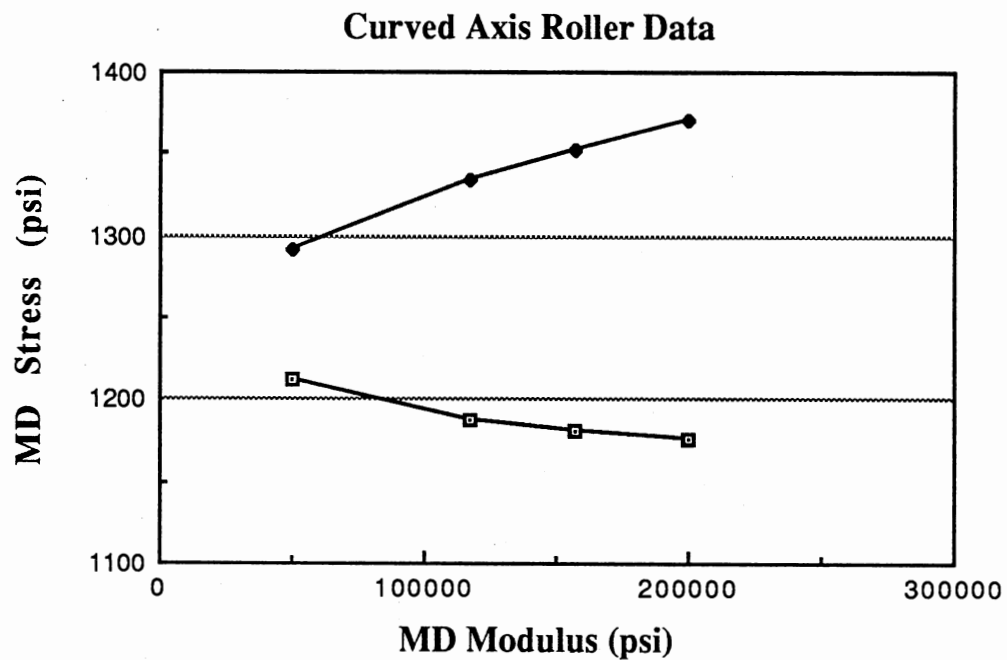
Figure 6-31. Curved Axis Roller - MD Stress vs. MD
Modulus

Curved Axis Roller Data
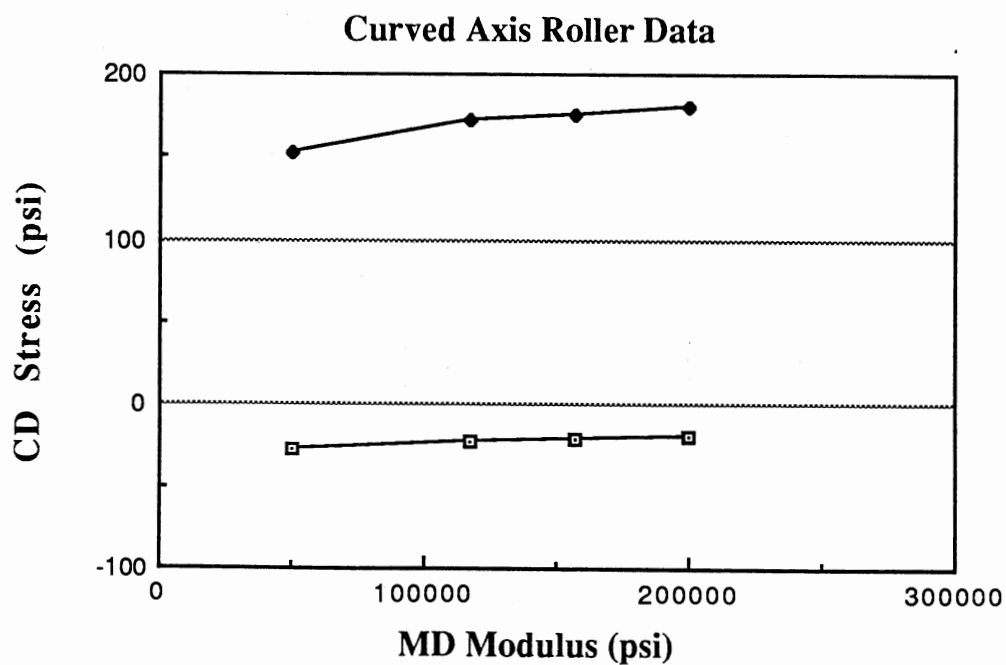
Figure 6-32. Curved Axis Roller - CD Stress vs. MD
Modulus

The curves for CD stress are consistent with the max spreading curves. The concave roller shows a significant increase in the max CD stress as MD modulus increases. This increase is the result of the significantly increased spreading. The curve for min CD stress is essentially flat for the concave roller. The curved axis roller shows a slight increase in the max CD stress and no change in the min stress.

Cross Machine Direction Modulus

Figures 6-33 through 6-36 show the effects of cross machine direction modulus on the concave roller, and figures 6-37 through 6-40 show the effects of CD modulus on the curved axis roller. Because the effects of CD modulus are different for the two rollers, they are discussed separately.

The concave roller shows both a sharp decrease in max spreading and a slight increase in the required coefficient of friction for increasing CD modulus. Spreading in the concave roller occurs because the MD strain profile causes a slight cross machine direction "bulge" in the entry span. The streamlines of the web are steered outward until the bulge is straightened and normal entry occurs. Increasing the CD modulus decreases the size of the bulge, therefore decreasing the amount of spreading required for normal entry.

The response of the friction curve for the concave roller is a combination of two opposing effects. First, because the amount of spreading decreases, the friction required to enforce that spreading should also decrease. But, for a fixed amount of spreading, increasing the CD modulus should result in an increase in the amount of friction

required. These two effects offset each other, resulting in only a slight increase in the amount of friction required.

The MD stress curves show essentially no variation in either the max or min stress for variations in CD modulus, while the CD stress curves show a slight variation. The max CD stress increases slightly with increasing CD modulus for the same reasons that the friction increased. It is the result of the same two opposing effects. The min CD stress shows a small decrease for increasing CD modulus.

The curved axis roller shows a very small decrease in the max spread curve for increasing CD modulus. This is consistent with the spreading mechanism for this roller. Spreading in the curved axis roller is primarily the result of CD velocity vector components of points on the roller cover, and is not effected by material properties to the same extent as the concave roller.

The curved axis roller shows a significant increase in the required coefficient of friction for increasing CD modulus. Because the amount of spreading is essentially constant, larger forces are required to spread a web with higher CD modulus.

The MD stress curves for the curved axis roller show a larger variation than was seen in the concave roller. The max stress curve increases slightly with CD modulus, while the min stress curve decreases. As was seen with the MD modulus data, the average MD stress remains constant, while the difference between the max and min curves increase. The average MD stress is not a function of the CD modulus.

Concave Roller Data
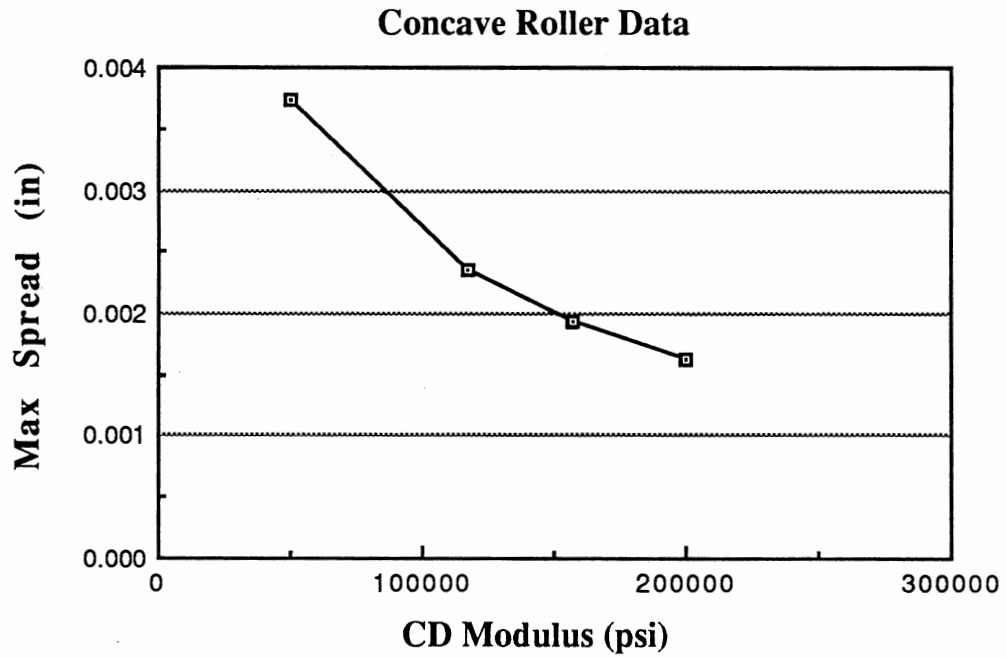
Figure 6-33. Concave Roller - Spread vs. CD
Modulus

Concave Roller Data
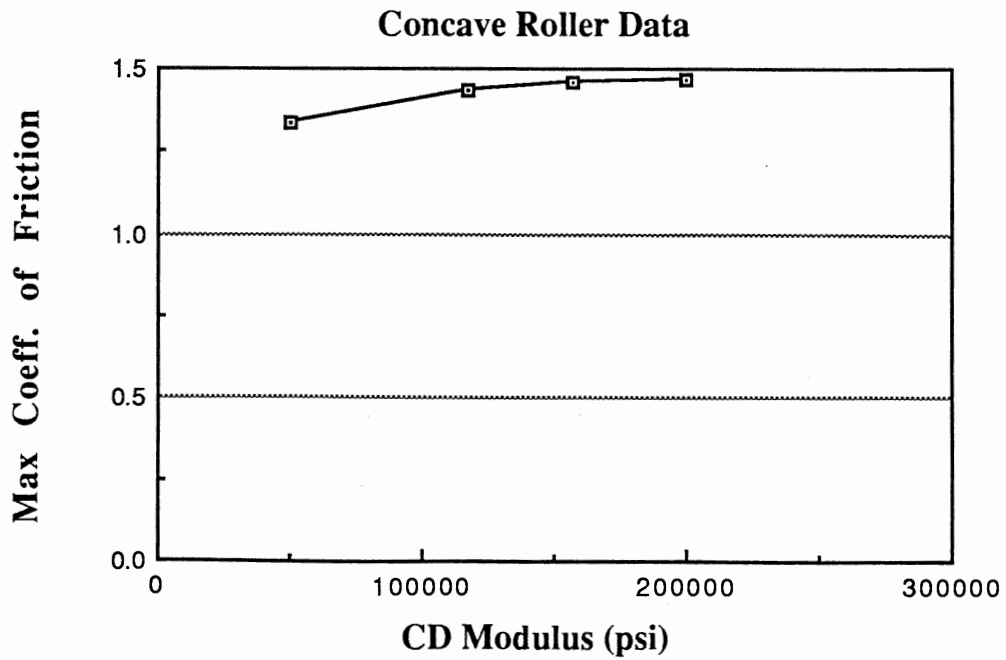
Figure 6-34. Concave Roller - Friction vs. CD
Modulus
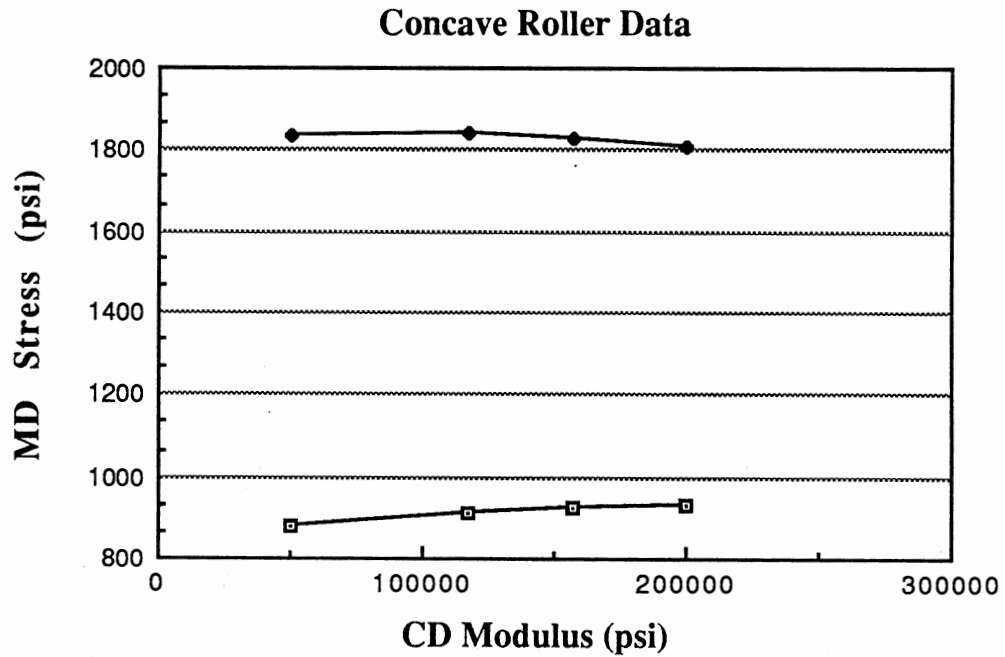
Figure 6-35. Concave Roller - MD Stress vs. CD Modulus
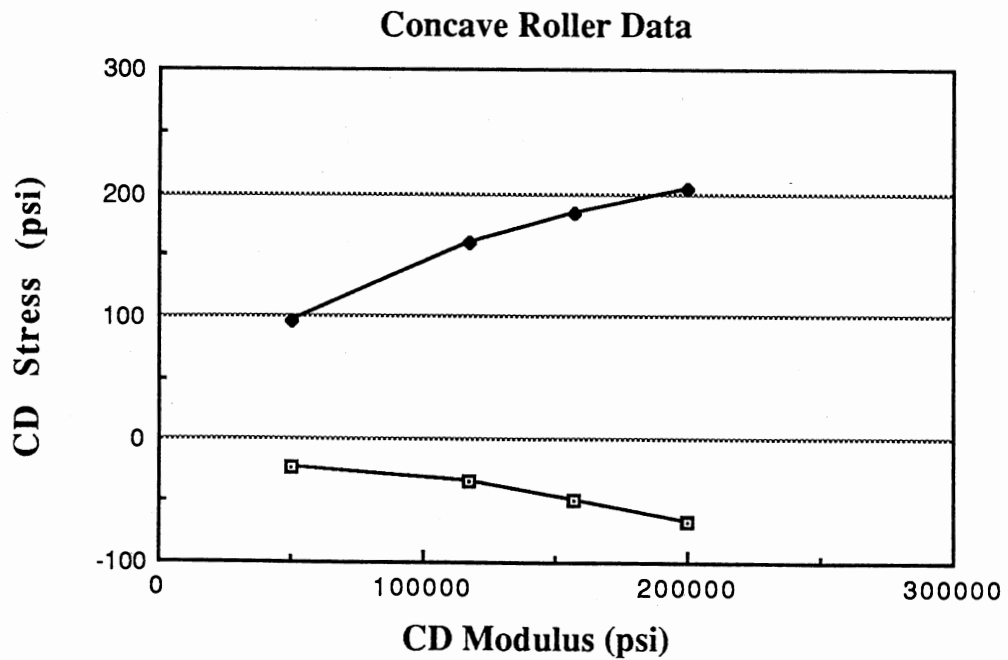
Figure 6-36. Concave Roller - CD Stress vs. CD Modulus

Curved Axis Roller Data
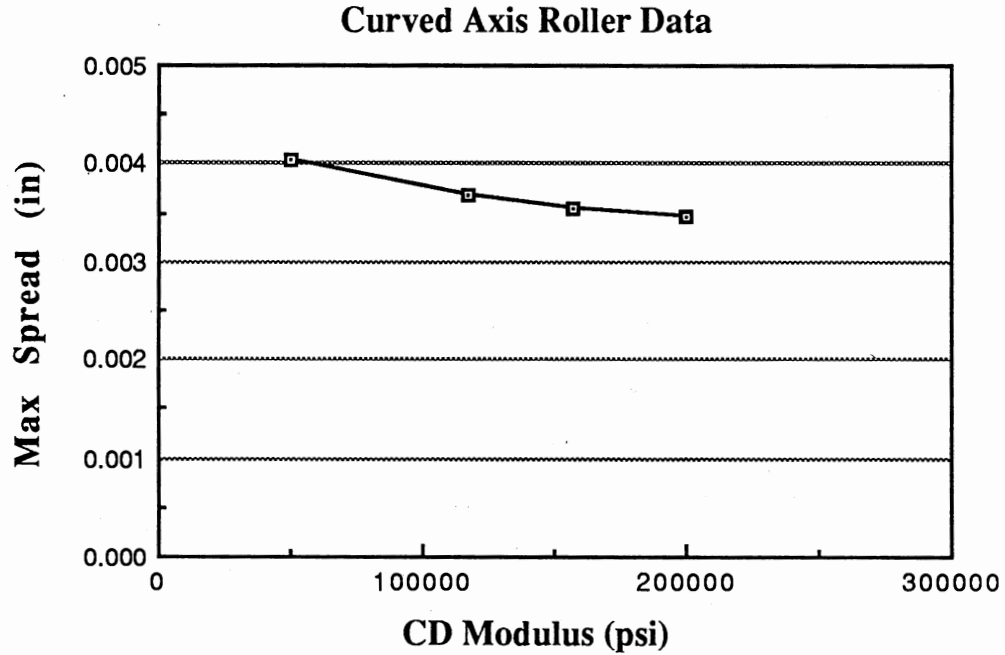
Figure 6-37.   Curved Axis Roller - Spread vs. CD
Modulus

Curved Axis Roller Data
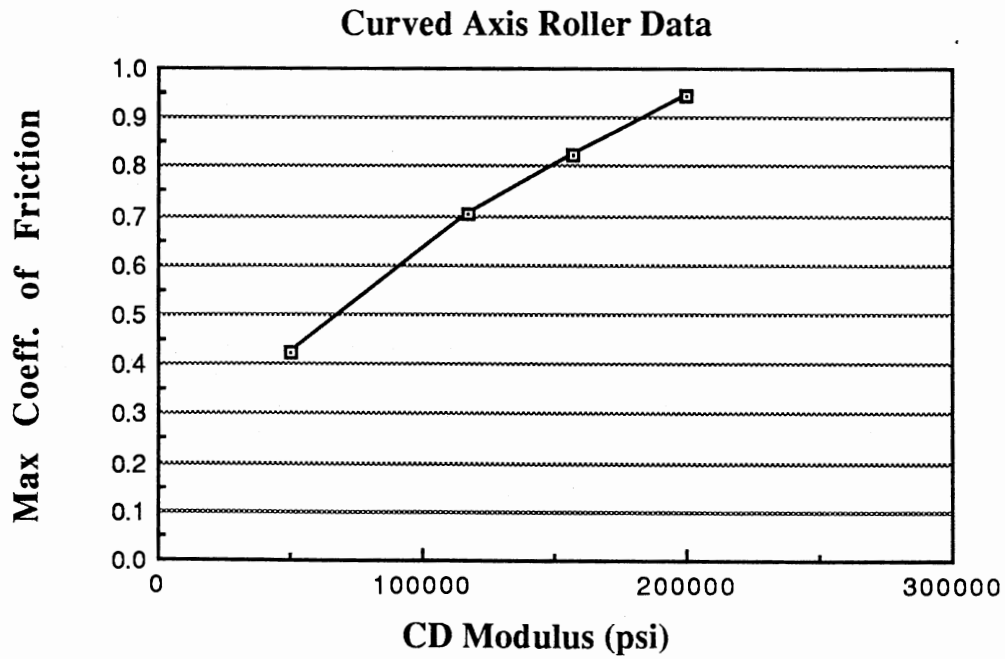
Figure 6-38.   Curved Axis Roller - Friction vs. CD
Modulus
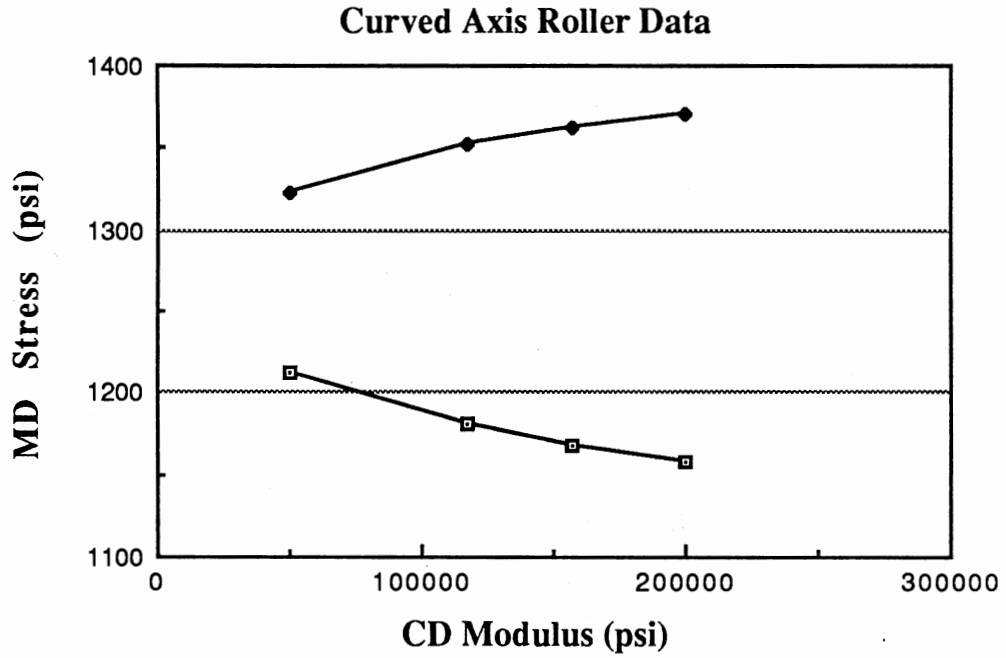
Figure 6-39. Curved Axis Roller - MD Stress vs. CD Modulus
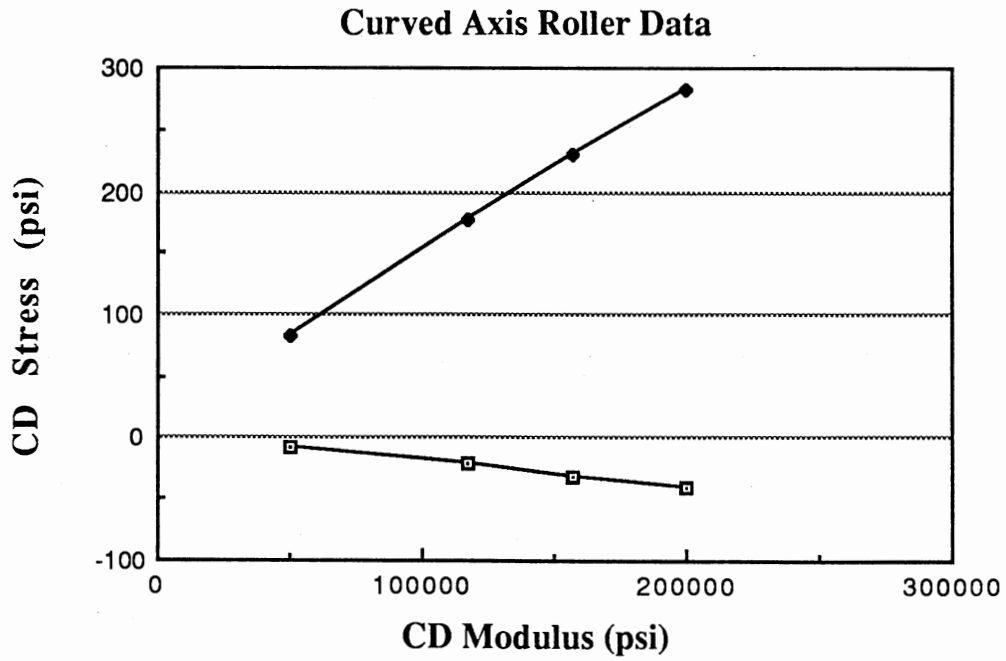
Figure 6-40. Curved Axis Roller - CD Stress vs. CD Modulus

The CD stress curves for the curved axis roller also parallel the friction curve. There is a large increase in the max CD stress as the CD modulus increases. For constant spreading, increasing the CD modulus requires higher spreading forces and therefore higher CD stresses. The min CD stress curve shows only a small decrease.

Machine Direction Poisson's Ratio

Figures 6-41 through 6-44 show the effects of cross machine direction modulus on the concave roller, and figures 6-45 through 6-48 show the effects of CD modulus on the curved axis roller. Of all the parameters used as input to the model, Poisson's ratio has the least effect on the behavior of the systems.

The concave roller shows a small decrease in spreading and friction with increasing Poisson's ratio. The MD stress curves are almost perfectly flat. The CD stress curve shows a small increase for increasing Poisson's ratio. The largest and most surprising effect is a moderate decrease (larger negative value) in the min CD stress.

The curved axis roller curves show even smaller variations for variations in Poisson's ratio. All of the curves are flat with the friction curve being the only exception. It shows a small decrease in the required friction.

Concave Roller Data
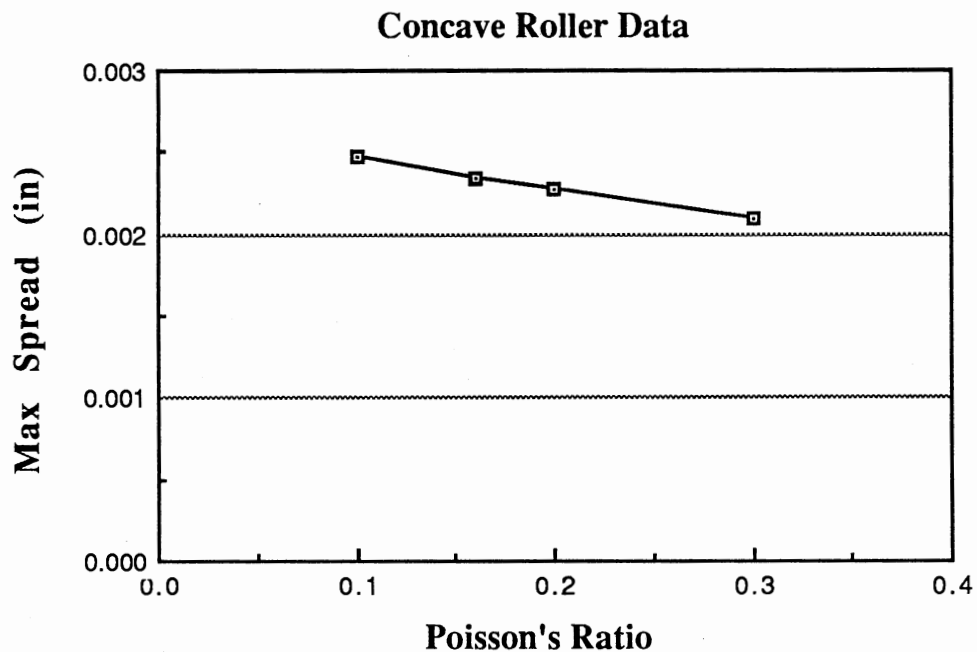
Figure 6-41. Concave Roller - Spread vs. Poisson's
Ratio

Concave Roller Data
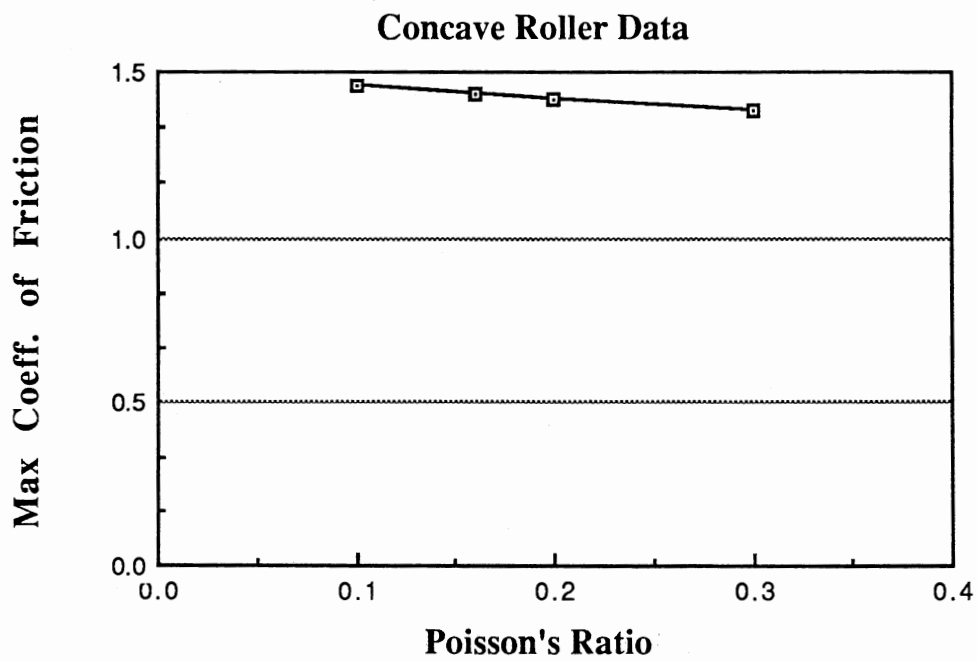
Figure 6-42. Concave Roller - Friction vs. Poisson's
Ratio

Concave Roller Data
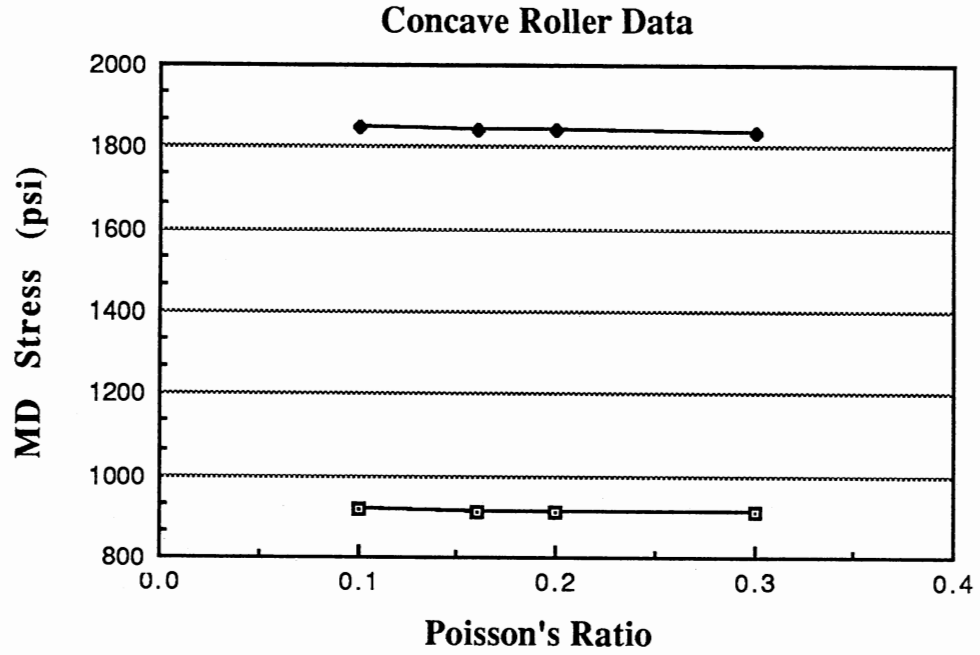
Figure 6-43.   Concave Roller - MD Stress vs.
Poisson's Ratio

Concave Roller Data
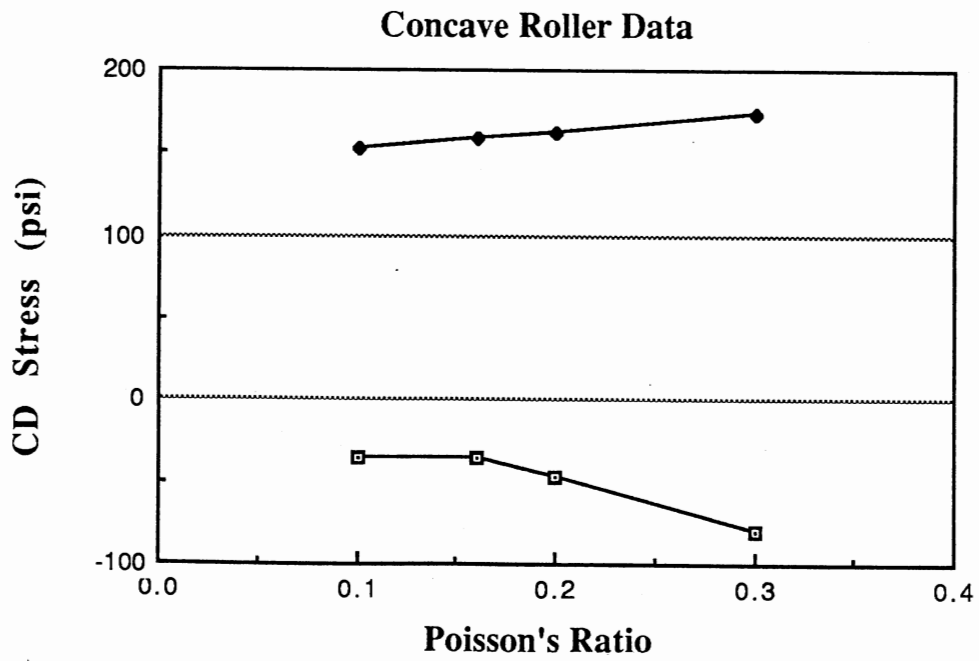
Figure 6-44.   Concave Roller - CD Stress vs.
Poisson's Ratio

Curved Axis Roller Data
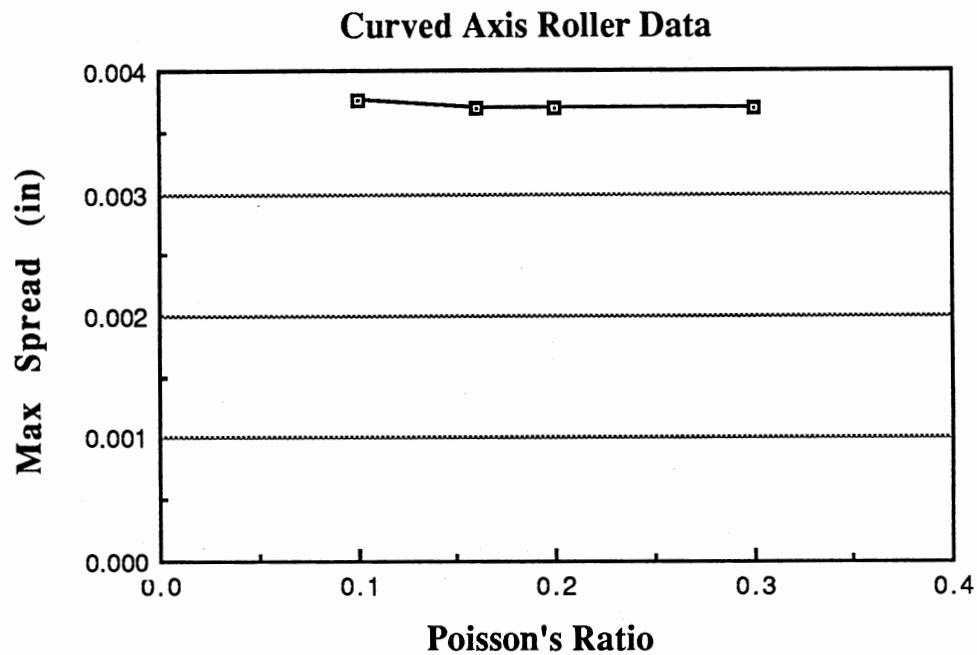
Figure 6-45.   Curved Axis Roller - Spread vs.
Poisson's Ratio

Curved Axis Roller Data
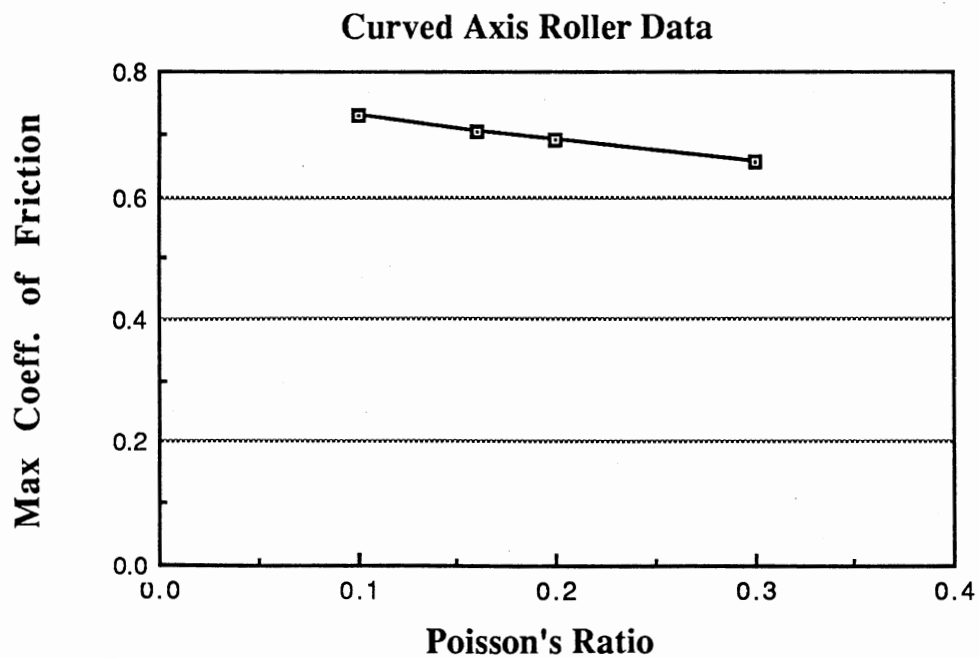
Figure 6-46.   Curved Axis Roller - Friction vs.
Poisson's Ratio

Curved Axis Roller Data
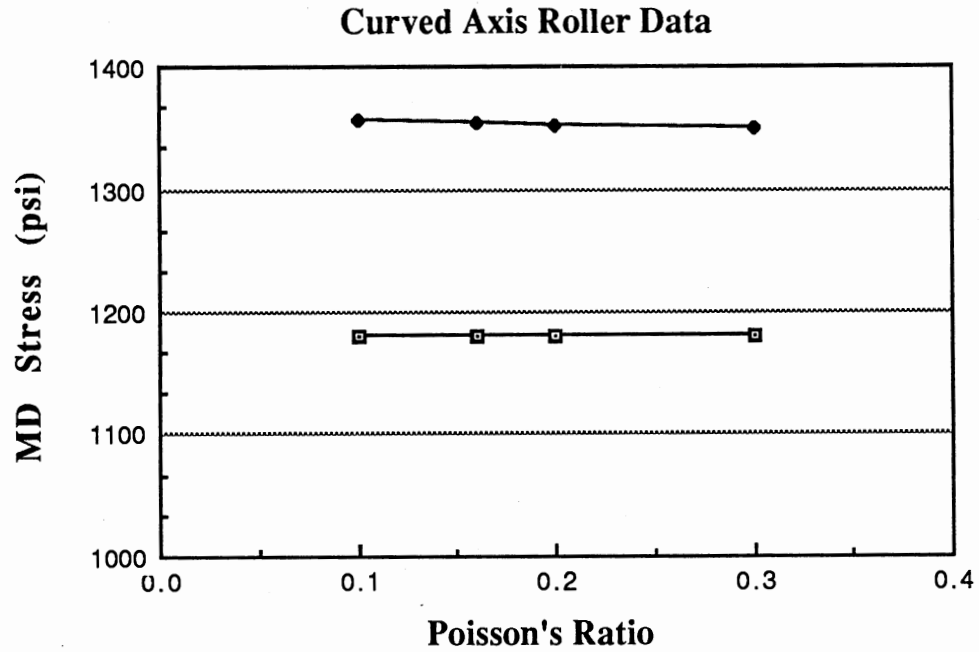
Figure 6-47.   Curved Axis Roller - MD Stress vs.
Poisson's Ratio

Curved Axis Roller Data
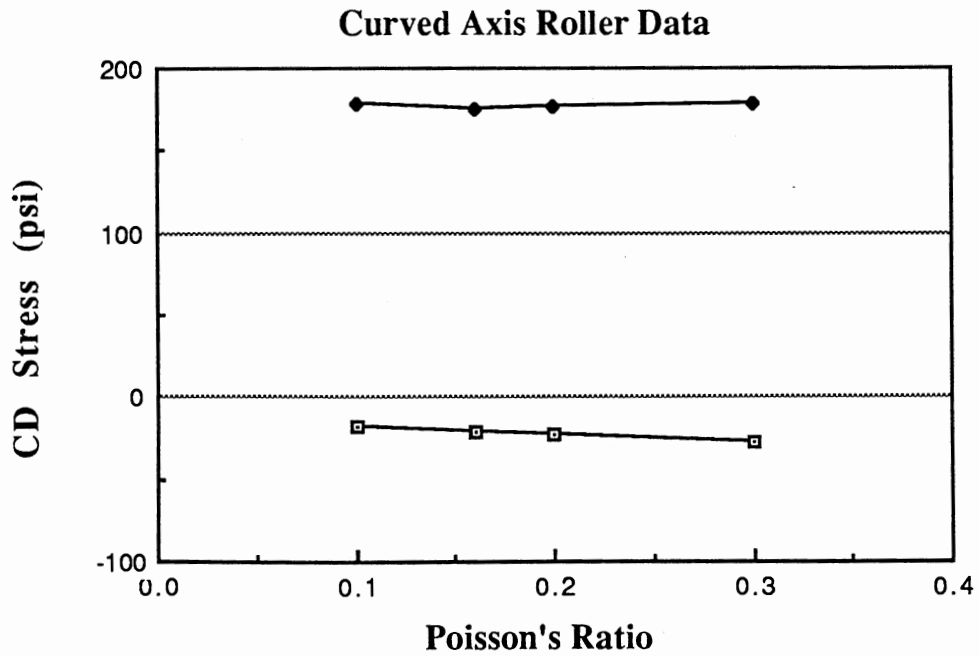
Figure 6-48.   Curved Axis Roller - CD Stress vs.
Poisson's Ratio

Web Width

Figures 6-49 through 6-52 show the effects of web width on the concave roller, and figures 6-53 through 6-56 show the effects of web width on the curved axis roller. All of the curves for both of the rollers show that the web width is a very significant parameter. This occurs with both rollers for the same reason. The only significance of having a wider web is that the edge of the web is interacting with the more extreme portion of the roller. The outer edge of the concave roller has both the largest diameter, and the largest rate of change in diameter. Likewise, the outer edge of the curved axis has the largest outward facing velocity vector components, and they have the largest rate of increase. Therefore, the contribution of web width to the behavior of these systems is due primarily to geometry of the roller with which it is able to interact, and not to the elastic behavior of a wider web.

For both types of rollers, the curves for max spread and max friction show a rapid increase with increasing web width. The concave roller shows twice as much spreading, and five times as much friction as the concave roller. For a 12 inch wide web, and the other base parameter values, the concave roller requires a coefficient of friction of five. This is clearly an unrealistic value. This says that the combination of roller curvature and web width must be chosen carefully so that the available friction is not exceeded.

For both rollers, the curves for max spread and max friction approach zero as the web width approaches zero. The drop is much faster for the concave roller, than for the curved axis roller.

Concave Roller Data
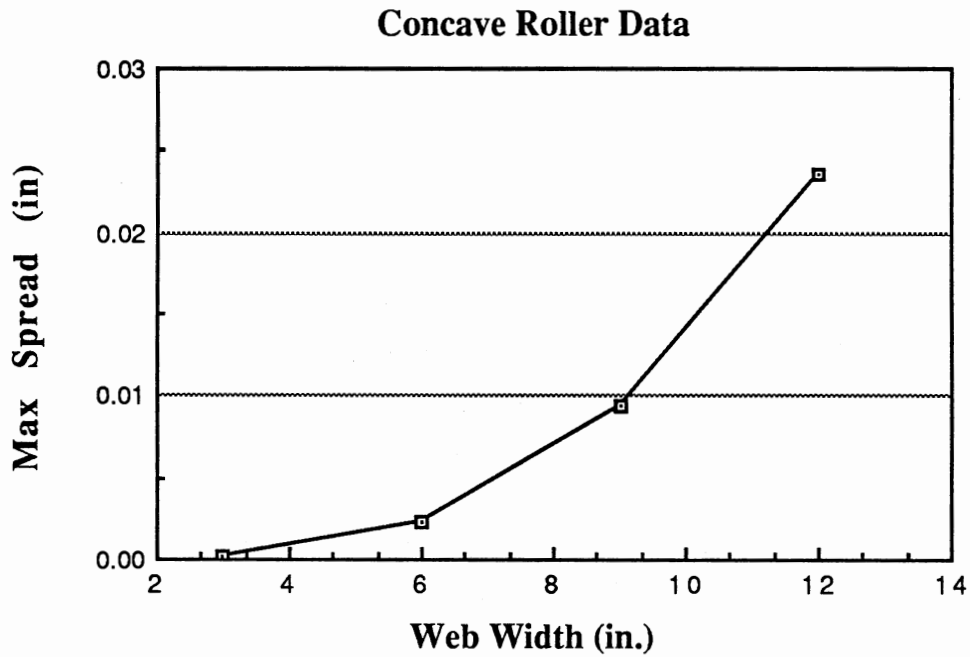
Figure 6-49.   Concave Roller - Spread vs. Web
Width

Concave Roller Data
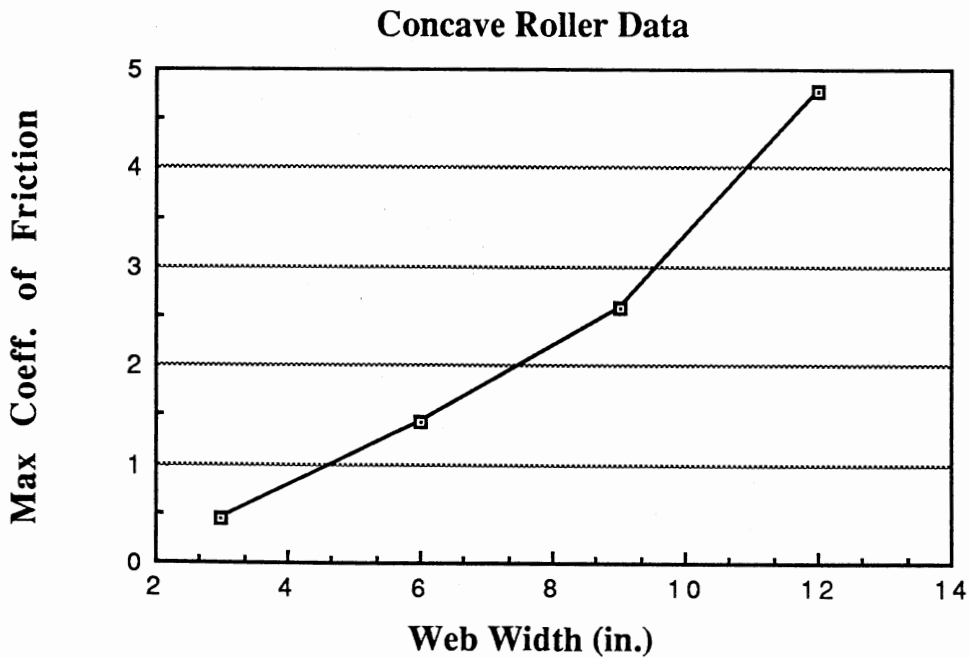
Figure 6-50.   Concave Roller - Friction vs. Web
Width

Concave Roller Data
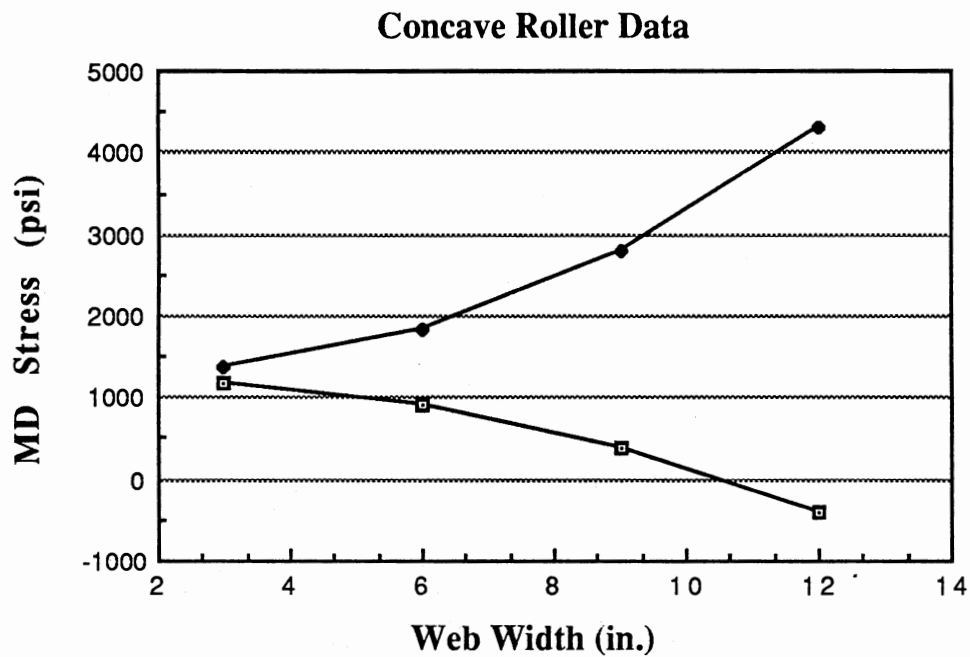
Figure 6-51.   Concave Roller - MD Stress vs. Web Width

Concave Roller Data
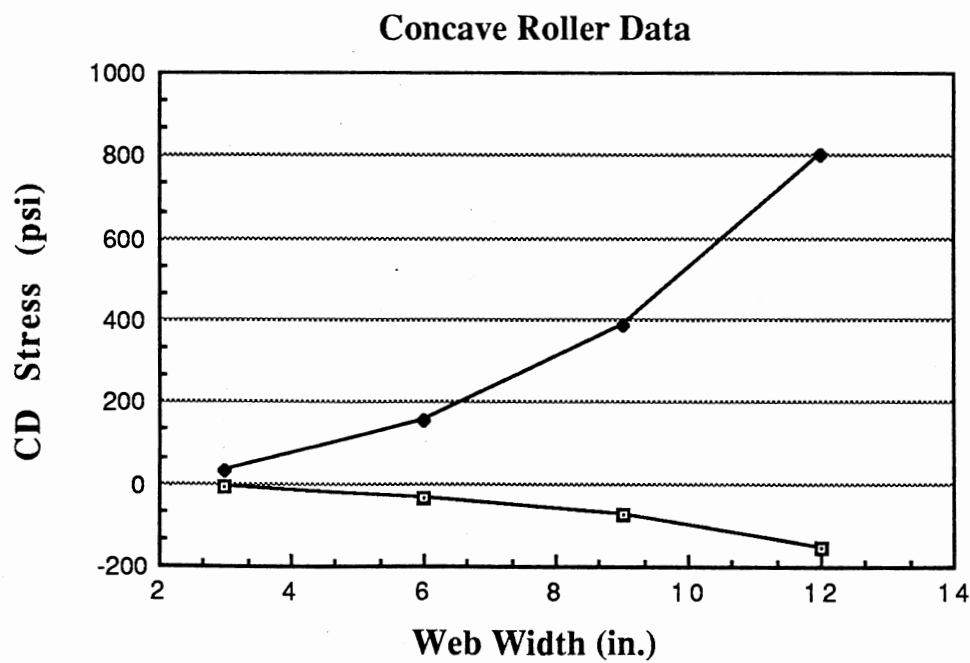
Figure 6-52.   Concave Roller - CD Stress vs. Web Width

Curved Axis Roller Data
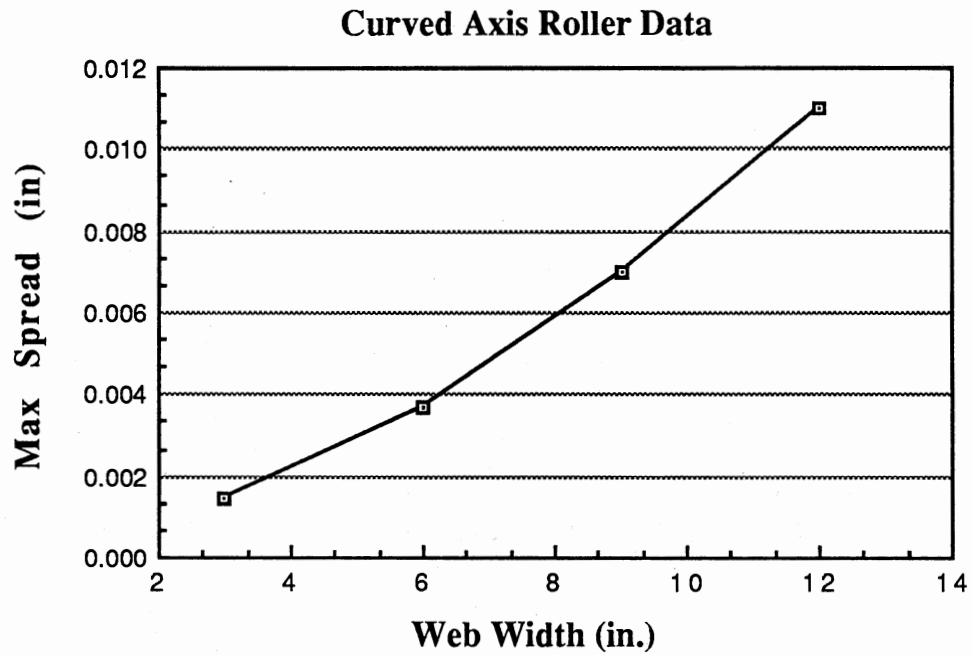
Figure 6-53. Curved Axis Roller - Spread vs. Web Width

Curved Axis Roller Data
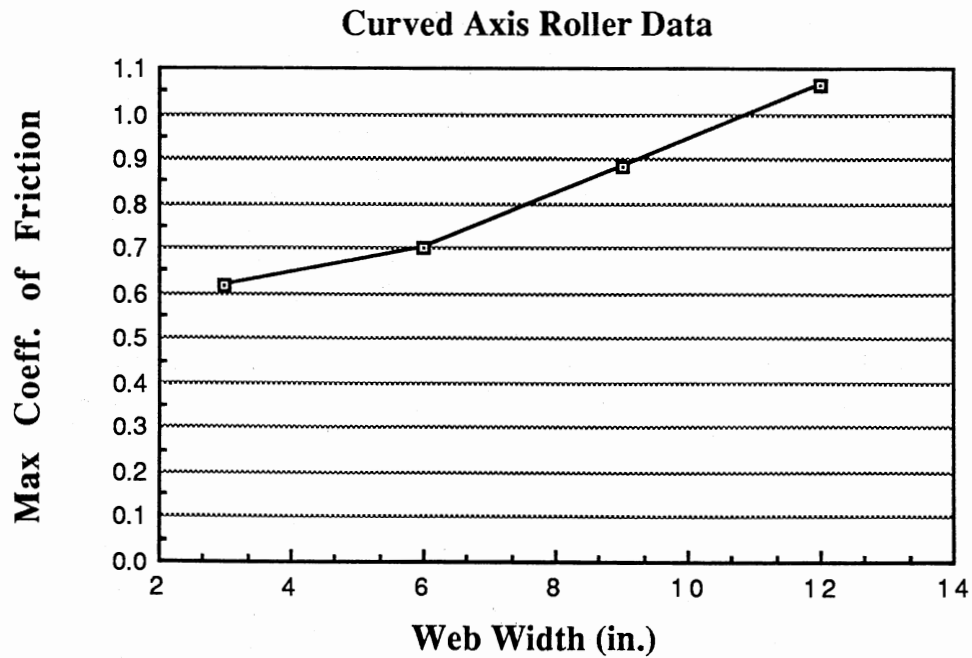
Figure 6-54. Curved Axis Roller - Friction vs. Web Width

Curved Axis Roller Data
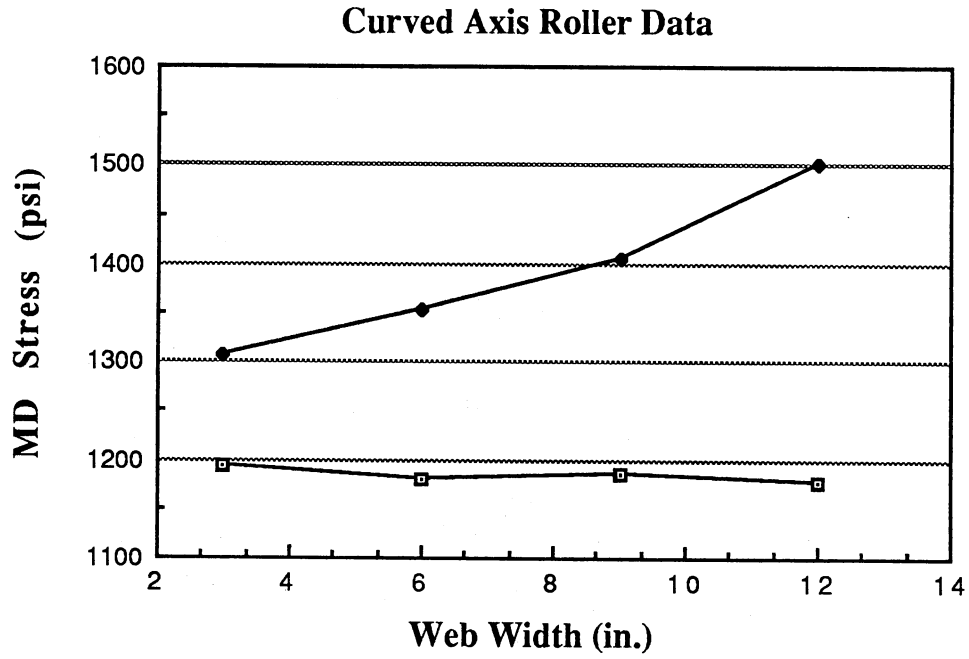
Figure 6-55.   Curved Axis Roller - MD Stress vs. Web Width

Curved Axis Roller Data
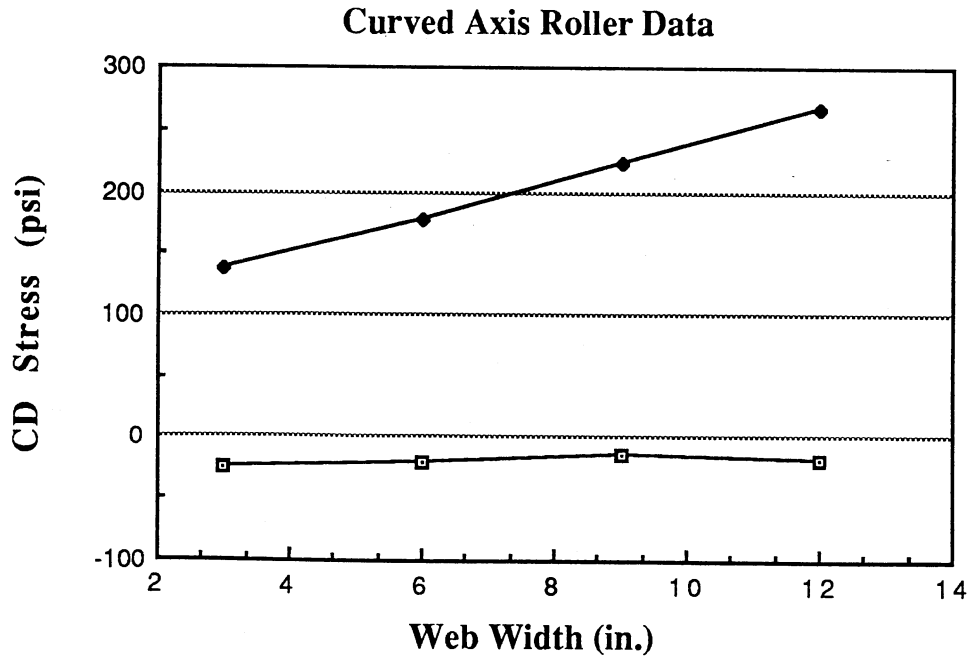
Figure 6-56.   Curved Axis Roller - CD Stress vs. Web Width

The stress curves for the concave roller also show extreme variations for variations in the web width. For the base parameters used, doubling the web width changes the max and min MD and CD stresses by a factor of three or four. Although an unrealistic amount of friction would be required to induce these stresses, these curves show that care must be taken in sizing the web-roller system so that the web material is not damaged.

Line Tension

Figures 6-57 through 6-60 show the effects of line tension on the concave roller, and figures 6-61 through 6-64 show the effects of line tension on the curved axis roller. The behavior of both rollers is nearly identical, and very predictable.

For both rollers, the max spread curves show no variation in spreading for variations in line tension. For the concave roller, it is the variation in the MD tensile forces that cause spreading, and not the absolute magnitude of those forces. For the curved axis roller, the cross machine direction parameters are of primary significance, while the machine direction parameters are of very little significance in spreading the web.

Concave Roller Data
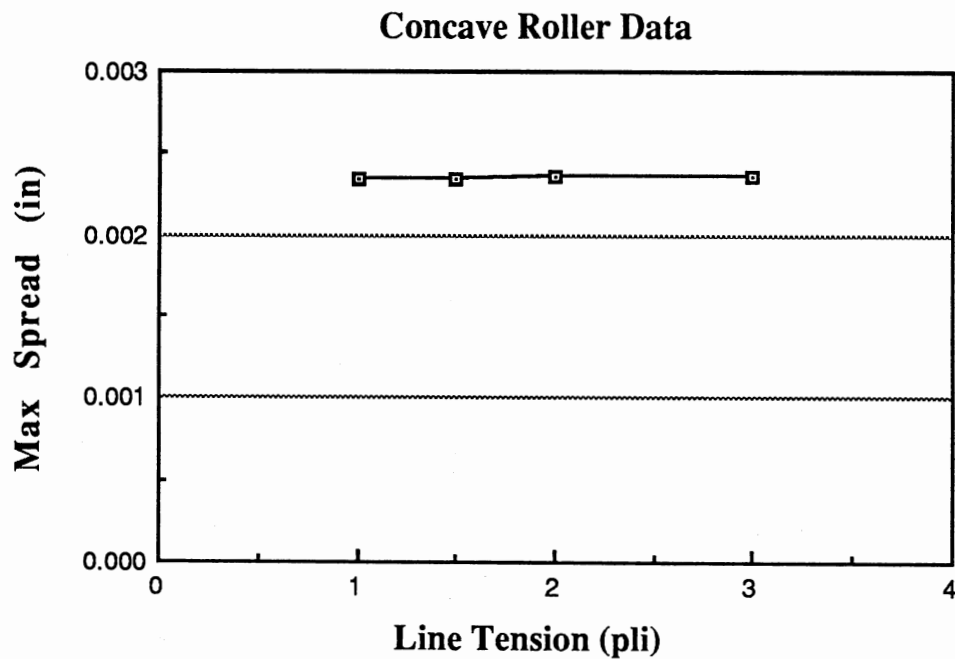
Figure 6-57.   Concave Roller - Spread vs. Line Tension

Concave Roller Data
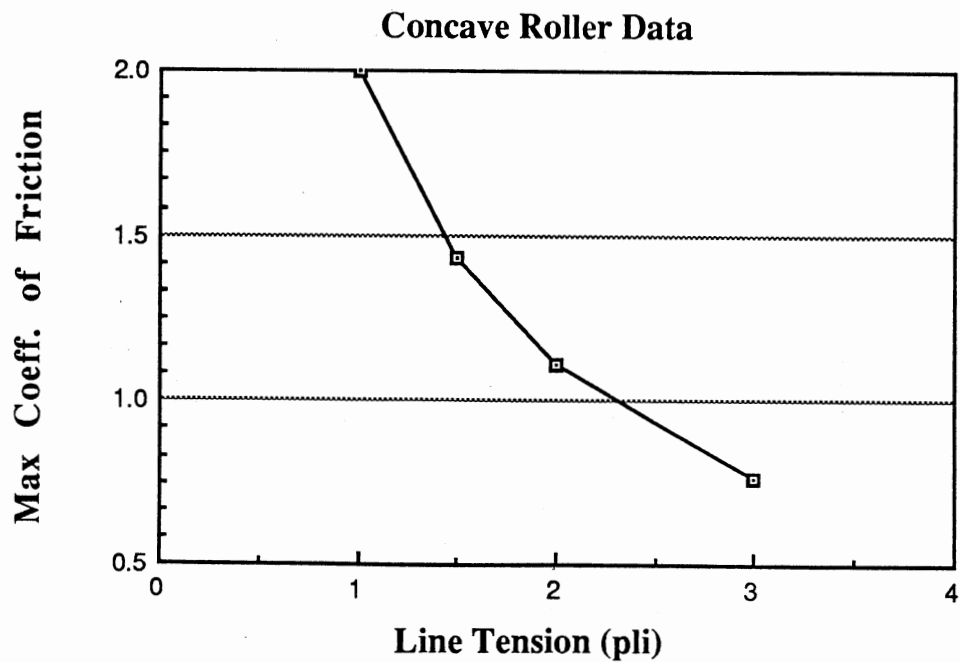
Figure 6-58.   Concave Roller - Friction vs. Line Tension

Concave Roller Data
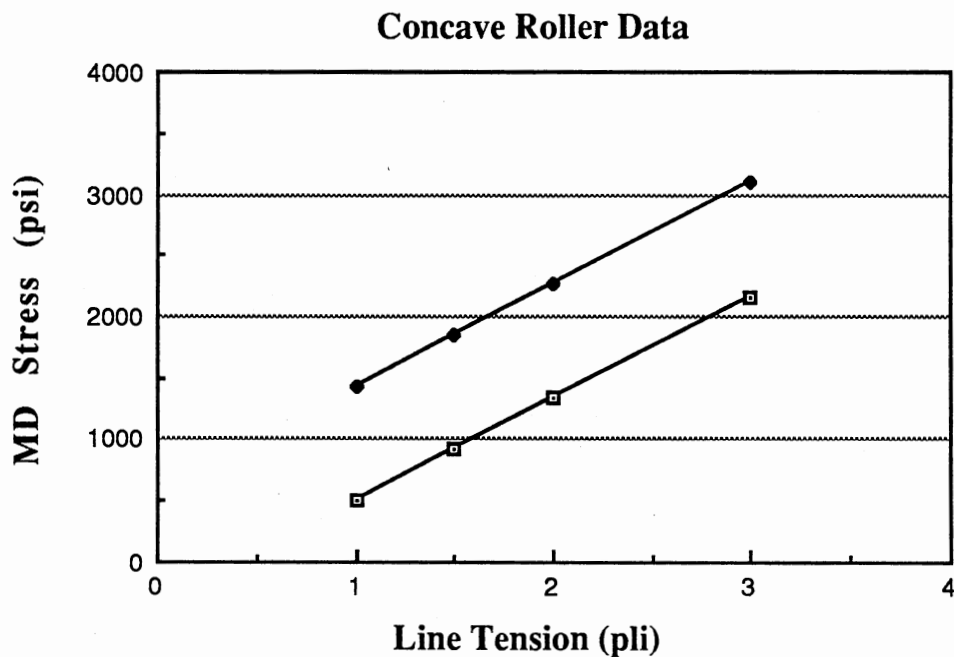
Figure 6-59. Concave Roller - MD Stress vs. Line
Tension

Concave Roller Data
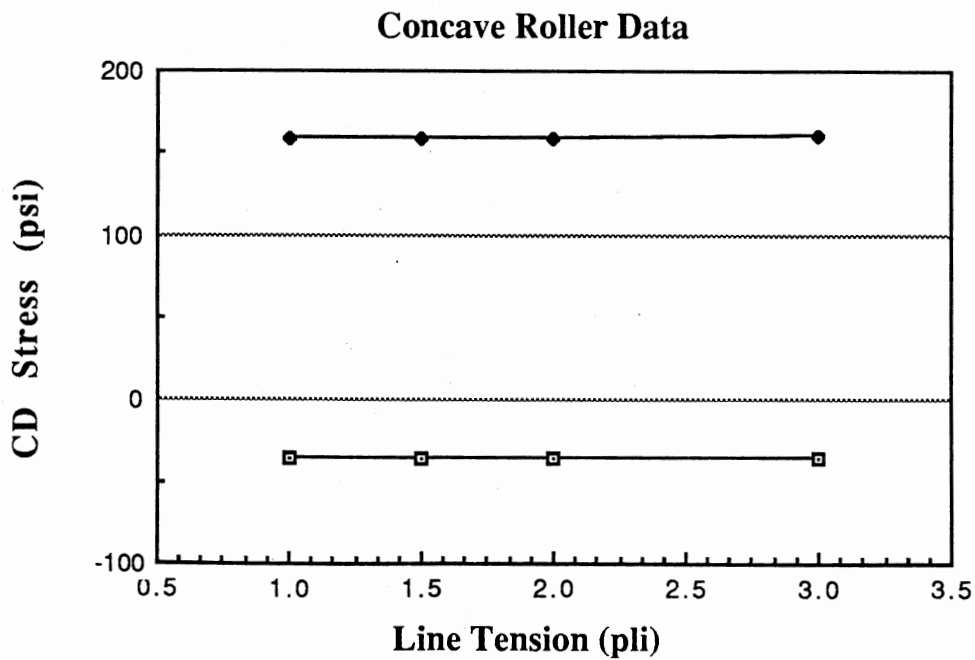
Figure 6-60. Concave Roller - CD Stress vs. Line
Tension

Curved Axis Roller Data
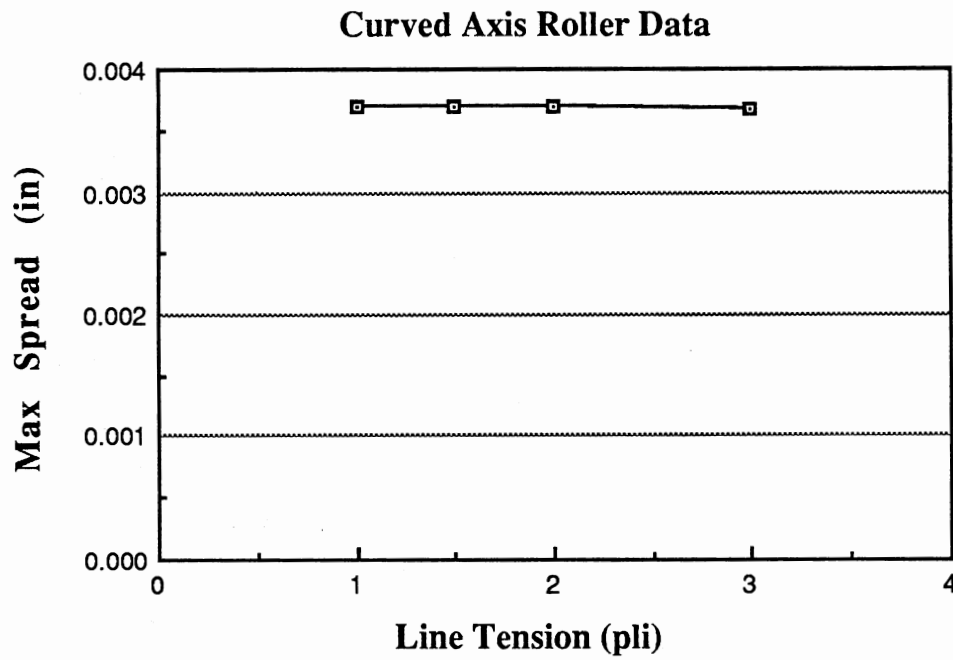
Figure 6-61.   Curved Axis Roller - Spread vs.
Line Tension

Curved Axis Roller Data
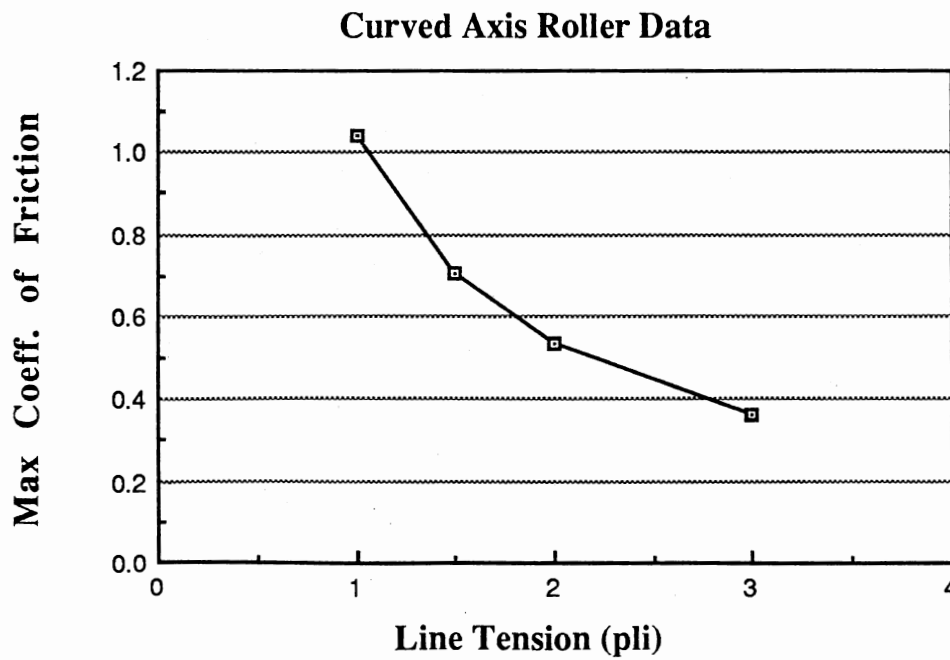
Figure 6-62.   Curved Axis Roller - Friction vs.
Line Tension

Curved Axis Roller Data
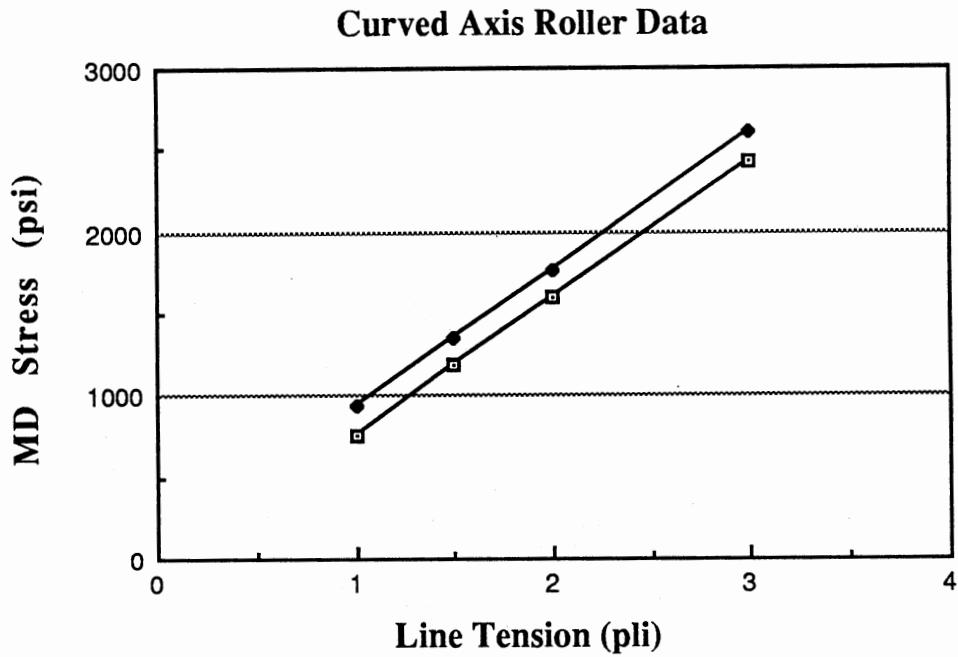
Figure 6-63. Curved Axis Roller - MD Stress vs.
Line Tension

Curved Axis Roller Data
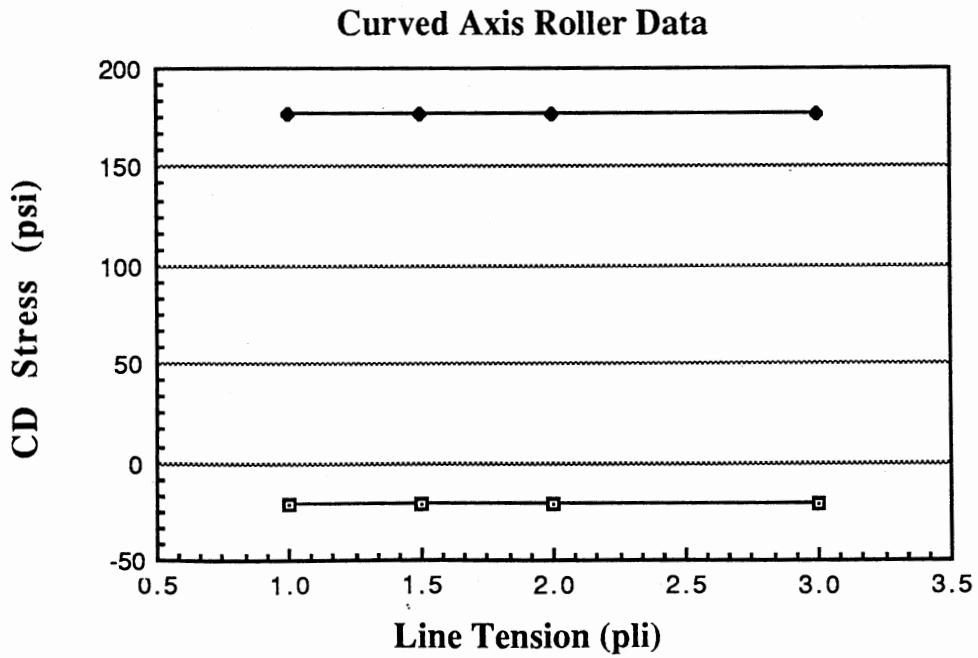
Figure 6-64. Curved Axis Roller - CD Stress vs.
Line Tension

While line tension has no effect on the amount that the web is spread, it has a tremendous effect of the coefficient of friction required to achieve that spreading. For constant web spreading displacements, the forces required to maintain that displacement remain constant. Increasing the line tension increases the normal force between the web and the roller. The ratio between the spreading (friction) forces and the normal forces therefore decreases as the line tension is increased.

The stress curves for both types of rollers show identical behavior in response to varying line tension. Both the max and min MD stresses increase linearly with increasing line tension, and the max and min curves remain a fixed distance apart. This shows that the line tension effects only the average value of MD stress, and has no effect on the MD stress variation. In addition, the max and min MD stress curves have slopes that would yield an average stress of zero for zero line tension, precisely as would be expected.

Both the max and min CD stress curves for both types of rollers are perfectly flat.

Roller Base Radius

Figures 6-65 through 6-68 show the effects of roller base radius on the concave roller, and figures 6-69 through 6-72 show the effects of roller base radius on the curved axis roller. The effects of roller radius on the behavior of the two types of rollers are entirely different.

Concave Roller Data
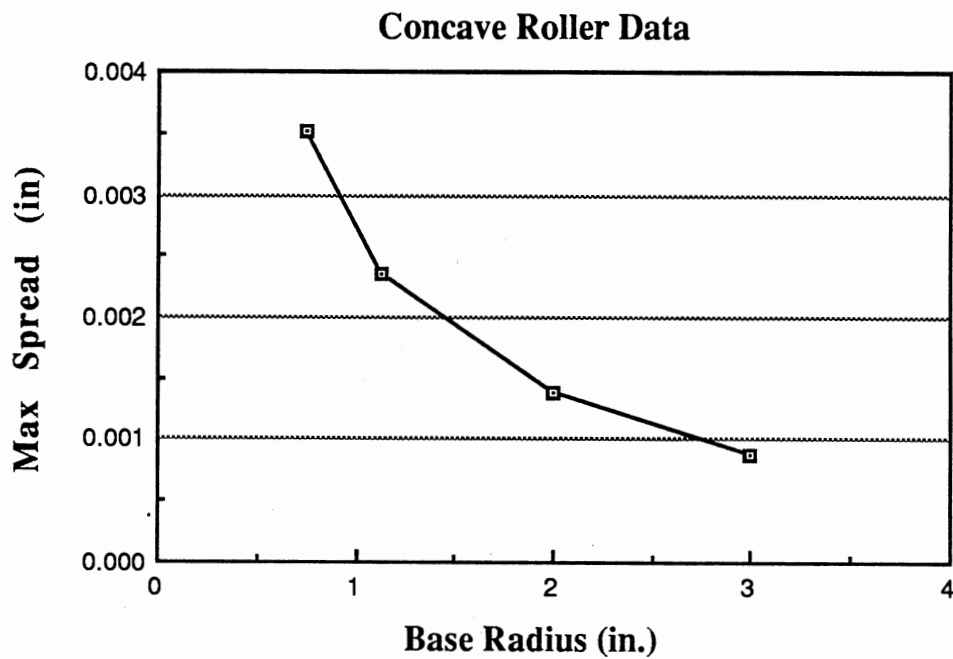
Figure 6-65.   Concave Roller - Spread vs. Base
Radius

Concave Roller Data
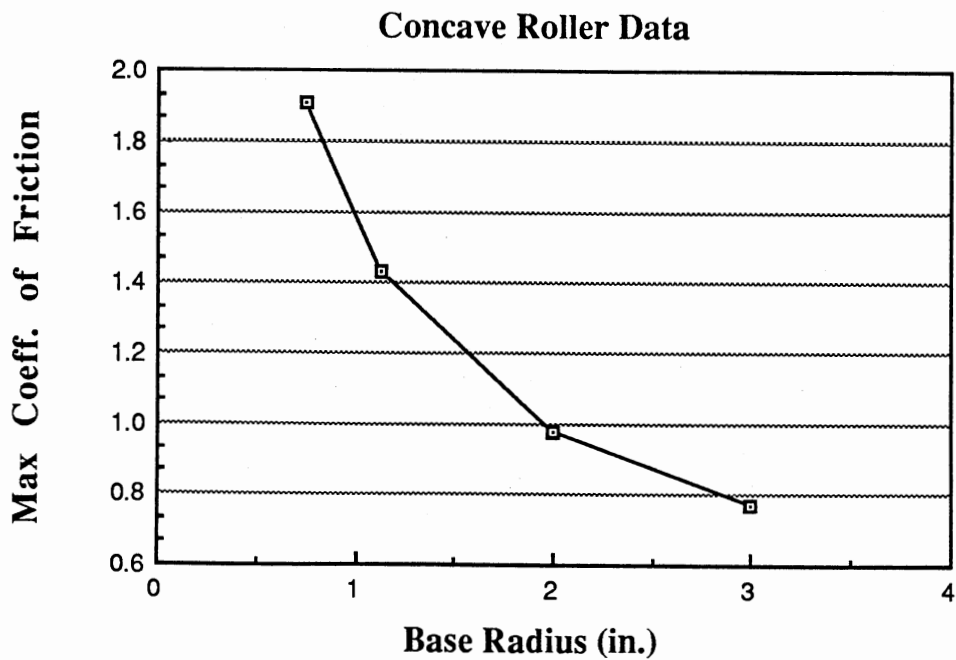
Figure 6-66.   Concave Roller - Friction vs. Base
Radius

Concave Roller Data
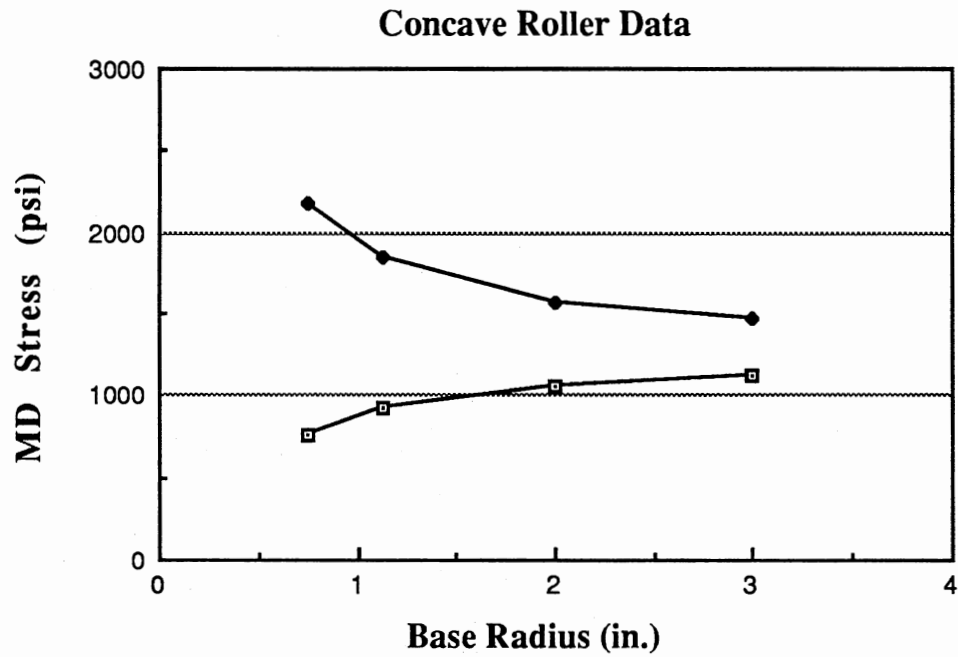
Figure 6-67. Concave Roller - MD Stress vs. Base
Radius

Concave Roller Data
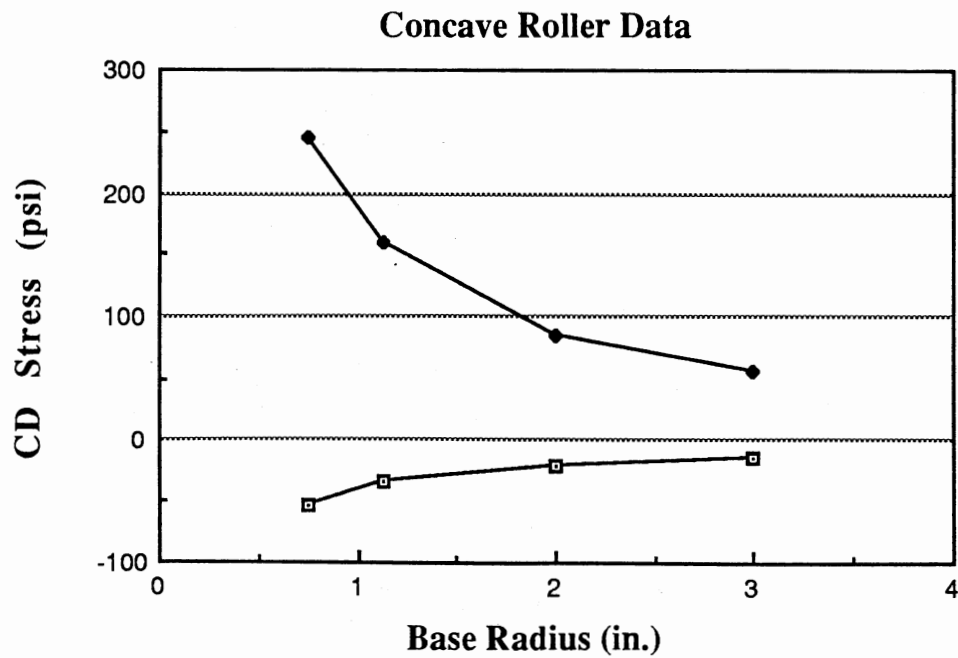
Figure 6-68. Concave Roller - CD Stress vs. Base
Radius

Curved Axis Roller Data
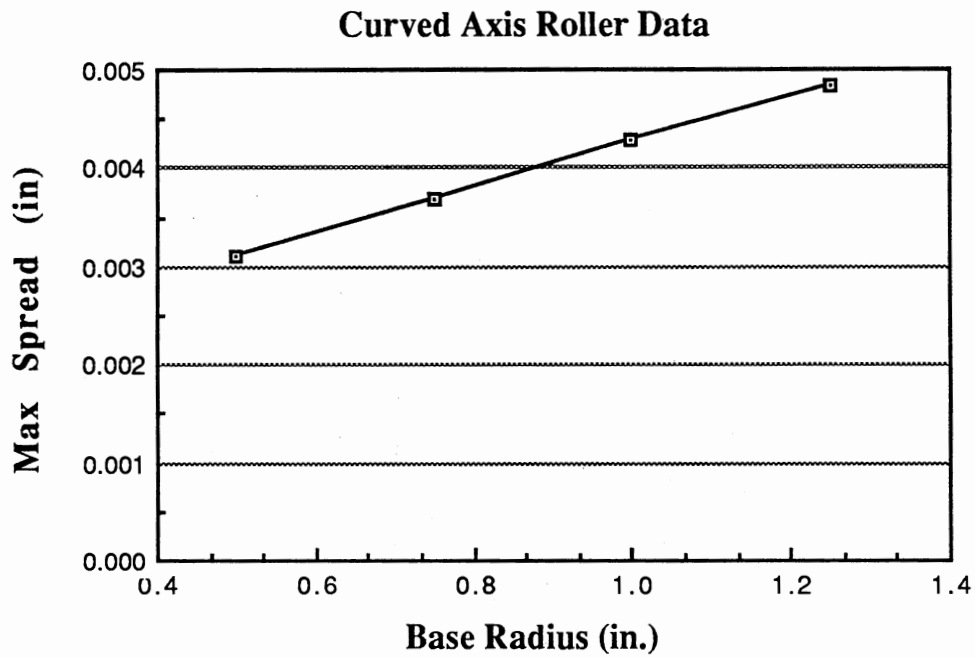
Figure 6-69. Curved Axis Roller - Spread vs. Base Radius

Curved Axis Roller Data
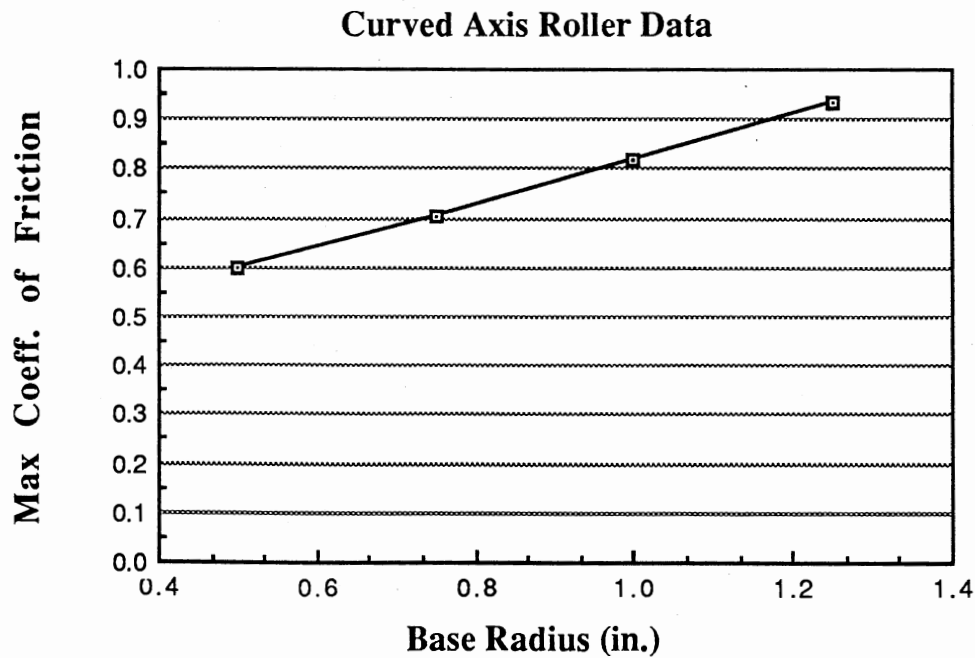
Figure 6-70. Curved Axis Roller - Friction vs. Base Radius
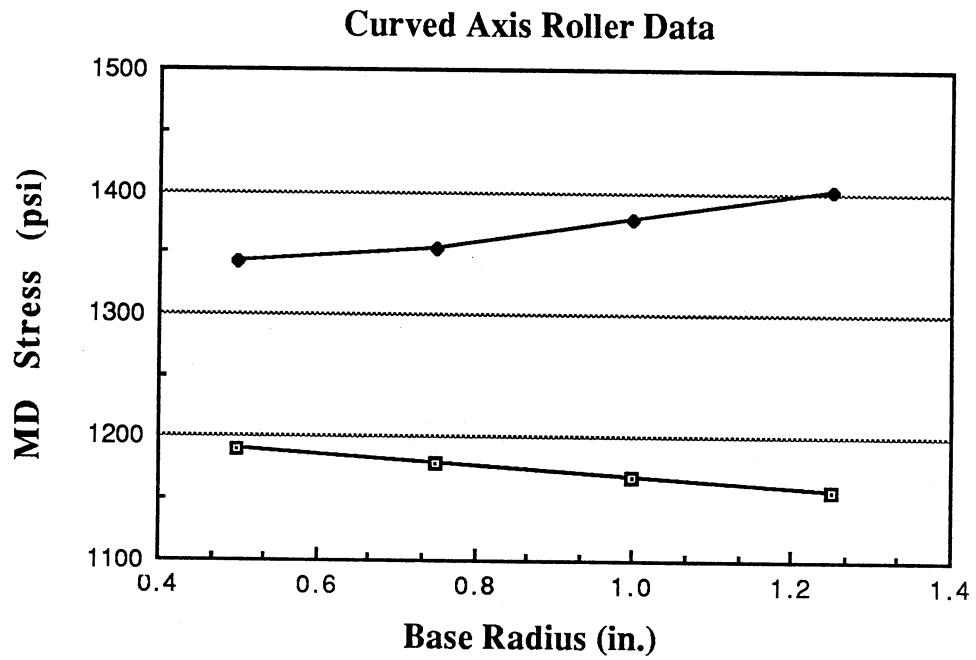
Figure 6-71. Curved Axis Roller - MD Stress vs.
Base Radius
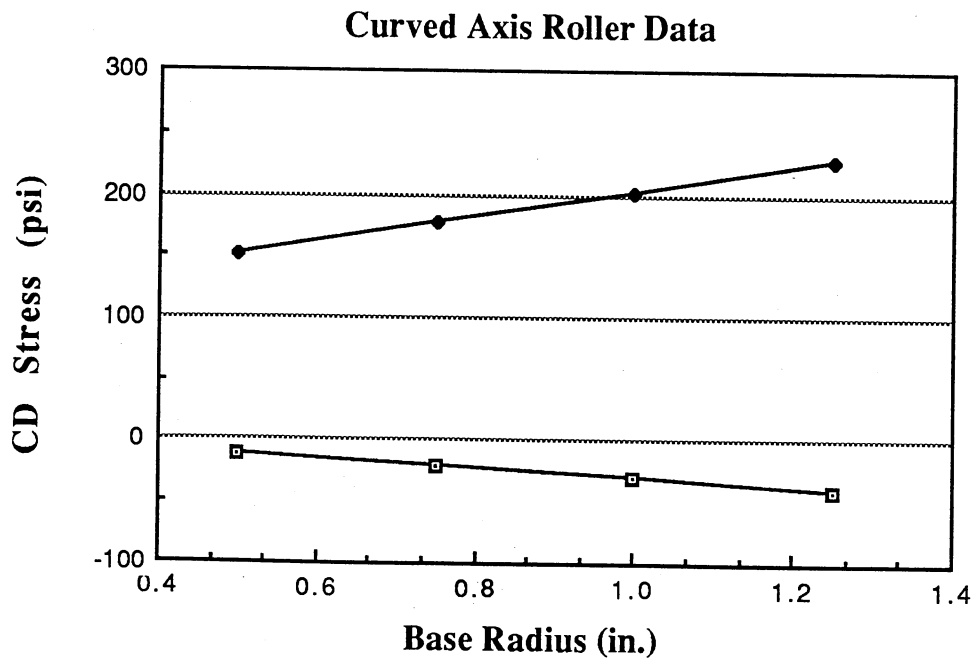
Figure 6-72. Curved Axis Roller - CD Stress vs.
Base Radius

For the concave roller, the primary spreading mechanism is related to the MD stress-strain distribution. With the no slippage between the web and the roller, the MD strain profile is related to the diameter ratio profile of the roller (diameter at a point divided by the average diameter). There are two significant roller dimensions that make up the diameter ratio profile, the average (base) roller radius, and the roller profile radius of curvature (which causes the roller to be non-cylindrical). For reference, a cylindrical roller has an infinite roller profile radius of curvature. For a given roller radius of curvature, a roller with a small average diameter will have a larger diameter ratio variation, than that of a roller with a large average diameter. Therefore, for a concave roller, reducing the roller base radius has the same effect as reducing the roller profile radius of curvature. Both of these cause larger MD strain variations.

The max spread curve for the concave roller shows a large amount of spreading for a small base radius, and a smaller amount of spreading for a larger base radius. The slope of the curve approaches infinity as the base radius approaches zero, while the slope of the curve approaches zero as the radius approaches infinity. This agrees with the conclusions of the previous paragraph.

The max friction curve is similar to the max spread curve for the concave roller. Rollers that produce large spreading deformations require large amounts of friction, while cylindrical rollers produce no spreading and require essentially no friction.

The stress curves for the concave roller show variations with base radius similar to the displacement and friction curves. Concave rollers that produce large spreading deformations produce large

positive max stresses and smaller (or more negative) min stresses in both the machine direction and the cross machine direction. For large values of roller base radius, the max and min MD stresses approach the same value, the nominal line tension. Similarly, the max and min CD stresses both approach zero.

The curved axis roller has a different spreading mechanism and therefore the curves have responses to variation in roller radius that differ from the concave roller. All points on the surface of the curved axis roller have the same velocity magnitude, but the velocity direction varies. The velocity magnitude is set by the web line speed and is independent of the roller radius. But, larger radius curved axis rollers magnify the effect of the outward components of the velocity vectors, and spread the web more than smaller rollers. This is shown in all of the curves for the curved axis roller.

The max spread curve shows a linear increase in spreading with increasing roller base radius. The max coefficient of friction curve shows a corresponding linear increase. The MD and CD stress curves show nearly linear increases in the maximum stresses, and decreases in the minimum stresses.

Roller Profile Radius of Curvature

Figures 6-73 through 6-76 show the effects of roller profile radius of curvature on the concave roller, and figures 6-77 through 6-80 show the effects of curvature on the curved axis roller. The roller radius of curvature is intuitively the most significant parameter for both types of roller. The roller curvature is the reason that both of these rollers spread the web. The amount of curvature

is the only thing that differentiates these rollers from simple cylindrical rollers. The curves show that the models produce results that match intuition.

For both types of rollers, the max spread and max friction curves show decreasing values with increasing radii of curvature. For both types of rollers, a radius of curvature of infinity produces a cylindrical roller. Thus, the behavior of these rollers should approach the behavior of a cylindrical roller as the radius of curvature approaches infinity. This behavior is shown by all of the curves for both the concave and the curved axis roller. For large radii, both the max spread and the max friction approach zero. In addition, both the max and the min MD stresses approach the nominal line tension, and the max and min CD stresses approach zero.

This behavior in the model lends additional credibility to the model. When a simple system is the limiting case for a more complex system, the model for the complex system should generate the theoretically correct response when the parameters of the simple limiting case are used.

Concave Roller Data
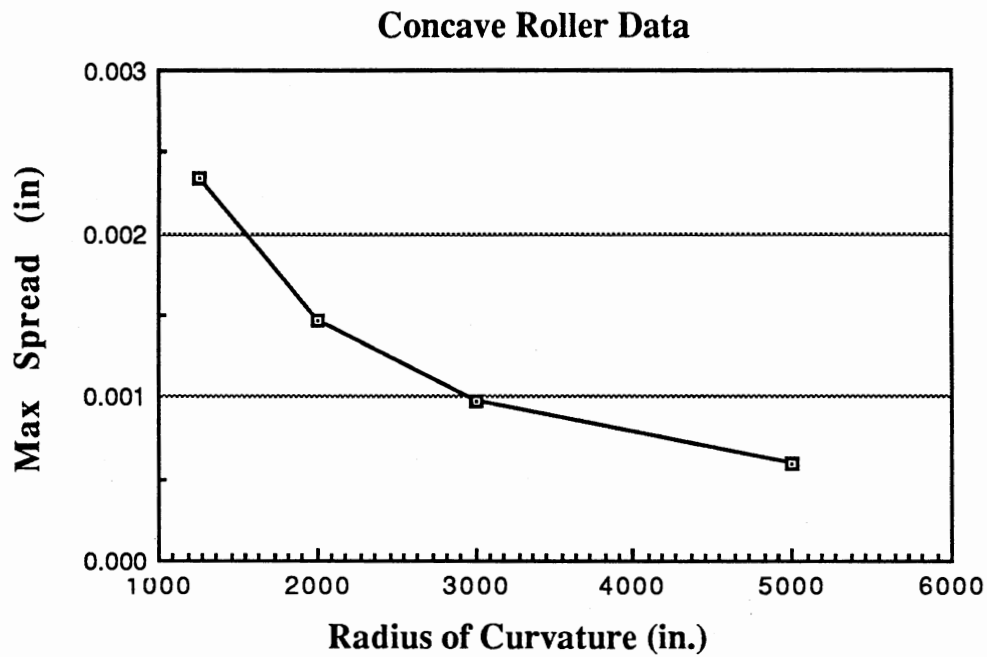
Figure 6-73.   Concave Roller - Spread vs. Radius of Curvature

Concave Roller Data
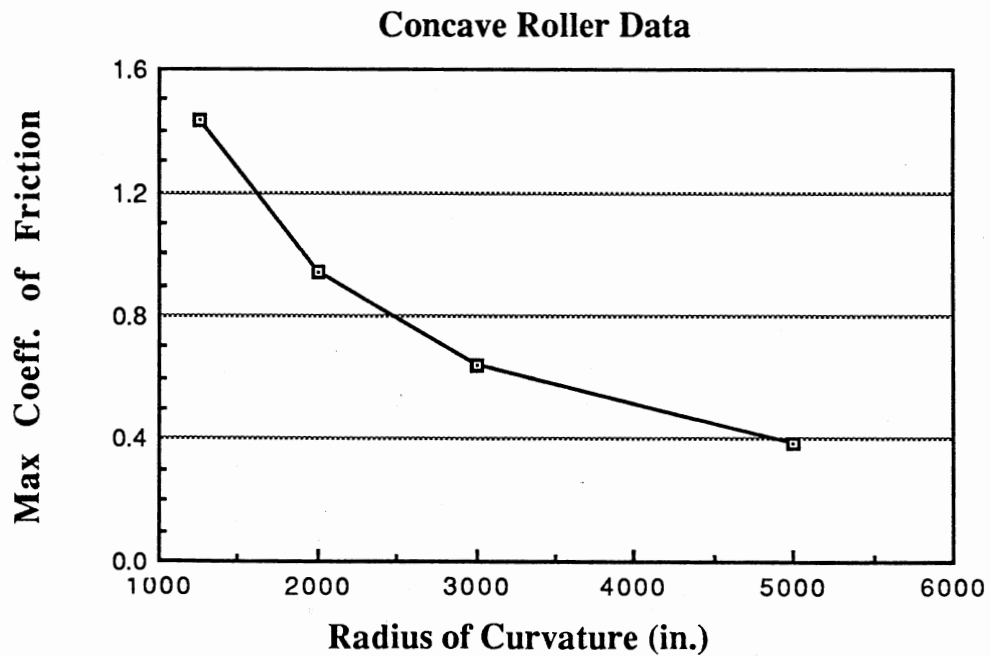
Figure 6-74.   Concave Roller - Friction vs. Radius of Curvature

Concave Roller Data
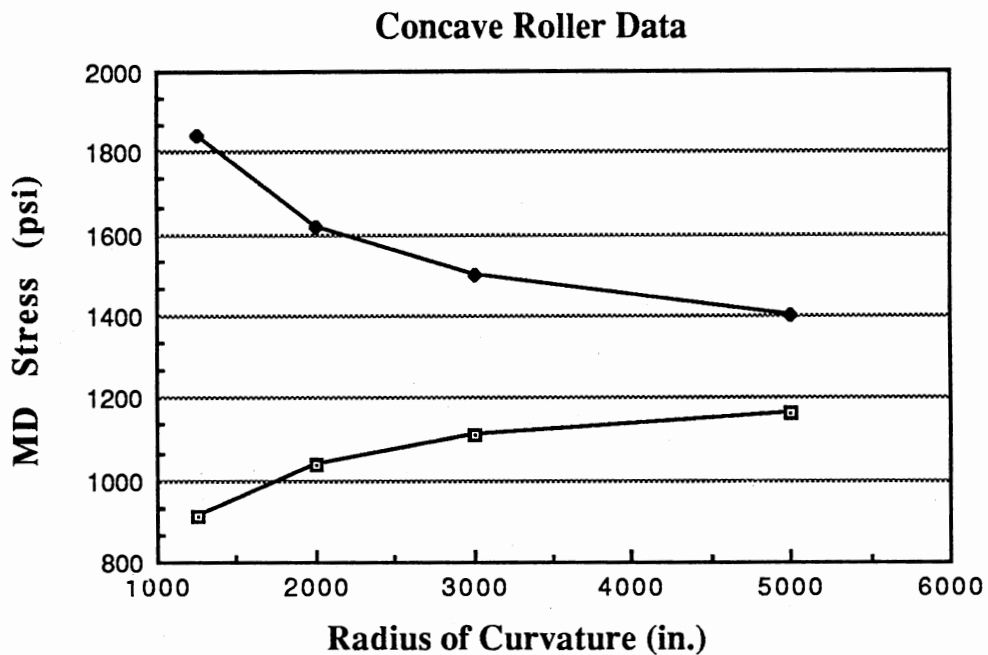
Figure 6-75.   Concave Roller - MD Stress vs. Radius
of Curvature

Concave Roller Data
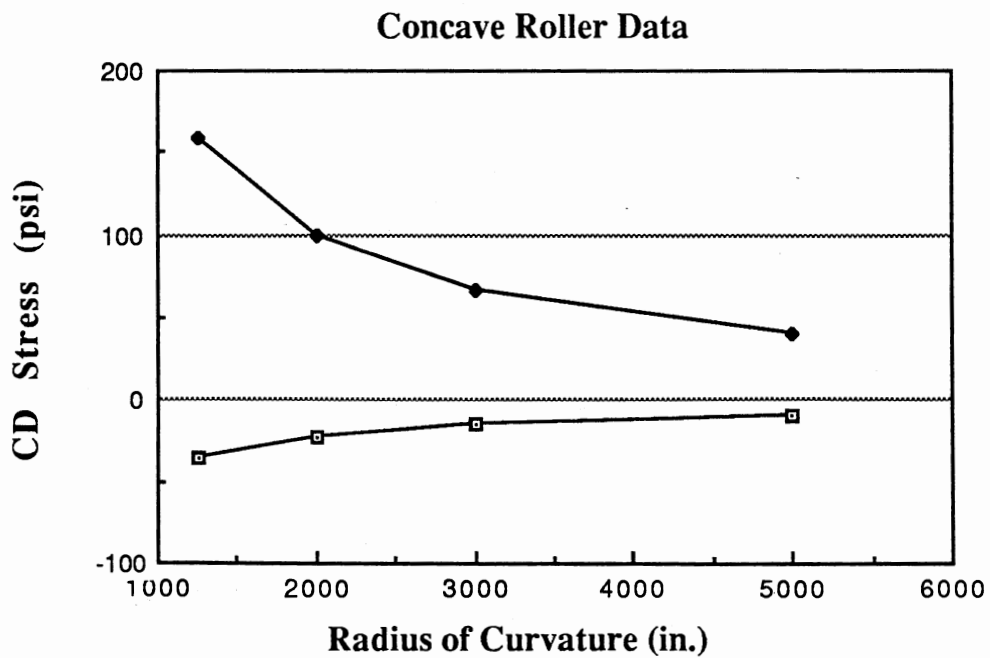
Figure 6-76.   Concave Roller - CD Stress vs. Radius of
Curvature

Curved Axis Roller Data
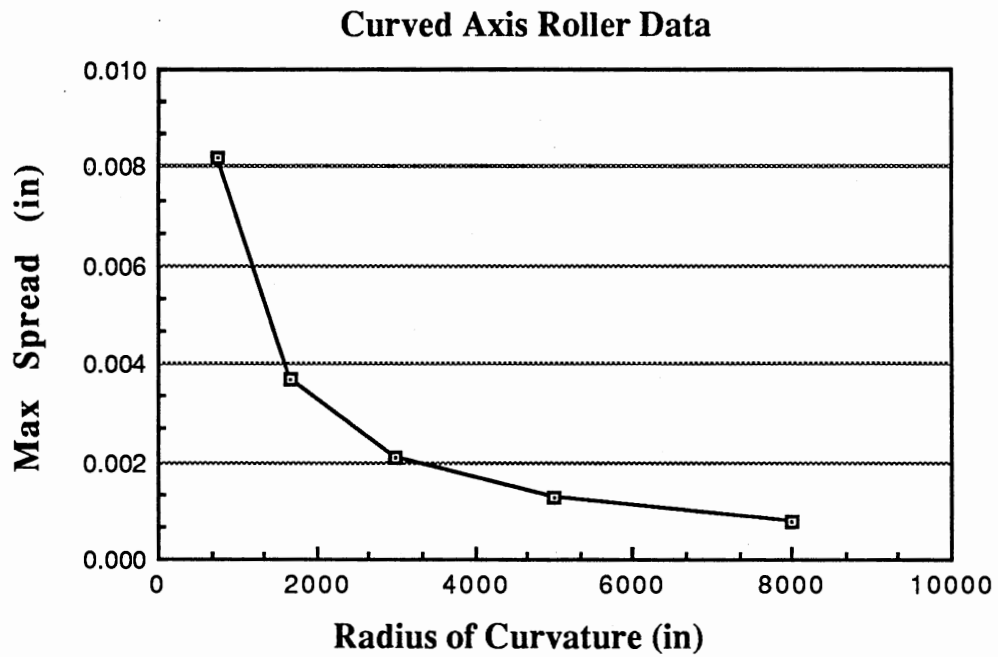
Figure 6-77. Curved Axis Roller - Spread vs. Radius
of Curvature

Curved Axis Roller Data
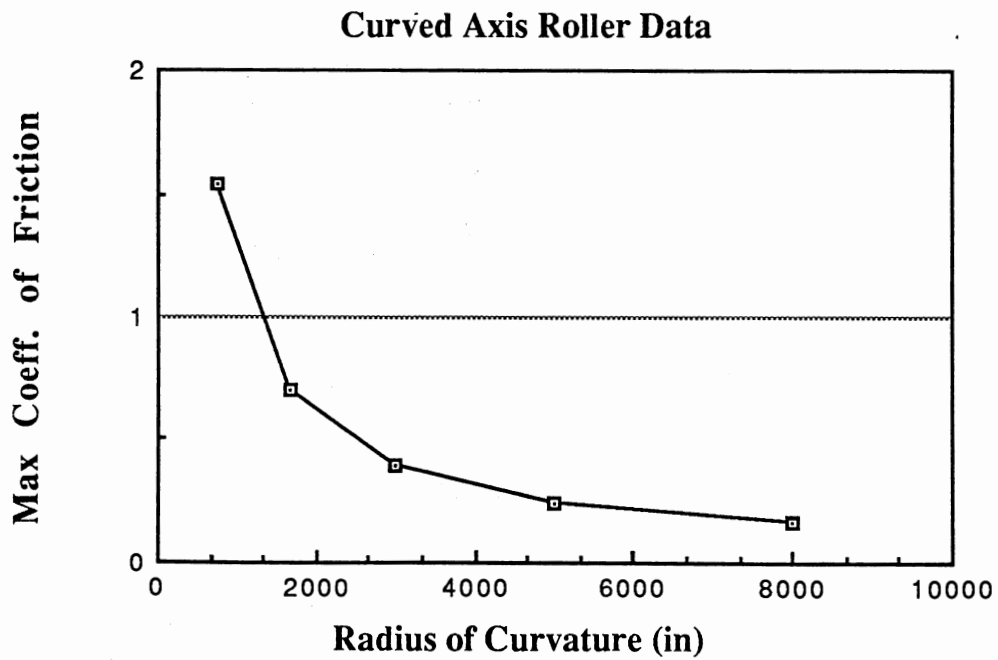
Figure 6-78. Curved Axis Roller - Friction vs. Radius
of Curvature

Curved Axis Roller Data
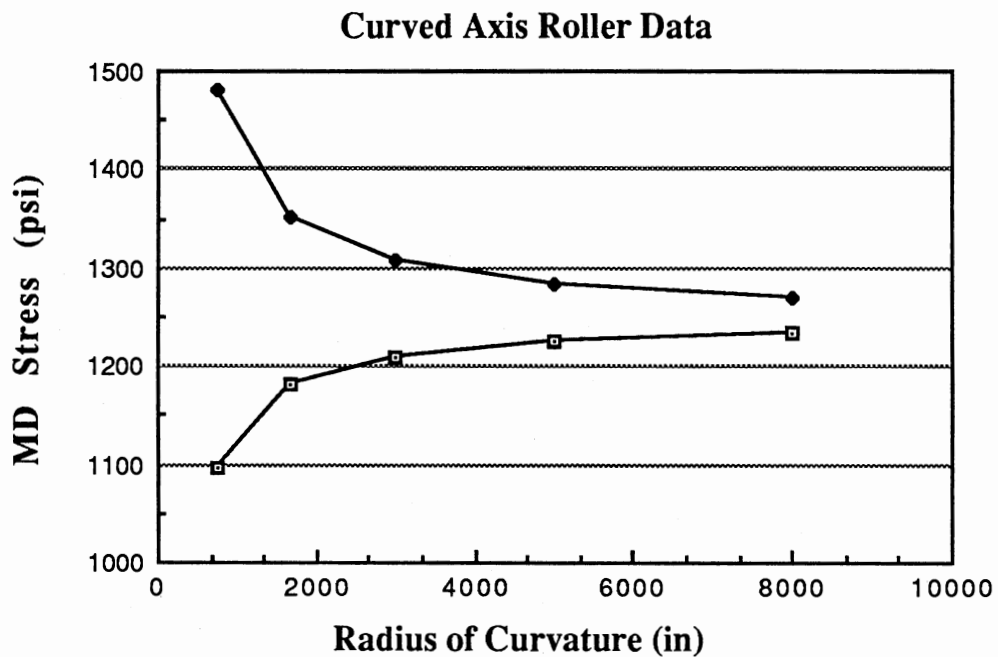
Figure 6-79.   Curved Axis Roller - MD Stress vs. Radius
of Curvature

Curved Axis Roller Data
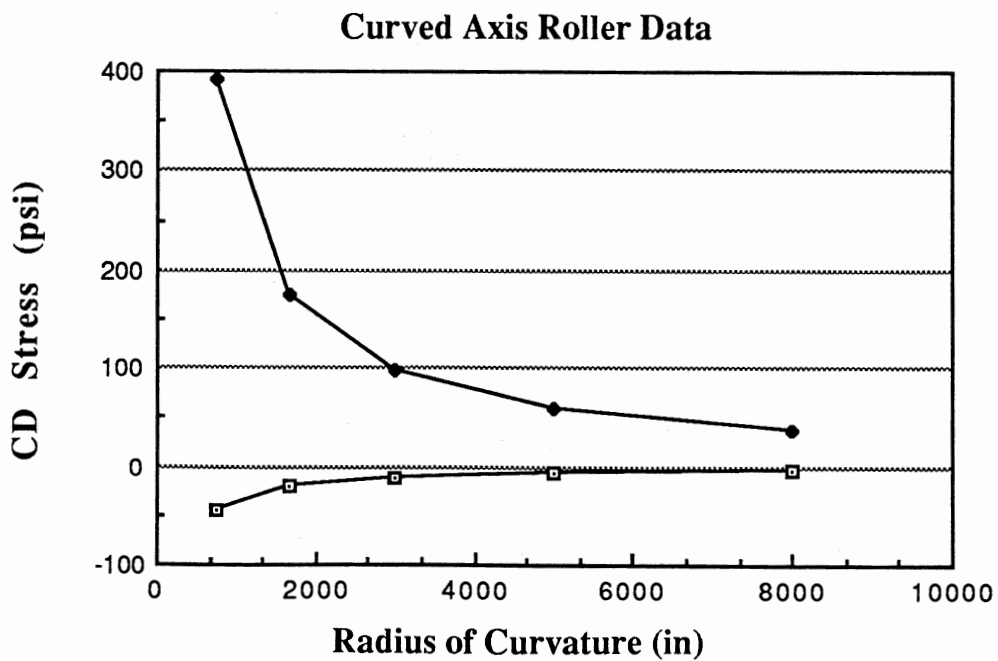
Figure 6-80.   Curved Axis Roller - CD Stress vs. Radius
of Curvature

Wrap Angle

Figures 6-81 through 6-84 show the effects of wrap angle on the concave roller, and figures 6-85 through 6-88 show the effects of wrap angle on the curved axis roller. Again, because the two types of rollers have different spreading mechanisms, the response of the models to the wrap angle is different.

For the concave roller, all of the spreading actually occurs in the entry span before the roller and not on the roller itself. The roller in contact with the web simply supplies sufficient forces to maintain the spreading. For this reason, the wrap angle has no effect on the geometry of spreading, and therefore no effect on the spreading displacements and stresses.

The sole effect of wrap angle on the concave roller is its effect on the forces available to maintain the spreading displacements. A wrap angle of zero would cause line contact between the web and roller. In addition, a wrap angle of zero would require no normal forces between the web and the roller surface. In this limiting case, there is no force available for maintaining either the MD strain variation, or the spreading displacements. This behavior is illustrated in the curve for max coefficient of friction which approaches infinity as the wrap angle approaches zero.

Again, the fundamental difference in the spreading mechanism between the curved axis roller and the concave roller results in different response to variations in the wrap angle. In the curved axis roller, spreading occurs both in the entry span before the roller, and on the surface of the roller. If sufficient friction were available,

the curved axis roller could spread the web even with zero wrap angle, assuming that the bow plane is in a correct orientation. One interesting aspect of the curved axis roller model is the essential relationship between the wrap angle and the bow plane angle.

The curve for max spread shows that variation in wrap angle does cause variation in the max spreading displacements. For the bow plane angle of 45 degrees, the curve shows that spreading increases with increasing wrap angle, but the increase tapers off at some point. For a given bow plane angle, (and as always, assuming sufficient friction) maximum spreading should occur with a wrap angle that causes the exit line to be in the plane of the bow plane. For a bow plane angle of 45 degrees, this would be a wrap angle of 135 degrees (90 + 45).

The curve for max coefficient of friction for the curved axis roller looks similar the same curve for the concave roller. Again, the wrap angle governs both the area through which friction forces may be transmitted, and the magnitude of those forces.

The MD stress curves for the curved axis roller show very interesting behavior. The max and min stress lines converge to nearly the same value as the wrap angle is increased from 30 degrees to 90 degrees. After 90 degrees, the max and min MD stress lines diverge. In the regions of the plot farthest from 90 degree wrap angle, the MD stress variation is extremely large.

Concave Roller Data
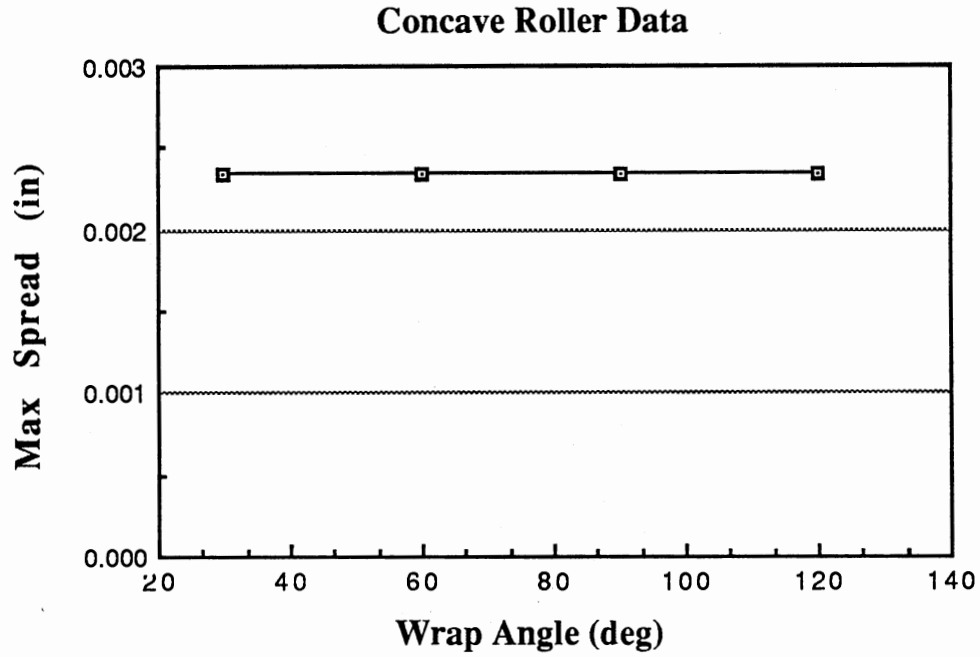
Figure 6-81.   Concave Roller - Spread vs. Wrap
Angle

Concave Roller Data
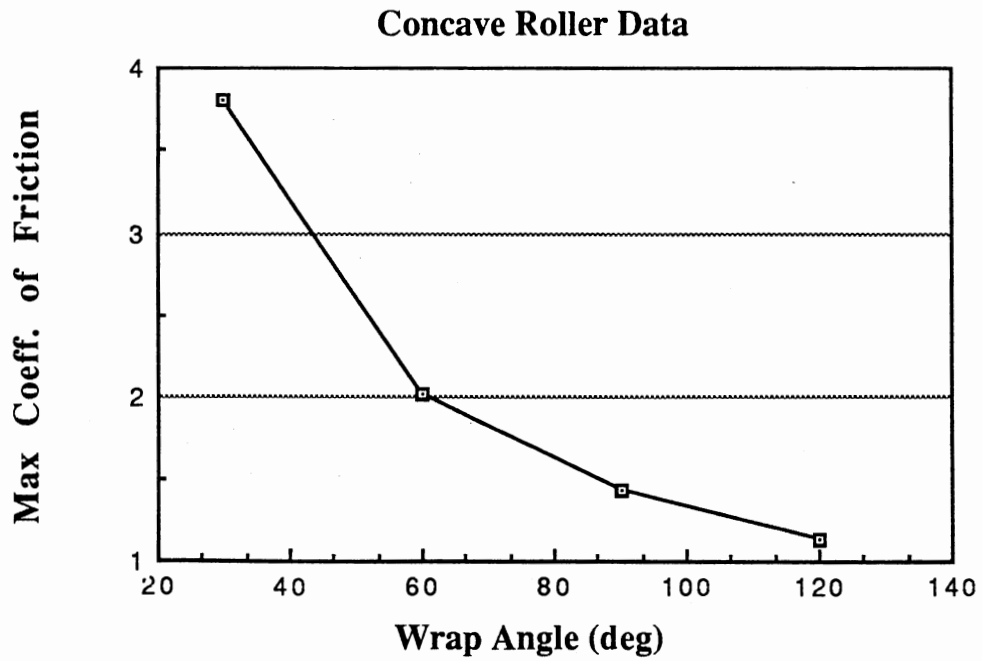
Figure 6-82.   Concave Roller - Friction vs. Wrap
Angle

Concave Roller Data
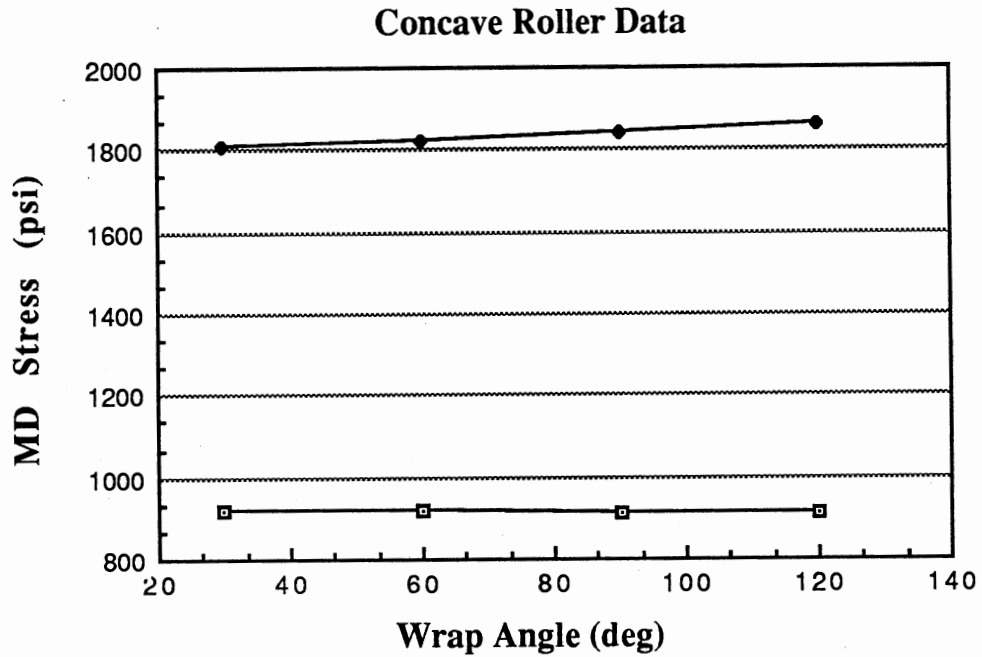
Figure 6-83.   Concave Roller - MD Stress vs. Wrap
Angle

Concave Roller Data
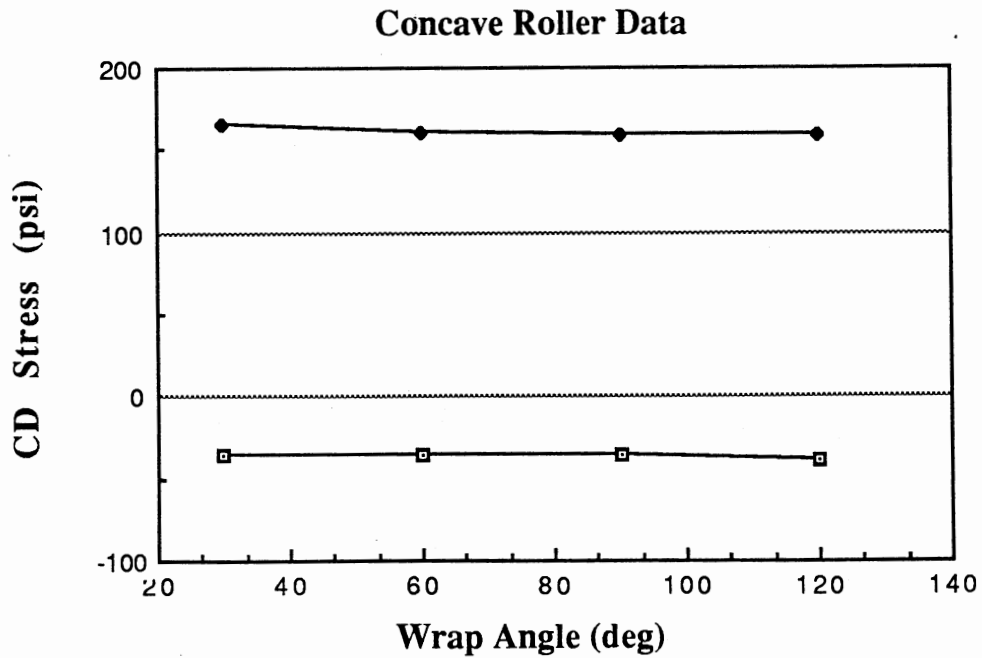
Figure 6-84.   Concave Roller - CD Stress vs. Wrap
Angle

Curved Axis Roller Data
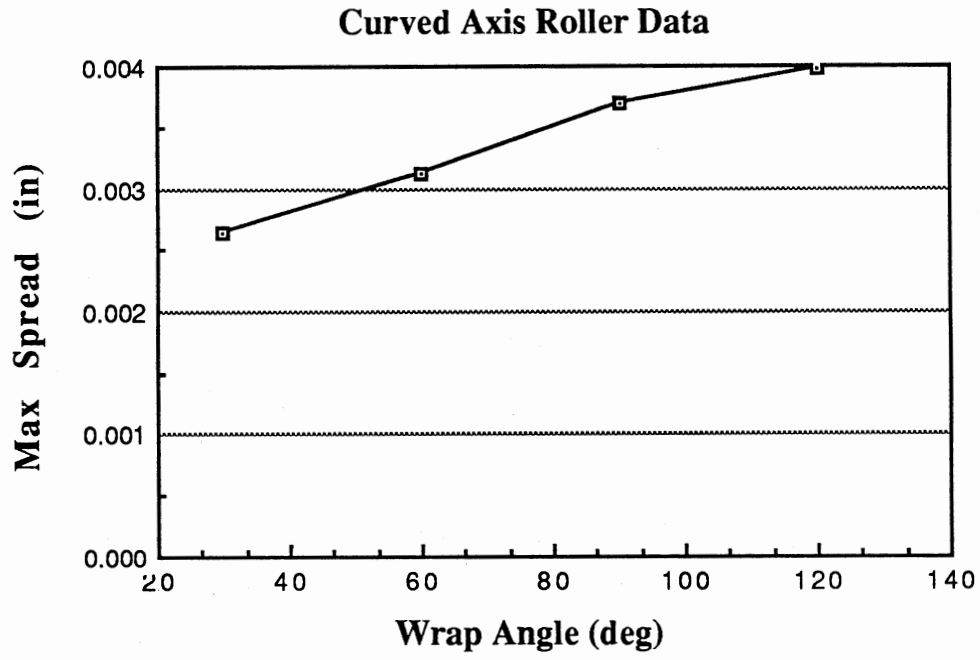
Figure 6-85.   Curved Axis Roller - Spread vs.
Wrap Angle

Curved Axis Roller Data
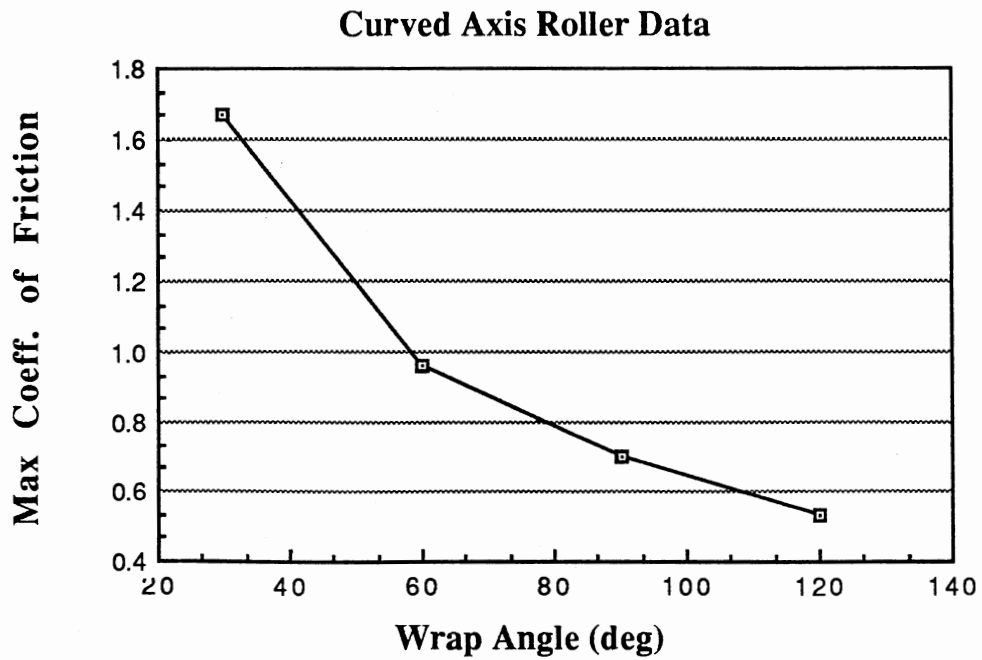
Figure 6-86.   Curved Axis Roller - Friction vs.
Wrap Angle

Curved Axis Roller Data
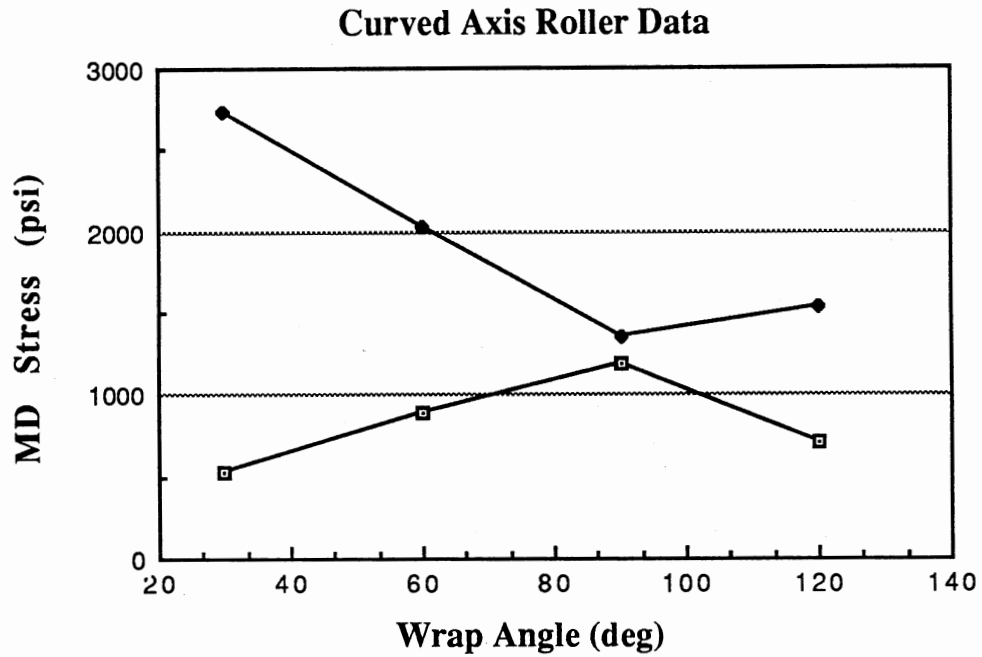
Figure 6-87. Curved Axis Roller - MD Stress vs. Wrap Angle

Curved Axis Roller Data
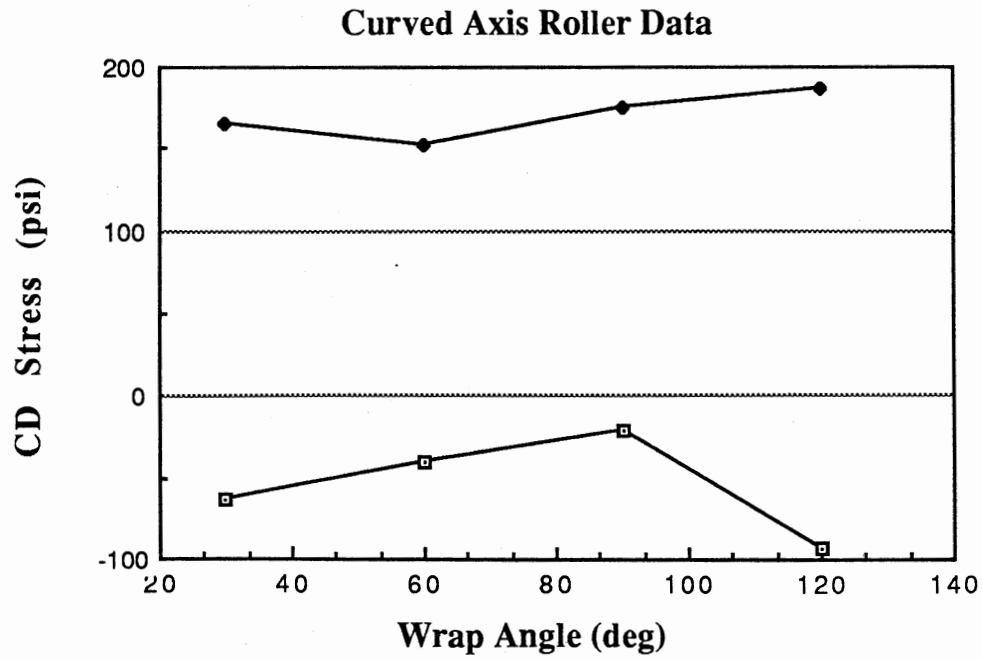
Figure 6-88. Curved Axis Roller - CD Stress vs. Wrap Angle

These curves suggest the reason for the configuration in which these rollers are normally used. The bow plane angle for the concave roller is normally selected so that the wrap angle is bisected by a plane perpendicular to the bow plane. For a 90 degree wrap angle, this would require a bow plane angle of 45 degrees down from the horizontal. The MD stress curves show that this gives the minimum variation in MD stresses. The reason that this minimum variation occurs in this configuration can be seen from the geometry of the roller. In this configuration, the total path length of all web streamlines are essentially equal. Any deviation from this optimal configuration results in different path lengths for different streamlines, and therefore a larger MD stress distribution.

The curves for max and min CD stress show only a small variation for variations in the wrap angle. It does show that the minimum CD stress reaches a maximum value (smallest negative value) for a wrap angle of 90 degrees.

Bow Plane Angle

Figures 6-89 through 6-92 show the effects of bow plane angle on the curved axis roller. The bow plane angle applies only to the curved axis roller. As was shown in the previous section, both the bow plane angle and the wrap angle cooperate to determine the response of the web. In the previous section, the curves showed the behavior when the bow plane angle was fixed at 45 degrees, while the wrap angle was varied from 30 to 120 degrees. In this section, the wrap angle is held fixed at 90 degrees, while the bow plane angle is varied between 30 and 60 degrees.

Curved Axis Roller Data
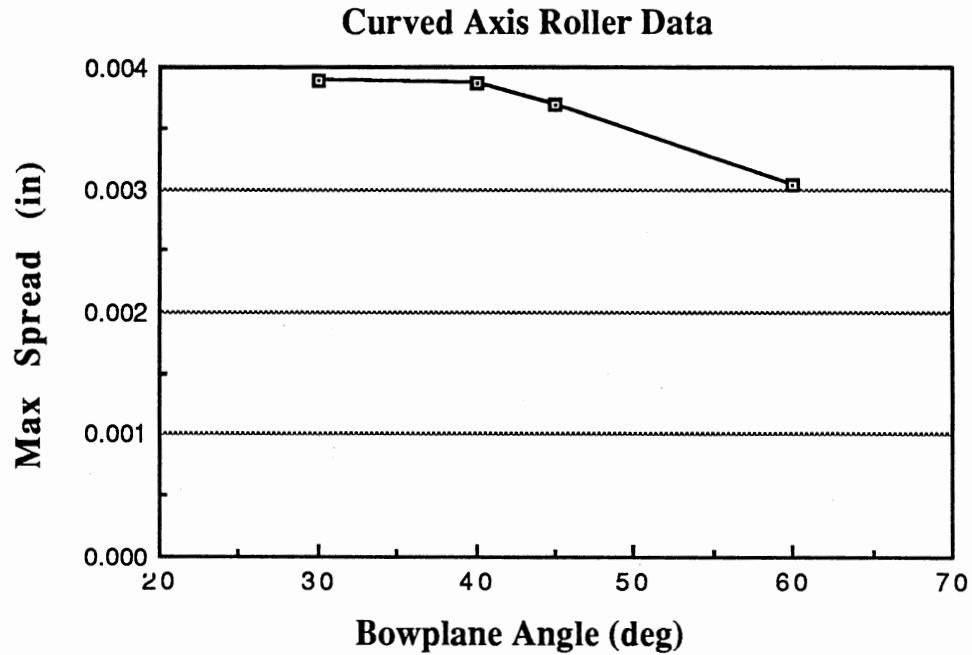
Figure 6-89.   Curved Axis Roller - Spread vs. Bow
Plane Angle

Curved Axis Roller Data
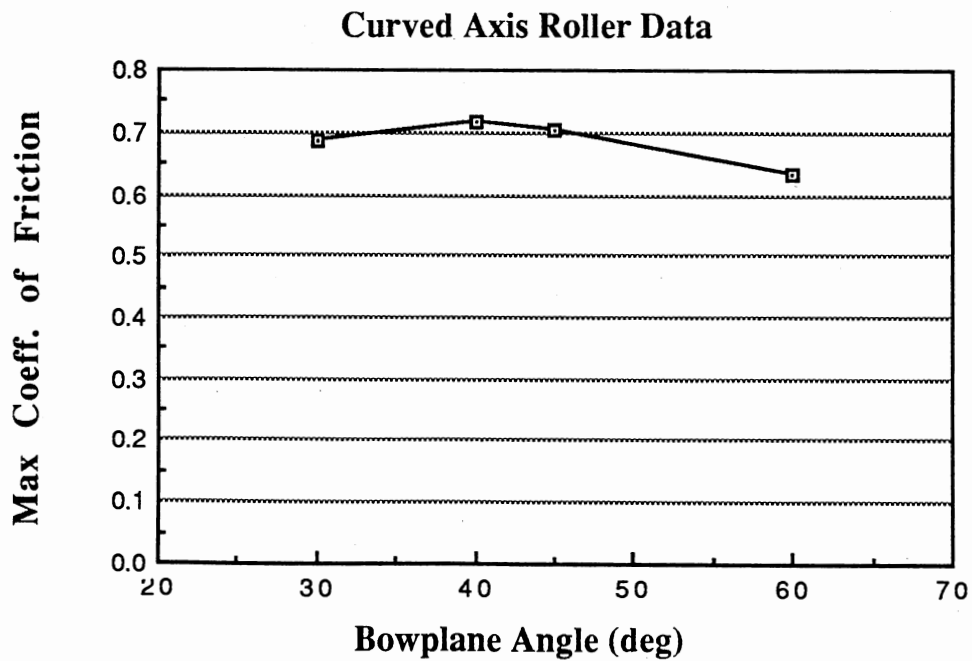
Figure 6-90.   Curved Axis Roller - Friction vs. Bow
Plane Angle

Curved Axis Roller Data
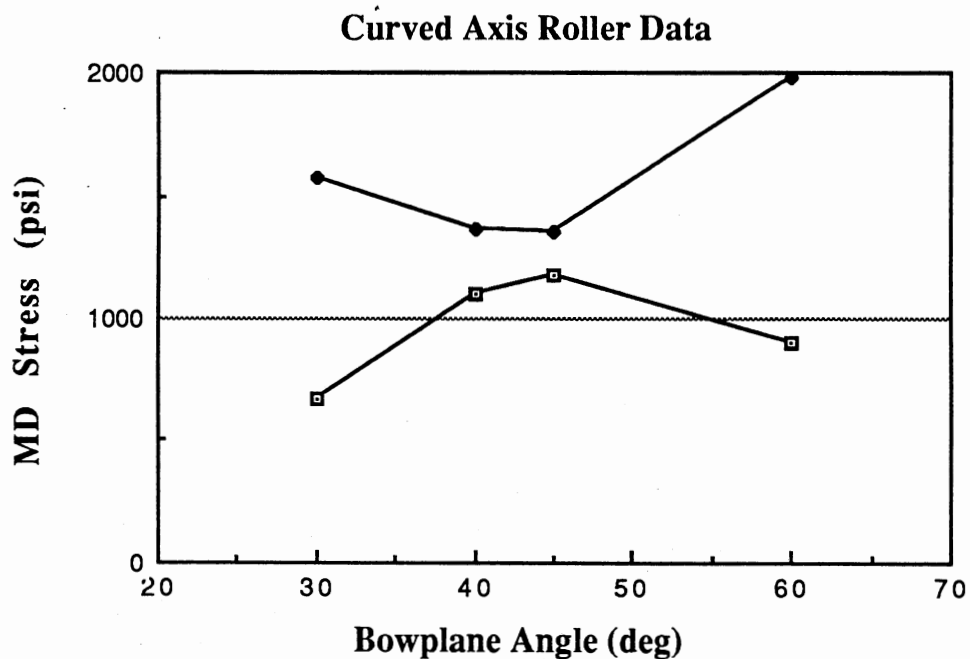
Figure 6-91.   Curved Axis Roller - MD Stress vs. Bow
Plane Angle

Curved Axis Roller Data
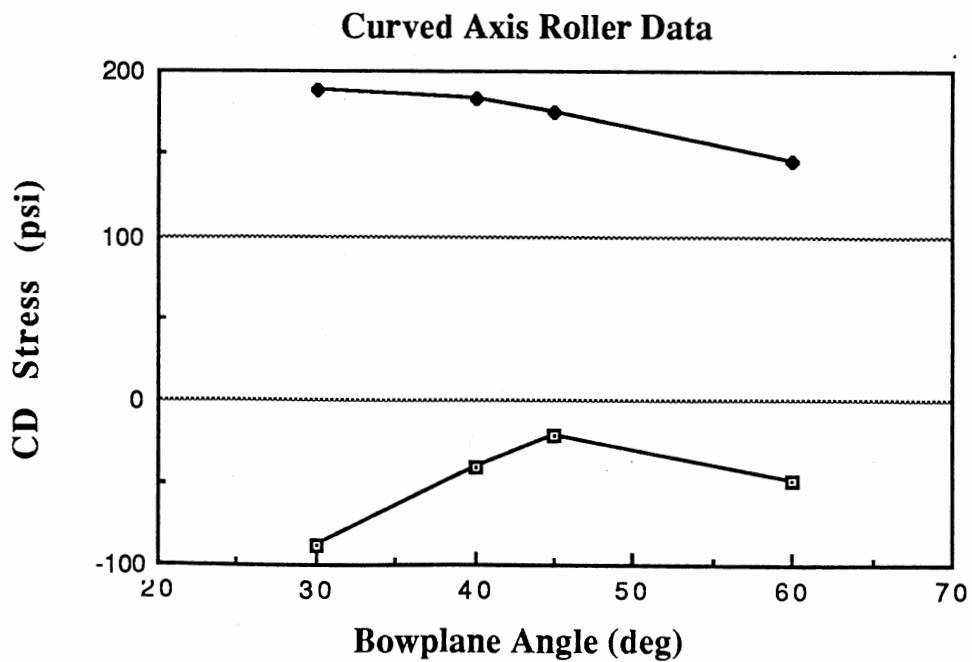
Figure 6-92.   Curved Axis Roller - CD Stress vs. Bow
Plane Angle

The curve for max spreading displacement shows a maximum displacement for bow plane angles between 30 and 40 degrees, with decreasing amounts of spreading for the larger angles. This behavior is the result of two conflicting conditions. The curved axis roller spreads the web both in the entry span, and on the roller. The spread in the entry span is caused by the web being steered to normal entry. The steering has maximum effect when the bow plane is oriented parallel to the entering web span (zero degrees wrap angle), because the spreading components of the velocity vectors are in the plane of the web. At any other angle, the velocity components must be projected into the plane of the web using a cosine function, diminishing the spreading effect on the entry span.

The spreading that occurs on the roller is also a combination of two things: the length of the web in contact with the roller, and the angle between the web surface and the bow plane. Maximum spreading on the roller occurs when the web is parallel to the bow plane. This optimum orientation occurs at only a single line of contact. The best orientation for spreading on the roller is the orientation most commonly used with the curved axis roller as was described in the previous section (bow plane of 45 degrees for a 90 degree wrap angle).

The bow plane orientation for maximum spreading in the entry span does not coincide with the orientation for maximum spreading on the roller. It stands to reason that the bow plane orientation for maximum total spreading is a compromise between these two orientations. The max spread curve shows that this compromise occurs somewhere near 30 degrees. If obtaining the maximum

spreading was the only objective, this curve would suggest that the industry change the manner in which curved axis rollers are installed. But, as was shown in the previous section, spreading is not the only consideration. The stresses induced in the web, and the forces required for spreading are also important.

The curve for max coefficient of friction shows that friction is not heavily dependent on the bow plane angle.

The curves for the max and min MD stresses show behavior similar to the curves in the previous section. The max and min stresses converge as the bow plane angle increases from 30 degrees to 45 degrees. After 45 degrees, the curves diverge. Again, the MD stress variation is larger as the bow plane angle deviates from the optimum value of 45 degrees.

The curves for max and min CD stress show only slight variation for variations in the bow plane angle. They do show larger CD stress variations for bow plane angles less than 45 degrees. In addition, the best value (smallest compressive stress) for the min CD stress occurs with a bow plane angle of 45 degrees.

Summary

In this chapter, the behavior of the spreading roller models was examined at two levels. First, the distribution of stresses and displacements over the entire web were examined using the base values of the model parameters. From this study, insight was gained into the total effect of these rollers on the web material being spread. Then, the parameters were varied one at a time about the base values. The results for each parameter were summarized in four

plots for each roller. These plots showed trends in the model that both enhanced the credibility of the models, and gave a better understanding as to why these rollers are used as they are commonly used.

CHAPTER VII

VALIDATION OF THE MODELS

Introduction

Chapter V described the device that was used to measure the amount the rollers spread the web. Chapter VI presented a study of the behavior of the spreading models for a wide range of input parameters. In this chapter, the results of the two previous chapters are combined in order to determine the validity of the spreading models.

The measured spreading data for both the concave and curved axis rollers is given in Appendix B. This data is overlayed on the spreading plots of the previous chapter so that a comparison may be made. These plots present the computer predicted spreading in the same manner as the previous chapter, a series of small squares connected by lines. The measured spreading data is shown as a combination of symbols. An asterisk is used to represent the average measured spreading, and a vertical bar is used to represent the entire range of measured values (min to max).

It is important to remember the definition of spreading that was presented in the previous chapter. The effective spreading of a web streamline is the change in the distance of that streamline from the web centerline. The location of the streamline at the beginning

of the entry span is used as the spreading reference. Therefore, by definition, all streamlines at the beginning of the entry span have zero spreading.

The maximum spreading for both models occurs at the line where the web exits the roller, and at the outer edge of the web. This is the value plotted on the vertical axis of the Max. Spread plots. This same location was used when measuring the web spreading.

Because is was not possible to accurately measure the change in distance between the web edge and the web centerline, the edge to edge distance (width) of the web was measured. These changes in web width are tabulated in Appendix B. In order to compare the measured spreading data to the spread predicted by the models, the measured data must be divided by 2.0 to give a center to edge distance.

<div align="center">Validation of the Concave Roller Model</div>

Figure 7-1 shows a plot of Max. Spread vs. Thickness for the concave roller. This plot includes both measured spreading data and spreading predictions from the model. The plot shows that there is a large difference between the amount of spreading predicted by the model, and the spreading that was measured. At first glance, it would appear that the model is severely in error. But, it is important that the fundamental assumption for the model be remembered.

The model is based on the assumption that there is no slippage between the web and the roller. All of the boundary conditions applied in the model are based on this assumption. The boundary displacements are calculated from the model geometry, and the

friction forces necessary to maintain those displacements are an output of the model. Therefore, the friction forces predicted by the model should be examined to find a possible explanation for the difference between the predicted and measured spreading.

Concave Roller Data
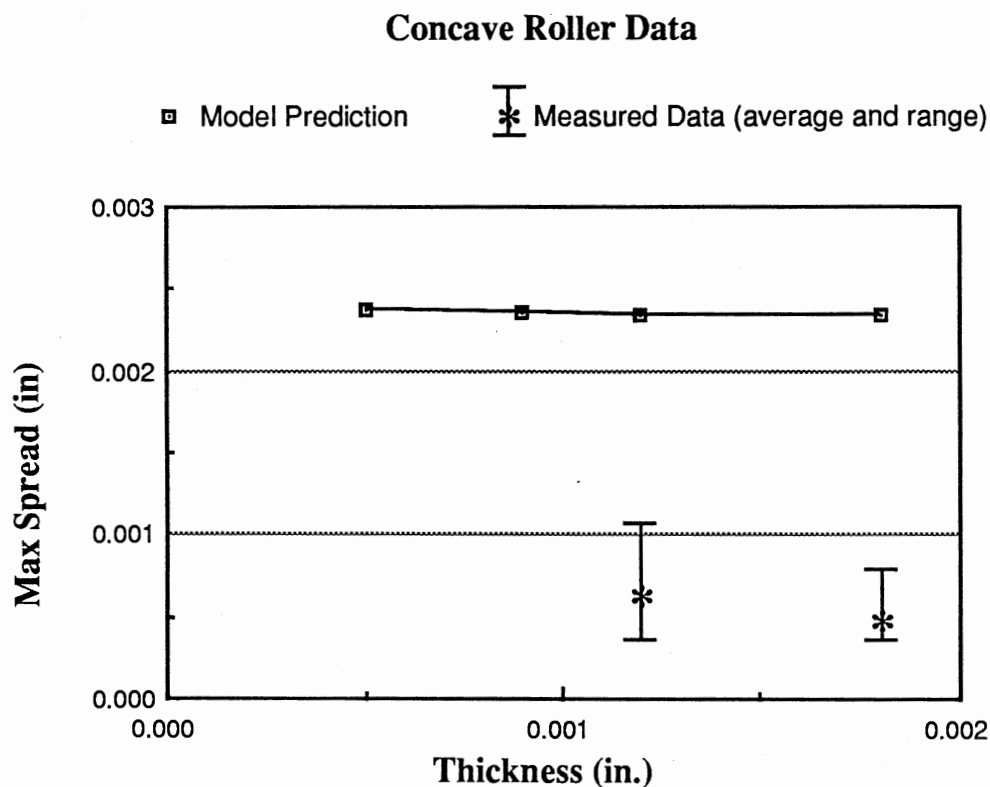
Figure 7-1. Concave Roller - Spread vs. Thickness

The Max Friction vs. Thickness plot from the previous chapter has been repeated here as figure 7-2. This figure clearly shows that for the combinations of webs and rollers used in the experiments, the

friction requirements are excessively large. A maximum coefficient of friction of 1.45 to spread a 0.0012 inch thick web, and a maximum coefficient of friction of 2.0 is required to spread the 0.0018 inch thick web. Coefficients of friction of these magnitudes are clearly unrealistic. This means that there is certainly slippage between the web and the roller, and this violates the fundamental assumption of the model.

Concave Roller Data
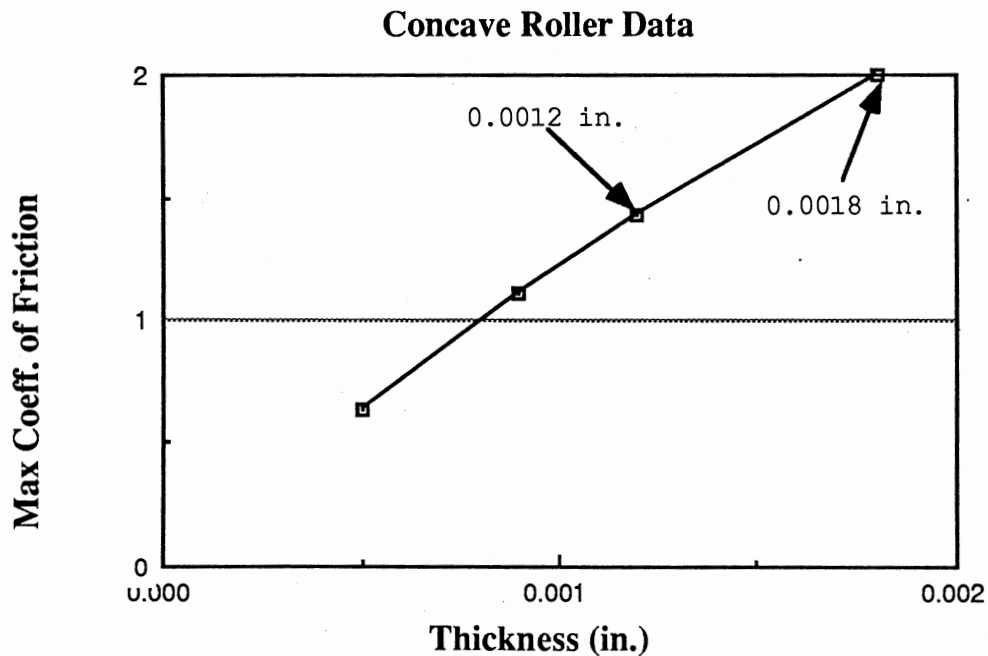
Figure 7-2. Concave Roller - Friction vs. Thickness

At this point, the model has predicted the amount of spreading based on the assumption that sufficient friction force is available,

and then predicts that there cannot be sufficient friction. The amount of friction predicted by the model implies that it cannot spread the web the predicted amount. This is the first point of agreement between the model and the measured data.

Because the model predicts slippage between the web and the roller, the measured data should be examined for any sign of slippage. Figure 7-1 shows that the thinner web was spread slightly more than the thicker web, while the model predicts that there should be no difference. If sufficient friction were available, both webs would spread the same amount. But, because the friction force is limited and insufficient in both cases, that limited force should be more effective at spreading the thinner web than the thicker web. Therefore, the measured data is consistent with a web that is slipping.

Another conclusive indication of slippage is the extreme measures that were required to measure any spreading at all. The initial measurements with the concave roller showed no spreading. It was only after the roller surface was covered with the 3-M spray-on glue that any spreading was measured. The additional friction supplied by the layer of dried glue allowed the roller to spread the web the amount measured.

At this point, the model is in partial agreement with the measured data. The model itself states that the amount of spreading predicted is unrealistic because of the friction required. But, this is not sufficient to consider the model verified. Further evidence for verifying the model could be obtained in any of three ways. First, a roller with less curvature (higher radius of curvature) could be made

and tested. Second, a much thinner web could be used. Figure 7-2 suggests that a 0.0004 inch thick web could be spread with a coefficient of friction of approximately 0.7. Finally, the model might be modified in some way to simulate a web and roller with limited friction.

One interesting characteristic of the concave roller model allowed a modification to incorporate limited friction in an indirect and simplified way. One of the boundary conditions applied to the concave roller model required pre-calculation of a machine direction displacement profile for all of the nodes on the roller. This displacement profile was required to simulate the fact that the edges of the web are pulled ahead of the centerline of the web. This occurs because the surface velocity of the concave roller is larger at the edges, where the radius is largest.

This boundary condition is interesting for two reasons. First, when this boundary condition is not included in the model, the model predicts nearly zero spreading! This means that this shearing of the edges is the primary factor in the concave roller's ability to spread the web. In addition, it is this boundary condition that generates most of the friction requirements predicted by the model. In the absence of this boundary condition, the model predicts that smaller coefficients of friction are required. For the concave roller, the feature that has the largest effect on spreading also has the largest effect on the friction requirements. Therefore, by modifying this boundary condition, it is possible to significantly alter both the spreading displacements and the friction forces predicted by the

model. This results in a simplified method for determining the effect of limited friction on the resulting spreading displacements.

In Chapter IV, the calculation of these MD displacements was described as a multi-step process. From the geometry of the roller and the material properties of the web, a MD strain profile is calculated. This strain profile is used to calculate a set of nodal forces. These forces are applied as boundary conditions to a simple Finite Element model of the entry span. The displacement profile calculated from this simple model is used as boundary conditions for the more complete model.

The process of modifying this boundary condition to simulate slipping is also a multi-step process. First, the force profile applied to the simple Finite Element model is modified. A suitable limit is placed on the magnitude of the forces that are applied. Forces smaller than this limiting value are applied without modification. The limiting force value is substituted for any forces calculated to be too large. Of course, the proper sign is used for the forces. Because the surface normal force between the web and the roller does not vary greatly over the roller, using a constant force limit is a reasonable approximation to a limit in the coefficient of friction.

This modified set of forces produces a smaller variation in the MD displacements predicted by the simplified entry span model. These smaller MD displacements produce less spreading and smaller friction requirements in the complete model. The process of choosing a force limit and calculating the friction requirement is repeated until the friction requirement matches the friction available from the web and roller materials.

Because of the importance of this boundary condition in both spreading and friction, this simplified analysis should yield a reasonable approximation of spreading displacements in a system that is slipping. This procedure was applied in a slightly different manner to the concave roller model using the parameter values of the experimental equipment.

The force limit described above was systematically varied in an iterative process. But, instead of stopping when the required friction converged to a known friction value, the process was stopped when the resulting displacements matched the displacements that were measured. For clarity, this process should be compared to the model described in Chapter IV and the modification described above.

The model in Chapter IV uses roller geometry and web material properties to calculate both the amount of spreading and the required friction. The amount of spreading is limited by geometry considerations, and not by available force. The first modification described above uses geometry, material properties, and a friction limit to calculate spreading displacements. The resulting displacements are smaller than those calculated when the friction is not limited. The final modification is simply a change in viewpoint from previous modification. It answers the question: "If the slipping system gives a known spreading displacement, what is the limiting coefficient of friction at which slipping occurs?"

In the final form, the model predicts that a coefficient of friction of 0.85 in a slipping model would produce the spreading displacements that were measured. Although the coefficient of

friction between dried 3-M glue and coated polypropylene was not measured, a value of 0.85 is very reasonable for these two materials.

Curved Axis Roller Data
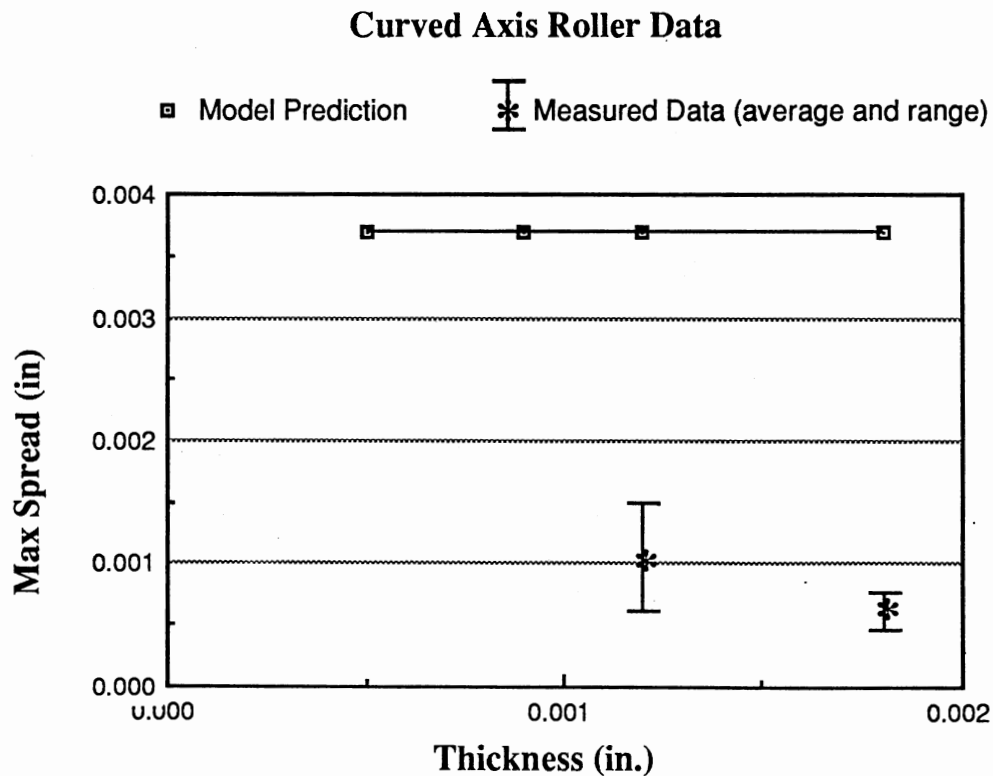
Figure 7-3. Curved Axis Roller - Spread vs. Thickness

Validation of the Curved Axis Roller Model

Figure 7-3 shows a plot of Max Spread vs. Thickness for the curved axis roller. This plot includes predicted and measured values of spreading. As in the concave roller, there is a substantial

difference between the predicted and measured spreading displacements. Again, this difference occurs because of slippage between the web and the roller.

Curved Axis Roller Data
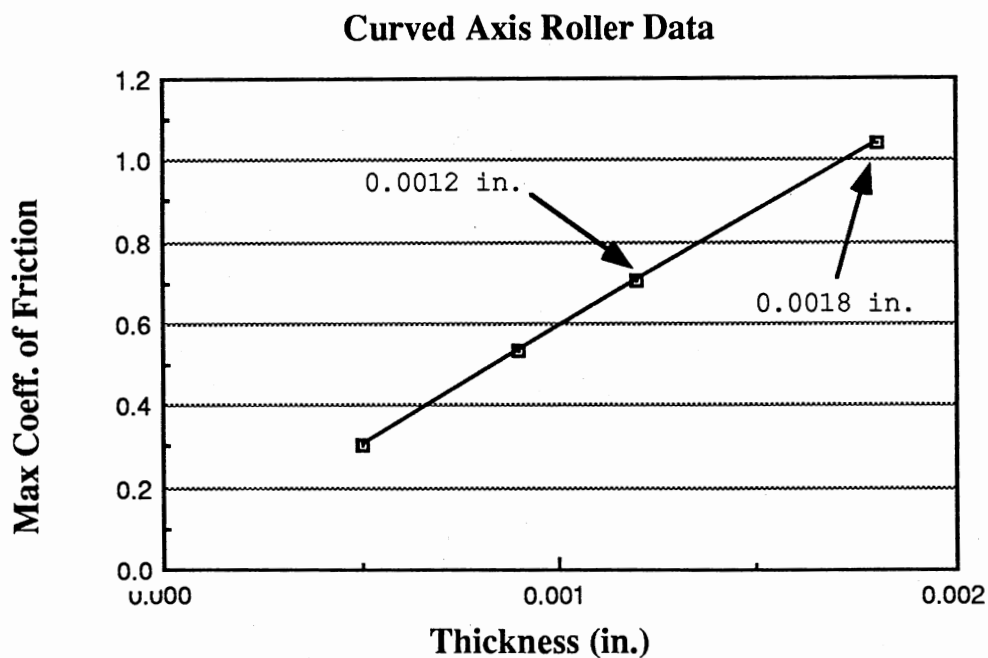
Figure 7-4. Curved Axis Roller - Friction vs. Thickness

Figure 7-4 shows that the curved axis roller model predicts a maximum required coefficient of friction of 0.7 and 1.0 for the thin and thick web respectively. Because the surface of the curved axis roller was not modified to increase the friction coefficient, these friction values are again unrealistic for these materials. As in the concave roller data, the curved axis data gives clear evidence of

slippage. The limited force is able to spread the thinner web a greater amount than it can spread the thicker web.

This situation is nearly identical to the situation with the concave roller, and the same alternatives are available for obtaining additional data for validating the model. In the case of the curved axis roller, there is no single factor controlling both spreading and friction that allows a simple model of a slipping web. Instead, the better option is to use a roller that is more gently curved.

Curved Axis Roller Data
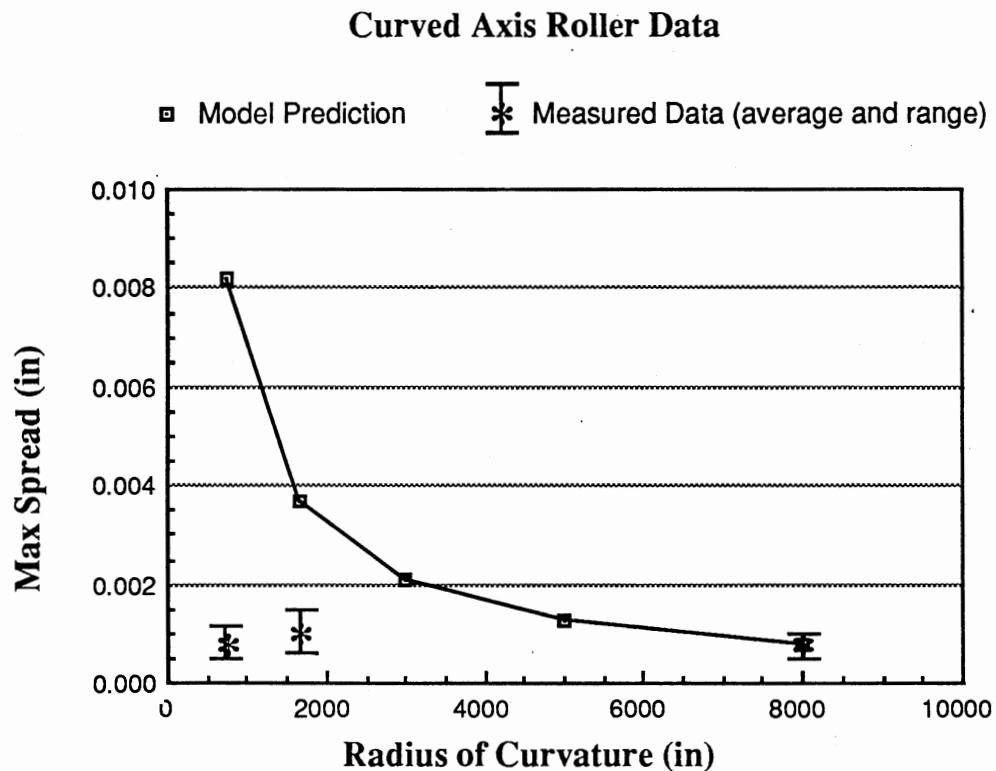
Figure 7-5. Curved Axis Roller - Spread vs. Radius of Curvature

Figure 7-5 shows a plot of Max Spread vs. Roller Radius of Curvature for the concave roller. In this plot the curvature is changed while the web thickness is held constant. This plot has two interesting features. First and most important is the nearly perfect agreement between the predicted and measured spreading displacements for a roller with a radius of curvature of 8000 inches. This point provides the verification needed for the curved axis roller model. The second interesting feature in this plot is that the 750 inch roller spreads the web less than the 1680 inch roller. Both of these rollers are slipping, but because the curvature in the 750 inch roller is more excessive, slipping occurs over a greater percentage of its surface. Therefore, it spreads the web less than the 1680 inch roller.

Figure 7-6 shows the Friction vs. Curvature plot for the curved axis roller. It shows that only the 8000 inch roller requires a reasonable amount of friction to operate without slipping.

Summary

In this chapter, experimental spreading measurements were compared to spreading values predicted by the models in order to validate the models. For both types of rollers, the roller geometry chosen for the initial measurements required excessive friction in order to operate without slipping. The excessive friction was predicted by the models, and verified by the spreading measurements.

Curved Axis Roller Data
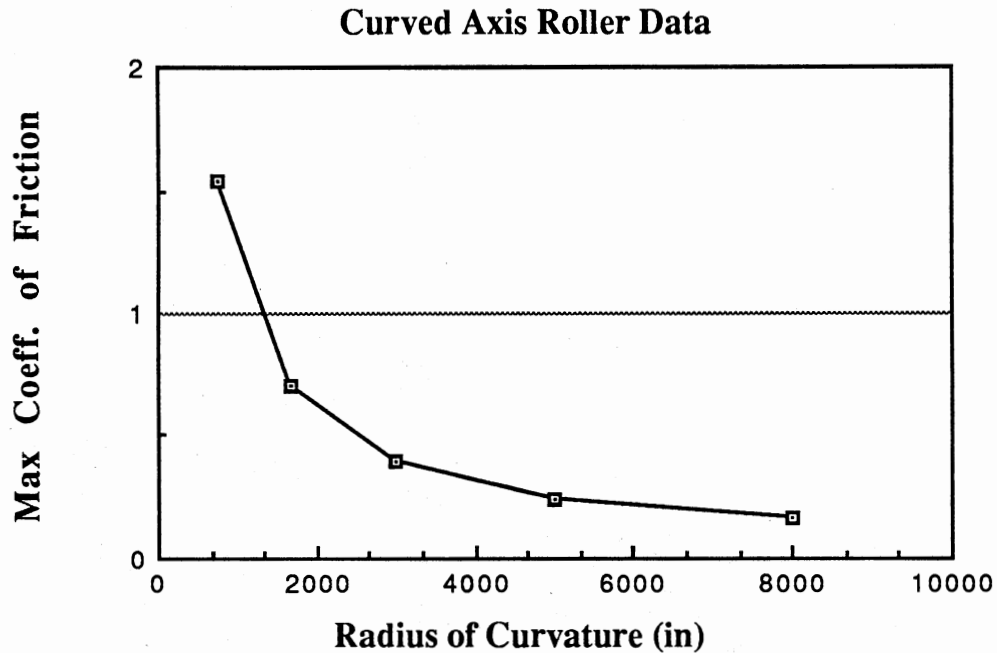
Figure 7-6. Curved Axis Roller - Friction vs. Radius
of Curvature

The concave roller model was modified in a simple but reasonable way to allow it to simulate a slipping roller. With this modification, the model predicted that the roller geometry chosen would produce the displacements measured if a coefficient of friction of 0.85 were available. This is a reasonable range of friction considering the coating applied to the surface of the roller.

The modification to the concave roller could not be applied to the curved axis roller model. Instead, a roller with an 8000 inch radius of curvature was manufactured. The average value of spreading measured using this roller matched the model prediction nearly perfectly.

CHAPTER VIII

CONCLUSIONS AND RECOMMENDATIONS

Conclusions

In accordance with the goals for this research that were stated in Chapter I, computational models have been developed for both the concave roller and the curved axis roller. These models use the web material properties and roller geometry as inputs to an iterative Finite Element analysis program which calculates the resulting web deformations, stresses, and friction forces.

In accordance with the sub-objectives, the models have been validated by comparison with measured spread data. Also, the models have been used in a study of the behavior of the roller systems in response to variations in the input parameters. Finally, many techniques were used to reduce both the total memory requirements and the execution time for the models.

One of the limitations of the program arose from the need to produce and distribute models that do not require a mainframe or super-computer to give reasonable execution times. The current versions of the models do not allow slippage between the rollers and the web. Instead the models enforce the no-slip boundary condition, and report the resulting friction forces. For this reason, the current versions of the models are best used as tools to design rollers that do

not slip. This is accomplished by varying roller geometry until the maximum friction requirements are lower than those known to be available.

The models can also be used to gain an understanding of existing spreading roller installations. By modeling the existing geometry, it can be determined whether or not the roller slips. This in itself is a significant piece of information. This model also gives an upper limit on the deformations and stresses in the web. If slipping occurs, both the deformations and stresses should be lower than those predicted.

Finally, an estimate of the deformations and stresses in the slipping roller can be obtained by varying the roller curvature and running the model until the available friction is reached. This is equivalent to designing a roller that is at impending slip. Figure 7-5 in Chapter VII shows the measured spreading for three different rollers. Two of the rollers show spreading deformations significantly smaller than those predicted by the model. Both of these rollers are slipping. The third roller shows very good agreement with the spreading predicted by the model. This roller is not slipping. It is interesting to note that the spreading deformations of all three rollers are of similar magnitude. This implies that the deformations of rollers that slip are similar to the deformations of a roller at impending slip. And, if the deformations are similar, the stresses should be similar.

Development of the Spreading Roller Models

In the use of the finite element method, there are three primary tasks required to create an accurate model. First, the unstrained geometry of the system must be described in sufficient detail. Then, the correct set of boundary conditions must be defined. Finally, the system of equations must be solved. For nonlinear systems, some form of iteration is required between the three tasks. In modeling the spreading rollers, there were significant developments in each of the three tasks.

Previous attempts at modeling these rollers allowed the web to conform to the doubly curved shape of these spreading rollers without incurring any strain in the material. Then the strains were simulated by adding local deformations. These local deformations had a significant effect on the calculated spreading. In the models produced by this research, the unstrained web was assembled around an average cylindrical roller. Then the correct set of boundary deformations was applied to cause the web to conform to the shape of the roller. This allowed both the web strains and deformations to be modeled more accurately.

In modeling the spreading process, nonlinear optimization techniques were used to find the correct set of spreading displacements. Those displacements were consistent with the fact that the streamlines in the web are steered to normal entry.

Throughout the modeling process, many techniques were used to allow the models to be run on machines with limited memory, and to perform the calculations in a minimum amount of time. These

techniques allow greater access to these models. In addition, many of these techniques may be reapplied in the continuation of this research.

Conclusions Reached from the Study of the
Models

The most surprising conclusion reached from the models is the high values of coefficient of friction that are required to prevent slippage between the web and the roller. This is particularly true in the concave roller. The largest forces in the concave roller are the MD forces near the edges of the web. These are the forces that shear the edges of the web ahead of the center. Coefficients of friction greater than 1.0 were predicted for concave rollers having curvature values that were thought to be in a reasonable range.

The curved axis roller model also predicted friction values that were higher than expected, although the friction values are lower than those predicted by the concave roller model. The MD forces in the curved axis roller are not the predominant forces. Both the MD and the CD forces are of similar magnitude.

The study of the models also leads to the expected conclusion that the roller geometry is the most significant parameter controlling web spreading deformations and stresses. The roller geometry includes both the roller nominal radius, and the roller profile radius of curvature. It has been suggested that the percent deviation from cylindrical geometry is a reasonable indicator of the spreading tendency of the roller. The results of the models are in complete agreement with this suggestion.

Common usage of the curved axis roller orients the roller so that the wrap angle between the web and the roller is bisected by a line perpendicular to the bow plane. For an incoming horizontal web with a 90 degree wrap angle, this would require a bow plane angle of 45 degrees down from horizontal. The curved axis roller model shows that this convention is used for very good reasons. This orientation produces acceptable spreading deformations, but it is the stress distribution that is the primary reason for using this orientation. Deviation from this optimal orientation results in significantly greater MD stress variations.

Conclusions Reached from Web Spreading
Measurements

The initial attempts at measuring web spreading confirmed the large friction requirements predicted by both of the models. The concave roller produced zero spreading until the friction carrying capability of the roller was increased using the spray-on glue. Even then, the roller showed smaller deformations than expected, indicating that the roller was still slipping. Modification of the model to account for limited friction force capability was required to reconcile the concave roller model with the measured spreading data.

Recommendations

Recommendations for extension of this work fall into two categories: additional capabilities in the model, and improvements in the measurement of web spreading. Three new capabilities in the models are of immediate interest to this author. First, the ability to

allow slipping should be added to the models. This will require a significant increase in computing power to perform the large number of iterations in a reasonable amount of time. Because of rapid improvements in computer speed, accompanied by reductions in price, machines capable of modeling slipping should be available to most engineers in the near future.

The models should also be modified to allow the web to move off of the centerline of the roller. Because these spreading rollers are destabilizing devices, it would be useful to calculate the maximum displacement of the web centerline, and the resulting stress distribution. This would be a first step in modeling the lateral dynamics of webs on spreading rollers.

Finally, the spreading models should be combined with a wrinkle model to investigate the ability of these rollers to prevent wrinkling. A very simple wrinkle model might be a lateral compressive force or displacement distribution at some point in the entry span. The maximum compressive stress remaining at the entrance of the roller should be a good indication of the ability of the roller to prevent wrinkling.

For better accuracy in measuring web spreading, the problems with the laser based measurement system should be solved. One possible solution is the use of automated online calibration immediately prior to the spreading measurement. This would remove the problem of the low speed drift in calibration. Another possibility would be to limit the time that the sensor is exposed to the laser with some type of shutter mechanism. This would remove

any heating effect caused by exposing the sensor to the laser for extended periods of time.

Finally, a device for accurately measuring web stresses would allow additional validation of the models. To be of use, the device would need to measure lateral and longitudinal stresses over a very small region and be small enough to collect data very near the roller entrance and exit points.

BIBLIOGRAPHY

1. "What is a Web" Unpublished Web Handling Research Center Information Brochure. Oklahoma State University, No date.

2. Swift, H. W., "Cambers for Belt Pulleys", <u>Proceedings, Institute of Mechanical Engineers (London)</u>, Vol. 122, June, 1932, pp. 627-683.

3. Sassaki, Hira, Abe, Yangagishima, Shimoyama, and Tahara, "Control of Strip Buckling and Snaking in Continuous Annealing Furnace", <u>Kawasaki Steel Technical Report</u>, No. 9, March, 1984.

4. Shelton, J. J., "Fundamentals of Lateral Web Behavior", Unpublished Web Handling Research Center Information Brochure, Feb., 1988.

5. Shelton, J. J., and Reid, K. N., "Lateral Dynamics of an Idealized Moving Web", <u>Journal of Dynamic Systems, Measurement, and Control,</u> September, 1971, pp. 187-192.

6. Shelton, J. J., and Reid, K. N., "Lateral Dynamics of a Real Moving Web", <u>Journal of Dynamic Systems, Measurement, and Control,</u> September, 1971, pp. 180-186.

7. Shelton, J. J., "Dynamics of Web Tension Control with Velocity or Torque Control", <u>Proceedings, 1986 American Control Conference</u>, Seattle, Washington, Vol. 3, pp. 1423-1427.

8. Pfeiffer, J. D., "Web Guidance Concepts and Applications", <u>TAPPI</u>, Vol. 60, No. 12, December, 1977.

9. Butler, T., "How Concave Rolls Can Correct Dryer Fabric Bowing", <u>Paper Trade Journal,</u> Vol. 169, No. 3, March 1985, pp. 70-72.

10. Gallahue, W. M., "Curved Rolls Used for Accurate Slit Separation", <u>Pulp and Paper</u>, February, 1974, pp. 84-85.

11. Daly, D. A., "Factors Controlling Traction Between Webs and Their Carrying Rolls", TAPPI, Vol. 48, No. 9, Sept., 1965.

12. Lucas, R. G., "Better Spreading of Web in the Winder - and How to Achieve It", Pulp and Paper, April, 1977, pp. 154-157.

13. Lucas, R. G., "Principles of Web Spreading", Presented at TAPPI 5th Finishing Conference, Houston, Texas, November 1, 1971.

14. Magill, M. A., "Contacting Web Biaxial Stress Transducer", M. S. Thesis, Oklahoma State University, 1988.

15. Feiertag, B. A., "Summary Report on the Use of Curved Axis Rolls for Wrinkle Prevention on Paper and Plastic", Fife Corporation, April 22, 1981.

16. Reynolds, B. H., "Stress Distribution Computation Within a Membrane Due to a Curved-Axis Roller", M. S. Thesis, Oklahoma State University, 1986.

17. Leport, M. L., "The Mechanics of Webs Encountering Concave Rollers", M. S. Thesis, Oklahoma State University, 1987.

18. Kliewer, G. A., "Parametric Analysis of Webs Encountering Concave Rollers", M. S. Thesis, Oklahoma State University, 1988.

19. Zienkiewicz, O. C., The Finite Element Method in Structural and Continuum Mechanics, London, McGraw Hill, 1967.

20. Segerlind, L. J., Applied Finite Element Analysis, 2nd. Ed., New York, John Wiley and Sons, Inc., 1984.

APPENDIXES

APPENDIX A

COMPUTER OUTPUT FROM PARAMETER STUDY RUNS

```
***********************************************************************
Title       : Concave Roller Base Run    .... th = 0.0012
Roller type : Concave Roller
Max Spread            :       0.002346
Max Friction Coeff. :       1.430200


         Sig-X       Sig-Y       Tau-XY      Sig-1       Sig-2      Tau-max
Min      915.50     -35.42      -16.54      916.45     -69.27      445.16
Max     1843.60     159.11      277.90     1878.85      158.47      933.08
***********************************************************************


***********************************************************************
Title       : th = 0.0005
Roller type : Concave Roller
Max Spread            :       0.002369
Max Friction Coeff. :       0.641990


         Sig-X       Sig-Y       Tau-XY      Sig-1       Sig-2      Tau-max
Min     2658.40     -35.85      -16.72     2658.80     -51.07     1318.10
Max     3597.30     160.69      280.75     3615.80      160.43     1792.70
***********************************************************************


***********************************************************************
Title       : th=0.0009
Roller type : Concave Roller
Max Spread            :       0.002351
Max Friction Coeff. :       1.110800


         Sig-X       Sig-Y       Tau-XY      Sig-1       Sig-2      Tau-max
Min     1330.50     -35.53      -16.58     1331.10     -61.77      652.80
Max     2261.10     159.62      278.58     2290.05      159.15     1135.40
***********************************************************************


***********************************************************************
Title       : th=0.0018
Roller type : Concave Roller
Max Spread            :       0.002340
Max Friction Coeff. :       1.999200


         Sig-X       Sig-Y       Tau-XY      Sig-1       Sig-2      Tau-max
Min      500.50     -35.33      -16.50      502.20     -83.41      238.10
Max     1426.05     158.36      277.22     1471.25      157.33      734.35
***********************************************************************


***********************************************************************
Title       : wrap=30
Roller type : Concave Roller
Max Spread            :       0.002333
Max Friction Coeff. :       3.799500


         Sig-X       Sig-Y       Tau-XY      Sig-1       Sig-2      Tau-max
Min      917.04     -35.36      -16.49      917.98     -53.96      450.18
Max     1807.45     165.68      278.54     1846.45      165.00      917.12
***********************************************************************
```

```
*********************************************************************
Title      : wrap=60
Roller type : Concave Roller
Max Spread          :     0.002339
Max Friction Coeff. :     2.024700


          Sig-X     Sig-Y     Tau-XY    Sig-1     Sig-2     Tau-max
Min      916.89    -35.39    -16.52    917.84    -62.94    448.33
Max     1825.25    161.00    278.29   1862.35    160.34    925.58
*********************************************************************


*********************************************************************
Title      : wrap=120
Roller type : Concave Roller
Max Spread          :     0.002345
Max Friction Coeff. :     1.131300


          Sig-X     Sig-Y     Tau-XY    Sig-1     Sig-2     Tau-max
Min      912.20    -39.36    -16.54    913.17    -74.67    441.81
Max     1861.95    157.59    277.39   1895.40    156.96    940.09
*********************************************************************


*********************************************************************
Title      : wrap = 150  .
Roller type : Concave Roller
Max Spread          :     0.002343
Max Friction Coeff. :     0.950560


          Sig-X     Sig-Y     Tau-XY    Sig-1     Sig-2     Tau-max
Min      906.68    -42.99    -16.54    907.67    -79.69    437.89
Max     1880.40    157.08    276.74   1912.10    156.46    946.95
*********************************************************************


*********************************************************************
Title      : emmd=50000
Roller type : Concave Roller
Max Spread          :     0.001016
Max Friction Coeff. :     0.513670


          Sig-X     Sig-Y     Tau-XY    Sig-1     Sig-2     Tau-max
Min     1153.00    -41.51     -5.18   1153.10    -46.42    564.06
Max     1418.70     85.81     95.41   1424.10     85.74    697.42
*********************************************************************


*********************************************************************
Title      : emmd=117000
Roller type : Concave Roller
Max Spread          :     0.001931
Max Friction Coeff. :     1.125100


          Sig-X     Sig-Y     Tau-XY    Sig-1     Sig-2     Tau-max
Min     1006.90    -37.27    -12.60   1007.50    -58.89    487.72
Max     1680.35    136.92    216.00   1703.70    136.56    841.53
*********************************************************************
```

```
********************************************************************
Title         : emmd=200000
Roller type : Concave Roller
Max Spread            :      0.002712
Max Friction Coeff. :      1.722900

            Sig-X      Sig-Y      Tau-XY      Sig-1      Sig-2     Tau-max
Min        813.93     -40.37     -20.31     815.57     -81.65     402.54
Max       2021.65     176.07     337.76    2069.35     175.03    1032.65
********************************************************************


********************************************************************
Title         : emmd=400000
Roller type : Concave Roller
Max Spread            :      0.003881
Max Friction Coeff. :      3.179200

            Sig-X      Sig-Y      Tau-XY      Sig-1      Sig-2     Tau-max
Min        309.13     -54.47     -33.35     322.67    -172.05     185.02
Max       2868.45     232.32     557.58    2961.70     228.27    1495.95
********************************************************************


********************************************************************
Title         : emcd=50000
Roller type : Concave Roller
Max Spread            :      0.003735
Max Friction Coeff. :      1.336000

            Sig-X      Sig-Y      Tau-XY      Sig-1      Sig-2     Tau-max
Min        881.07     -22.75     -13.66     881.92     -34.10     448.35
Max       1883.50      94.76     225.97    1906.85      94.19     951.78
********************************************************************


********************************************************************
Title         : emcd=157000
Roller type : Concave Roller
Max Spread            :      0.001928
Max Friction Coeff. :      1.455600

            Sig-X      Sig-Y      Tau-XY      Sig-1      Sig-2     Tau-max
Min        925.61     -49.97     -16.86     926.63     -87.52     440.94
Max       1826.65     184.31     289.13    1865.05     183.64     922.39
********************************************************************


********************************************************************
Title         : emcd=200000
Roller type : Concave Roller
Max Spread            :      0.001618
Max Friction Coeff. :      1.471500

            Sig-X      Sig-Y      Tau-XY      Sig-1      Sig-2     Tau-max
Min        933.70     -65.72     -16.84     934.76    -105.77     439.14
Max       1812.00     204.44     294.89    1852.25     203.76     911.57
********************************************************************
```

```
*******************************************************************
Title       : pois=0.1
Roller type : Concave Roller
Max Spread            :     0.002466
Max Friction Coeff. :     1.456100

          Sig-X      Sig-Y     Tau-XY     Sig-1      Sig-2    Tau-max
Min       916.21    -35.31     -17.39    916.99    -51.68    437.99
Max      1849.65    153.38     288.98   1887.00    152.72    944.41
*******************************************************************


*******************************************************************
Title       : pois=0.2
Roller type : Concave Roller
Max Spread            :     0.002269
Max Friction Coeff. :     1.415400

          Sig-X      Sig-Y     Tau-XY     Sig-1      Sig-2    Tau-max
Min       914.89    -48.06     -16.54    915.97    -81.35    449.96
Max      1840.40    162.45     271.02   1874.40    161.81    926.06
*******************************************************************


*******************************************************************
Title       : pois=0.3
Roller type : Concave Roller
Max Spread            :     0.002095
Max Friction Coeff. :     1.384900

          Sig-X      Sig-Y     Tau-XY     Sig-1      Sig-2    Tau-max
Min       913.46    -81.06     -17.14    914.88   -113.20    460.33
Max      1836.05    173.13     255.30   1867.15    172.50    910.50
*******************************************************************


*******************************************************************
Title       : width=3
Roller type : Concave Roller
Max Spread            :     0.000199
Max Friction Coeff. :     0.452250

          Sig-X      Sig-Y     Tau-XY     Sig-1      Sig-2    Tau-max
Min      1192.50     -9.22      -2.20   1192.50     -9.90    587.55
Max      1362.70     29.97      52.94   1364.20     29.96    679.37
*******************************************************************


*******************************************************************
Title       : width=9
Roller type : Concave Roller
Max Spread            :     0.009376
Max Friction Coeff. :     2.588800

          Sig-X      Sig-Y     Tau-XY     Sig-1      Sig-2    Tau-max
Min       392.25    -76.90     -40.49    410.93   -270.98    205.20
Max      2799.30    386.84     714.62   2958.75    379.22   1487.05
*******************************************************************
```

```
*********************************************************************
Title      : width=12
Roller type : Concave Roller
Max Spread          :      0.023561
Max Friction Coeff. :      4.794400


           Sig-X       Sig-Y      Tau-XY      Sig-1       Sig-2     Tau-max
Min      -393.15     -152.61      -56.69      -33.56     -834.07      60.60
Max      4318.45      800.14     1390.00     4707.60      749.46     2394.40
*********************************************************************


*********************************************************************
Title      : tension=1
Roller type : Concave Roller
Max Spread          :      0.002340
Max Friction Coeff. :      1.999200


           Sig-X       Sig-Y      Tau-XY      Sig-1       Sig-2     Tau-max
Min       500.50      -35.33      -16.50      502.20      -83.41     238.10
Max      1426.05      158.36      277.23     1471.25      157.33     734.35
*********************************************************************


*********************************************************************
Title      : tension=2
Roller type : Concave Roller
Max Spread          :      0.002351
Max Friction Coeff. :      1.110800


           Sig-X       Sig-Y      Tau-XY      Sig-1       Sig-2     Tau-max
Min      1330.50      -35.52      -16.58     1331.10      -61.77     652.80
Max      2261.10      159.62      278.58     2290.05      159.15    1135.40
*********************************************************************


*********************************************************************
Title      : tension=3
Roller type : Concave Roller
Max Spread          :      0.002363
Max Friction Coeff. :      0.764230


           Sig-X       Sig-Y      Tau-XY      Sig-1       Sig-2     Tau-max
Min      2160.40      -35.73      -16.67     2160.80      -53.82    1068.55
Max      3096.25      160.29      279.94     3117.55      159.98    1545.15
*********************************************************************


*********************************************************************
Title      : profile=2000
Roller type : Concave Roller
Max Spread          :      0.001467
Max Friction Coeff. :      0.939620


           Sig-X       Sig-Y      Tau-XY      Sig-1       Sig-2     Tau-max
Min      1040.00      -22.16      -10.34     1040.30      -36.09     512.27
Max      1620.95       99.51      173.89     1636.65       99.27     811.19
*********************************************************************
```

```
*********************************************************************
Title      : profile=3000
Roller type : Concave Roller
Max Spread          :      0.000976
Max Friction Coeff. :      0.639850

          Sig-X      Sig-Y     Tau-XY      Sig-1      Sig-2    Tau-max
Min     1109.10    -14.80      -6.89    1109.20     -21.17     550.02
Max     1497.25     65.76     116.01    1504.80      65.65     746.16
*********************************************************************


*********************************************************************
Title      : profile=5000
Roller type : Concave Roller
Max Spread          :      0.000587
Max Friction Coeff. :      0.383100

          Sig-X      Sig-Y     Tau-XY      Sig-1      Sig-2    Tau-max
Min     1164.60     -9.01      -4.14    1164.60     -11.37     579.36
Max     1398.35     40.63      69.64    1401.25      40.59     696.11
*********************************************************************


*********************************************************************
Title      : base radius=0.75
Roller type : Concave Roller
Max Spread          :      0.003507
Max Friction Coeff. :      1.905700

          Sig-X      Sig-Y     Tau-XY      Sig-1      Sig-2    Tau-max
Min      750.05    -53.97     -24.76     752.60    -126.05     344.74
Max     2181.60    245.01     416.30    2250.60     243.49    1119.45
*********************************************************************


*********************************************************************
Title      : base radius = 2
Roller type : Concave Roller
Max Spread          :      0.001319
Max Friction Coeff. :      0.976670

          Sig-X      Sig-Y     Tau-XY      Sig-1      Sig-2    Tau-max
Min     1058.80    -20.02      -9.31    1059.00     -32.29     528.66
Max     1570.20     84.78     156.46    1582.40      84.59     785.36
*********************************************************************


*********************************************************************
Title      : base radius = 3
Roller type : Concave Roller
Max Spread          :      0.000881
Max Friction Coeff. :      0.769110

          Sig-X      Sig-Y     Tau-XY      Sig-1      Sig-2    Tau-max
Min     1119.00    -13.71      -6.21    1119.10     -19.95     561.63
Max     1459.55     56.11     104.31    1464.95      56.03     727.73
*********************************************************************
```

```
*******************************************************************
Title        : Curved axis roller base run
Roller type : Curved Axis Roller
Max Spread            :      0.003694
Max Friction Coeff. :       0.702250


          Sig-X      Sig-Y      Tau-XY     Sig-1      Sig-2      Tau-max
Min     1180.45     -20.71     -57.56    1180.65     -25.08     537.60
Max     1353.35     176.83      76.29    1363.60     176.06     675.87
*******************************************************************


*******************************************************************
Title        : Curved Axis = th=0.0012 profile=756
Roller type : Curved Axis Roller
Max Spread            :      0.008199
Max Friction Coeff. :       1.537400


          Sig-X      Sig-Y      Tau-XY     Sig-1      Sig-2      Tau-max
Min     1097.75     -46.09    -127.94    1098.75     -67.01     433.02
Max     1480.95     392.55     169.24    1525.65     389.09     744.55
*******************************************************************


*******************************************************************
Title        : Curved Axis - th=0.0018  profile= 1680
Roller type : Curved Axis Roller
Max Spread            :      0.003691
Max Friction Coeff. :       1.041000


          Sig-X      Sig-Y      Tau-XY     Sig-1      Sig-2      Tau-max
Min      764.46     -20.70     -57.50     764.76     -27.17     329.74
Max      936.83     176.52      76.21     951.36     175.61     468.73
*******************************************************************


*******************************************************************
Title        : Curved Axis - th=0.0018  profile=756
Roller type : Curved Axis Roller
Max Spread            :      0.008206
Max Friction Coeff. :       2.287200


          Sig-X      Sig-Y      Tau-XY     Sig-1      Sig-2      Tau-max
Min      681.69     -45.99    -128.02     683.33     -76.30     227.26
Max     1064.67     392.55     169.07    1125.53     386.72     541.33
*******************************************************************


*******************************************************************
Title        : th=0.0005
Roller type : Curved Axis Roller
Max Spread            :      0.003686
Max Friction Coeff. :       0.304950


          Sig-X      Sig-Y      Tau-XY     Sig-1      Sig-2      Tau-max
Min     2928.05     -20.83     -57.40    2928.15     -22.68    1411.55
Max     3102.05     176.93      76.62    3106.55     176.58    1549.30
*******************************************************************
```

```
****************************************************************
Title      : th=0.0009
Roller type : Curved Axis Roller
Max Spread          :      0.003691
Max Friction Coeff. :      0.531740


            Sig-X       Sig-Y       Tau-XY      Sig-1       Sig-2       Tau-max
Min      1596.55     -20.76      -57.50     1596.70     -24.05      745.70
Max      1769.65     176.79       76.37     1777.50     176.11      883.52
****************************************************************


****************************************************************
Title      : th=0.0018
Roller type : Curved Axis Roller
Max Spread          :      0.003691
Max Friction Coeff. :      1.041000


            Sig-X       Sig-Y       Tau-XY      Sig-1       Sig-2       Tau-max
Min       764.46     -20.70      -57.50      764.76     -27.17      329.74
Max       936.83     176.52       76.21      951.36     175.61      468.73
****************************************************************


****************************************************************
Title      : emmd=50000
Roller type : Curved Axis Roller
Max Spread          :      0.003133
Max Friction Coeff. :      0.424770


            Sig-X       Sig-Y       Tau-XY      Sig-1       Sig-2       Tau-max
Min      1212.55     -27.00      -28.88     1212.65     -28.04      552.34
Max      1292.75     153.43       37.27     1296.25     153.13      648.43
****************************************************************


****************************************************************
Title      : emmd=117000
Roller type : Curved Axis Roller
Max Spread          :      0.003578
Max Friction Coeff. :      0.625080


            Sig-X       Sig-Y       Tau-XY      Sig-1       Sig-2       Tau-max
Min      1188.20     -22.12      -48.90     1188.35     -25.32      541.09
Max      1334.35     171.66.      65.30     1342.65     170.94      666.09
****************************************************************


****************************************************************
Title      : emmd=200000
Roller type : Curved Axis Roller
Max Spread          :      0.003765
Max Friction Coeff. :      0.766020


            Sig-X       Sig-Y       Tau-XY      Sig-1       Sig-2       Tau-max
Min      1175.25     -19.67      -64.62     1175.45     -25.13      535.12
Max      1370.10     180.47       85.34     1381.85     180.00      685.34
****************************************************************
```

```
********************************************************************
Title       : bowplane= 30
Roller type : Curved Axis Roller
Max Spread            :       0.003892
Max Friction Coeff. :        0.687940


          Sig-X       Sig-Y       Tau-XY      Sig-1       Sig-2       Tau-max
Min        671.08     -89.35      -61.96      693.59     -111.87      402.72
Max       1566.90     188.51       78.04     1566.90      188.05      726.08
********************************************************************


********************************************************************
Title       : bowplane = 40
Roller type : Curved Axis Roller
Max Spread            :       0.003861
Max Friction Coeff. :        0.716630


          Sig-X       Sig-Y       Tau-XY      Sig-1       Sig-2       Tau-max
Min       1098.80     -40.50      -59.97     1102.90      -44.98      533.48
Max       1361.00     184.47       70.23     1371.60      183.50      665.47
********************************************************************


********************************************************************
Title       : bowplane=60
Roller type : Curved Axis Roller
Max Spread            :       0.003025
Max Friction Coeff. :        0.634980


          Sig-X       Sig-Y       Tau-XY      Sig-1       Sig-2       Tau-max
Min        902.79     -49.00      -47.06      902.79      -57.77      440.81
Max       1973.60     145.27       92.86     1974.40      144.51      960.83
********************************************************************


********************************************************************
Title       : base rad. = 0.5
Roller type : Curved Axis Roller
Max Spread            :       0.003098
Max Friction Coeff. :        0.598770


          Sig-X       Sig-Y       Tau-XY      Sig-1       Sig-2       Tau-max
Min       1191.85     -11.67      -48.82     1192.00      -16.06      553.34
Max       1341.25     150.73       76.30     1344.35      150.42      676.12
********************************************************************


********************************************************************
Title       : base rad. = 1
Roller type : Curved Axis Roller
Max Spread            :       0.004278
Max Friction Coeff. :        0.816560


          Sig-X       Sig-Y       Tau-XY      Sig-1       Sig-2       Tau-max
Min       1169.20     -29.69      -65.99     1169.50      -34.03      523.47
Max       1378.85     202.85       76.29     1392.05      201.68      677.79
********************************************************************
```

```
********************************************************************
Title       : base rad. = 1.25
Roller type : Curved Axis Roller
Max Spread          :      0.004842
Max Friction Coeff. :      0.935910


        Sig-X     Sig-Y     Tau-XY    Sig-1     Sig-2     Tau-max
Min     1158.50   -41.19    -74.38    1158.85   -43.65    509.52
Max     1401.50   228.19     76.30    1417.85   226.69    680.52
********************************************************************


********************************************************************
Title       : poison = 0.1
Roller type : Curved Axis Roller
Max Spread          :      0.003748
Max Friction Coeff. :      0.729940


        Sig-X     Sig-Y     Tau-XY    Sig-1     Sig-2     Tau-max
Min     1180.15   -17.90    -60.11    1180.30   -22.68    532.61
Max     1356.20   178.81     79.83    1367.00   178.38    678.62
********************************************************************


********************************************************************
Title       : poisson=0.2
Roller type : Curved Axis Roller
Max Spread          :      0.003692
Max Friction Coeff. :      0.690900


        Sig-X     Sig-Y     Tau-XY    Sig-1     Sig-2     Tau-max
Min     1180.05   -22.27    -56.36    1180.25   -26.39    539.87
Max     1352.75   177.53     74.10    1362.75   176.65    674.53
********************************************************************


********************************************************************
Title       : poisson = 0.3
Roller type : Curved Axis Roller
Max Spread          :      0.003629
Max Friction Coeff. :      0.653530


        Sig-X     Sig-Y     Tau-XY    Sig-1     Sig-2     Tau-max
Min     1180.90   -27.16    -53.16    1181.15   -30.74    546.02
Max     1349.80   178.15     69.15    1358.90   177.99    670.85
********************************************************************


********************************************************************
Title       : width = 3
Roller type : Curved Axis Roller
Max Spread          :      0.001466
Max Friction Coeff. :      0.614360


        Sig-X     Sig-Y     Tau-XY    Sig-1     Sig-2     Tau-max
Min     1194.10   -24.95    -38.86    1194.10   -25.77    556.37
Max     1306.50   138.90     38.14    1311.45   138.45    650.06
********************************************************************
```

```
************************************************************************
Title      : width=9
Roller type : Curved Axis Roller
Max Spread            :      0.006957
Max Friction Coeff. :      0.880600

           Sig-X       Sig-Y      Tau-XY      Sig-1      Sig-2     Tau-max
Min     1186.05      -15.38      -95.67     1186.05     -25.19      518.40
Max     1406.00      224.15      114.32     1410.10      223.43      709.75
************************************************************************


************************************************************************
Title      : width=12
Roller type : Curved Axis Roller
Max Spread            :      0.011021
Max Friction Coeff. :      1.064500

           Sig-X       Sig-Y      Tau-XY      Sig-1      Sig-2     Tau-max
Min     1177.25      -19.05     -133.34     1177.30     -24.66      495.35
Max     1500.00      268.00      152.41     1504.60      267.71      747.10
************************************************************************


************************************************************************
Title      : tension=1
Roller type : Curved Axis Roller
Max Spread            :      0.003691
Max Friction Coeff. :      1.041100

           Sig-X       Sig-Y      Tau-XY      Sig-1      Sig-2     Tau-max
Min      764.47      -20.70      -57.50      764.77     -27.17      329.74
Max      936.83      176.53       76.21      951.36      175.61      468.73
************************************************************************


************************************************************************
Title      : tension=2
Roller type : Curved Axis Roller
Max Spread            :      0.003691
Max Friction Coeff. :      0.531780

           Sig-X       Sig-Y      Tau-XY      Sig-1      Sig-2     Tau-max
Min     1596.55      -20.76      -57.50     1596.75     -24.06      745.70
Max     1769.70      176.80       76.37     1777.55      176.12      883.52
************************************************************************


************************************************************************
Title      : tension=3
Roller type : Curved Axis Roller
Max Spread            :      0.003677
Max Friction Coeff. :      0.360760

           Sig-X       Sig-Y      Tau-XY      Sig-1      Sig-2     Tau-max
Min     2428.95      -20.85      -57.26     2429.05     -23.07     1162.15
Max     2602.00      176.32       76.53     2607.40      175.90     1299.40
************************************************************************
```

```
****************************************************************
Title       : emcd=50000
Roller type : Curved Axis Roller
Max Spread           :     0.004042
Max Friction Coeff. :     0.424190

           Sig-X      Sig-Y     Tau-XY     Sig-1      Sig-2    Tau-max
Min      1212.20      -6.69     -37.03    1212.25      -8.26     583.09
Max      1323.90      82.57      45.53    1327.15      82.46     664.34
****************************************************************


****************************************************************
Title       : emcd=157000
Roller type : Curved Axis Roller
Max Spread           :     0.003557
Max Friction Coeff. :     0.823340

           Sig-X      Sig-Y     Tau-XY     Sig-1      Sig-2    Tau-max
Min      1168.40     -30.37     -65.57    1168.65     -36.08     512.62
Max      1362.60     229.61      87.54    1376.90     229.03     680.91
****************************************************************


****************************************************************
Title       : emcd=200000
Roller type : Curved Axis Roller
Max Spread           :     0.003456
Max Friction Coeff. :     0.945820

           Sig-X      Sig-Y     Tau-XY     Sig-1      Sig-2    Tau-max
Min      1157.70     -39.73     -71.60    1158.10     -46.62     488.68
Max      1370.40     283.71      96.48    1389.20     281.86     685.48
****************************************************************


****************************************************************
Title       : wrap angle = 30
Roller type : Curved Axis Roller
Max Spread           :     0.002635
Max Friction Coeff. :     1.671900

           Sig-X      Sig-Y     Tau-XY     Sig-1      Sig-2    Tau-max
Min       533.75     -63.29     -42.41     576.37     -79.83     288.53
Max      2737.75     166.25     102.03    2740.55     163.50    1288.54
****************************************************************


****************************************************************
Title       : wrap angle = 60
Roller type : Curved Axis Roller
Max Spread           :     0.003130
Max Friction Coeff. :     0.963380

           Sig-X      Sig-Y     Tau-XY     Sig-1      Sig-2    Tau-max
Min       883.04     -41.02     -49.60     883.04     -51.66     417.22
Max      2032.15     152.79     102.49    2034.55     151.83     982.56
****************************************************************
```

```
************************************************************************
Title      : wrap angle = 120
Roller type : Curved Axis Roller
Max Spread        :     0.003981
Max Friction Coeff. :     0.533500


        Sig-X     Sig-Y    Tau-XY    Sig-1     Sig-2    Tau-max
Min     712.99    -93.03   -81.29    721.76    -101.78   411.76
Max     1540.80   187.78    59.54    1540.80   187.43    718.73
************************************************************************


************************************************************************
Title      : profile=756
Roller type : Curved Axis Roller
Max Spread        :     0.008199
Max Friction Coeff. :     1.537400


        Sig-X     Sig-Y    Tau-XY    Sig-1     Sig-2    Tau-max
Min     1097.75   -46.09  -127.94    1098.75   -67.01    433.02
Max     1480.95   392.55   169.24    1525.65   389.09    744.55
************************************************************************


************************************************************************
Title      : profile=3000
Roller type : Curved Axis Roller
Max Spread        :     0.002068
Max Friction Coeff. :     0.400120


        Sig-X     Sig-Y    Tau-XY    Sig-1     Sig-2    Tau-max
Min     1210.45   -11.61   -32.19    1210.45   -12.99    575.75
Max     1307.40    98.95    42.73    1310.70    98.67    652.80
************************************************************************


************************************************************************
Title      : profile=5000
Roller type : Curved Axis Roller
Max Spread        :     0.001245
Max Friction Coeff. :     0.247470


        Sig-X     Sig-Y    Tau-XY    Sig-1     Sig-2    Tau-max
Min     1225.60    -6.93   -19.34    1225.60    -7.43    595.14
Max     1284.15    59.52    25.64    1285.40    59.42    641.50
************************************************************************


************************************************************************
Title      : Profile = 8000
Roller type : Curved Axis Roller
Max Spread        :     0.000777
Max Friction Coeff. :     0.161530


        Sig-X     Sig-Y    Tau-XY    Sig-1     Sig-2    Tau-max
Min     1234.20    -4.33   -12.05    1234.20    -4.52    606.21
Max     1270.95    37.11    16.03    1271.45    37.08    635.21
************************************************************************
```

```
*********************************************************************
Title       : Profile = 999999
Roller type : Curved Axis Roller
Max Spread          :     0.000006
Max Friction Coeff. :     0.039865

            Sig-X      Sig-Y      Tau-XY     Sig-1      Sig-2      Tau-max
Min       1248.40      -0.01      -0.03     1248.40      -0.01      624.21
Max       1250.15       0.29       0.13     1250.15       0.29      625.06
*********************************************************************


*********************************************************************
Title       : Profile=1e20
Roller type : Curved Axis Roller
Max Spread          :     0.000000
Max Friction Coeff. :     0.039485

            Sig-X      Sig-Y      Tau-XY     Sig-1      Sig-2      Tau-max
Min       1248.40      -0.12      -0.03     1248.40      -0.12      624.21
Max       1250.05       0.04       0.11     1250.05       0.04      625.03
*********************************************************************
```

APPENDIX B

WEB SPREADING MEASUREMENT DATA

214

Roller Type:	Concave Roller
Roller Base Radius:	1.125 in.
Roller Profile Radius:	1250 in.
Material:	0.0012 in. Coated Polypropylene

Spreading Measurements (in.)				
0.0015	0.0012	0.0021	0.0011	0.0008

Roller Type:	Concave Roller
Roller Base Radius:	1.125 in.
Roller Profile Radius:	1250 in.
Material:	0.0018 in. Coated Polypropylene

Spreading Measurements (in.)				
0.0009	0.0016	0.0008	0.00075	0.001

Roller Type:	Curved Axis Roller
Roller Base Radius:	0.75 in.
Roller Profile Radius:	756in.
Material:	0.0012 in. Coated Polypropylene

Spreading Measurements (in.)				
0.0018	0.0010	0.0013	0.0013	0.0023

Roller Type:	Curved Axis Roller
Roller Base Radius:	0.75 in.
Roller Profile Radius:	756in.
Material:	0.0018 in. Coated Polypropylene

Spreading Measurements (in.)				
0.0011	0.0018	0.0014	0.0013	0.0018

Roller Type:	Curved Axis Roller
Roller Base Radius:	0.75 in.
Roller Profile Radius:	1680in.
Material:	0.0012 in. Coated Polypropylene

Spreading Measurements (in.)				
0.0019	0.0017	0.0030	0.0017	0.0013

Roller Type:	Curved Axis Roller
Roller Base Radius:	0.75 in.
Roller Profile Radius:	1680 in.
Material:	0.0018 in. Coated Polypropylene

Spreading Measurements (in.)				
0.0014	0.0009	0.0015	0.0013	0.0013

Roller Type:	Curved Axis Roller
Roller Base Radius:	0.75 in.
Roller Profile Radius:	8000 in.
Material:	0.0012 in. Coated Polypropylene

Spreading Measurements (in.)				
0.0015	0.0020	0.0010	0.0015	0.0015

VITA 2

Ronald David Delahoussaye

Candidate for Degree of

Doctor of Philosophy

Thesis: ANALYSIS OF DEFORMATIONS, STRESSES, AND FORCES IN
WEBS ENCOUNTERING SPREADING ROLLERS

Major Field: Mechanical Engineering

Biographical:

Personal Data: Born in Jennings, Louisiana, February 11,
1957, the son of Dave and Carolyn Delahoussaye.

Education: Graduated from Jennings High School, Jennings,
Louisiana in May 1975; received Bachelor of Science
Degree in Mechanical Engineering from Louisiana Tech
University in May 1979; received Master of Science
Degree in Mechanical Engineering from Georgia Institute
of Technology in August 1982; completed the
requirements for the Doctor of Philosophy Degree in
Mechanical Engineering in December 1989.

Professional Experience: Graduate Assistant, Instructor,
Lecturer, and Assistant Professor, Department of
Mechanical and Aerospace Engineering, Oklahoma State
University, January 1984 to present; Visiting Assistant
Professor, Department of Mechanical Engineering,
Louisiana Tech University, September 1982 to December
1983; Graduate Assistant, Department of Mechanical
Engineering, Georgia Institute of Technology, August
1981 to August 1982; Design Engineer, Pratt and Whitney
Aircraft, May 1979 to August 1981.